

**SENSOR AND CNC INTERNAL SIGNAL EVALUATION TO
DETECT TOOL AND WORKPIECE MALFUNCTIONS IN
THE DRILLING PROCESS**

Electronics and Computing Department



To obtain the title of

DOCTOR IN APPLIED ENGINEERING

Presented by

AITOR DUO ZUBIAURRE

Supervised by

ROSA MARIA BASAGOITI ASTIGARRAGA
Electronics and Computing Department

PEDRO JOSE ARRAZOLA ARRIOLA
Mechanics and Industrial Production Department

In ARRASATE in 2021

This work is distributed under a licence Creative Commons
Attribution-NonCommercial-NoDerivatives 4.0 International.



ABSTRACT

To boost competitiveness and meet changing customer demands, the manufacturing sector is taking advantage of Information and Communication Technologies (ICT). Machining is no exception, and machining processes are moving toward a more intelligent and connected network to become part of an industrial digital ecosystem.

Despite the advances made to date, there are still considerable opportunities for improvement because of the complexity of machining processes. In this context, extracting and analysing data from machining operations can provide valuable information to predict undesirable aspects, and take actions to reduce or prevent them.

The machining process taken as the focus of the present work is drilling. Drilling is one of the most commonly used and critical machining operations on many machined components. It is carried out in the last stages of product manufacture, where a mistake can result in a defective part. In this thesis, a comparison and selection of the sensors with the best prediction capacity of tool condition and surface roughness is carried out for the development of data driven models that predict the mentioned parameters of the drilling process.

Various sensors were installed on a drilling machine, as well as internal machine signals, to take series of physical measurements of the tool condition and the machined component. The resulting data determines relationships for the creation of predictive models to identify errors that may have occurred in the drilling operation based on acquired signals.

Through statistical analysis (t-test) of the results obtained from the data-driven models, insight was gained into the predictive capability of each sensor. The most viable ones for tool condition monitoring systems were then selected.

The features of the signals that best adapt to specific surface finish were established. Based on a series of random measurements of the machined surface roughness, a methodology was developed to map the signal features that best suit the roughness distribution of the machined holes. By using hierarchical clustering and principal component analysis of the mapped signal features, clusters are created to identify holes with damaged surfaces.

The adaptability of machining process monitoring systems to various input parameters is a fundamental challenge for the automatic reconfiguration of such systems. For this reason the dimensions of the features obtained were reduced to two dimensions using principal component analysis as t-distributed stochastic neighbour embedding to be able to better identify the input parameters.

LABURPENA

Lehiakortasuna bultzatzeko eta bezeroen eskaera aldakorrei erantzuteko, fabrikazio sektorea Informazio eta Komunikazio Teknologiak (IKT) aprobetxatzen ari da. Mekanizazioa ez da salbuespena, eta mekanizazio prozesuak sare adimentsuago eta konektatuago baterantz doaz ekosistema digital industrial baten parte izateko.

Mekanizazio prozesuen konplexutasuna dela eta orain arte aurrerapenak lortu diren arren, oraindik hobetzeko aukerak daude. Testuinguru horretan, mekanizazio prozesuetatik ateratako datuak, material edo erremintarako egoera arriskutsuak aurreikusteko eta prebenitzeko informazio iturri bat izan daitezke.

Lan honen ardatz nagusia zulaketa prozesua da. Zulaketa, mekanizatutako atal askotan gehien erabiltzen den operazio kritikoenetakoa da eta produktuaren fabrikazioko azken etapetan egiten denez, akats batek pieza hondatu dezake. Tesi honetan sentsoerek barautzen desgastea eta piezan lortutako zimurtasuna iragartzeko duten gaitasuna aztertzen da datuetan oinarritutako ereduak bidez aipatutako parametroen iragarpena egiteko.

Hainbat sentso instalatu ziren zulatzeko makina batean, baita makinaren barneko seinaleak ere, erremintaren eta mekanizatutako atalen egoeraren zeharkako neurketa emateko. Zulaketa prozesuan gerta litezkeen akatsak identifikatzeko, lortutako datuek parametro fisikoekin dituzten korrelazioek zehazten dute iragarpen ereduak sortzeko gaitasuna.

Datuetan oinarritutako ereduetatik lortutako emaitzen analisi estatistikoaren (t-test) bidez, sentso bakoitzaren gaitasun iragarleari buruzko ezagutza lortu zen. Erremintaren egoera kontrolatzeko sistemarako bideragarrienak hautatzea bideratuz.

Ebaketa prozesuen errepikakortasunaren zehaztasuna funtsezko alderdi bat da mekanizatutako piezaren akabera jakin bat bermatzeko. Mekanizatutako laginen artean, zimurtasunaren ausazko neurketen arabera, zimurtasun profilarren distribuzioari gehien egokitzen zaizkien seinaleen ezaugarrien aukeraketa egiten da. Taldekatze hierarkikoa aplikatuz, aukeratutako ezaugarrien osagai nagusiak aztertuz eta sortutako taldeak irudikatuz, kaltetutako edo ez kaltetutako zuloen bereizketa erakusten da.

Mekanizazio prozesuak kontrolatzeko sistemak sarrerako parametroetara egokitzea oinarritzko erronka da sistema horien birkonfigurazio automatikoa lortzeko. Hori dela eta, instalatutako sentso eta barne seinale bakoitzetik lortutako ezaugarrien osagai nagusien analisisian eta t distribuzioan banatutako bizilagunen txertatze estokastikoaren analisiak konparatuz sarrerako parametroak bi dimentsiotan ikustea eta sailkatzea lortzen da.

RESUMEN

Para impulsar la competitividad y satisfacer las cambiantes demandas de los clientes, el sector de la fabricación está aprovechando las tecnologías de la información y la comunicación (TIC). El mecanizado no es una excepción, y los procesos de mecanizado están avanzando hacia una red más inteligente y conectada para formar parte de un ecosistema digital industrial.

A pesar de los avances logrados hasta la fecha, todavía existen considerables oportunidades de mejora debido a la complejidad de los procesos de mecanizado. En este contexto, la extracción y el análisis de los datos de las operaciones de mecanizado pueden proporcionar información valiosa para predecir los aspectos no deseados y tomar medidas para reducirlos o prevenirlos.

El proceso de mecanizado en el que se centra el presente trabajo es el taladrado. El taladrado es una de las operaciones de mecanizado más utilizadas y críticas en muchos componentes mecanizados. Se lleva a cabo en las últimas etapas de la fabricación del producto, donde un error puede dar lugar a una pieza defectuosa. En esta tesis se realiza una comparación y selección de los sensores con mejor capacidad de predicción del estado de la herramienta y de la rugosidad superficial para el desarrollo de modelos basados en datos que predigan los parámetros mencionados del proceso de taladrado.

Se instalaron diversos sensores en una máquina de taladrado, así como señales internas de la máquina, para tomar medidas indirectas físicas del estado de la herramienta y del componente mecanizado. Los datos resultantes determinan relaciones para la creación de modelos predictivos que permitan identificar los errores que puedan haberse producido en la operación de taladrado.

Mediante el análisis estadístico (prueba t) de los resultados obtenidos de los modelos basados en datos, se obtuvo una visión de la capacidad de predicción de cada sensor. A continuación, se seleccionaron los más viables para los sistemas de monitorización del estado de las herramientas.

Se establecieron las características de las señales que mejor se adaptan al acabado superficial específico. A partir de una serie de mediciones aleatorias de la rugosidad de la superficie mecanizada, se desarrolló una metodología para mapear las características de las señales que mejor se adaptan a la distribución de la rugosidad de los agujeros mecanizados. Mediante el uso de la agrupación jerárquica y el análisis de componentes principales de las características de las señales mapeadas, se crean clusters para identificar los agujeros con superficies dañadas.

La adaptabilidad de los sistemas de monitorización del proceso de mecanizado a diversos parámetros de entrada es un reto fundamental para la reconfiguración automática de dichos sistemas. Por este motivo, las dimensiones de las características obtenidas se redujeron a dos dimensiones utilizando el análisis de componentes principales como incrustación de vecinos estocásticos distribuidos en t para poder identificar mejor los parámetros de entrada.

ACKNOWLEDGEMENTS

First of all, I would like to thank my supervisors Dr. Rosa Basagoiti Astigarraga from Data Analysis and Cybersecurity research group and Dr. Pedro J. Arrazola Arriola from High Performance Machining research group, who with their knowledge and support guided me through each of the stages of this project.

I would also like to thank Mondragon Unibertsitatea for providing me with all the necessary resources and tools to carry out the research process. I would not have been able to arrive at these results if it not been for their help.

I want to add the University of Naples Federico II where I did my PhD stay. Professor Roberto Teti, who with his help I was able to collaborate with the Department of Chemical, Materials and Industrial Production Engineering and the Department of Industrial Engineering.

Azkenik, nire lankide, lagun eta senide guztiei eskerrak eman nahi nizkieke, nire gogoahula zenean ere laguntzeagatik. Bereziki, H. Otálora, A. Sela, G. Ortiz de Zarate eta X. Lazkano lankideak, nire lagun Pello Heriz eta Mikel Zumeta eta nire gurasoak, Jon Duo eta Ana Zubiaurre aipatu nahiko nituzke, beti egon baitziren laguntza hitzak eta besarkada lasaigarri bat emateko.

Eskerrik asko denoi.

CONTENTS

Abstract	i
Acronyms	xv
Nomenclature	xvii
1 INTRODUCTION	1
2 LITERATURE REVIEW	11
2.1 Machining	11
2.1.1 Orthogonal cutting	12
2.1.2 Three-dimensional cutting processes (3D)	15
2.1.3 Industrial parameters to control	17
2.1.4 Cutting process modelling	31
2.2 Process monitoring	34
2.2.1 Industrial monitoring systems	34
2.2.2 A framework for intelligent process monitoring	38
2.3 Summary	61
3 DATA COLLECTION, PROCESSING AND CLEANING METHODOLOGIES	65
3.1 Preliminary tests	67
3.2 Tests on BLS 35CrMo4 Low S	70
3.3 Tests on Inconel 718	73
3.4 Signal cleaning and feature extraction	75
3.5 Surface integrity data collection	79
4 TOOL CONDITION CLASSIFICATION THROUGH SIGNAL PERFORMANCE EVALUATION IN BLS 35CRMO4 LOW S STEEL MATERIAL WITH PREVIOUSLY WEAR-INDUCED TOOLS	81
4.1 Methodology	82
4.1.1 Sensitivity analysis through machine learning algorithms	82
4.1.2 Testing with different drill bits	84
4.2 Sensitivity of the signals to tool wear	85
4.3 Model testing for different tool geometries	86
4.4 Conclusions	90
5 TOOL FLANK WEAR CURVE RECONSTRUCTION IN END-OF-LIFE TESTS AND SUBSEQUENT PREDICTION OF TOOL BREAKAGE IN INCONEL 718	93
5.1 Methodology	94
5.1.1 Wear target estimation	94
5.1.2 Feature selection	96
5.1.3 Algorithm selection and flank wear curve prediction	96
5.1.4 Tool breakage prediction	98
5.2 Tool flank wear curve modelling through machine learning algorithms	101
5.2.1 Model performance in BH04.5D tool geometry	108

5.3	Tool breakage prediction through logistic regression	109
5.3.1	Logistic model trees for each sensor for tool breakage detection	113
5.4	Surface integrity analysis	118
5.4.1	Roughness	119
5.4.2	Material damage	122
5.5	Conclusions	125
6	SURFACE ANOMALY DETECTION IN BLS 35CRMO4 LOW S STEEL ON A LONG MACHINED TIME	127
6.1	Methodology for surface anomaly detection	128
6.1.1	Acquired signal segmentation and feature extraction	129
6.1.2	Roughness parameter selection for clustering	131
6.1.3	Surface roughness clustering based on signal features	134
6.2	Visualization of obtained clusters	136
6.3	Validation of obtained clusters	140
6.4	Conclusions	146
7	INFLUENCE OF TOOL GEOMETRY, MATERIAL AND CUTTING CONDITIONS IN SENSOR SIGNALS: DIMENSIONALITY REDUCTION AND DATA ANALYSIS	149
7.1	Methodology	149
7.2	Visualization and classification of different input parameters	152
7.3	Conclusions	156
8	CONCLUSIONS AND FUTURE LINES	159
8.1	Tool condition monitoring	160
8.2	Surface condition monitoring	161
8.3	Input parameter recognition through sensors	162
8.4	Future Development	162
9	CONTRIBUTIONS	165
	BIBLIOGRAPHY	167

LIST OF FIGURES

Figure 1.1	Industrial evolution	1
Figure 1.2	Data-driven manufacturing	4
Figure 1.3	Process monitoring framework	7
Figure 1.4	Research methodology	8
Figure 2.1	Cutting process	12
Figure 2.2	Orthogonal cutting process	13
Figure 2.3	Different chip formations	14
Figure 2.4	Turning process and variables related to cutting conditions . .	15
Figure 2.5	Drilling operation and related variables	16
Figure 2.6	Cutting forces in drilling	17
Figure 2.7	Wear mechanism in metal cutting	19
Figure 2.8	Types of drill wear	20
Figure 2.9	Flank and margin wear on drill bit according to cutting speed and drill minor cutting edge/material interaction areas	21
Figure 2.10	Different surface roughness profiles with same Ra parameter .	23
Figure 2.11	Surface roughness in drilling and helical milling	24
Figure 2.12	Residual stresses in turning	25
Figure 2.13	Residual stresses in drilling	26
Figure 2.14	Example of micro-structural damage	27
Figure 2.15	SEM close view of the severe plastic deformation layers	27
Figure 2.16	Grain boundary deformation in drilling process	28
Figure 2.17	Nanohardness profiles under the abusive drilling	29
Figure 2.18	Types of burr in drilling process	29
Figure 2.19	Graphic representation of geometrical tolerances	30
Figure 2.20	Roundness error for microdrilling at different cutting conditions	31
Figure 2.21	Model-based manufacturing and data-driven manufacturing . .	33
Figure 2.22	Spike system polar plot	35
Figure 2.23	Static fixed limits and part defined limits on Montronix system	36
Figure 2.24	Nordmann system floating limit monitoring strategy	37
Figure 2.25	Sandvik coroplus dynamic limits	37
Figure 2.26	Thrust force and torque signal relationship with tool wear in drilling process	39
Figure 2.27	Acoustic emission sources in machining	40
Figure 2.28	Evolution of energy of detail after Wavelet Packet Transform of acoustic emissions in turning operation	41
Figure 2.29	Magnitude of power spectrum of spindle noise and flank wear in turning	42
Figure 2.30	Spindle power and torque comparison in drilling process	45

Figure 2.31	Three-level wavelet packet transform (WPT) decomposition, where blackened fields indicate the frequency band of the original signal	49
Figure 2.32	Conceptual representation of a dendrogram	55
Figure 2.33	Data leakage problem in tool wear prediction	59
Figure 3.1	Employed set-up configuration in preliminary tests	68
Figure 3.2	Input/Outputs on preliminary tests	69
Figure 3.3	Drill bit geometries and considered tool wear levels	70
Figure 3.4	Employed set-up configuration and signal simultaneous acquisition	72
Figure 3.5	Input/Outputs on BLS 35CrMo4 Low S steel tests	73
Figure 3.6	Tool condition before and after tests for each tool geometry . .	74
Figure 3.7	Input/Outputs on Inconel 718 tests	74
Figure 3.8	Tool geometries used in end-of-life tests on Inconel 718	75
Figure 3.9	Signal segmentation strategy	76
Figure 3.10	Wavelet packet transform obtained from vibrations in Z	76
Figure 3.11	Signals acquired by sensors and corresponding drilling states .	77
Figure 3.12	Machine internal signals and corresponding drilling states . . .	78
Figure 3.13	Cutting procedure for surface roughness and material damage inspection	79
Figure 4.1	Model training and testing using different geometries of drill bits	84
Figure 4.2	Performance of all the strategies and algorithms tested for the third version of dataset (V3)	88
Figure 4.3	Confusion matrices applying strategies 2 and 3 for the IBK algorithm and the TV2 and Fz signals	89
Figure 4.4	Confusion matrix: J48 algorithm for TV2 signal	90
Figure 5.1	Tool wear measurements, third-degree polynomial curve and tool breakage measured hole for each repetition	95
Figure 5.2	Complete feature space, feature selection process and reduced feature spaces for each sensor	97
Figure 5.3	Model interpretation through logistic model trees	99
Figure 5.4	Followed methodology for tool breakage detection	100
Figure 5.5	Results of algorithms using the complete feature space and reduced feature space of accelerometer signals	102
Figure 5.6	Results of algorithms using the complete feature space and reduced feature space of dynamometer signals	103
Figure 5.7	Results of algorithms using the complete feature space and reduced feature space of internal signals	104
Figure 5.8	Best and worst tool wear prediction performances for each sensor reduced feature space from bootstrapping process on geometry MDS080SK for FC_RFS	105
Figure 5.9	Best and worst tool wear prediction performances for each sensor reduced feature space from bootstrapping process on geometry MDS080SK for ACC_RFS	106

Figure 5.10	Best and worst tool wear prediction performances for each sensor reduced feature space from bootstrapping process on geometry MDS080SK for INT_RFS	107
Figure 5.11	Confusion matrices for each sensor reduced feature space for S5 (stage 5)	110
Figure 5.12	Results obtained in S6 (stage 6) for each of the sensors in testing subset	112
Figure 5.13	Logistic model function based on Internal signals Reduced Feature Space (INT_RFS)	118
Figure 5.14	Surface integrity testing points for 2 different tool geometries on different tool conditions	119
Figure 5.15	Tool condition in the last testing point for each tool in both cutting edges (rake face, flank face and margin)	120
Figure 5.16	Kernel Density estimations of roughness profiles on different tool wear levels	121
Figure 5.17	Surface roughness profiles on each tool condition for tool geometry MDS080SK on repetition 3	123
Figure 5.18	Material damage on holes performed with MDS080SK and BH04.5D tool geometries in different tool conditions	124
Figure 5.19	Material damage generated on the last testing point for tool geometry MDS080SK on repetition 3 at hole entry and hole exit	124
Figure 6.1	External and Internal signal acquired for each tool geometry	129
Figure 6.2	External and Internal signal statistical feature selection for hole surface anomaly detection	130
Figure 6.3	Uncorrelated ($R^2 < 0.99$) surface parameters and their respective dendrograms for R204.6D and BH04.5D	131
Figure 6.4	Individual roughness parameters (R_a , R_{ku} , R_{sk}) coloured based on clustering results	132
Figure 6.5	Example of Alicona measurements for hole 196 of R204.6D tool and hole 287 of BH04.5D tool	133
Figure 6.6	Comparison of different distribution function assumption for roughness profiles	134
Figure 6.7	Clustering of measured holes using the signal statistical features of signals shown in Table 6.1	135
Figure 6.8	Dendrograms using the statistical features of all the holes for each of the cutting tools used	135
Figure 6.9	Visualization of two principal components for obtained clusters a) R204.6D tool b) BH04.5D tool	137
Figure 6.10	Principal component analysis of selected features for R204.6D and BH04.5D tools	138
Figure 6.11	Validation data for BH04.5D (straight edge) tool	141
Figure 6.12	Hole surfaces and surface profiles obtained with BH04.5D tool	142
Figure 6.13	Validation data for R204.6D (curved edge) tool	143
Figure 6.14	Hole surfaces and surface profiles obtained with R204.6D tool	145

Figure 7.1	Different input parameters to the drilling process considered in this chapter	150
Figure 7.2	Compared two scenarios for the same objective a) PCA based model b) tSNE based model)	151
Figure 7.3	PCA based on sensor fusion	153
Figure 7.4	t-SNE based on Sensor fusion	154
Figure 7.5	Input parameter combination changes used on section 5.2.1 to predict tool flank wear	157

LIST OF TABLES

Table 2.1	Roughness parameters	22
Table 2.2	Sensor and monitoring strategies used by industrial tool condition monitoring systems	35
Table 2.3	Types of tool wear found in vibration signal spectrum	44
Table 2.4	Signal feature expressions	47
Table 2.5	Summary of indirect tool conditions monitoring techniques through automatic learning algorithms	59
Table 2.6	Summary of indirect roughness monitoring techniques through automatic learning algorithms	61
Table 3.1	Acquired signals, sampling frequency and sensor details	67
Table 3.2	Chemical composition of the workpiece material (BLS 35CrMo4 Low S)	68
Table 3.3	Cutting conditions, cutting edge geometry and number of holes related to drill number	71
Table 3.4	Chemical composition of the workpiece material (Inconel 718)	75
Table 4.1	Generalized example of a signal dataset. Constituted by statistical features extracted from the signal, process input parameters, and the class	83
Table 4.2	Statistical significance of signals in a two tailed paired T-test for accuracy in predicting BH04.5D tool flank wear	86
Table 4.3	Statistical significance of signals in a two tailed paired T-test for accuracy in predicting R204.6D tool flank wear	87
Table 5.1	Model evaluation metrics used for regression	98
Table 5.2	Model performance from bootstrapping process for each tool and the mean value of considered metrics for each sensor reduced feature space	108
Table 5.3	Model performance on BH04.5D tool geometry after training on MDS080SK in each sensor selected feature space	108
Table 5.4	Label imputation for transition phase during tool breakage	110
Table 5.5	Mean in MCC for each of the sensors and p values of t-test results	111
Table 5.6	Logistic model for stage 5 using FC_RFS	114
Table 5.7	Logistic model for stage 6 using FC_RFS	114
Table 5.8	Logistic model 1 st leave for stage 5 using ACC_RFS	114
Table 5.9	Logistic model 2 nd leave for stage 5 using ACC_RFS	115
Table 5.10	Logistic model 3 rd leave for stage 5 using ACC_RFS	115
Table 5.11	Logistic model 1 st leave for stage 6 using ACC_RFS	115
Table 5.12	Logistic model 2 nd leave for stage 6 using ACC_RFS	116
Table 5.13	Logistic model 3 rd leave for stage 6 using ACC_RFS	116

Table 5.14	Logistic model 4 th leave for stage 6 using ACC_RFS	116
Table 5.15	Logistic model for stage 5 using INT_RFS	117
Table 5.16	Logistic model for stage 6 using INT_RFS	117
Table 6.1	Correlations higher than 90% between acquired signal statistical features and roughness measured parameters	134
Table 6.2	Cluster centroids for R204.6D tool drilled holes and feature contribution to each dimension	138
Table 6.3	Cluster centroids for BH04.5D tool drilled holes and feature contribution to each dimension	139
Table 6.4	Intra cluster distance and distance between measured holes and cluster centroids R204.6D tool	139
Table 6.5	Intra cluster distance and distance between measured holes and cluster centroids BH04.5D tool	139
Table 7.1	Comparison of the success rate between PCA and tSNE for identifying process input parameters	155

ACRONYMS

ACC_RFS	Accelerometer Reduced Feature Space
AE	Acoustic Emission
ANFIS	Adaptive Neuro Fuzzy Inference System
ANN	Artificial Neural Network
ARMA	Auto Regressive Moving Average
BUE	Built-Up Edge
CFRP	Carbon Fiber Reinforced Plastic
CIRP	International Academy for Production Engineering
CNC	Computer Numerical Control
DFT	Discrete Fourier Transform
DWT	Discrete Wavelet Transform
FC_RFS	Dynamometer Reduced Feature Space
FDSS	Fuzzy Decision Support System
GA	Genetic Algorithm
HDL	Heavily Distorted Layer
HSS	High Speed Steel
HWC	Harmonic Wavelet Coefficients
ICT	Internet and Communication Technology
IoT	Internet of Things
INT_RFS	Internal signals Reduced Feature Space
LR	Logistic Regression
LMT	Logistic Model Tree
MAE	Mean Absolute Error
MAMP	Moving Average Mean Power
ML	Machine Learning
MLP	Multi Layer Perceptron
MP	Mean Power
MCC	Matthews Correlation Coefficient
MESA	Maximum Entropy Spectral Analysis
MVMP	Moving Variance Mean Power
PCA	Principal Component Analysis
PSD	Power Spectral Density
RF	Random Forest
RMS	Root Mean Square
RUL	Remaining Useful Life
RBFN	Radial Basis Function Network
RMSE	Root Mean Square Error
SPD	Severe Plastic Deformation

STFT	Short Time Fourier Transform
SSLW	Signal Stable Length Window
SVM	Support Vector Machine
SH	Strain Hardening
SSA	Singular Spectrum Analysis
SMOTE	Synthetic Minority Oversampling Technique
tSNE	t Distributed Stochastic Neighbour Embedding
TDA	Time Direct Analysis
WPT	Wavelet Packet Transform
WL	White Layer

NOMENCLATURE

Symbol	Description	Unit
V_c	Cutting speed	$m \cdot \text{min}^{-1}$
n	Spindle speed	rpm
f	Feed per revolution	$\text{mm} \cdot \text{rev}^{-1}$
a_v	Feed rate	$\text{mm} \cdot \text{min}^{-1}$
a_p	Depth of cut	mm
L	Hole depth	mm
h	Uncut chip thickness	mm
ϕ	Shear angle	$^\circ$
λ	Rake angle	$^\circ$
α	Clearance angle	$^\circ$
\varnothing	Drill diameter	mm
r	Cutting edge radius	μm
β	Cutting edge angle	$^\circ$
β'	Worn cutting edge angle	$^\circ$
V_b	Flank wear	mm
$V_{b_{\max}}$	Maximum flank wear	mm
W_m	Margin wear	mm
R_a	Average roughness of profile	μm
R_q	Root-Mean-Square roughness of profile	μm
R_t	Maximum peak to valley height of roughness profile	μm
R_z	Mean peak to valley height of roughness profile	μm
R_{\max}	Maximum peak to valley height of roughness profile	μm
R_p	Maximum peak height of roughness profile	μm
R_v	Maximum valley height of roughness profile	μm
R_c	Mean height of profile irregularities of roughness profile	μm
R_{sm}	Mean spacing of profile irregularities of roughness profile	μm
R_{sk}	Skewness of roughness profile	
R_{ku}	Kurtosis of roughness profile	
R_{dq}	Root-Mean-Square slope of roughness profile	
R_t/R_z	Extreme Scratch/Peak value of roughness profile	
R	Resultant force	N
F_c	Cutting force acting on cutting velocity direction	N
F_x	Cutting force in X axis direction	N

F_y	Cutting corfe in Y axis direction	N
F_z	Thrust force	N
M_z	Torque	$N \cdot m$
ACC_x	Vibrations in x axis	$m \cdot s^{-2}$
ACC_y	Vibrations in y axis	$m \cdot s^{-2}$
ACC_z	Vibrations in z axis	$m \cdot s^{-2}$
AE	Acoustic emissions	V
SP	Sound pressure	Pascal
TV2	Z-axis motor torque	N
TV50	Spindle motor power feedback	W
TV51	Active power supplied by the drive	W
TV3	Power percentage respect to the maximum on servo system	%
V_x	Tool speed in x axis	$mm \cdot s^{-1}$
V_y	Tool speed in y axis	$mm \cdot s^{-1}$
V_z	Tool speed in z axis	$mm \cdot s^{-1}$
$ACCEL_x$	Tool acceleration in x axis	$mm \cdot s^{-2}$
$ACCEL_y$	Tool acceleration in y axis	$mm \cdot s^{-2}$
$ACCEL_z$	Tool acceleration in z axis	$mm \cdot s^{-2}$
$JERK_x$	Tool jerk in x axis	$mm \cdot s^{-3}$
$JERK_y$	Tool jerk in y axis	$mm \cdot s^{-3}$
$JERK_z$	Tool jerk in z axis	$mm \cdot s^{-3}$
f_s	Sampling frequency	Hz
\bar{X}	Arithmetic mean	
σ^2	Statistical variance	
σ	Standard deviation	
g_1	Skewness	
g_2	Kurtosis	

INTRODUCTION

The technologies employed in industrial environments have always been in a state of continuous evolution. Figure 1.1 shows the evolution of industrial and Machine Learning (ML) from the point of view of complexity over time. After a long trajectory, the so-called fourth industrial revolution at the turn of the 21st century has witnessed the emergence of concepts such as the Internet of Things (IoT), big data and cyber-physical systems. The application of these advances to industrial contexts has given rise to a new concept of intelligent factories. In these environments, the exploitation of the information captured during the manufacturing processes is essential to the implementation of new production strategies.

The digital transformation of industrial processes and the introduction of the concept of Industry 4.0 has opened up a wide range of opportunities in manufacturing environments. This most recent revolution aims to adapt to the needs and variability of production processes to increase resource allocation efficiency. The digitisation of

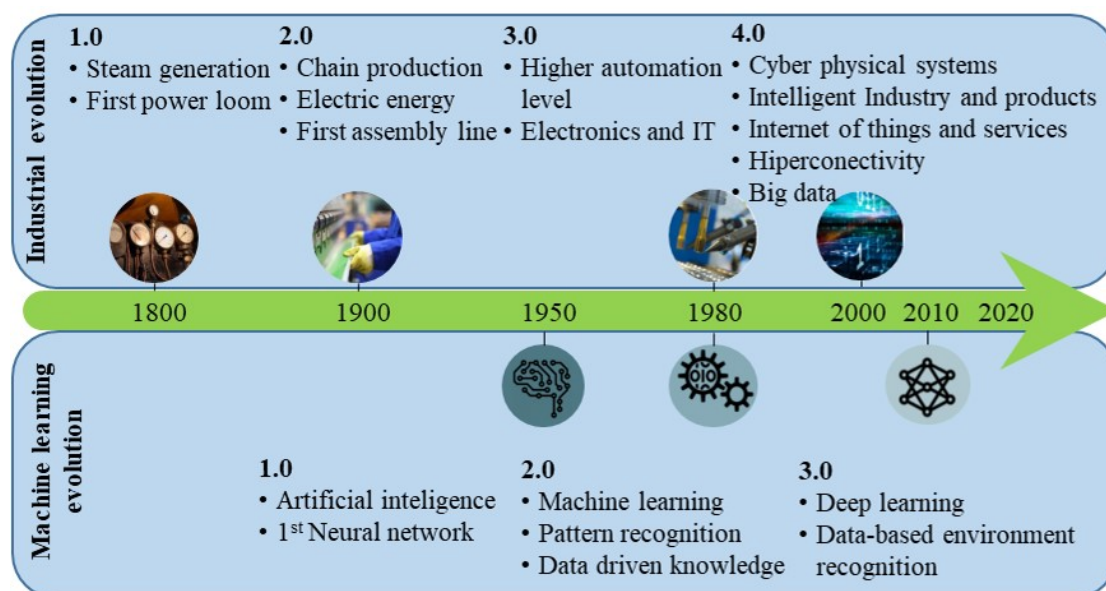


Figure 1.1 The evolution of Industrial and Artificial Intelligence, complexity over time

manufacturing means that we can reduce the time taken to market; increase process flexibility, product quality, and energy efficiency; and improve the security of our industrial networks. This all results in reduced costs and a more sustainable industrial environment.

This shift towards industry 4.0 is brought about by integrating Internet and Communication Technology (ICT) into manufacturing processes. In this scenario, diverse physical objects are interconnected through the Internet. Collaboration between networked elements, together with interaction with humans, can give machines greater autonomy as they learn to recognise the surrounding environment based on previous states. This close link between physical objects and the Internet is causing innovative technologies to emerge continually, bringing with it a number of advantages:

Efficiency: With increased human-machine activity, decisions can be taken much faster and more efficiently.

Reliability: With data analysis, more reliable products are obtained, which allows both the quality control of the products and even the improvement of the quality.

Agility: When the link between the specifications of a product and its own production process is tightened, it accelerates the entire production processes.

Innovation: Since Industry 4.0 production lines can accommodate high mix and low volumes, they are ideal for the introduction of new products and experimentation in design.

Customer experience: The responsiveness of customer requirements and greater availability of information in Industry 4.0 means that manufacturers can offer customers better service.

Costs: While Industry 4.0 requires initial investment, once intelligence is built into products and processes, costs will fall significantly. Fewer quality problems lead to less material waste, as well as lower personnel and operating costs.

According to the International Academy for Production Engineering (CIRP), machining covers almost half of all manufacturing processes. The term machining refers to a range of processes where the manufacturing of components is made by material removal: turning, drilling, milling etc. These processes are used in a range of applications where in general high accuracy, productivity, reliability is required (Schmitz and Smith, 2009).

Some of the most strategic sectors where machining is applied are automotive, energy, aerospace and railway. In the automotive sector, machining is applied to produce the steering, transmission and central unit components. The energy sector has applications in all sources, including thermal, nuclear, hydroelectric, wind, oil, and solar. In the aerospace industry, manufacturing turbines, landing gears, and stabilisers are produced by cutting tool machines, as are the railway sector rails and train wheels.

However, in the US alone more than \$10 billion is wasted annually due to non-optimal practices in the machining industry (Umbrello et al., 2004; Jawahir and Wang,

2007; Equeter et al., 2020). These include incorrect use of cutting conditions, improper selection of cutting tools and premature tool replacement. These losses would be even greater, if the number of discarded components that do not meet specific sector standards were to be aggregated. Additionally, it should be considered that surface material properties can be modified by machining and thus the useful life of the machined component can be reduced. Correcting only 1% of the abovementioned malpractices could save \$100 million per year.

The development of unmanned processes capable of performing human operator tasks, can deliver significant improvements in productivity, cost and quality. Such processes are created in human-machine collaborative environments, that allow machines to gain autonomy from the operator experience through the use of appropriate ML tools. In the context of machining, intelligence developed in the machine can learn to: (I) replace cutting tools when they result in a defective state, (II) evaluate the quality of the machined component, (III) modify the cutting conditions if necessary, and (IV) detect situations that endanger the integrity of the part, tool or machine tool (collisions, lack of coolant or chip tangling).

The collection and storage of sensor data can ensure more efficient use of cutting tools and more effective selection of cutting condition parameters. Sensor data is not merely a measurement of a physical parameter produced by a component. It also has predictive capabilities for physical parameters that cannot be measured during the manufacturing process. To ensure the closest information to what happens in the process, sensors should be located as close as possible to the cutting process without obstructing operations. The signals acquired are categorised as "far from the process" or "close to the process" (Abubakr et al., 2021). The former includes machine current, machine voltage, motor driver temperature, and motor power; while the latter refers to dynamometers, accelerometers, acoustic emissions, strain, sound or temperature measurements.

The selection of input parameters is a critical step in machining, with a very real impact on the performance of the final part. The direct measurement of machined component parameters describes the process performance, and the input parameters are adapted to obtain the required product quality. Cleaning and adapting the data to obtain signal features that provide information about the physical parameters of interest, and the application of ML techniques to obtain explanatory or predictive models are fundamental steps in moving towards a more automated, efficient and sustainable production environment.

Through the use of ML technologies, machines learn for themselves the optimal behaviour to meet production requirements. Furthermore, process monitoring makes decision-making more efficient therefore, faster. This is called data-driven manufacturing; where unlike physical models, decisions are based on the data collected during the cutting process, eliminating assumptions and impressions. Figure 2.21 shows the data-driven manufacturing cycle. The data generated in the production processes is acquired either physically, through direct measurements, such as material properties,

and tool condition; or via sensor measurements, such as vibrations, cutting forces, and acoustic emissions. The data is then stored for analysis and subsequent decision making.

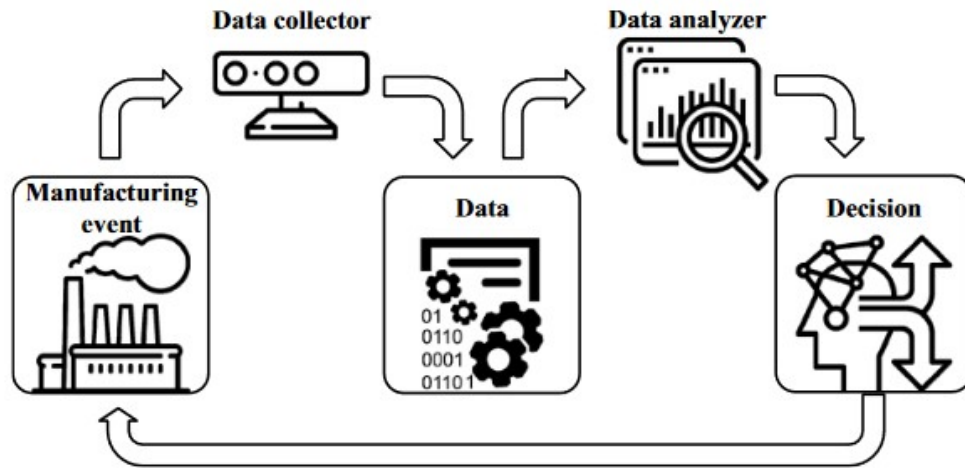


Figure 1.2 Data-driven manufacturing (Xu et al., 2020)

In data-driven manufacturing, the machine should be in charge of predicting its condition. Automatic alarm systems or notifications about the cutting process state are fundamental for the future of machined parts. The data is the basis of this transition, and will greatly assist the machine learning process and the prediction of future events.

The amount of data currently available to the scientific community to develop monitoring strategies is very limited, as data acquisition can be costly. The present research therefore analyses approaches for developing predictive models capable of answering the demands of the industrial environment, from the design and execution of process experiments to the creation of models with acceptable results. ML techniques that could be of great applicability in machining are explored by analysing and comparing different sensor data sources. This gives a more comprehensive vision of each the effectiveness of each sensor for different monitoring purposes.

The manufacturing process which we take as our focus is drilling. The drilling process is a widely employed machining operation and one of the most demanding operations in terms of chip removal processes. It is also one of the most critical steps in a component production chain since it is performed, together with other finishing operations, in the final stages of the manufacturing process. A failure generated during drilling can spoil or lead to the premature deterioration of the desired component.

There is thus a clear need to optimise the drilling operation, increase the accuracy of the machined parts, and reduce costs. Given the specifications to be met by the machined part, improved monitoring and control of processes is also essential. Through the use of the proper data analysis tools, the virtualisation and control of operations becomes a reality, and steps are being taken towards transforming the machine tool sector to a more automatic environment.

RESEARCH OBJECTIVES

To determine the predictive capacity of each of the sensors installed in a drilling machine and to find those variables that best adapt to certain characteristics of the cutting process, the following objectives have been defined:

General objective: Establish a methodology that working on parameters such as acoustic emission, cutting forces, vibrations, and those provided by the machine allows discriminating tool condition, surface roughness and material damage that would have occurred in the drilling operation to create data-driven predictive models for timely decision-making.

Specific objectives:

- Design and development of an experimental set-up to perform drilling tests collecting the sufficient quantity of signals and physical measurable parameters.
 - Establish the drilling experiments to be carried out.
 - Set up the different sensors and design the system for simultaneous acquisition of the internal machine signals and the installed sensors.
 - Perform detailed measurements of tool condition, surface roughness and material damage.
- Obtain reliable signal features to find robust relationships with those physical parameters measured in the laboratory.
 - Clean the signals to obtain the specific machining parts.
 - Use feature extraction techniques from acquired signals.
- Label unknown observations based on the signal features and the limited number of physical parameters measured during data acquisition.
 - Employ machine learning techniques to establish relationships between the physical parameters measured and their respective signal features at the measured observations.
 - From the relationships found, impute labels to the unknown observations.
- Apply ML algorithms to understand the features of the most representative signals for different monitoring objectives of the drilling process.
 - Employ machine learning algorithms on the collected signals to predict tool condition, surface roughness or material damage.
 - Perform statistical comparison of the results obtained with each of the signals and the algorithms used.

- Make a limited selection of physical sensors to detect tool condition, surface roughness and material damage errors that may have occurred during the drilling process.
 - Identify signal features with the best predictive capability for the physical parameters measured.
 - On the basis of the most suitable features, select the sensors that have the best predictive capability for the measured parameters.

This dissertation presents a data-driven process monitoring framework of drilling process. This framework is envisaged in four layers, as shown in Figure 1.3. In the machine layer, where the cutting takes place, several output parameters are generated, and these are then collected in the data acquisition layer. The output parameters are classified into two categories: industrial and scientific. Industrial parameters are physical parameters that are to be improved or controlled and are usually measured directly, stopping the cutting process. Scientific parameters on the other hand, are measured by sensors, and provide information about physical process behaviour. Therefore, the setup and data acquisition methodology was designed to be acquire the full range of drilling process variability. In the data preparation layer analysis of the raw data is carried out by processing, extracting features, and preparing sensor signals for the measured physical parameters or target variables. The target variables are the tool condition and aspects related to surface integrity (roughness and material damage). In the machine learning layer, the most relevant features related to the defined target variable are obtained. Once the most suitable signal features are identified, models are generated to make predictions about future data.

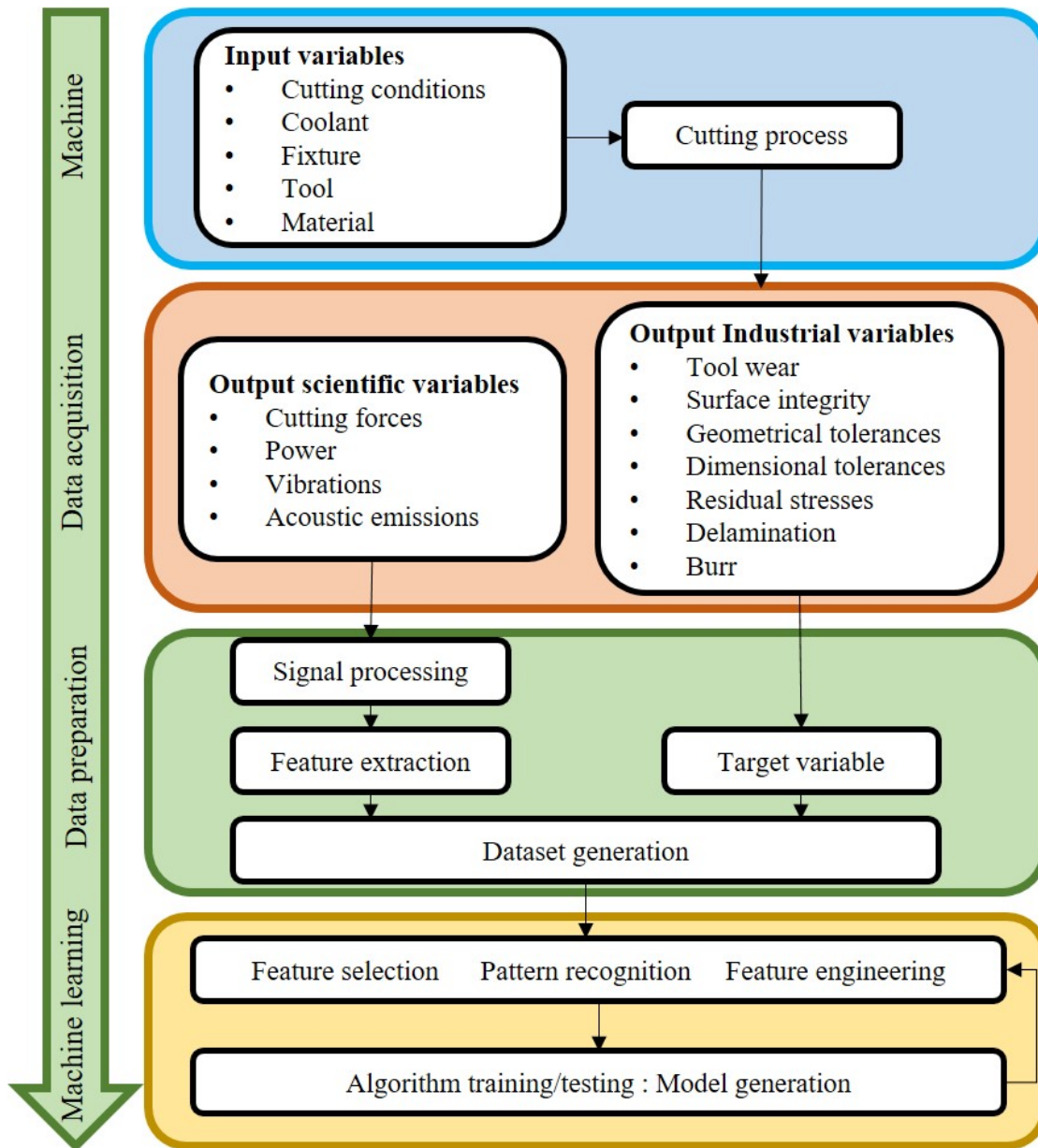


Figure 1.3 Process monitoring framework

DISSERTATION STRUCTURE

The dissertation contains 8 chapters represented in Figure 1.4 . The following are the summaries of each one of them.

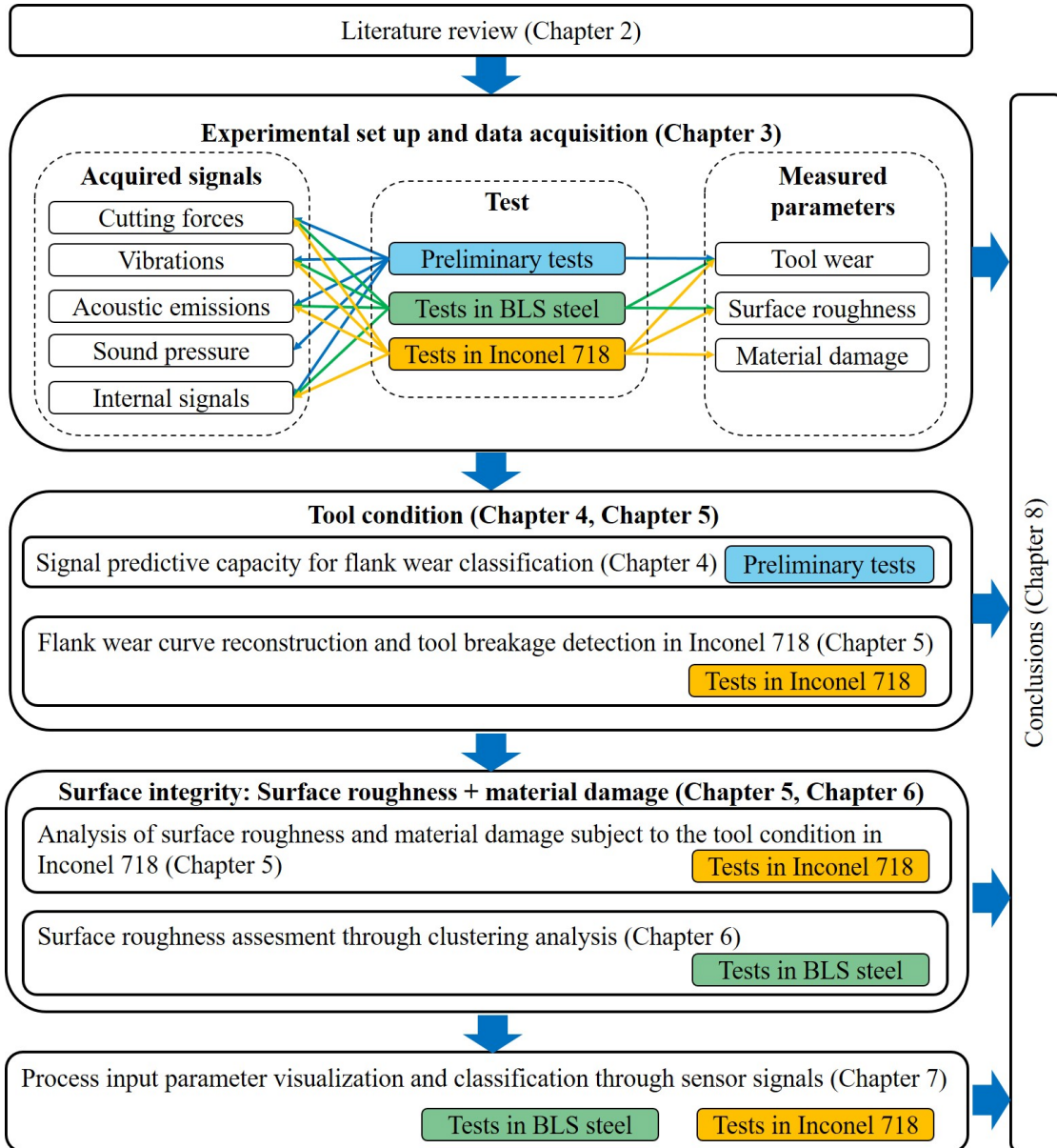


Figure 1.4 Research methodology

Chapter 2

Literature review: This chapter describes the fundamentals of cutting processes. It shows those scientific variables used to control or understand the desired industrial variables for process monitoring purposes. It also shows the most advanced applications in this area, making a more in depth analysis of drilling processes. This chapter aims to explore in depth the framework for monitoring cutting processes, particularly the drilling process.

Chapter 3

Drilling process data collection, processing and cleaning methodologies: This chapter focuses on the methodology employed for data collection during and after drilling operations, data cleaning and signals feature extraction. The collection of data is the key to the development of the thesis. The data collection was carried out in three test batches on BLS 35CrMo4 Low S Steel with two different tool geometries and on Inconel 718 with three tool geometries.

Chapter 4

Tool condition classification through signal performance evaluation in BLS 35CrMo4 Low S Steel material with previously wear induced tools: In this chapter, the predictive capacity of statistical features in the time domain of internal and external signals for the prediction of flank wear in drilling processes is analysed. To this end, a methodology based on automatic learning algorithms was developed. Secondly, once the most sensitive signals to flank wear were identified, algorithms with signals of a specific tool geometry were trained, and a model was obtained to predict the flank wear of a different tool geometry. The results show that the feed force (external) and the z-axis motor torque (internal) are able to perform the task adequately.

Chapter 5

Tool wear curve reconstruction in end-of-life tests and subsequent prediction of tool breakage in Inconel 718: This chapter presents the results obtained in drilling process monitoring carried out on Inconel 718. The main objective was to evaluate the capacity of each acquisition source to reconstruct the flank wear curve and, subsequently, the tool breakage detection. The methodology used to analyse the data makes it possible to have a comparative analysis of each of these sources potential for tool flank wear monitoring during the drilling process. The results indicate that cutting forces from internal signals or external signals can carry out this task accurately. At the same time of

data acquisition, detailed tool wear measurements were added. In addition, roughness and material damage were analysed to examine the effect of tool wear on these two characteristics of the machined component.

Chapter 6

Surface anomaly detection in BLS 35CrMo4 LoW S steel on a long machined time: When analysing the surface generated, inevitable variability in the roughness profiles obtained can be observed. External signal to the machine tool was acquired with sensors (cutting forces, vibrations and acoustic emissions) as well as internal signals (spindle power, spindle torque in the Z-axis, spindle current and positions, speeds, accelerations and jerk of the tool tip in the three axes of the machine). The hierarchical clustering of the process external and internal signals statistical features was compared with clusters obtained using roughness parameters. Results show that clusters appear using signals positively related to the roughness parameters obtained from the measured profiles, confirming a mapping between the acquired signals during the machining process and the roughness profile parameters.

Chapter 7

Influence of tool geometry, material and cutting conditions in sensor signals: dimensionality reduction and data analysis: The input parameters of a cutting process are fundamental for the creation of predictive models of the process. Systems must be able to detect and identify changes in the input parameters and adapt the predictions to the demands of the moment. This chapter question is to what extent changes in input parameters can be interpreted in the signal features acquired during the drilling process. Thus, discriminate the input parameter used in the proposed process window. Two techniques of dimensionality reduction and visualisation were used; PCA and tSNE.

Chapter 8

Conclusions and future development: The general conclusions and future developments of the research work are presented.

Chapter 9

Contributions: The scientific contributions made during the development of the thesis are mentioned, as well as journal articles, attended conferences and open-access datasets.

LITERATURE REVIEW

This chapter aims to present the basic principles of the cutting process, define the variables of interest in industrial environments and describe which signals are used by the scientific community to explain these industrial key features. Finally, a review of industrial applications and different works carried out up to date regarding the monitoring of cutting processes based on ML, especially drilling are shown.

2.1 MACHINING

Machining is defined as an industrial process in which a piece of material is shaped by removing unwanted material (Schmitz and Smith, 2009). The geometrical specifications of a component are produced by the relative movements of the tool and the workpiece. These processes are a fundamental production branch of the automotive, railway, naval, aviation, appliances and construction sectors. All these sectors require innovative manufacturing processes for the development of new products with improved quality and durability properties and, at the same time, reduce the production cost. Monitoring and control of the cutting processes are essential to achieve customer specifications.

The cutting process can be presented as a set of input elements and output elements, as shown in Figure 2.1. The input parameters are physical components and quantitative parameters that define the process behaviour. Two concepts define the output of the process, the industrial parameters and scientific parameters. Industrial parameters are those which are desired to control or improve (surface roughness, tool life-cost, material damage, etc.) because they define the characteristics of the component and scientific parameters (cutting forces, vibrations, acoustic emissions, spindle power, etc.) which are used to understand the cutting process.

Although almost all machining operations are performed in three dimensions, many investigations are simplified to two dimensions to understand some of the complexities of this process. Thus, this chapter will introduce the cutting process in 2D (Orthogonal cutting), where the basic principles (chip formation process, cutting forces and heat generation) are explained. The cutting process in 3D will then be presented, starting with the turning process and followed by the drilling process.

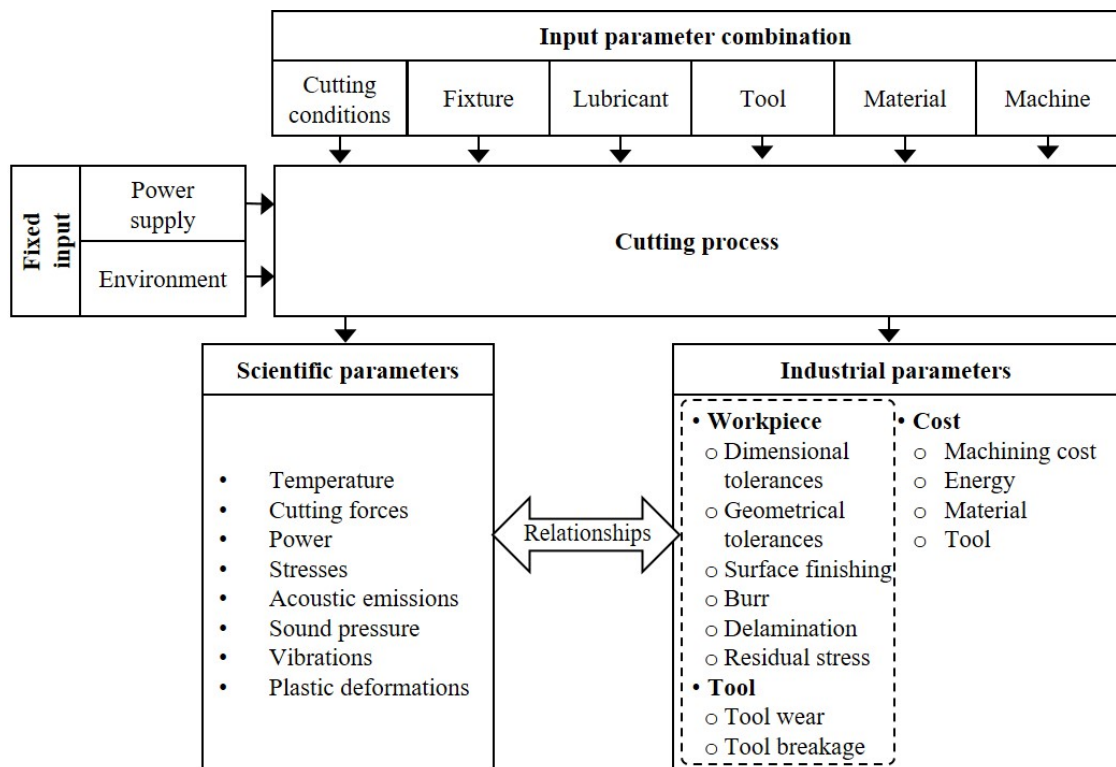


Figure 2.1 Input/output parameters of a cutting process

2.1.1.1 Orthogonal cutting

The most popular simplification for the cutting process analysis is the orthogonal cutting system since it reduces the complications derived from the most advanced tool geometry (El-Hofy, 2019).

The orthogonal cutting consists of sliding a wedge-shaped tool with a straight cutting edge relative to the working material where a layer of metal of a given thickness (h) is removed to form the chip.

Figure 2.2 shows the basic principles of the orthogonal cutting process. The workpiece moves against the cutting tools at the cutting speed (V_c). The thickness of the material to be removed is known as the uncut chip thickness (h), and it is expressed in (mm).

The tool geometry is defined by a series of surfaces oriented by angles. The surfaces and angles defining a basic tool geometry for 2D are the following:

Rake face: It is the surface over which the chip slides.

Flank face: It is the surface in front of the generated surface.

Cutting edge: It is edge generated by the intersection of the rake and flank faces.

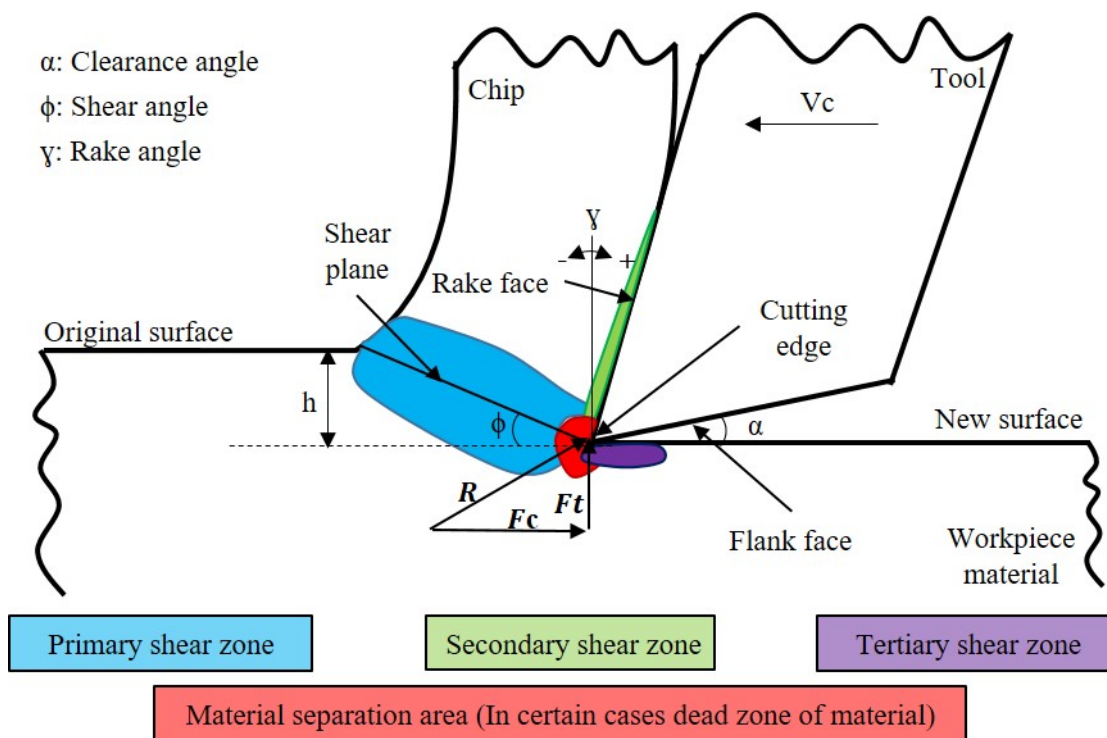


Figure 2.2 Orthogonal cutting process, shear zones and cutting conditions

Rake angle (γ): This angle defines the orientation of the rake surface and has a remarkable influence on the chip formation process. As its value becomes more positive, cutting forces will be decreased.

Clearance angle (α): This angle, also known as relief angle, defines the orientation of the flank face. This angle should be positive to prevent the flank from rubbing against the material.

Shear angle (Φ): The angle made by the shear plane and the new surface.

When the workpiece material faces the cutting tool, it is deformed plastically in three zones/areas (Kilicaslan, 2009).

Primary shear zone is the area where, according to some research works, the major amount of plastic strain is produced to form the chip.

Secondary shear zone: It is the area where the chip is in contact with the rake surface. Apart from the plastic deformation, friction between the tool and chip is produced, generating a relevant temperature area.

Tertiary shear zone: is the area where the fresh surface generated rubs against the tool. If the tool is fresh, the amount of plastic work and friction generated is low. However, if the tool is worn, this area becomes very relevant, generating high temperatures, which promotes microstructure damage and affects the surface integrity condition.

Dead zone of material: In some cases, due to the high mechanical loads, a dead zone is created over the cutting edge Built-Up Edge (BUE), which modifies the geometry of the cutting tool generating the chip formation process.

Cutting forces need to be applied by the cutting tools to generate the chip and the plastic work. Two forces are defined in the orthogonal cutting:

F_c: Cutting force acting on cutting velocity direction.

F_t: Thrust force acting on thrust direction.

The resultant cutting force (**R**), is decomposed into two components **F_t** and **F_c**. **F_c** is the force acting in the direction of the cutting speed (V_c) and is the amount of force required to move the cutting tool through a given distance. The force **F_t** does no work, but both components produce a deflection in the workpiece and in the cutting tool during operation.

The plastics deformation produced at high strain rates generates a large amount of heat distributed in the chip, tool and workpiece. The heat generated by friction in the secondary zone adds an additional heat source to the process.

According to the working condition and workpiece material, different types of chips morphologies can be formed. Figure 2.3 shows four basic shapes that can take the chip; these are examples of the types of chips that can be formed in machining processes.

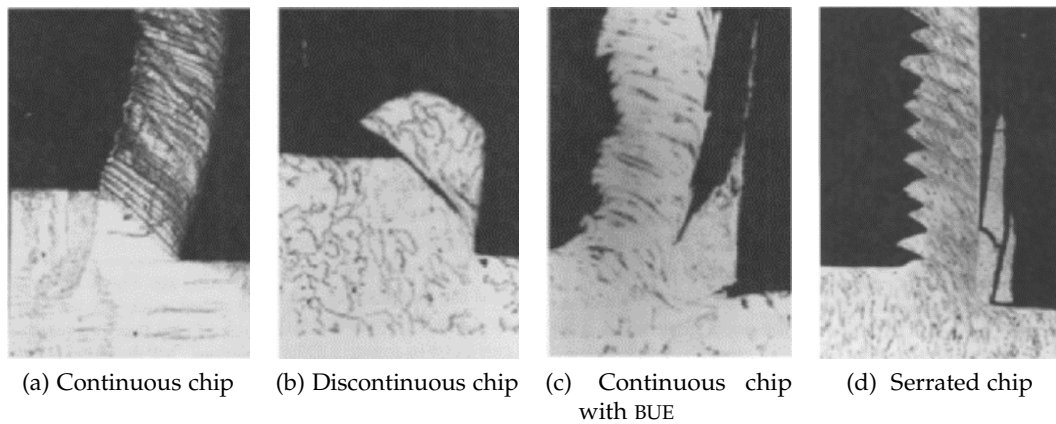


Figure 2.3 Different chip formations (Childs et al., 2000)

Continuous chip is formed by cutting ductile metals at high cutting speeds, while the discontinuous chip is generated at low cutting speeds in the same type of materials or fragile materials. The continuous chip with BUE is created when low carbon steels are machined with high-speed steel tools under low cutting speeds. Finally, the serrated chip is the frequent chip morphology during high-speed machining of ductile materials (Kilicaslan, 2009).

2.1.2 Three-dimensional cutting processes (3D)

The most common machining operations are turning, milling and drilling. This section aims to explain the metal cutting process in 3D, specifically the drilling process. For this purpose, the turning process is described first since its nature is the most straightforward process mentioned above. Next, the drilling process is explained.

2.1.2.1 Turning

Turning is the most common process in cutting processes by chip removal (Figure 2.4). It is a process in which cylindrical parts are produced using a single-edged cutting tool. In this operation, the workpiece is the one that rotates, keeping the tool stationary. The cutting conditions to consider in this operation are the cutting speed V_c ($\text{m} \cdot \text{min}^{-1}$), the depth of cut a_p (mm) and feed rate f ($\text{mm} \cdot \text{rev}^{-1}$), which is the one that makes the difference compared to the simplified cutting process explained in the previous section. V_c is considered the linear velocity of the periphery of the part in contact with the tool material, so the cutting speed varies along the cutting edge.

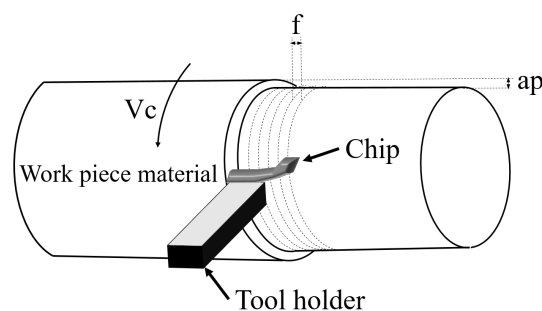


Figure 2.4 Turning process and variables related to cutting conditions

The turning process involves different operations: external turning, internal turning, longitudinal turning, profiling, or facing. Each operation affects the choice of tool and cutting conditions. Besides, each of the operations may be either roughing or finishing, affecting the initial decisions for turning.

2.1.2.2 Drilling

Drilling is the most productive method for machining holes (Figure 2.5). Before starting a drilling process, the most critical parameters to consider are diameter, depth and quality (tolerance, surface finish and straightness). These parameters influence the choice of the tool to be used. In this process, it is the tool that carries out the cutting movements. In this case, the cutting conditions to take into account are the cutting speed (V_c) and the feed per revolution (f).

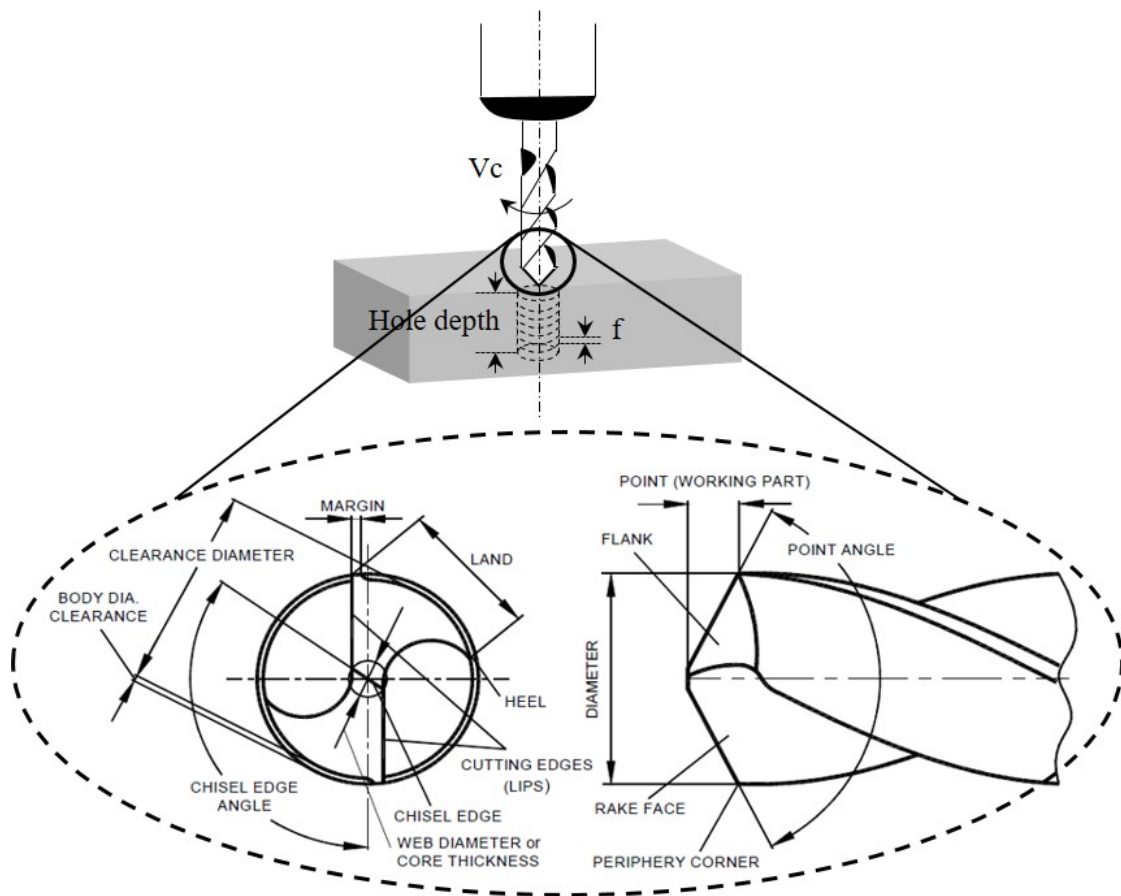


Figure 2.5 Drilling operation and related variables (Adapted from: Astakhov (2010))

This operation usually occurs in the final stages of the production of an element, followed by some finishing operations, boring, reaming, etc.; therefore, it is one of the most critical manufacturing operations. According to Jindal (2012), an almost finished part can be destroyed during the drilling process, causing a higher cost or leaving the production line inactive for a while. Thus, it is an operation in which the control and optimization of the process itself are of great importance to avoid problems and detect the different errors in time.

The cutting speed varies along the cutting edge in drilling operations, with 0 at the centre and $V_{c_{max}}$ at the drill periphery. For this reason, the mechanisms of generation of the chip will be very different according to which it is the chip entry zone (Zhao et al., 2015).

A twist drill usually has two cutting edges that cut the material as in a turning process, while in the centre of the drill, the material is removed by extrusion by the chisel edge (Swinburne, 2005) which is the main responsible for geometrical errors and high thrust forces (Smith, 2008). Figure 2.5 shows a drill geometry with two cutting edges.

An unlimited number of cutting tool designs can be found for drilling processes. Each one of them designed to eliminate specific problems that occur during the cutting process: increase the useful life of the tool, facilitate chip evacuation, reduce cutting forces by increasing the penetration rate, improve the roughness of the machined part, improve dimensional tolerances, etc.

Figure 2.6 represents a schematic view for cutting force generation in drilling process. Assuming that the drill geometry is perfectly symmetrical, the cutting lips produce most of the torque with a small part contributed through the chisel edge while rotating against the resistance opposed by the workpiece material. The thrust force results from several parameters involved in the drilling process: feed speed, hardness of the working material, and coolant presence on the cutting lips. The cutting lips must be of symmetrical length for the proper balancing of the cutting process, the chisel edge is the part that has the highest contribution to the thrust force, and finally, the edges of the drill bit, through friction, also contribute to the increase of the thrust force (Smith, 2008).

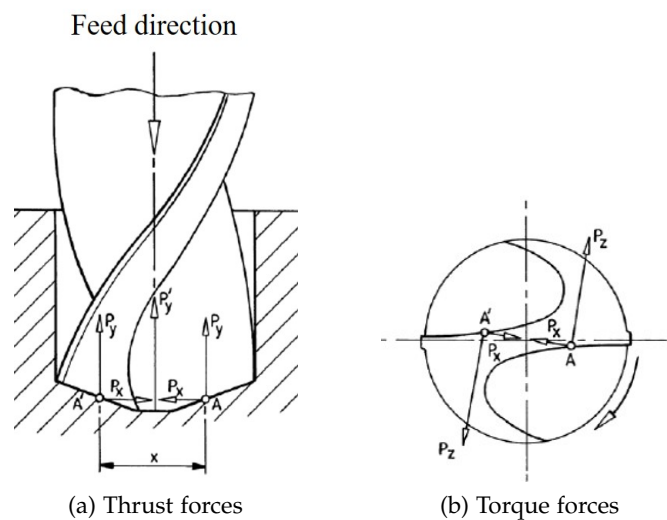


Figure 2.6 Compensation of cutting forces in drilling processes (Smith, 2008)

The thermal loads generated in drilling processes are essential as they affect the deformation process for chip generation, workpiece finishing conditions and tool wear. The distribution of the heat generated during drilling depends on the tool, workpiece and chip thermal properties. Cooling of the cutting zone allows for greater chip control and to reduce cutting temperatures during machining.

2.1.3 Industrial parameters to control

In cutting processes, surface integrity, dimensional deviations, and burr characteristics provide information about the machined component quality. All these parameters could be conditioned by tool wear, one of the major causes of faults in the machined part. In

this section, a literature review is made on works related to these characteristics of the machined part to identify the cutting process parameters that can have a relation with them.

2.1.3.1 *Tool wear*

During the machining processes, the thermomechanical loads reached in the cutting tool generate tool wear. This tool wear is responsible for some defects found in machined workpieces, such as bad surface integrity condition, burr formation and inadequate geometrical and dimensional tolerances. If the tool wear value is too high, sudden tool breakage may destroy the machined part. One of the industrial techniques to avoid premature tool failure or to guarantee a component surface integrity is to change the tool frequently (Arrazola et al., 2014). The use of this technique increases the manufacturing costs of specific components as well as paralysing the production process for a certain period. This is why it is necessary to create optimisation mechanisms that allow prolonging its useful life.

Tool wear mechanisms

Tool wear mechanisms can be mechanical, thermal or chemical and are defined as follows by Trent and Wright (2000):

Abrasion: This mechanism takes place at the moment when a hard particle slides over a softer surface. Therefore, it is a wear mechanism that depends on the composition of both the working material and the tool. If the workpiece material has harder particles than the tool, the wear is accelerated.

Diffusion: The wear created by this type of mechanism is due to the chemical affinity between two materials. The atoms of the tool material are displaced to the surface being machined due to high temperatures. At low cutting speeds, the crater wear formed by this mechanism occurs slowly. It depends on the high temperatures and the flow with which the material is removed from the working material surface.

Oxidation: Nitrogen plays an important role in protecting the tool from this mechanism, the areas where the temperature is high and are more exposed to oxygen are mostly affected by this problem.

Fatigue: Both (I) mechanical and (II) thermal fatigue are factors that affect tool life, and this mechanism can fracture the tool before other mechanisms become more visible. (I) Intermittent loads applied against the tool can cause the tool to fracture at the early stages of an operation. (II) Thermal fatigue causes small cracks in the tool due to shrinkage and expansion of the tool surface layers as the tool heats up during the cutting process and cools down between cutting operations. If there are a large number of cracks, the tool could fracture.

Adhesion: Also known as BUE. It is the adhesion of the chip to the cutting tool. Over time, the chip becomes unstable, taking with it pieces of the tool material. However, the BUE can sometimes protect the tool causing a positive effect on the process.

The wear mechanisms appear depending on the conditions in which the machining is being produced. Figure 2.7 shows the locations where the wear mechanisms occur and their relationship to the machining process conditions.

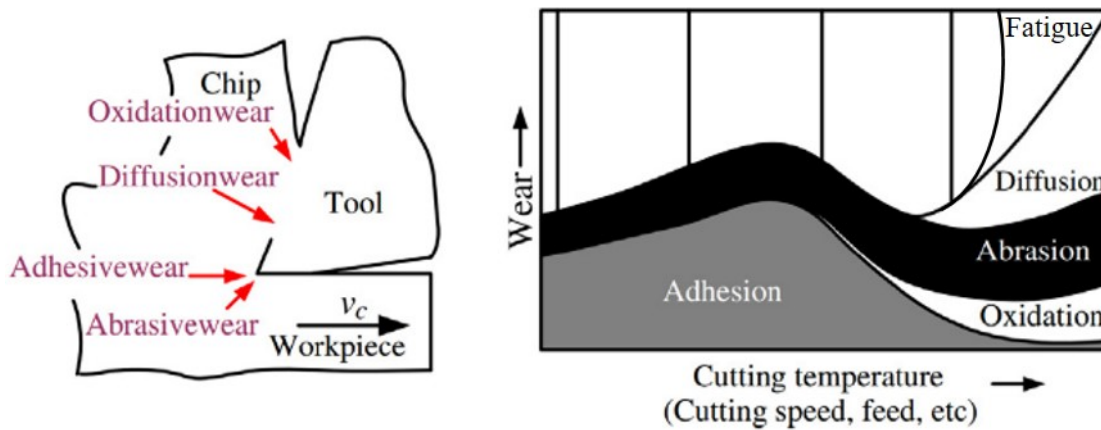


Figure 2.7 Wear mechanism in metal cutting (Adapted from: Gao et al. (2015))

The wear mechanisms are dependent on the cutting temperature. At low cutting temperatures, mechanisms such as adhesion BUE or abrasion are predominant. At high cutting temperatures, the material adhered parts become more unstable thanks to the material softening. However, other wear mechanisms such as diffusion and oxidation appear.

Types of tool wear

From the above mechanisms, different defects can occur on the surface of the tool faces. High temperatures, frictions or chemical affinity between the tool material and the workpiece material negatively affect the tool life. Figure 2.8 shows the main tool wear types.

Regarding the creation of monitoring systems, the most desired wear is flank wear, since it predominates in the early stages of cutting processes, as it has been observed in different works, (Eckstein et al., 2016; El-Wardany et al., 1996). In Khleif and Abdullah (2017) the flank wear is described according to ISO 8688:1989 (Tool-life testing in milling) and ISO 3685:1993 (Tool-life testing with single-point turning tools) as the loss of tool particles along the cutting edge, and it is classified into three categories:

- **Uniform flank wear:** wear maintains a constant width along the entire cutting edge.

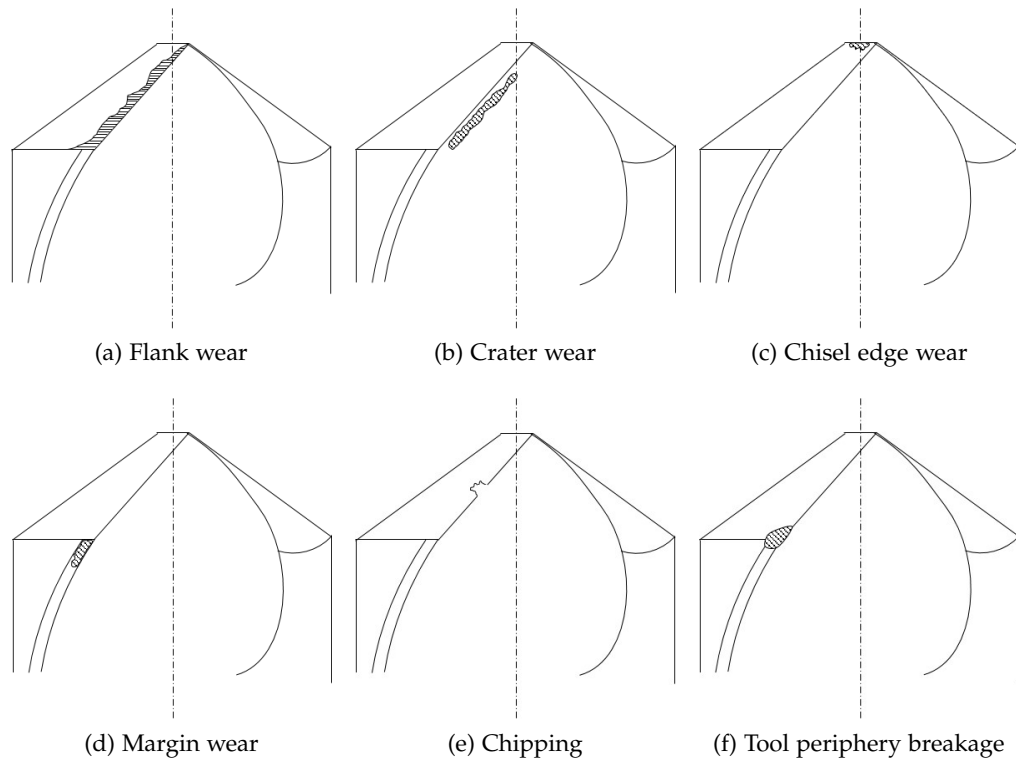


Figure 2.8 Types of drill wear

- **Irregular flank wear:** wear is at fixed points along the cutting edge.
- **Fixed location flank wear:** wear occurs at a fixed point on edge.

Figure 2.9 shows the flank V_b and margin wear W_m represented in a two cutting edge drill and the interaction between minor cutting edges and workpiece material. The flank wear measurement is an approximation of real wear since the average wear length is V_b . The $V_{b_{max}}$ is the maximum wear length found on the flank face, and it is measured perpendicular to the major cutting edge. Wear is accelerated with the cutting speed, so it is common for the tool to suffer more significant wear where the speed is maximum. However, the minor cutting edge is where the new surface of the machined material is generated. So this area is of great interest as far as drilling is concerned.

The tool geometry defines the aggressiveness with which the cut occurs; this is fundamental for less damage to the surface of the material. Sharman et al. (2008) studied the machinability of Inconel 718 with a curved edge drill with radius on the periphery and a straight edge drill with a sharp periphery showing that the first option results in longer tool life.

The coating protects the tool from the various wear mechanisms. Rahim and Sharif (2007) made a comparison between the TiAlN and supernitride coatings, concluding that the supernitride coating having a higher Al concentration protects the tool better when Ti-6Al-4V material is machined. Uzun and Kaplan (2017) made a comparison between

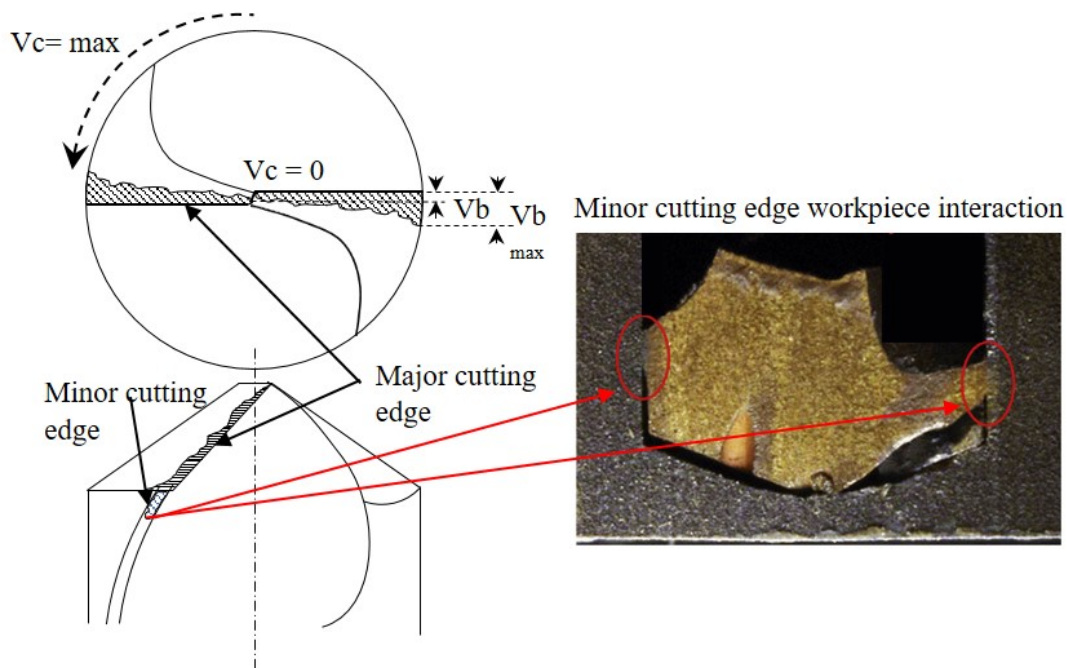


Figure 2.9 Flank and margin wear on drill bit according to cutting speed and drill minor cutting edge/material interaction areas (Adapted from: Kwong et al. (2009a))

plasma-nitride coated High Speed Steel (HSS) and uncoated HSS bits. Concluding that this type of coating increases the hardness of the drill bit extending its useful life.

Tool wear is subject to the cutting conditions used in the cutting process. At high cutting speeds, the tool useful life is reduced. Increasing the cutting speed, the temperatures generated during the cutting process increase, accelerating the erosion process. This causes the generation of low-quality holes (Rahim and Sharif, 2006; Jindal, 2012).

2.1.3.2 Surface integrity

The surface integrity (roughness, residual stresses, material damage, etc.) condition of a component will define its behaviour, aspects such as fatigue life, tribology or corrosion. According to Moussaoui et al. (2013), this characteristic of the machined component is defined based on three parameters:

Geometrical parameter: roughness

Mechanical parameter: residual stresses

Metallurgical parameter: microhardness and microstructure

Surface specifications will be different depending on the function of the machined component. Some components will have (I) mechanical functions, which will suffer mechanical loads. Others will have to fulfil (II) thermal functions, heat-resistant components with high thermal conductivity. Components with (III) tribological functions

interact with other components. Components with (IV) optical functions with high light reflection capacity or (V) flow functions that will be in contact with fluids.

Surface roughness

Surface roughness is a widely used indicator of technical requirements of a component (Benardos and Vosniakos, 2003). Gadelmawla et al. (2002) defined the parameters that can be calculated from roughness profiles. They explained measures of amplitude, space and hybrids. Some of these parameters need to be adapted to the user requirements, depending on the component application.

As reported by Bhushan (2000), among the different ways of measuring roughness (contact roughness meter, optical profilometry, atomic force microscopes, etc.), they showed that optical profilers are non-contact and can produce three-dimensional profiles rapidly and without any lateral motion between the optical spindle and the sample. Three-dimensional roughness height data can be processed to calculate a variety of amplitude and spatial functions and parameters. 3D measurements can provide more information than 2D measurements. In industrial environments, 3D measurement practice can be difficult, given the constraints of the environment (dust or vibrations from the environment) and the preparation of the area to be measured. Table 2.1 shows the parameters that can be obtained from roughness profiles.

Table 2.1 Roughness parameters (Source: ISO 4287-1997 (1998))

Name	Description	Unit
R_a	Average roughness of profile	μm
R_q	Root-Mean-Square roughness of profile	μm
R_t	Maximum peak to valley height of roughness profile	μm
R_z	Mean peak to valley height of roughness profile	μm
R_{max}	Maximum peak to valley height of roughness profile within a sampling length	μm
R_p	Maximum peak height of roughness profile	μm
R_v	Maximum valley height of roughness profile	μm
R_c	Mean height of profile irregularities of roughness profile	μm
R_{sm}	Mean spacing of profile irregularities of roughness profile	μm
R_{sk}	Skewness of roughness profile	
R_{ku}	Kurtosis of roughness profile	
R_dq	Root-Mean-Square slope of roughness profile	
R_t/R_z	Extreme Scratch/Peak value of roughness profile, ($>= 1$), higher values represent larger scratches/peaks	

Among all these parameters, the most used one is R_a . However, this parameter alone does not explain the entire roughness profile. Most of the common machining processes produce surfaces with asymmetric (non-Gaussian) profiles. Turning and shaping generate rough surfaces with positive skewness. Whereas grinding, honing and milling generate rough surfaces with negative skewness and high kurtosis, a surface with negative skewness always has a larger contact area ratio (Zhang et al., 2014). In the case of drilling processes, Wern et al. (1993) showed that this process generates a negative skewness and high kurtosis. Figure 2.10 a) shows two different

roughness profiles with the same Ra and different skewness, Figure 2.10 b) shows two different roughness profiles with the same Ra and different kurtosis. Amor et al. (2015) showed that profiles with the same level of roughness Ra and different degree of skewness Rsk do not have the same contact properties. They also showed that the negative skewness and the lower value of Ra are advisable to achieve a high normal contact stiffness. The profile with positive skewness shows a smaller support area. However, the negative skewness profile can lead to fracture propagation and can hurt a component fatigue life. Thus, it is important to consider more than one parameter among those obtained from the roughness profile to reference the requirements to be fulfilled by the machined component. The kurtosis value Rku indicates the uniformity of peaks along with the measured roughness profile. This value provides information about lubrication retention problems on in-service components or wear on industrial components caused by random peaks on the machined surface (Smith, 2008).

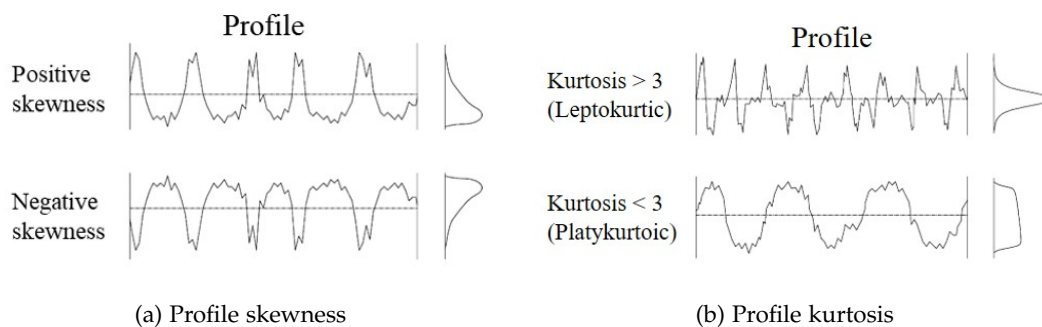


Figure 2.10 Surface roughness profiles with same Ra parameter a) different skewness distributions b) different kurtosis distributions (Adapted from: Gadelmawla et al. (2002))

Rahim and Sharif (2006) investigated the effect of cutting speed on the tool and surface integrity when drilling two different titanium alloys. They showed that a worse roughness is achieved at low cutting speeds, but the tool life is extended. On the contrary, at high cutting speeds, the tool wear is accelerated, but a better roughness is obtained. They suggest that this effect could be due to the increase in temperature of the cutting area which leads to a modification of the separation mechanisms of the material.

In the aeronautical industry, a finishing operation is necessary to meet the requirements for the assembly of components in many cases. Eckstein et al. (2016) analysed the drilling of holes on Inconel 718 using both the roughing process (drilling) and the finishing process (reaming). The roughness tends to be similar in both cases obtaining better results in the finishing process. The roughness improves in the early stages in both processes, and it is suggested that this tendency is due to the rounding effect of the cutting edges. Zhao et al. (2015) compared the roughness of holes made by drilling and helical milling (Figure 2.11), concluding that drilling resulted in a better roughness.

According to Benardos and Vosniakos (2003) the roughness could be influenced by the workpiece properties: hardness, diameter, length. The cutting tool properties: nose

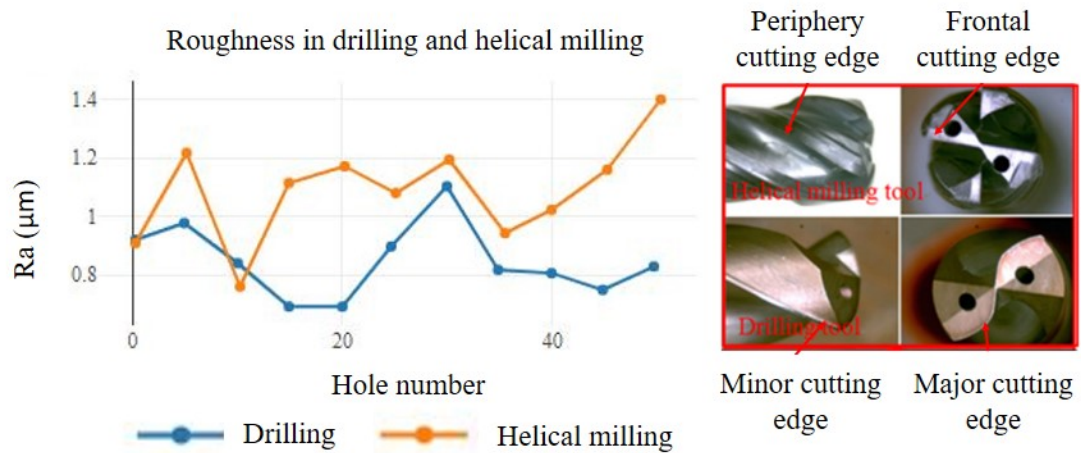


Figure 2.11 Surface roughness in drilling and helical milling (Adapted from: Zhao et al. (2015))

radius, tool material, tool shape. Machining parameters: process kinematics, tool angle, step-over, depth of cut, feed rate, cutting speed, and the machine itself and cutting phenomena involved in the process like vibrations, accelerations, chip formation and friction in the cutting zone affect the roughness profile.

At first instance, it seems that the feed is the most influential parameter in the machined part roughness. The most used parameters to characterize the surface roughness are Ra , Rz and Rt . These parameters only explain the amplitude details of the roughness profile. As we have already seen, the parameter Ra can adopt the same values independently of the shape of the profile. Therefore several statistical parameters concerning the roughness profile are needed to evaluate a machined surface.

In drilling, roughness is more complicated than in other processes. When deepening in the hole, the tool and generated chip both exert rubbing on the machined part. Therefore, the roughness profile could be altered from the machined roughness profile to the obtained roughness profile.

Residual stresses

As reported by Kudryavtsev (2008) residual stresses in a structural material or component are those stresses that exist in the object without applying any service or other external loads. Residual stress could be caused by localised yielding of the material because of a sharp notch or specific surface treatments like shot peening or surface hardening.

Residual stresses are introduced into the machined parts in manufacturing processes by plastic deformations or metallurgical deformations (Smith, 2008). This influences both the fatigue strength and the fracture strength of the machined component, including corrosion resistance (Lu, 2002). Tensile stresses (positive stresses) tend to reduce component fatigue life, while compressive stresses (negative stresses) tend to increase

this characteristic as it was observed by Zhao et al. (2015). Therefore to increase the fatigue strength of a component, compressive stresses are of major interest.

König et al. (1993) analysed the residual stresses in a turning process, Figure 2.12 shows the distribution of the residual stresses they obtained in their research. It can be seen that tensile residual stresses do not appear in the surface layer until machining has been carried out for a certain period. Thus, these results confirm that the tensile residual stresses are affected by the tool wear V_b .

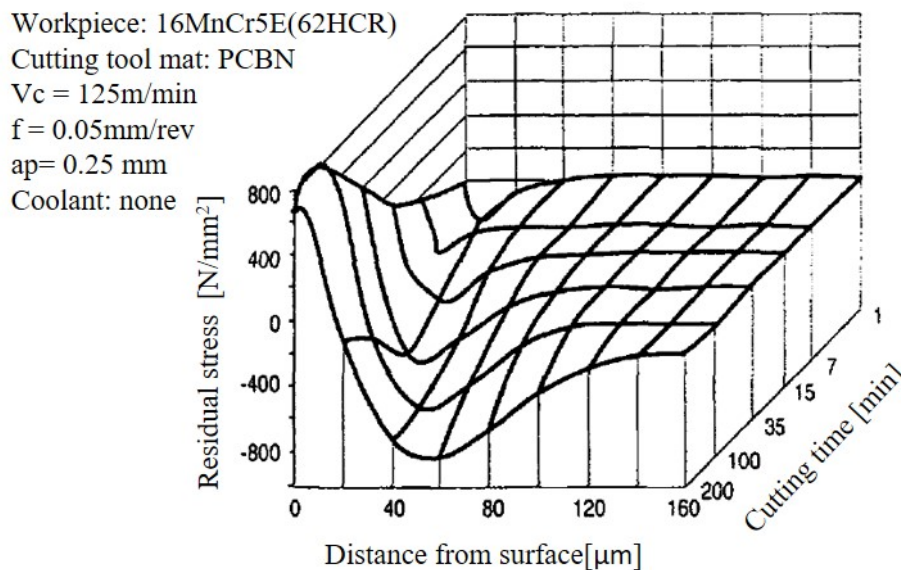
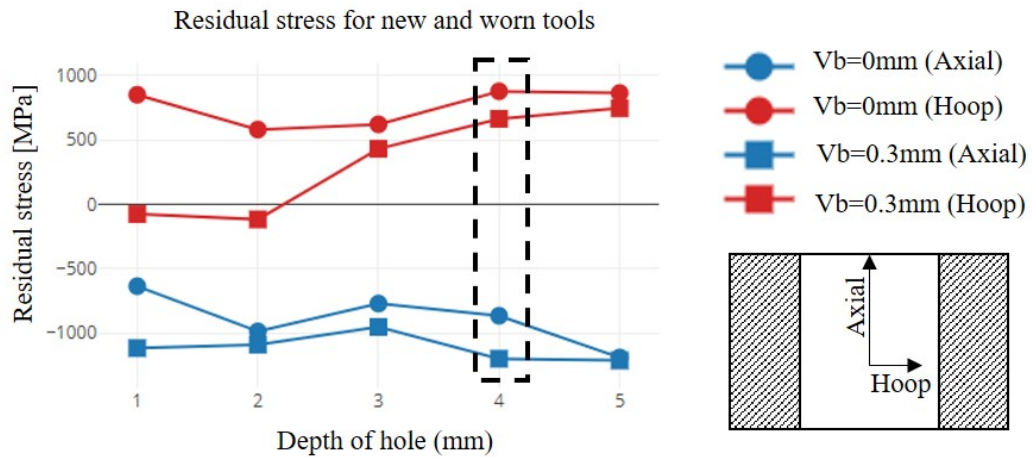


Figure 2.12 Residual stresses in turning (Adapted from: König et al. (1993))

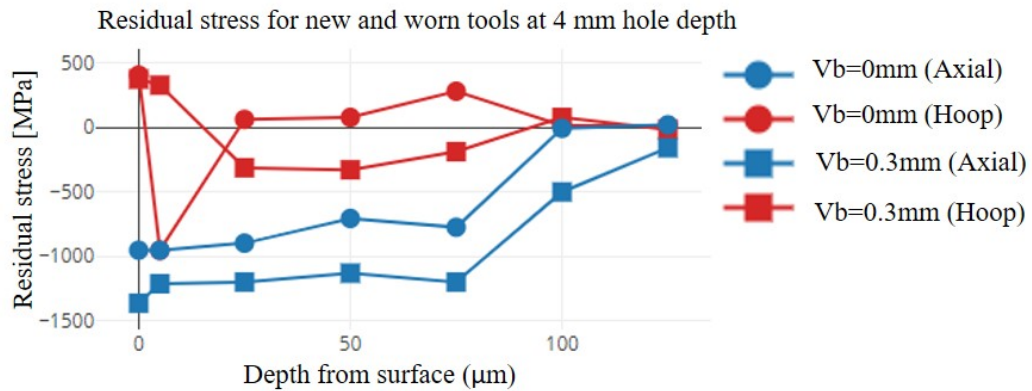
Kwong et al. (2009a) measured residual stresses in drilling process of RR1000 alloy for new and worn tools along the hole depth (Figure 2.13 a). They showed compressive residual stresses in axial direction while in hoop direction the trend was mainly tensile. When the tool is worn, compressive residual stresses were observed at the entrance of the hole due to the friction generated by the interaction of the worn minor cutting edge and the workpiece material. In other work made by Kwong et al. (2009b) the residual stress profile measured at 4mm hole depth was observed (Figure 2.13 b)), showing that in the hoop direction at the surface there are tensile stresses becoming compressive as it deepens into the posterior layers.

Micro-hardness and micro-structure

The main defects found in the machined microstructure are feed marks, chip redeposition on the machined surface, grain deformation, particle plucking and particle redeposition. These particles can cause dragging and tearing (Ulutan and Ozel, 2011).



(a) Residual stress through hole depth ($f = 0.1\text{mm/rev}$, $n = 1061 - 1592\text{rpm}$) (Adapted from: Kwong et al. (2009a))



(b) Residual stresses at 4mm hole depth ($MRR \approx 10000\text{mm}^3/\text{min}$, $\varnothing = 1.1\text{mm}$) (Adapted from: Kwong et al. (2009b))

Figure 2.13 Residual stress profile along depth of hole and at 4mm subsurface residual stresses

Figure 2.14 shows examples of material damage with the white layer or plastic deformations found by Zhao et al. (2015) in drilling and helical milling. When the tool is worn, the white layer of the surface is discontinuous. The increase of friction between the flank and the workpiece material causes the temperature to increase, breaking the white layer.

According to Herbert et al. (2012), the characteristics of the deformed layers found during drilling are somewhat different from other processes. This is probably due to increased contact between the workpiece surface and the worn major and minor cutting edges, which resulted in the removal/fracture of the white layer as the drill advances into the workpiece. Formation of the white layer during drilling can be removed if the process is followed by plunge milling.

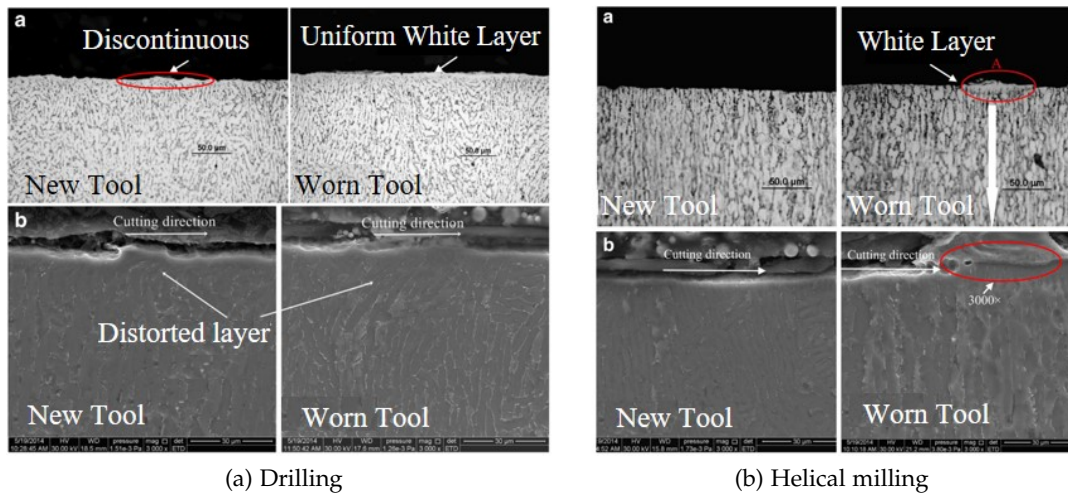


Figure 2.14 Example of micro-structural damage a) Drilling operation b) Helical milling finishing operation (Adapted from: Zhao et al. (2015))

Thakur and Gangopadhyay (2016) revealed that alloy 720Li and RR1000 having smaller grain size, higher yield strength and ultimate tensile strength than waspalloy and alloy 718 demonstrated higher thickness of Severe Plastic Deformation (SPD) white layer during abusive drilling as shown in Figure 2.15. Moreover, the same layer for alloy 720Li and RR1000 also exhibited delamination and cracks near the free surface and at the interface between layer and bulk material due to more pronounced thermomechanical loading. The white layer can also be specified and evaluated based on cutting parameters, cutting environment, type of tools and tool wear. The hard and brittle nature of this widely deformed region contributes to fatigue failure of the machined component in a given operating environment. Therefore, the study of how to minimise the thickness of this deformed region is of great importance.

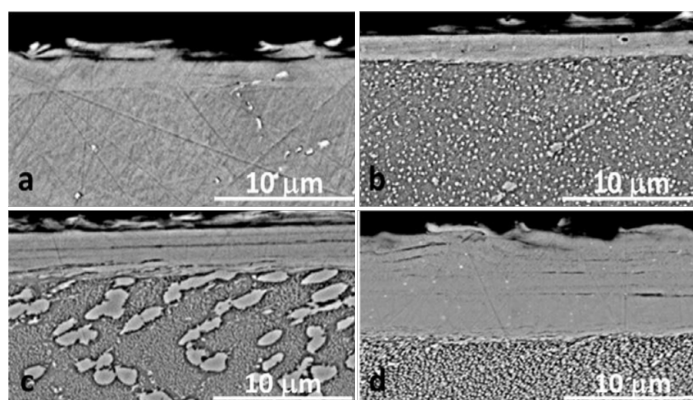


Figure 2.15 SEM close view of the severe plastic deformation layers produced by abusive drilling (V_c of 35 m/min, f of 0.12 mm/rev, dry environment) of a) Alloy 718, b) Waspalloy, c) Alloy 720Li, d) and RR1000 (Thakur and Gangopadhyay, 2016)

Sharman et al. (2008) analysed the deformed layer of the material with different tool geometries in drilling processes on Inconel 718. They showed that there is no significant increase in the deformed layer despite the different tool wear patterns. The depth of the deformed layer with each tool geometry obtained in this study can be seen in Figure 2.16. They did not expect these results. However, they said that the cutting action of minor cutting edges could significantly influence the material damage since they have closer contact with the generated surface.

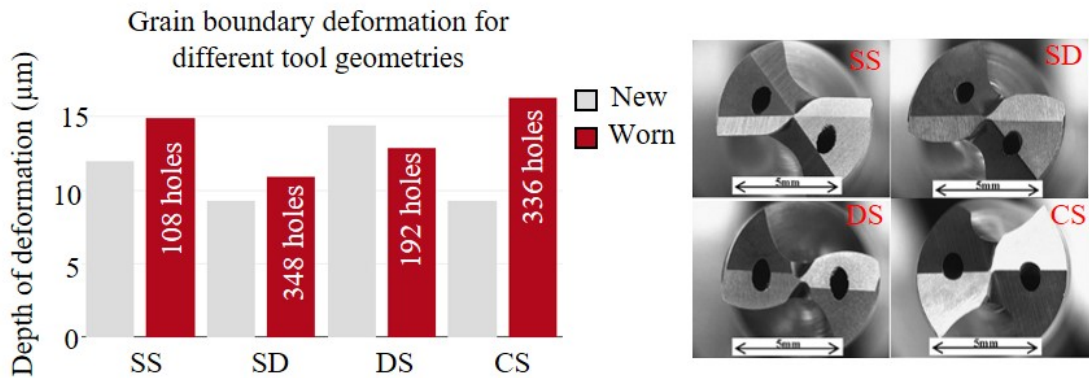


Figure 2.16 Grain boundary deformation in drilling process for Inconel 718 with different tool geometries, $V_c = 25\text{m/min}$, $f = 0.1\text{mm/rev}$ (Adapted from: Sharman et al. (2008))

Zhao et al. (2015) observed how in drilling operations, the micro-hardness decreases concerning the raw material at the hole entrance because of the thermal softening. As the tool advances, the micro-hardness increases again, decreasing at the hole exit to values equal to the bulk material. In contrast with the helical milling, they obtain a maximum in the micro-hardness at the hole entrance to decrease until the exit. The same phenomenon has been observed in both cases for worn and new tools.

As stated by Thakur and Gangopadhyay (2016) workpiece hardening phenomena can be effectively captured by progressively measuring micro-hardness at various depths below the machined surface. The results indicate that the machined surface hardness gradually approaches its bulk value as distance increases away from the machined surface. Alloy 720Li and RR1000 showed a higher value of nano-hardness along with the deformed layer than those for waspalloy and alloy 718. Variation of work hardening of different materials is shown in Figure 2.17.

2.1.3.3 Burr

Some of the cutting processes do not generate well-finished edges on machined parts. Irregular edges, raised surfaces known as burring, can appear (Lee and Dornfeld, 2005).

The formation of burrs in drilling processes is a problem for the machined component durability and the assembly with other parts. Therefore, second operations are necessary

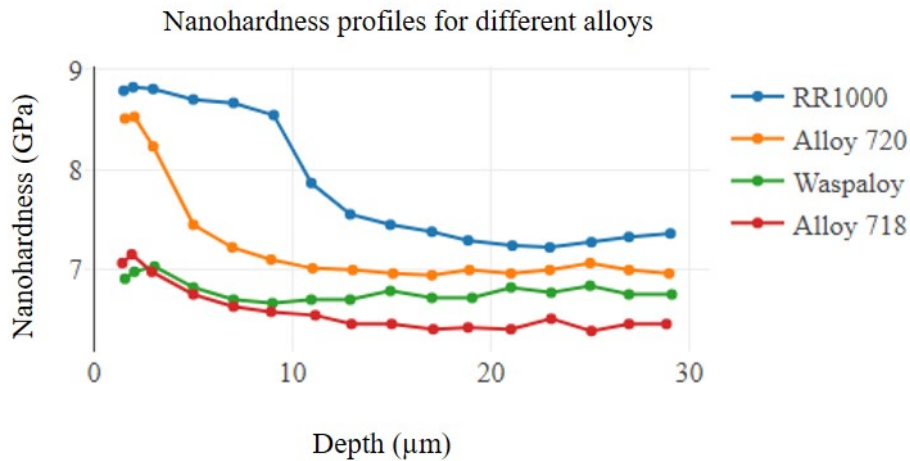


Figure 2.17 Nano-hardness profiles under the abusive drilling (V_c of 35 m/min, f of 0.12 mm/rev, dry environment) of the four Ni-based superalloys (Adapted from: Thakur and Gangopadhyay (2016))

to remove the burrs formed during the process. Figure 2.18 shows some cases of burr in the drilling process.

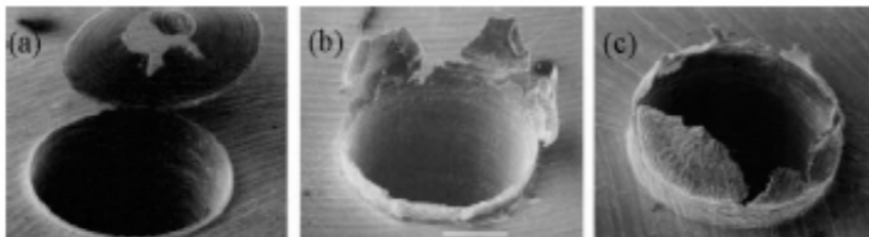


Figure 2.18 Types of burr in drilling process (Min et al., 2001)

The appearance of burrs in drilling processes is formed by the tool geometry, properties of the working material and cutting conditions. The most controllable parameters are the cutting conditions. Specifically, the feed per revolution and the cutting speed (Abdelhafeez et al., 2015).

Karnik and Gaitonde (2008) showed that there is a non-linear relationship between cutting conditions and burr height. The interaction between different parameters and the height of the burr is different from the width of the burr. The feed is the most significant parameter in burr formation, while the cutting speed is negligible in terms of burr height. The lower the clearance angle, the lower the height and width of the burr.

In micro milling processes, deburring can be a problem due to the machined part small size. Conventional deburring processes cannot be easily applied. Besides, the deburring process can introduce dimensional errors and could destroy the machined part. Lee and Dornfeld (2005) studied the effect of cutting conditions when machining

holes in micro-milling processes observing that burr height is related to tool wear and feed per revolution. Zhao et al. (2015) showed that finishing a hole with helical milling produces less burr than conventional drilling.

2.1.3.4 Dimensional and geometrical tolerances

In specific industries, the precision with which a hole is machined is essential in assembly requirements. This is why a proper selection of cutting conditions must be made before a part is machined. Incorrect selection of cutting conditions can lead to rougher surfaces and dimensional errors, which can cause a deviation from the correct operation of the assembled part.

Various factors such as diameter deviation, hole tapering, angularity or location errors can be analysed (Dechow, 1998). Dimensional errors can also be measured in terms of circularity and cylindricity (Sultan et al., 2015). Each of these aspects is measured depending on the application and requirements of the machined part.

Circularity is a 2D dimension measured in any portion transversal to the axis of the hole, which indicates whether a hole in that position meets previously established tolerances. This measure can be applied to any circular body such as spheres, cones, etc. On the other hand, cylindricity is a 3D dimension, and it can be only be applied to cylindrical shapes. This measure indicates if the whole hole respects a previously established tolerance along the whole axis (Sultan et al., 2015). Figure 2.19 shows the measurement of these dimensions graphically.

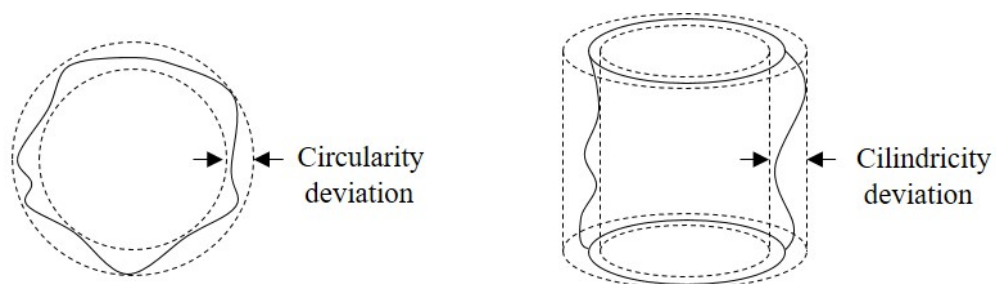


Figure 2.19 Graphic representation of geometrical tolerances (Adapted from: Souza et al. (2012))

Jindal (2012), Abdelhafeez et al. (2015), and Waqar et al. (2016) reported that the diameter of the hole is larger at the entrance than at the exit. This is because the tool is in continuous contact with the holes entry, and there is a displacement of the drill when it comes into contact with the working material. Both Abdelhafeez et al. (2015) and Waqar et al. (2016) found no linear relationship between the cutting conditions and the deviation of the hole diameter, so other factors affect this parameter as the vibrations, diameter of the tool, etc. On the contrary Sultan et al. (2015) registered that there is less deviation from the diameter at a low cutting speed. This is because the spindle vibrates less when the cutting speed is low.

Ranjan et al. (2020) analysed the roundness errors of various cutting conditions in a microdrilling process. They observed an increase in the mean roundness error subject to increasing cutting speed and increasing feed rate (Figure 2.20). They also showed that the roundness error is similar to vibration with respect to the drilled hole number.

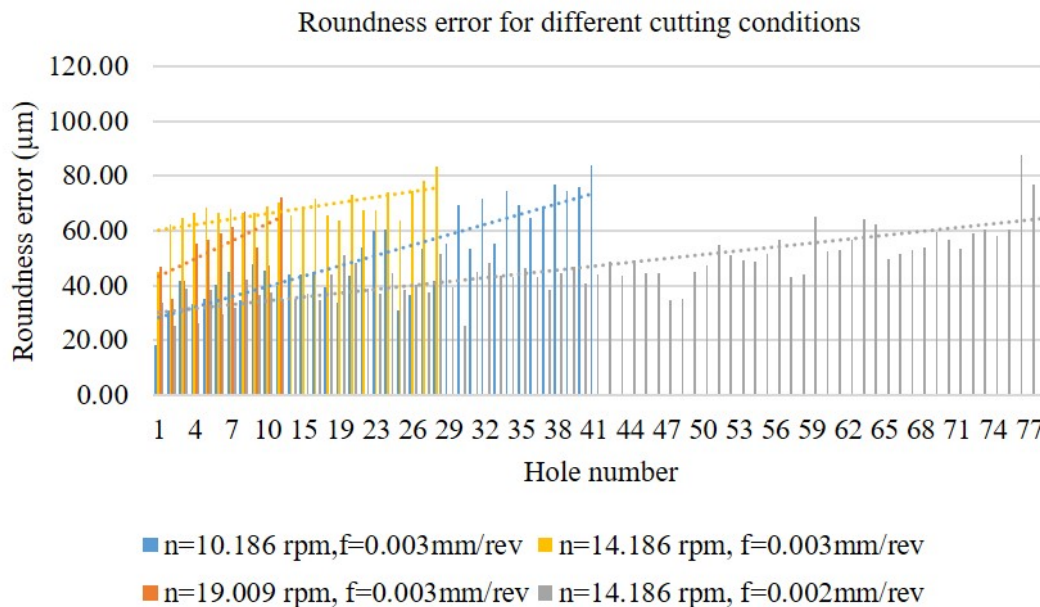


Figure 2.20 Roundness error for microdrilling at different cutting conditions (diameter=0.4mm) (Adapted from: Ranjan et al. (2020))

2.1.4 Cutting process modelling

The modelling allows to obtain a precise analysis in order to have a better control over the cutting process. Given the variety of physical phenomena involved in cutting processes (thermomechanical coupling, friction or material failure), there are several techniques for modelling and simulate cutting processes: analytical, experimental, finite element, mechanistic and data-driven modelling. This section presents the fundamentals of each of these methods and briefly discusses them.

Analytical modelling represents the system in terms of a set of mathematical equations that specify the parametric relationships and associated parameter values as a function of time, space and other system parameters. Most studies try to determine equations without any experimental work that can be used to look for relationships with other parameters, such as tool wear (Markopoulos, 2013). However, in the review made by Ehmann et al., 1997, it is stated that analytical models do not obtain accurate results because the model response depends on more variables than the analytical model takes into account. The cutting mechanism, the interaction between the tool

flank and the workpiece material and the interaction between the chip and the cutting tool are the main reasons.

Experimental methods seek to find relationships between the cutting parameters and the phenomena that occur during cutting processes. However, the physical phenomena are ignored, and the view of the dynamics of the process is lost. Although expressions have been found that relate the parameters involved in material removal to the phenomena, in most cases, these methods are not practical for many applications.

Mechanistic modelling, which is not purely analytical as it depends on coefficients obtained from experimental tests. It is a combination of analytical and experimental methods. They are based on understanding the behaviour of the components of a system. It aims to establish a mechanical relationship between inputs and outputs, and it is difficult to incorporate information from multiple spatial and temporal scales with precision. Once validated, can be used as a predictive tool where experiments are difficult or costly to perform. Mathematical methods introduce some numerical errors, and the determination of model coefficients can be a costly task.

Numerical simulation by the finite element method has proven to be a reliable alternative to analyse several metal forming operations. Plastic deformation takes place in small areas, and the temperature increase in the local area due to plastic deformation and friction induces softening and changes the material properties of the part in terms of strain rates and temperatures. Therefore, it is necessary to take the temperature rise into account in the calculations performed, which means that, in addition to the mechanical problem, a heat transfer problem must be treated in a simulated form, thus requiring a coupled analysis. In the finite element method, the basic principle is the replacement of a continuum by finite elements forming a mesh. This procedure is called discretisation. Each finite element is simpler in geometry and, therefore, easier to analyse than the whole structure. However, it needs high computational power to produce accurate results (Markopoulos, 2013).

Experience gained from machining processes, audio-visual observations and human intelligence have contributed to a better understanding of the cutting process. However, analytical, empirical, mechanistic, and finite element modelling have to simplify since accurate predictions require tedious trial-and-error processes and excessive computing power for validation. Thus, data-driven models have emerged as an alternative to the methods mentioned above. Figure 2.21 shows the difference between conventional process modelling methods and data-driven manufacturing.

In opposition to conventional modelling methods, data-driven is based on the data obtained from the cutting process, which is the key enabler to realise smart manufacturing. A model is trained to accurately predict the target in the limit of the input data provided for training without considering any physical parameters. These methods are characterised by modelling nonlinear and multidimensional problems with a fast response that makes them feasible for real-time monitoring. The disadvantages are (i) the large amount of data required for training and (ii) some algorithms are based on

the black box concept, which does not allow to understand the key variables that allow obtaining the output.

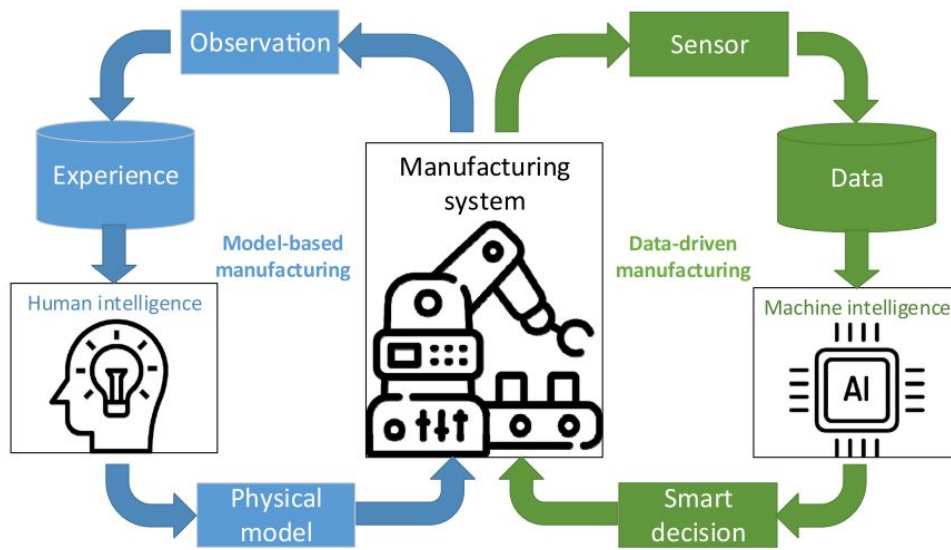


Figure 2.21 Model-based manufacturing and data-driven manufacturing (Xu et al., 2020)

2.2 PROCESS MONITORING

The monitoring of cutting processes is a fundamental branch to avoid problems during the production of components to achieve greater automation and reduce operating costs. Current approaches used in the industry exhibit disadvantages in their reliability due to process uncertainties. Therefore, the strategies employed by the scientific community are an alternative to the disadvantages present in the industry. This section first introduces industrial monitoring systems and then presents the framework developed within the scientific community to overcome the limitations of the strategies of industrial monitoring systems.

2.2.1 *Industrial monitoring systems*

There are several industrial products for tool condition monitoring, employing, most of them, the same methods like those presented by Jemielniak (1999). The monitoring strategies in the industry are based on fixing limits based on the acquired signal and triggering alarms if a new signal exceeds the established limits. Static limits can be of three types: (I) The limits can be established from the beginning by the user, (II) or they can be fixed by a signal acquired after one part machining with a new tool automatically, these first two are offered by most of the suppliers of tool wear monitoring systems. (III) In the case of using floating limits, the program resets the limits from one machined part to another. The option to use this type of limits only allows for Montronix (Montronix, n.d.) and Nordmann (Nordmann, n.d.) systems. (IV) Dynamic limits in which the system itself adapts the limits taking into account the fluctuations that could occur in a given signal are offered by Sandvik coroPlus system (Sandvik Coromant, n.d.). In Table 2.2 the sensors and monitoring strategies used by industrial systems can be consulted.

The Promicron spike technology uses a dedicated tool holder to measure forces and bending moment in the X and Y directions directly on the tool. In milling processes, polar coordinate displays are used to detect tool wear (Figure 2.22). The successive polar coordinate system is compared against the original one to see each of the leaves formed in the visualisation chart.

Fixed limits are set at N% above the learning curve and N% below, using various limits. For example, the recorded signal represents the 100%, the limit₁ is fixed at 200% while the limit₂ is fixed at 150%, finally the limit₃ is fixed at 50%. If the signal exceeds the limit₁ an alarm is triggered for tool change. If the signal exceeds the limit₂ indicate a worn tool. In the event that the curve falls below the lower limit prematurely (limit₃), an alarm will also be given to indicate a missing tool. Figure 2.23 shows an example of the fixed and part defined limits of the Montronix systems (Montronix, n.d.).

The floating limits are a type of fixed limit and are automatically reset to the next cycle based on the previous cycles, resetting the established limits. This allows detecting

Table 2.2 Sensor and monitoring strategies used by industrial tool condition monitoring systems

Suppliers	Sensors							Monitoring strategy		
	Cutting forces	Acoustic emissions	Accelerometer	Strain	Power	Displacement	Internal signals	Static limits	Dynamic limit	Floating limits
Promicron spike (Promicron, n.d.)	x							x		
Artis CTM (ARTIS, n.d.)		x	x		x		x	x		
Montronix (Montronix, n.d.)	x	x	x	x	x		x			x
Sandvik coroPlus (Sandvik Coromant, n.d.)	x	x	x		x		x	x	x	
Nordmann (Nordmann, n.d.)	x	x		x	x	x		x		x
Caron Eng. TMAC 3.0 (Caron, n.d.)			x	x	x			x		
WattPilote (Wattpilote, n.d.)			x		x			x		

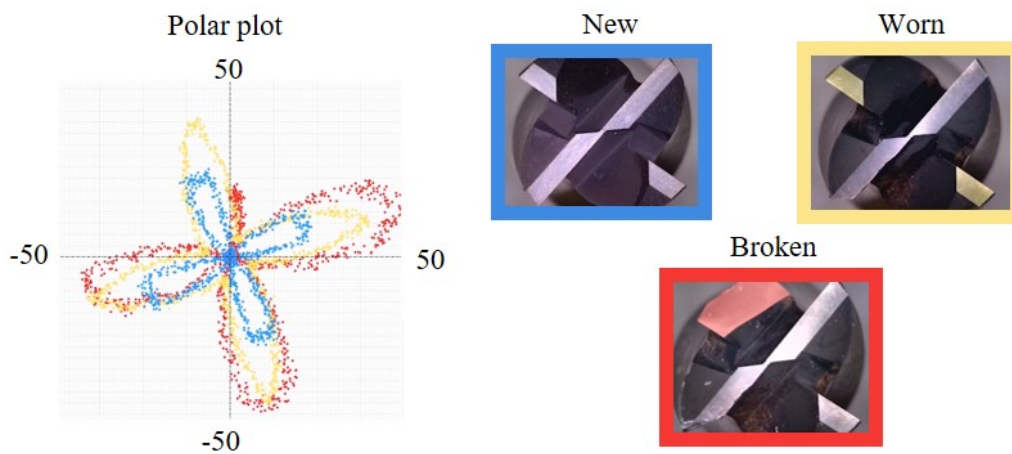
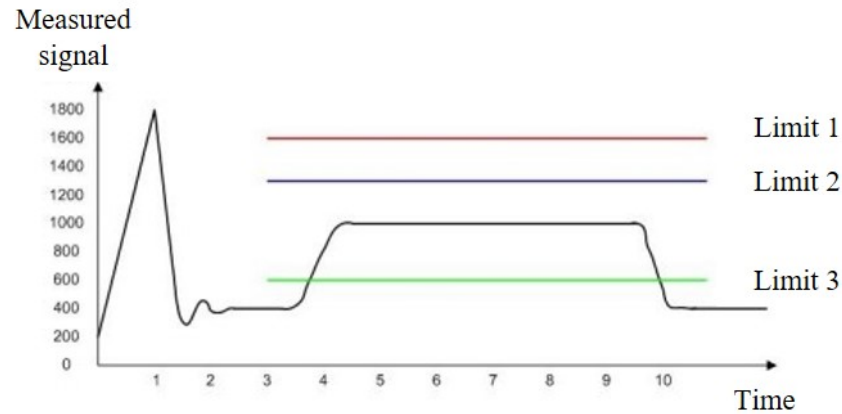
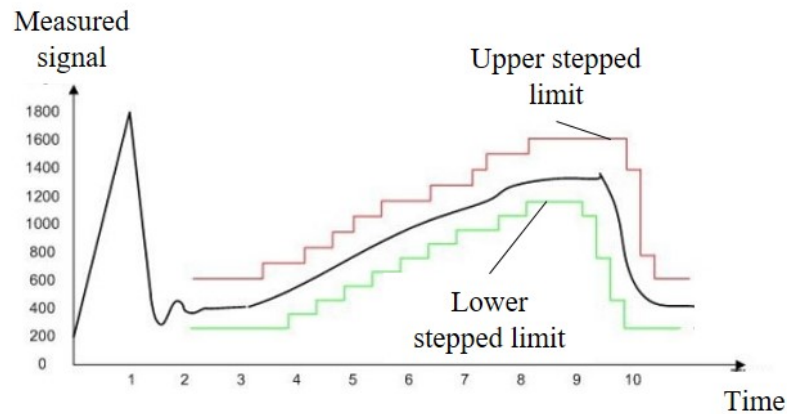


Figure 2.22 Spike system polar plot for milling process tool condition detection (Adapted from: Promicron (n.d.))

tool breakage without exceeding the limit of tool wear, e.g. in multispindle applications (Montronix, n.d.; Nordmann, n.d.). Figure 2.24 shows an example of Nordmann’s monitoring system in drilling. It shows an example of drill bit breakage detection in multi-spindle with 6 drill heads. The changes in measured value height due to the breakage of a single drill are smaller than the changes due to the wear of all drills. The sliding envelope limit (limit2) changes from workpiece to workpiece in height due to



(a) Fixed limit



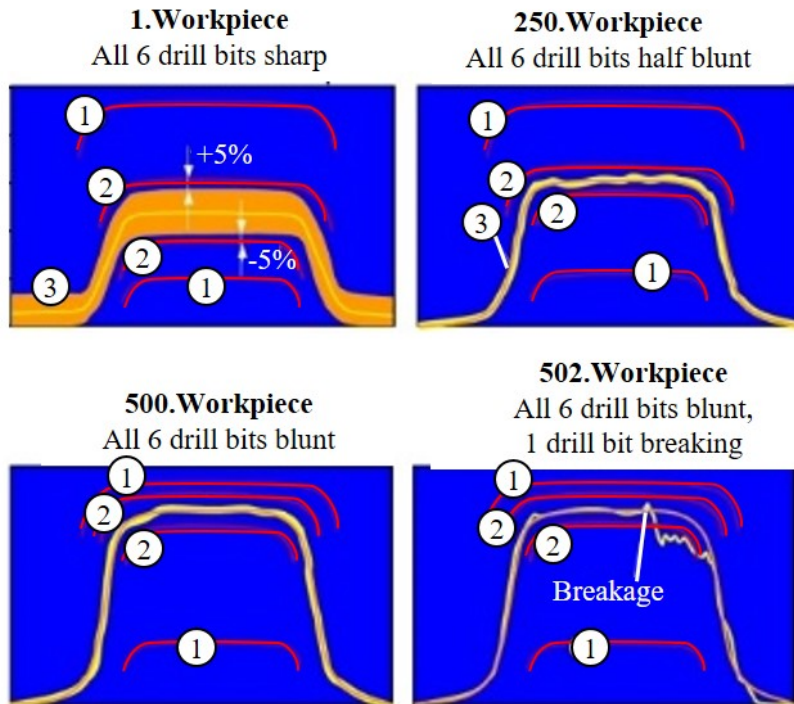
(b) Part defined limit

Figure 2.23 Static fixed limits and part defined limits on Montronix system (Adapted from: Montronix (n.d.))

tool wear. This allows a much smaller distance between the envelope (limit2) and the measuring curve.

The Sandvik Coroplus system offers dynamic limits (Figure 2.25) where they are basically to detect tool breakage. An adjustable relative distance is used, which accompanies the signal in a variable way. The signal only exceeds the limit with a rapid change (with adjustable sensitivity). This helps to detect breakage without the risk of setting the limits too low or too high.

The use of these techniques may be limited to tool diameters or cutting conditions employed during the cutting process because the cutting forces and the power generated can be very low. Among the suppliers of such systems, specified limits may range from $\varnothing = 0.1\text{mm}$ on the Nordmann (n.d.) systems, $\varnothing = 1\text{mm}$ on Wattpilote (n.d.) systems or $\varnothing < 3\text{mm}$ on Montronix (n.d.) systems.



- ① Fixed envelopes
- ② Sliding envelopes continually readjust from workpiece to workpiece
- ③ Averaged measurement curve (temporary enlarged after changing a new sharp tool)

Figure 2.24 Nordmann system floating limit monitoring strategy based on motor effective power measurement (Adapted from: Nordmann (n.d.))

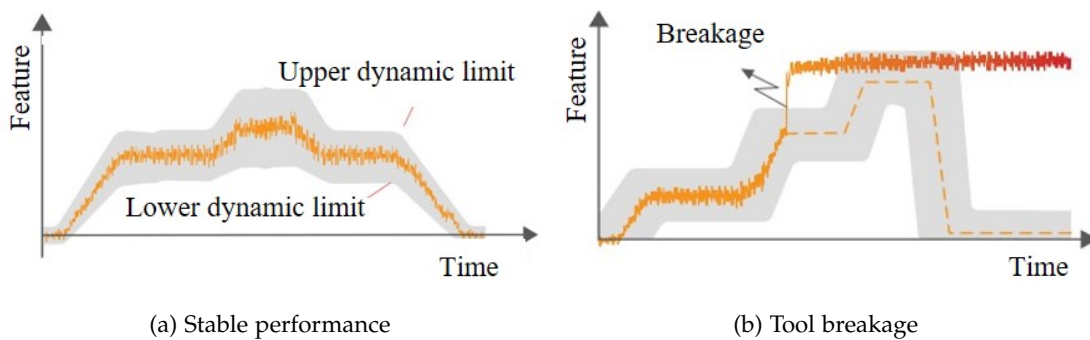


Figure 2.25 Sandvik coroplus dynamic limits for tool wear monitoring (Adapted from: Sandvik Coromant (n.d.))

Industrial tool monitoring systems have employed the same strategies for years. The system offered by Promicron spike is one of the most different from the rest because of the visualisation strategy and the smart tool holder it employs. Most of these systems lead to false positives due to process uncertainties, especially in flexible machining

processes, and therefore the reliability is questionable (O'Donnell et al., 2001). These systems often have close ranges of performance or require considerable training or set-up time to operate properly.

2.2.2 *A framework for intelligent process monitoring*

This section defines the most commonly used signals for monitoring cutting processes, to detect the premature tool breakage, tool wear and component finishing conditions, without disturbing the machining process and an easy and cost effective maintenance.

2.2.2.1 *Sensing techniques*

Sensor signals facilitate the detection of premature tool breakage, tool wear and component finishing conditions. This must be done without disturbing the machining process. Besides, maintenance should be easy and cost-effective. This section defines the most commonly used signals for monitoring cutting processes.

Cutting forces

The cutting force is mainly affected by cutting conditions (V_c , f , a_p), cutting tool geometry and workpiece material properties. According to Rahim and Sharif (2006) and Wei et al. (2016) the thrust force (F_z) decreases with increasing V_c . This happens as a result of increasing temperatures in the cutting process. As the cutting speed increases, the shear angle also increases, and the shear plane length decreases decreasing also the generated chip thickness. Reducing the shear plane length requires less cutting force to produce the necessary stress for the workpiece material deformation. As the process continues under specific cutting conditions, the micro-geometry of the tool is altered (tool wear), thus increasing the friction between the material and the flank face in the tertiary shear zone and increasing the thrust force (Arrazola et al., 2014).

Subramanian and Cook (1977) showed that the cutting forces are dependent on the hardness of the material. They concluded that cutting forces for tool wear monitoring is only possible if there is a tolerance of 5% in the hardness of the workpiece material. It is also known that the increase in temperature varies essentially in proportion to the hardness. They found a very rapid increase in flank wear at the end of tool life, accompanied by a significant increase in torque, thrust, and spindle power. They said that unless the workpiece hardness value is closely controlled, thrust force cannot be used as a meaningful variable for sensing drill wear. Similar arguments can be extended for the torque measurements also.

Brinksmeier (1990) showed that by installing a sensor to measure the cutting torque in the drill shank, the measurement is more sensitive to the cutting process due to the closeness to the cutting area. The spindle mass and the drive unit damping char-

acteristics are of minor importance. Therefore, accurate measurements were achieved and he showed that it is also possible to predict tool fracture by evaluating the higher frequency content of drill torque.

In Balsamo et al. (2016) the tool breakage was detected in the turning process from time domain features extracted from the three components (F_x, F_y, F_z) of the cutting forces, creating a robust system capable of detecting tool catastrophic failure in early stages of the turning process with the mean and variance of these signals.

Shah et al. (2010) showed the linear relationship between tool wear and F_z / M_z signals (Figure 2.26) recorded by an stationary dynamometer in drilling process. Despite the high relationship, they said that the acquisition of these signals is more expensive than other measurements due to sensor costs and geometrical limitations.

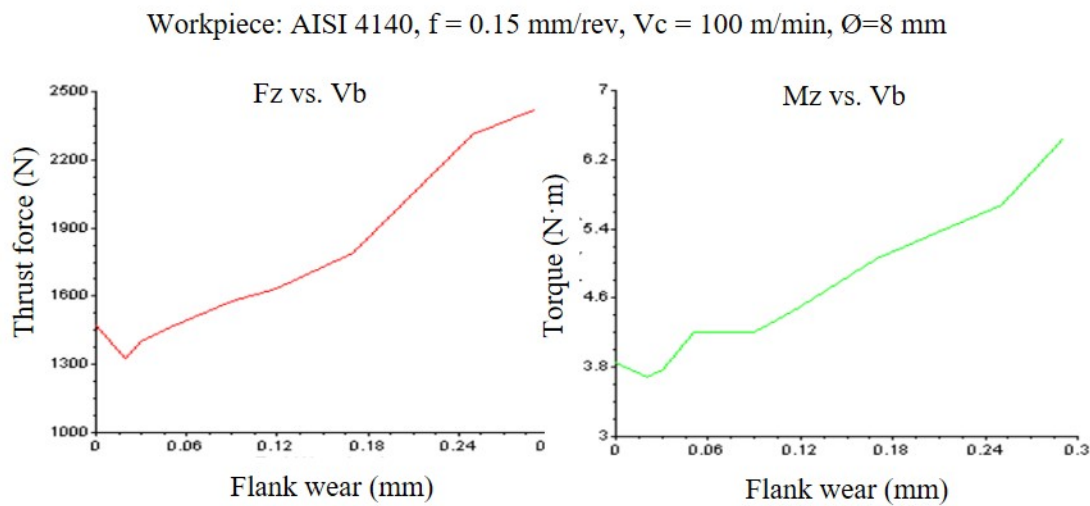


Figure 2.26 Thrust force and torque signal relationship with tool wear in drilling process (Adapted from: Shah et al. (2010))

To sum up, cutting forces are signals that are sensitive to the tool geometry. Therefore, when modifying the micro-geometry of the tool, the tool wear increases cutting forces. The assembly and adjustment of dynamometer sensors can be a problem in industrial production environments, so it is considered the use of other types of measurements. Problems like geometric constraints on three-axis dynamometers where the size of the part is restricted by the size of the dynamometer.

Acoustic emissions

Acoustic Emission (AE) are a way of identifying different phenomena in materials or structures in a wide range of frequency, from 100 to 900kHz. In general, this signal is used to locate micro-cracks, plastic deformations, corrosion, etc. In machining operations locating the source of the acoustic emissions is a difficult task. Therefore, the most common use is to detect transient signals (Grosse and Linzer, 2008). According

to Bhuiyan et al. (2016), this signal is based on two types of components, continuous and transient. The continuum is caused by the plastic deformations that take place in the cutting process. Transients are components of the signal caused sporadically by micro-cracking, corrosion, etc. AE is a wave of tension that travels through the material due to some sudden release of tensile energy. It can also be defined as the elastic energy released spontaneously during a local, dynamic and irreversible change in the microstructure of the material (Maia et al., 2015). Figure 2.27 shows the different types of sources that can have this type of signals in machining operations.

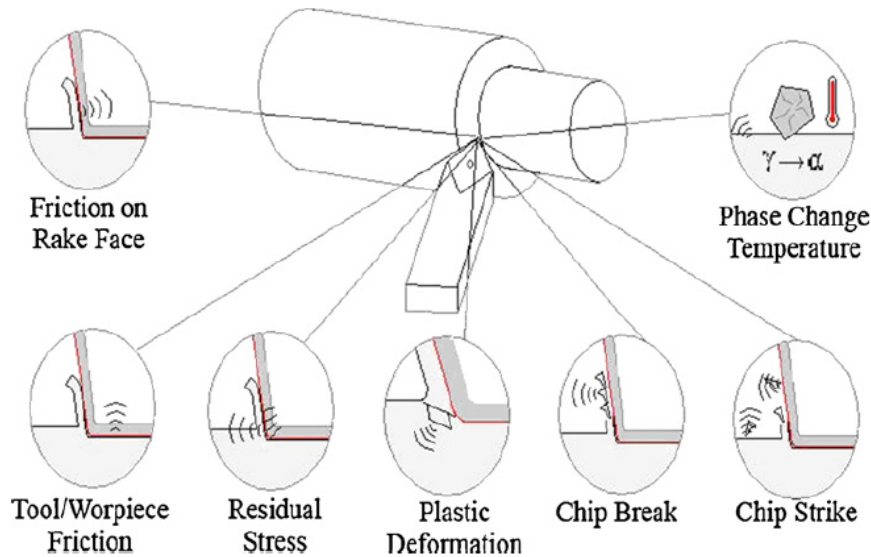


Figure 2.27 Acoustic emission sources in machining (Karpuschewski, 2001)

In Gómez et al. (2010) different features of acoustic emissions were studied to detect tool wear. It was proposed to use Mean Power (MP) as a parameter for monitoring. In this case, the Moving Average Mean Power (MAMP) as a function of Moving Variance Mean Power (MVMP) are the parameters that best represent tool conditions.

Patra (2011) used the wavelet packet method for the decomposition of acoustic emissions. They showed that the features extracted from the packages could be indicators for the prediction of tool wear. This work tries to extract wear sensitive features from the analysis of AE sensor signals at low-frequency range to avoid massive data storage and retrieval memory requirements for high-frequency analysis. The acquired AE signals were filtered through a bandpass (500 Hz - 50 kHz) digital filter.

One of the biggest challenges lies in obtaining the necessary information for the characterization of each of these phenomena in AE. Babatunde et al. (2017) said that observing the amplitude of the acoustic emissions is sufficient to monitor tool wear in milling finishing processes. The acoustic emission amplitude increases with tool wear due to increased friction between the flank and the working material. However, other phenomena could be detected with this signal, such as chipping, plucking, chip shape or surface drag. These phenomena arise more spontaneously, so advanced signal analysis

techniques and advanced knowledge in acoustic emissions are needed. Jemielniak and Kossakowska (2010) showed a good relationship between machining time and acoustic emissions after wavelet packet transform shown in Figure 2.28.

In a recent study Sun et al. (2020) proposed a tool breakage monitoring method based on acoustic emission signal for milling process based on 12 features (rise time, rms, absolute energy, average signal level, etc.) extracted from Short Time Fourier Transform (STFT) over the signal. The results are promising, although the authors comment that the limitations are the input conditions. The results are promising, but the authors comment that in case of changing the cutting conditions, the model has to be retrained.

To sum up, acoustic emissions seem to contain much information, and the problem lies in separating that information from the data and identifying what causes the transient energy outputs that occur when machining. Any impact on the material, the chip evacuation, and the simple fall of the chip on the workpiece material can cause transient signals that confuse the different phenomena.

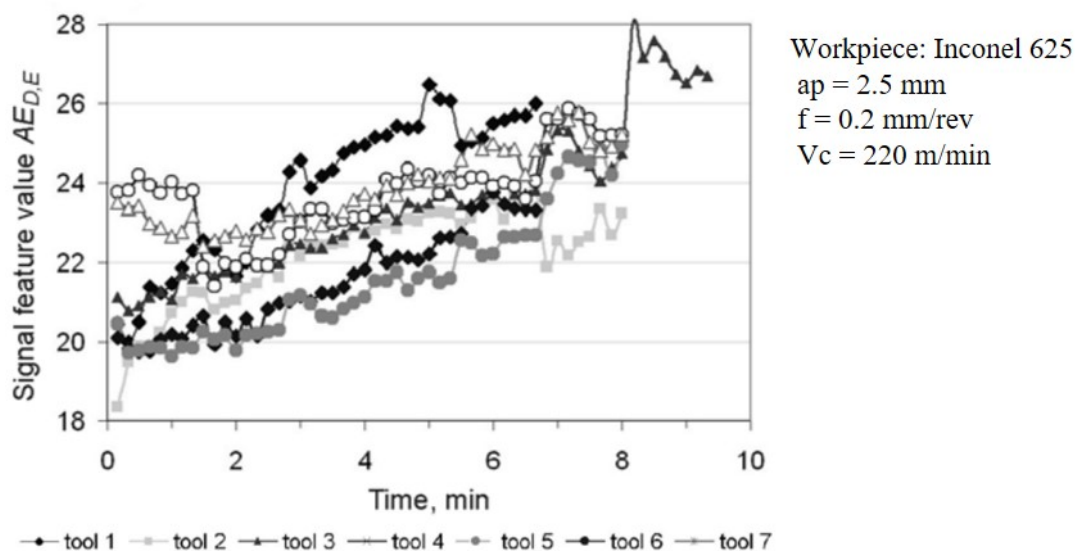


Figure 2.28 Evolution of energy of detail after Wavelet Packet Transform of acoustic emissions in turning operation for different repetitions (Adapted from: Jemielniak and Kossakowska (2010))

Sound pressure

This measurement technique does not require direct contact with any part involved in the process as it is the atmospheric variation transmitted through the air, the acquisition of such signals is quite simple as it can be recorded by a microphone and the frequency range varies from 0 to 20kHz. However, sound pressure-based monitoring has several drawbacks. Noise caused by systems outside the cutting process (other machining

centres, noise caused by the operator during the cutting process, etc.) can hurt the measurement of such signals, so the sensor positioning concerning the cutting area is essential for the correct measurement of the signal. Therefore the reduction of noises that can affect the measurements is of great importance (Huo et al., 2014).

Kothuru et al. (2017) proposed a monitoring method based on audible sound signals for tool wear prediction. They processed the signal every one second to obtain the Fourier transform and used a unique value extracted from the spectrum as a feature. They obtained good results, although the need for more sophisticated data processing methods is required to extract more robust features.

Rafezi et al. (2012) studied different features of sound pressure, and it was concluded that the Root Mean Square (RMS), peak and variance of the signal in the time domain are the most sensitive variables to tool wear. In particular, the signal value RMS has a strong relationship with the increase in tool flank wear. Also, the frequency domain of sound pressure was studied to determine which frequency bands tool wear affects. The analysis in the frequency domain was carried out in two stages. On the one hand, the Fourier transform was performed to determine which bands are affected by tool wear. The analysis was then performed based on the Wavelet Packet Transform (WPT) to extract the information from the frequency bands where tool wear affects.

Seemuang et al. (2016) tried to predict tool wear with the spindle audible sound signal in turning operation, concluding that the magnitude of spindle noise frequency spectrum and its cumulative value could be used as monitoring features in tool condition monitoring as shown in Figure 2.29.

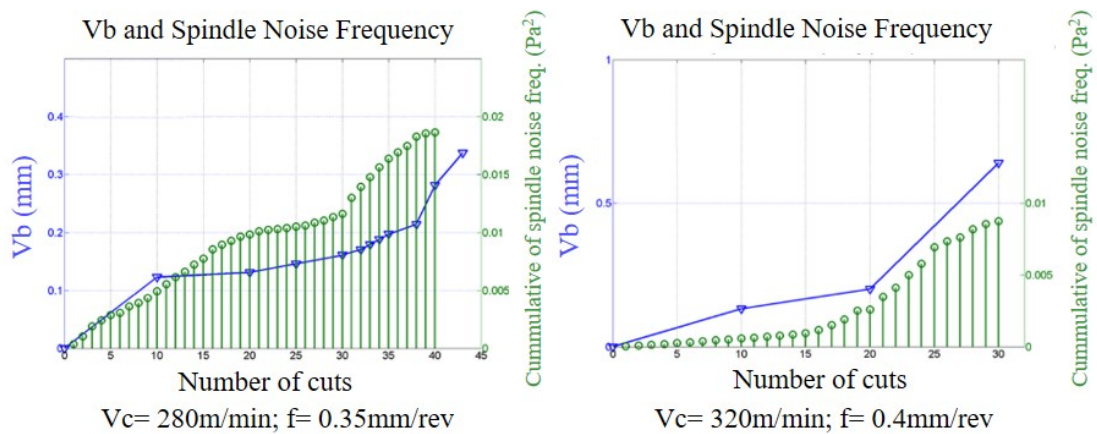


Figure 2.29 Magnitude of power spectrum of spindle noise and flank wear in turning process (Adapted from: Seemuang et al. (2016))

Although a relationship can be established between sound pressure features and characteristics of the cutting process, this practice is limited by the effect of the surrounding environment and is not as widespread as the measurement of the other signals presented in this section. The signal processing used is very dedicated to a

specific application, and the search for the most relevant features may change from application to application and requires expert knowledge to perform the task.

Vibrations

Vibrations are a widely used signal to monitor cutting processes. Vibrations arise from cyclic variations in dynamic cutting forces. The vibration signal arising from the metal cutting process is such that it incorporates aspects of free, forced, periodic and random types of vibration (Dimla Snr., 2000; Bhuiyan and Choudhury, 2014). The advantage of this method is the simplicity of deployment, which does not involve any alteration of the machine tool or workpiece fixture. The disadvantages are the dependence of the recorded signals on the workpiece material, cutting conditions, machine structure and clamping force (Heyns, 2007).

Harun et al. (2017) monitored the tool condition based on features obtained from triaxial accelerometer vibration signals by performing single spectrum analysis in the drilling process. Rmili et al. (2016) proposed a monitoring system for the three phases of tool wear (initial wear, steady-state or accelerated wear) in drilling processes. The analysis was carried out based on the average signal power, which seems to be a parameter sensitive to the various transitions suffered by a cutting tool. They concluded that it is a valid parameter for detecting the different tool wear phases. These three phases consist of a transition where the tool wear is accelerated, another transition where the wear remains stable and the last transition where the wear is accelerated until the tool breakage. A variation in amplitude of vibration signals caused due to variation in distance between accelerometer position and the hole was found by Nakandhrakumar et al. (2016) in the drilling process. This clarified that the position of the sensor affected the wear monitoring and increased uncertainty in prediction. They proposed a normalisation procedure to nullify the distance between the sensor and the drill hole on the received vibration signals.

El-Wardany et al. (1996) induced to the cutting tools a set of artificial defects to later machine and measure the vibrations produced with each one of them and identify each of the errors produced in the spectrum of the vibration signal. Subsequently, carrying out an end-of-life tool test, checks that the features identified in the signal spectrum correspond to those identified in the end-of-life test. Besides, a cepstrum analysis was performed to detect tool breakage. In the study, different holes were made until the tool breakage was reached, being able to detect the phenomena that are represented in the Table 2.3.

García Plaza and Núñez López (2017) concluded that it is possible to monitor the value Ra of the roughness using vibration signals and Singular Spectrum Analysis (SSA). They proved that SSA applied to the sum of the three vibration components acquired on the tool of a turning process allows faster predictions than applying the analysis to the individual components. To make an adequate prediction of the parameter Ra of

Table 2.3 Types of tool wear found in vibration signal spectrum (El-Wardany et al. (1996))

Hole N°	Phenomenon	Spectrum band
6	Plastic deformations and chisel edge wear	3.9 y 5.3 kHz
21	Corner wear	3.2 kHz
32	Margin wear	4.5 kHz
60	The magnitude of vibrations increases	2.4 a 5.8 kHz
128	Flank, chisel, corner and margin wear	Increasing amplitude in the interval 2.4 to 5.8 kHz
151	BUE (Built up edge) chisel edge	4.8 kHz
211	High amplitude peaks	
217	Start of tool failure	

the machined surface, the author assumes all the machined surface profiles are equal, which implies a dangerous assumption.

Spindle power

Spindle power is easy to collect and the sensor easy to install there is a strong relationship between the spindle power and the tangential cutting force. In Corne et al. (2017) the possibility of using spindle power to predict tool wear instead of thrust force was considered. In this case, although the thrust force maintains a higher relationship with tool wear, it was concluded that it is possible to monitor tool wear using the spindle power thanks to its high relationship with the torque. Figure 2.30 shows a comparison between the two signals having a significant relationship between both for fresh and worn tool conditions.

Patra et al. (2006) observed that the magnitude of the current increases with increasing drill wear when all other cutting conditions remain constant. The magnitude of the current also depends on the cutting conditions. Time-domain features are susceptible to cutting conditions, so it is challenging to develop a tool wear monitoring system suitable for a wide range of machining conditions. Ao and Qiao (2010) stated that spindle current is sensitive to the wear in medium and heavy cutting conditions. So the use in low cutting conditions or micro-drilling processes could be limited. Franco-Gasca et al. (2006) also showed that spindle current is related to the cutting process dynamics allowing to determine the moment of tool change after performing Discrete Wavelet Transform (DWT).

Drouillet et al. (2016) used a power sensor to measure the RMS of spindle power to predict Remaining Useful Life (RUL) in milling processes. After normalizing the values for different cutting speeds, they can predict the RUL for different cutting speeds. The normalization of the values is done to reference the nominal value for different cutting conditions.

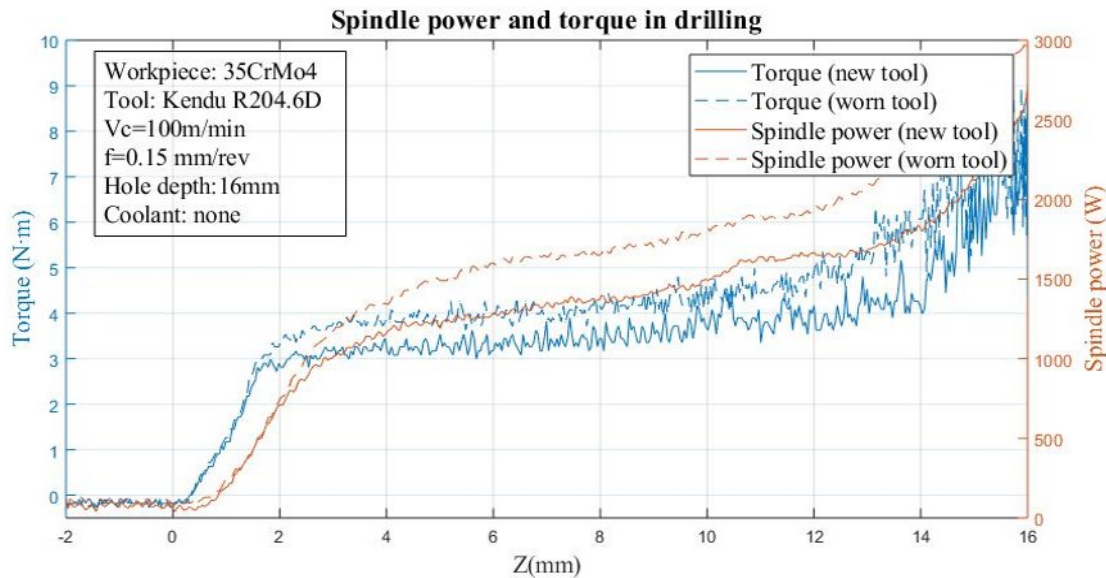


Figure 2.30 Spindle power and torque comparison in drilling process (Duo et al., 2019)

In Stavropoulos et al. (2016), the average of the spindle electrical current is used to study its correlation with tool wear. In this case, it was concluded that the spindle electrical current provides better results than the vibration signal since it is not affected by external noises and is easier to process.

Sensor fusion

The use of various sensors to extract statistical features and their combination allows obtaining more information about the state of the cutting process. In the literature, several sensors for detecting the tool condition can be observed as a trend. This principle is based on the experience that if several sensors indicate a malfunction of the tool condition, the response of the system is more credible (Bhuiyan and Choudhury, 2014). The fundamental problem is that a tool condition detection system must be scalable, cost-effective and not obstruct the cutting process. One of the unknowns is the improvement of a tool condition detection system based on a single sensor or a fusion of sensors. Furthermore, in the event of a failure of one of the sensors, whether the system would continue to give the same response.

Several works showed efforts to use different sensors for the detection of the tool condition. Caggiano et al. (2017) used the cutting forces, acoustic emissions and vibrations signals for tool state monitoring in turning processes. Once the time domain features have been extracted, the most relevant variables have been selected based on the Pearson correlation coefficient. The RMS value of the acoustic emissions is established together with the features of the cutting force signals in the three axes (F_x , F_y , F_z) as the most representative in terms of tool wear. In another study Caggiano (2018) also collected the same signals to select the most robust variables through a Principal

Component Analysis (PCA) analysis on the features; mean, variance, skewness and kurtosis of the cutting forces of the three axes, the AE RMS signal and vibrations in the three axes. From the 28 of the total features extracted, they reduce the dimensionality to two features.

Jemielniak et al. (2011) used a dynamometer (Kistler 9017B) and an acoustic emission sensor (Kistler 8152B121) for tool condition monitoring in rough turning. The authors said that use of features of two sensors improved the performance of the system. Statistical analysis would have confirmed the hypothesis that the signals acquired from the two sensors have a relevant impact on the performance over employing sensors individually.

The monitoring system proposed by Rajeev et al. (2017) for turning processes is based on the mean value of the cutting forces and the power spectral density of the vibration signal in the 4.5-5.5 kHz band. In the study, it is observed that these variables are feasible for tool wear monitoring. Like Dimla and Lister (2000) in the Z-axis, a greater amplitude of the vibrations is obtained, the reason why it is the component of the vibrations with more meaningful information.

Vibrations and cutting forces are the most commonly used signals for detecting tool wear. So Wu et al. (2017b) used these two signals on the three axes together with the acoustic emissions to detect tool wear in milling processes. They extract the mean, median, standard deviation and maximum and then use them in a wear prediction model from all the collected signals.

Nowadays, numerical controls offer the opportunity to obtain machine-internal signals. These signals can also be used for tool condition monitoring and complemented with a single sensor or obtain responses from two different systems for the same purpose. A multi-sensor system to only establish the current status of the tool is an expensive practice. This is why a selection of sensor features best suited to a particular purpose must be made to establish monitoring of the status of the cutting and finishing process of the complete workpiece and make a monitoring system even more cost-effective in this sense.

2.2.2.2 *Feature extraction*

Signal processing techniques are applied to obtain feasible features related to the cutting process conditions. First, it involves the pre-processing of the acquired signal: signal cleaning, drift removal or filtering. Time domain, frequency domain and time-frequency domain are the methods used for this purpose. According to Jemielniak (2019) as many features as possible should be extracted from the available signals as most of them are considered irrelevant.

The acquisition of signals to obtain information about the cutting process results in large volumes of data. According to ISO/IEC/IEEE 60559:2011 a double floating-point of 8 bytes covers the range from $4.94065645841246544e^{-324}$ to $1.79769313486231570e^{308}$ (positive or negative), knowing this and assuming that we are storing each sample

based on this type of data and that we are acquiring with a sampling rate of 1Mhz, we would acquire one Gb in 125s. For this reason, the manipulation and extraction of information must be done appropriately, making a selection of the features that best express the physical quality of the cutting process to be controlled and storing data containing relevant information about the cutting process.

Time domain analysis

Different features describing the signal distribution while preserving the relevant information must be obtained, as have been seen in different works (Caggiano et al., 2018a; Caggiano et al., 2018b; Elangovan et al., 2011; Scheffer and Heyns, 2001). The most common features in the time domain can be seen in Table 2.4.

Table 2.4 Signal feature expressions

Name	Features	Observations
Mean	$\bar{X} = \frac{\sum_{i=1}^r x_i n_i}{N}$	
Variance	$\sigma^2 = \frac{\sum_{i=1}^r (x_i - \bar{x})^2 n_i}{N}$	
Standard deviation	$\sigma = \sqrt{\sigma^2}$	
Kurtosis	$g_1 = \frac{\sum_{i=1}^r (x_i - \bar{x})^3 n_i}{N} \frac{3}{\left(\frac{\sum_{i=1}^r (x_i - \bar{x})^2 n_i}{N} \right)^{\frac{3}{2}}}$	$g_1 = 0$ Symmetrical distribution $g_1 > 0$ Asymmetrical right-hand or positive distribution $g_1 < 0$ Asymmetrical left-hand or negative distribution
Skewness	$g_2 = \frac{m_4}{\sigma^4} - 3$	$g_2 = 0$ Similar to normal distribution. Mesokurtic distribution $g_2 > 0$ Positive kurtosis. Leptokurtic distribution $g_2 < 0$ Negative kurtosis. Platykurtic distribution
Root Mean Square	$RMS = \sqrt{\frac{\sum_{i=1}^r x_i^2 n_i}{N}}$	

Frequency and time-frequency domain analysis

The frequency-domain can contribute additional information about a signal. The analysis of the frequency components of a signal can present information about the events that occur in a cutting process. Representation in the different domains sometimes provides insight and points out properties that are hard to discern or see in other representations. Besides, there are helpful techniques to represent the signal in time-frequency.

- *Discrete Fourier transform*

The Discrete Fourier Transform (DFT) is used in a discrete and periodic data set to obtain the frequency domain of a signal. Having a x_i signal, the Fourier transform is done using the equation 2.1.

$$X_k = \sum_{i=0}^{N-1} e^{-j\frac{2\pi}{N}kn} x_i \quad (2.1)$$

When calculating the signal spectrum, two main problems can appear; aliasing and leakage. Aliasing implies that there is not enough data to represent the high-frequency components. The solution is to filter the signal before it is discretised to eliminate those high-frequency components or increase the sampling frequency. Spectral leakage is a phenomenon that takes place due to finite windowing of the data. In addition to the lobe due to the frequency components, additional lobes start appearing in the DFT spectrum. Therefore, if a non-rectangular window can be used and its frequency domain characteristics are uniform in nature, the effect can be reduced. The spectrogram based on STFT is another tool for displaying the frequency components of a signal. In this case, it assumes the representation of these frequency components in time (Teti et al., 2010).

- *Discrete wavelet transform and wavelet packet transform*

The wavelet packages are another way to visualise the data without losing information. It consists of separating the signal into fragments, and the original signal is systematically filtered with a high pass filter and a low pass filter. Having the approximations in high scale, low frequency and the details in low-scale, high-frequency. The DWT is described with the following equation.

$$W(j, k) = \sum_j \sum_k x(k) 2^{(-j/2)} \Psi(2^{-j}n - k) \quad (2.2)$$

$\Psi(t)$ is a time function with finite energy and fast decay called the mother wavelet. The DWT analysis can be performed using a fast, pyramidal algorithm related to multi-rate filter-banks. As a multi-rate filter-bank, the DWT can be viewed as a constant Q filter-bank with octave spacing between the filter centres. Each sub-band contains half the samples of the neighbouring higher frequency subband. The signal is analysed at different frequency bands with different resolution in the pyramidal algorithm by decomposing the signal into a coarse approximation and detail information. The coarse approximation is then further decomposed using the same wavelet decomposition step. This is achieved by successive high-pass and low-pass filtering of the time domain signal and is defined by the following equations:

$$Y_{low}[n] = \sum_{k=-\infty}^{\infty} x[k]g[2n - k] \quad Y_{high}[n] = \sum_{k=-\infty}^{\infty} x[k]h[2n - k] \quad (2.3)$$

Where $h[n]$ and $g[n]$ are typically called low-pass and high-pass filters in the associated filter bank. In fact, the signals Y_{low} and Y_{high} are the convolutions of $x[k]$ with the filters $h[n]$ and $g[n]$ followed by a down-sampling of factor 2. The graphical representation of this method can be seen in Figure 2.31.

In the WPT both approximations and details are decomposed to provide more frequency bands, increasing the probability of obtaining relevant features from the original signal. As seen in the work done by Jemielniak and Kossakowska (2010) the WPT is most valued for obtaining relevant features for tool condition monitoring. Other works have applied the WPT by obtaining relevant signal features related to measured physical parameters, like tool wear Kumar et al. (2015) or hole roundness errors Ranjan et al. (2020).

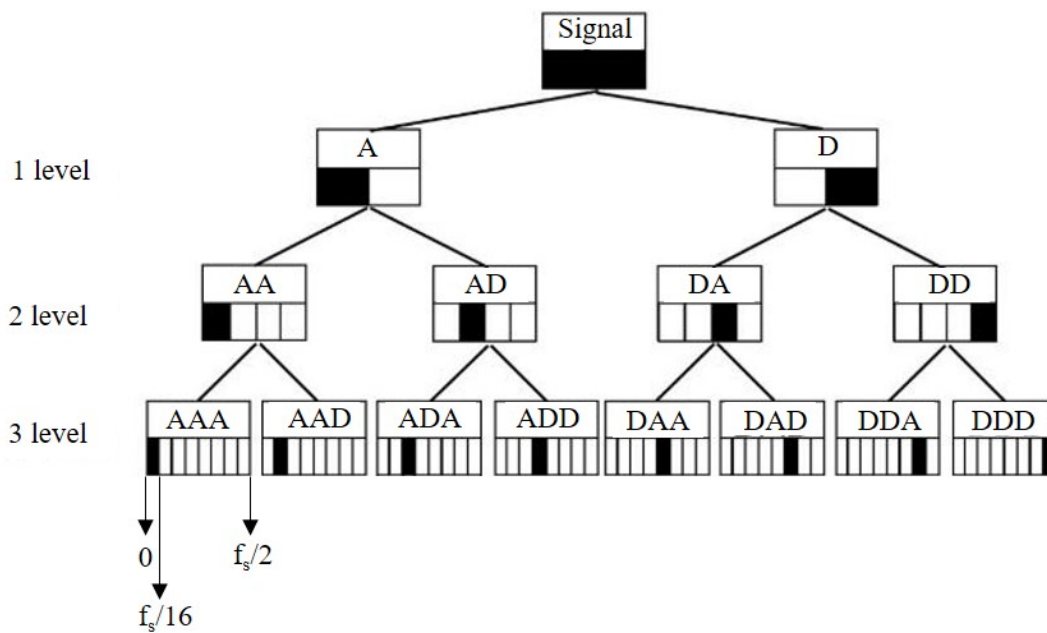


Figure 2.31 Three-level WPT decomposition, where blackened fields indicate the frequency band of the original signal (Adapted from: Jemielniak et al. (2011))

2.2.2.3 Feature selection

Feature selection is based on the selection of a subset of features from an original set of features. The main idea is to eliminate irrelevant and redundant features, which can be beneficial to obtain more accurate results and reduce learning time (Cai et al.,

2018). Teti et al. (2010) said that only 15% used some technique for the selection of relevant features during tool condition monitoring. Overall, applying feature selection will always provide benefits such as providing insight into the data, a better classifier model, enhance generalisation and identification of irrelevant variables. Mehmood et al. (2012) commented that there is no method for selecting variables consistently superior to the rest. It is probable to be an interaction between the method and the data properties. There are several criteria for the selection of variables, which are briefly described below.

Filter methods

Filtering methods do not incorporate any learning techniques and evaluate each feature relative to the target variable. The existing filter algorithms are computationally cheaper, but they fail to identify and remove all redundant features. Besides, there is a danger that the features selected by a filter method can decrease the correlation coefficient of a learning algorithm (Karagiannopoulos et al., 2007). The most used filtering method for variable selection is the Pearson correlation coefficient (equation 2.4) that assumes a Gaussian distribution to each variable and reports on their linear relationships.

$$r_{XY} = \frac{\sum_{i=1}^n (X_i - \bar{X})(Y_i - \bar{Y})}{\sqrt{\sum_{i=1}^n (X_i - \bar{X})^2} \sqrt{\sum_{i=1}^n (Y_i - \bar{Y})^2}} \quad (2.4)$$

Another filtering method is Information Gain (IG), based on entropy reduction between the independent variables and the target variable. It tries to find those variables with the highest information gain, which in turn minimises entropy. The algorithms find weights of independent variables basing on their correlation with a continuous class attribute.

$$IG = H(\text{target}) + H(\text{attribute}) - H(\text{target}, \text{attribute}) \quad (2.5)$$

where $H(X)$ is Shannon entropy for variable X and $H(X,Y)$ is a joint Shannon entropy for a variable X with a condition to Y .

Wrapper methods

Wrapper methods use a ML algorithm to measure the quality of subsets of features without incorporating knowledge about the specific structure of the classification or regression function and can therefore be combined with any machine learning algorithm. The sequential selection algorithms start with an empty set (Forward selection) or a complete set (Backward selection) and add features or remove features until the

maximum objective function is obtained. A problem with forward selection is that it may fail to include interdependent attributes, as it adds variables one at a time. However, it may locate small effective subsets quite rapidly, as the early evaluations, involving relatively few variables, are fast. In contrast, in the backward selection, interdependencies are well managed, but early evaluations are relatively expensive (Liu and Motoda, 1998).

In Sequential Backward Search, the primary idea is to sequentially remove features from the given features list consisting of N features to reach the list of K -features, where $K < N$. At each stage of removal, the feature that causes the least performance loss gets removed. The search for features is based on a combinatorial search algorithm where the subset of features get selected from a combination, and the score is calculated for the subset and compared to other subsets.

Embedded methods

In contrast to filter and wrapper approaches, the learning part and the feature selection part can not be separated in embedded methods. Some induction algorithms models include implicitly a search for optimal features with respect to the target. It is the case of Random Forest (RF) trees that allows to obtain a ranking of the most important variables to create a model. In each split of the tree, the feature used for the splitting is the one that has an impact of the overall error of the model.

Apart from that, regularization is a form of regression that discourages learning a more complex or flexible model to avoid the risk of overfitting. There are two regularization algorithms, LASSO and ridge regression (Zou and Hastie, 2005). The main difference is that LASSO regression is better than ridge regression at reducing variance if there are useless features. Elastic Net is a regularisation based on LASSO and Ridge regression that tries to minimize the loss function of equation 2.6.

$$L_{\text{ElasticNet}} = \frac{\sum_i (y_i - \beta'x_i)^2}{2n} + \lambda \left(\alpha \sum_{k=1}^K |\beta_k| + \frac{1-\alpha}{2} \sum_{k=1}^K \beta_k^2 \right) \quad (2.6)$$

If $\alpha = 1$ the expression corresponds to LASSO regression, and if $\alpha = 0$, the expression corresponds to ridge regression. With a cross-validation process, it was possible to tune different λ values for different α values and get a suitable group of features with this method and reduce overfitting.

2.2.2.4 *Machine learning for machining process monitoring*

Learning algorithms allow extracting unknown information from previously collected data. This information can offer advantages in decision-making and provide knowledge about the problem.

In machining processes, learning algorithms are generally used to learn the behaviour of a process based on previous data. The learned models can detect subsequent unwanted or desired phenomena, both in the machined part and in the cutting tool. There are two different processes that a pattern recognition system executes in the acquired instances. On the one hand, the system must be trained with a series of known instances. Once the training phase has concluded, there is the operational mode where the system makes decisions.

An automatic learning system must have four different fundamental characteristics in order to make predictions autonomously (Wu et al., 2017b):

- It should train the system automatically and improve results as more data input arrives, this means that the system must be self-updating and learning periodically.
- Discover or recognise patterns and intelligence with input data.
- Predicate on unknown data.
- The system should acquire knowledge from data and solve problems.

There are two categories of ML, supervised and unsupervised. In supervised training, all instances belong to a particular class (classification). On the other hand, in non-supervised training, the system does not recognise the entry instance, so it assigns a new class and adjusts the clustering parameters.

Active learning is a ML approach that lets users play an active role in the learning process. An active learning approach can ask a user (e.g., a domain expert) to label an example, from a set of unlabeled examples or synthesised by the learning program. The goal is to optimise the model quality by acquiring knowledge from human users, given a constraint on how many examples they can be asked to label.

The algorithms used can provide more or fewer advantages, depending on the case to be analysed. Therefore, it is essential to compare the results obtained. The algorithms can be compared concerning the following criteria according to Han et al. (2012):

Predictive accuracy: It is the ability of the model to predict a class correctly.

Speed: It is the cost of computing that the model needs for learning or use.

Robustness: The model can make predictions with data with noise or lack of attributes.

Scalability: Ability to create an efficient model providing large volumes of data.

Interpretation: It is the ability to understand what the model provides as information.

Supervised learning

In this category are problems of (I) classification, which tries to map inputs to output labels, and (II) regression, which tries to map inputs to a continuous variable. There are several strategies for accomplishing both tasks. The most commonly used are briefly

described below. The works cited in each of the strategies are discussed in section 2.2.2.5.

- *Instance based learning*

Instance-based algorithms compare new observations with the observations in the training set based on distance measures. One of the advantages of this type of algorithm is the ability to adapt to observations not included in the training set. These types of algorithms can be used to perform classification or regression. The most commonly used distance is the Euclidean distance, but there are other distance measures such as Hamming, Manhattan or Mikowski. Instance-based learning was used by Dheeraj Simon and Deivanathan (2019) and Kilundu et al. (2011).

- *Probability based algorithms*

This type of algorithm, such as the Naive Bayes classifier, uses the probability that an event has occurred before to obtain the probability of the event covered by the new observation (posterior probability). One of the disadvantages is that a new observation not covered in the training set will get a probability of 0 (Kumar et al., 2015). Bayes theorem provides a way to calculate the posterior probability (equation 2.7).

$$P(c|x) = \frac{P(x|c)P(c)}{P(x)} \quad (2.7)$$

- *Decision trees*

They are a family in which data is continuously separated based on certain input parameters. These types of algorithms are based on the idea of divide and conquer. The input data is divided into subsets until the subsets are sufficiently homogeneous. Although they are simple to construct, they can be over-trained, and creating a tree can become very complex if there are small changes in the input data (Elangovan et al., 2011; Krishnakumar et al., 2015).

- *Support vector machines*

This type of algorithms identifies hyperplanes that separate groups of data. The hyperplanes are decision boundaries, and the hyperplane dimension depends on the number of input features for the prediction. When there are 2 features, the hyperplane is a line, and if there are 3 features, the hyperplane is a plane. The support vectors are the points closest to the hyperplane and are the ones that allow maximising the margin of the classifier (Wu et al., 2017b).

- *Neural Networks*

A neural network trains a set of weights associated with each input to the neuron based on the training set. A basic neural network consists of an input layer, a hidden layer and an output layer. Most neural networks are fully connected, and each connection has an associated weight. The larger the weight, the more influence the neuron will

have on the output. Optimising the weights associated with each neuron is done using backpropagation, comparing the actual and predicted output and updating the weights to minimise the error produced (Caggiano et al., 2017; Abu-Mahfouz, 2003; Jaini et al., 2020).

Unsupervised learning

This practice results in learning the structure of the data without having the data labels. In this category, the common use results in the exploratory analysis of the data.

Clustering is an unsupervised method that allows the understanding of groups and could improve the knowledge about the process, dealing with unlabelled data and explaining groups created from this data. Clustering methods organise the observations into an efficient representation that characterises the target population of the sample (Maimon and Rokach, 2011). Unsupervised methods can be divided into two groups, (i) hierarchical or (ii) partitioning methods. (i) Hierarchical methods build the groups by dividing the observations recursively. The result is a dendrogram representing the groupings of observations and their level of similarity. (ii) Partitioning methods create an initial partition and reallocate observations from one group to another. These methods usually require the number of groups to be selected previously. The hierarchical methods are divided into two groups, agglomerative methods, which consider each of the observations as an independent cluster and group them. Divisive methods, which consider the whole set of observations as a cluster and separate them into subgroups. Among the agglomerative methods, different inter-group proximity measures may show more or less interpretable results in the same group of observations (Everitt et al., 2011).

- Hierarchical clustering

Hierarchical clustering is a tool for unsupervised data analysis. Specifically, it consists of grouping independent observations that are closest to each other. In bottom-up or agglomerative hierarchical clustering, a tree is built by joining small subsets of observations until the central node of the tree contains all the elements. This is done iteratively by joining the two most similar clusters in each iteration.

The distance between two observations can be calculated in different ways (Hamming, Manhattan, Minkowski distances). The most commonly used is the Euclidean distance (equation 2.8).

While for the linkage (the criteria for merging two clusters), the Ward criterion (equation 2.9), which tries to minimise the error sum of squares, is the one that more stable results achieve with numerical data (Mingoti and Lima, 2006).

$$D(p, q) = \sqrt{\sum_{i=1}^N (p_i - q_i)^2} \quad (2.8)$$

$$\delta(X_i, X_j) = \frac{n_i n_j}{n_i + n_j} \|c(X_i) - c(X_j)\|^2 \quad (2.9)$$

This creates a dendrogram, depicted in Figure 2.32. From the created dendrogram, clusters are obtained by horizontal cuts at a specified height, which represents the degree of similarity of groups.

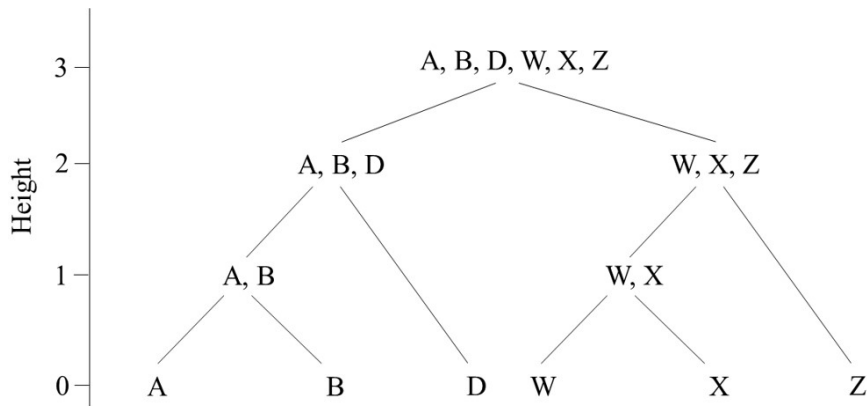


Figure 2.32 Conceptual representation of a dendrogram

Dimensionality reduction

Dimensional reduction techniques allow visualising possible hidden data patterns in a dataset. PCA is one of the most popular algorithms for dimensional reduction. It was originally developed by Pearson (1901) to overcome the problem of visualising a data system on a limited feature space. It is a method to describe a feature space on a set of non-correlated linear components. t Distributed Stochastic Neighbour Embedding (tSNE) (Maaten and Hinton, 2008) is a non-linear dimensionality reduction data visualization method. It models each high-dimensional object by a two- or three-dimensional point in such a way that similar objects are modelled by nearby points, and distant points model dissimilar objects with high probability. The main difference between both approaches is that tSNE does not preserve the input feature space characteristics like PCA. Thus, it can not be used as a preprocessing method directly. To overcome this limitation, Oliveira et al. (2018) used first tSNE for dimensionality reduction and then a neural network for new data mapping to the reduced feature space.

- Linear dimensionality reduction: Principal component analysis

PCA allows to reduce a big feature space d into lower feature space k , where $k < d$, preserving the original d dimensional space information. Each k dimensions will be transformed as linear combinations of d dimensional feature space. The dimensions on the k feature space are called principal components, and each principal component Dim_n will have the form of,

$$\text{Dim}_1 = a_1x_1 + a_2x_2 + \dots + a_nx_n \quad (2.10)$$

The Dim_1 is obtained so that the variance is the maximum subject to the total variance that remains fixed. This is achieved by calculating eigenvalues and eigenvectors. In the PCA method, each of the principal components corresponds to an eigenvector, and the order of components is established by decreasing the order of eigenvalue. Thus, the first component is the eigenvector with the highest associated eigenvalue. This is a powerful tool to simplify data visualisation.

- *Non-linear dimensionality reduction: t stochastic neighbour embedding*

tSNE tries to place a point from a high-dimensional space in a low-dimensional one so as to preserve neighbourhood identity. The similarity of x_i to the point x_j in high dimensionality is obtained by the joint probability p_{ij} using a Gaussian distribution expressed in equation 2.11.

$$p_{ij} = \frac{\exp(-\|x_i - x_j\|^2 / 2\sigma^2)}{\sum_k \sum_{l \neq k} \exp(-\|x_k - x_l\|^2 / 2\sigma^2)} \quad (2.11)$$

In low dimensionality uses a Student's t-distribution distribution to measure similarities y_i and y_j of the high-dimensional data points x_i and x_j , it is computed a similar joint probability denoted by q_{ij} .

$$q_{ij} = \frac{(1 + \|y_i - y_j\|^2)^{-1}}{\sum_k \sum_{l \neq k} (1 + \|y_k - y_l\|^2)^{-1}} \quad (2.12)$$

And minimizes a single Kullback-Leibler divergence between a joint probability distribution, P , in the high-dimensional space and a joint probability distribution, Q , in the low-dimensional space:

$$\text{KL}(P \parallel Q) = p_{ij} \log \frac{p_{ij}}{q_{ij}} \quad (2.13)$$

The differences between P and Q must be 0. To obtain these probabilities, a sigma value must be selected. For dense regions, a smaller sigma value is more appropriate than for sparse regions. A search for the sigma value is performed using a user-defined perplexity value which is the number of neighbouring observations used in each local estimate.

2.2.2.5 Tool condition monitoring based on indirect sensing techniques

The most widely known regression algorithm is linear regression. However, limited ability and simplicity are often not applicable to real-life data. Therefore, the use of other types of algorithms capable of dealing with non-linear data should be employed. Neural networks are widely used for tool wear monitoring, Caggiano et al. (2018b) employed backpropagation Artificial Neural Network (ANN) for tool wear curve prediction in Carbon Fiber Reinforced Plastic (CFRP) drilling operation, obtaining a minimum RMSE = 0.00023. They used time-domain features of thrust force and torque. In a similar work, Caggiano et al. (2018a) in addition to the thrust force and the cutting torque, they acquired the acoustic emissions, in this occasion, they applied PCA on the features with high correlation coefficient with tool wear curve always obtaining an RMSE < 0.00217. Liu and Anantharaman (1994) employed dynamometer data for tool wear curve prediction based on time-domain features of cutting forces and ANN with adaptive activation-function slopes concluding that adaptive activation functions are a better solution than conventional neural networks. Mohsen et al. (2020) employed Adaptive Neuro Fuzzy Inference System (ANFIS) for tool wear regression making a comparison of different activation functions concluding that the sigmoid function is the most suitable for the regression of the wear curve in turning processes. Corne et al. (2017) compared different backpropagation algorithm performances for tool wear prediction in drilling operations based on spindle power data, and they conclude that the Levenberg Marquart algorithm was the best option. Balazinski et al. (2002) made a comparison between three different ML methods, ANN, a Fuzzy Decision Support System (FDSS) and ANFIS for tool wear curve reconstruction in turning process. They did not see any superior method to the rest, but they concluded that ANFIS was the most practical ML algorithm given its practicality. Making use of the same process data and the same algorithms, Ren et al. (2010) added to the comparison the Takagi-Sugeno-Kang (TSK) fuzzy modelling based on subtractive clustering method, showing its superiority to the rest ML algorithms. Garg et al. (2010) compared Radial Basis Function Network (RBFN) trained based on k-means clustering and Genetic Algorithm (GA) in drilling operation for tool wear curve prediction showing the best result for GA training.

Elangovan et al. (2011) employed C4.5 decision trees to classify different tool wear levels using the vibration signal. They made a comparison between a feature selection made through C4.5 and using the best two principal components (PCA) of acquired features, concluding that the features based on the decision tree obtain a better result with a classification accuracy of 77.22%. Remarkably, PCA is not a feature selection method, it is the rotation of dimensions of the feature space based on linear combinations of all the feature space. Jaini et al. (2020) used a gap sensor for tool condition classification in the drilling process. By obtaining the head movement kurtosis and skewness features, they can classify 11 drills with different damage. Multi Layer Perceptron (MLP) was used in this study with two hidden layers. Dheeraj Simon and Deivanathan (2019) used the vibration signal time-domain features to detect the presence of wear in drilling processes, using the K-Star algorithm. Wu et al. (2017a) made a comparison between

algorithms based on ANN, Support Vector Machine (SVM) and Random Forest (RF), showing the superiority of RF over the other methods. Ao and Qiao (2010) used Logistic Regression (LR) and Auto Regressive Moving Average (ARMA) models to predict the RUL. Abu-Mahfouz (2003) classified artificially induced wear types using the vibration signal. For this purpose, he used frequency Harmonic Wavelet Coefficients (HWC) and Maximum Entropy Spectral Analysis (MESA) features and time-domain features of vibration signals and ANN. He compared different input combinations of features concluding that frequency domain features provide better classification accuracy.

Deep learning has also been employed for tool wear prediction. By constructing images from the polar coordinates of the cutting forces in milling processes (Gouarir et al., 2018) and using convolutional neural networks, a cloud-based system capable of classifying the level of tool wear was deployed by Terrazas et al. (2018). Although the authors state that this is not a cost-effective solution given the type of sensor used, they showed the applicability of the system. Table 2.5 summarises the main works consulted on the subject.

Based on the information revealed by the table above, most of the works employ neural networks for tool wear prediction based on features obtained in the time domain. Some compare different algorithms for the same purpose to get a broader view of the capability of different algorithms. As a target, the most commonly used unit is the tool wear curve itself, since by its nature and because it is a continuous value, it makes more sense to reconstruct the wear curve progressively based on previous data. A few works face the problem as a classification of different tool wear levels, although this may involve different criteria when defining the boundaries at which each level will be found. As has already been seen, different types of wear can appear on the tool, and some works focus on identifying the presence of the different types of wear that may appear, this being subject to the conditions of the cutting process and the wear mechanisms that may be activated throughout the process. Finally, few of the papers employ feature selection techniques that are best suited to the prediction of tool wear, and it appears that the practice of variable selection has been increasing in recent years. Among the techniques employed are correlation coefficients between features and tool wear or variable selection techniques embedded in algorithms, such as decision trees, variables that contribute most to the principal components, or variable discrimination techniques.

Some works used a data partitioning method for the training and testing phase (i.e. 70% for training and 30% for testing) (Wang et al., 2013; Shankar et al., 2018). Indirectly, data leakage is induced on the testing phase, which can lead to better results than those obtained in a real system overestimating the produced model. The testing phase should be carried out in a completely new tool to obtain adequate results and validate the created model. The data leakage problem for tool wear curve estimation is illustrated in Figure 2.33.

The monitoring process is different in each of the cutting operations. The tool, cutting conditions or the resources available to make the acquisitions of the signals

Table 2.5 Summary of indirect tool conditions monitoring techniques through automatic learning algorithms

Sensor	Process	Feature extraction	Algorithm	Output	Feature selection	Ref.
Dynamometer Acoustic emission Accelerometer Current Sound Gap sensor Strain Drilling Others		Time domain Frequency domain Time-frequency domain	ANN ANFIS FDSS Bayesian Network TSK-FL SVM Decision trees Distance based Regression	Wear curve Wear levels Wear types	RUL Filter Embedded	
x	x	x	x	x	x	Caggiano et al. (2017)
x x	x	x	x	x	x	Caggiano et al. (2018a)
x	x	x		x	x	Elangovan et al. (2011)
x	x	x		x		Wang et al. (2013)
x	x	x x	x		x	Abu-Mahfouz (2003)
x	x	x	x		x	Jaini et al. (2020)
x x	x	x	x	x		Shankar et al. (2018)
x	x	x		x	x	Dheeraj Simon and Deivanathan (2019)
x	x	x x	x	x		Patra (2011)
x	x	x	x	x		Liu and Anantharaman (1994)
x	x	x	x	x	x	Krishnakumar et al. (2015)
x	x	x	x x	x x	x	Kilundu et al. (2011)
x x x	x	x	x	x x	x	Wu et al. (2017b)
x	x	x x x	x	x	x	Scheffer and Heyns (2001)
x	x	x		x x	x	Ao and Qiao (2010)
x	x	x	x	x		Patra et al. (2006)
x	x	x x	x x	x	x	Kumar et al. (2015)
x	x	x	x	x		Panda et al. (2006)
x	x	x x		x x		Sudev and Ravindra (2008)
x x x x	x	x	x	x		Kandilli et al. (2007)
x	x	x	x	x		Mohsen et al. (2020)
x	x	x	x x x	x		Balazinski et al. (2002)
x	x	x	x x x x	x		Ren et al. (2010)

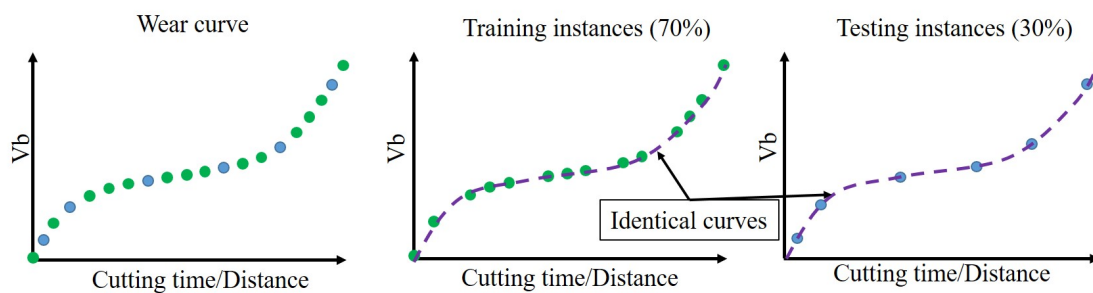


Figure 2.33 Data leakage problem in tool wear prediction

that best represent the phenomenon could condition the predictions. Identifying the features related to the phenomenon in consideration is essential since it allows the creation of simpler and lighter models. Addressing the problem as a classification does not establish criteria for deciding what flank wear limits should be established as a

target for the predictions. Furthermore, depending on the machining operation, cutting conditions or the tool used, these criteria may vary. Trying to address the problem as regression can be costly as the whole process wear curve must be constructed with the number of measurements that imply. Signal fusion for tool wear prediction is common in laboratory environments; however, increasing the number of sensors in an industrial plant for a particular machine can be expensive and not practical. It seems essential to design and develop hybrid systems for industrial applications to benefit from the different advantages of the different algorithms and information sources to scale and introduce more process complexity based on different sensors.

2.2.2.6 *Surface roughness monitoring based on indirect sensing techniques*

The increase in demand for components with more precise finishes means that quality inspection of machined parts is becoming more critical and must be carried out with greater precision. This is a challenge for repetitive parts that must meet specific requirements, but also for the production of small batches of high benefit components. Decisions regarding critical events that may occur during a process must be made as quickly as possible. Automation tasks for the quality control of components play an important role in increasing the reliability of components with specific requirements.

Venkata Rao et al. (2014) used neural networks to predict roughness in a boring process using the cutting conditions and geometry of the tool used as input, obtaining an error percentage of 4.51%. In the same way, Vrabel et al. (2012) monitored the Ra parameter in drilling processes on Udimet 720, using the cutting conditions and the thrust force as inputs to the neural network. However, they only test the neural network in 9 of the 41 holes made. They obtain good results ($RMSE = 12.7\%$), but they did not test all the cutting conditions used. Akincioğlu et al. (2013) were conducting a similar study on steel intending to predict the Ra parameter. They used different cutting conditions for each hole they make, so they do not consider the phenomena that could appear during the drilling of holes under established cutting conditions in long cutting time. 32 holes were drilled, 26 were used for the learning phase and 6 for the testing phase obtaining $RMSE = 0.010$. Mia and Dhar, 2016 compared different supervised learning algorithms for Ra prediction in turning processes using cutting conditions, material hardness and dry or High-Pressure Coolant as input variables obtaining acceptable results, $RMSE = 0.031$. Rodríguez et al. (2016) compared 35 different machine learning algorithms to classify Ra and Rz parameters based on ISO 4288 : 1996 standard levels in milling process. Among all the algorithms, they concluded that decision tree J48 was the best method due to its simplicity and accuracy of 79.75%. In a similar work Samanta (2009) tested ANFIS, ANFIS-GA and ANN networks for Ra parameter prediction in the milling process, showing the superiority of ANFIS-GA over other 2 algorithms. Table 2.6 shows the works identified in the literature to predict the Ra parameter.

García Plaza et al. (2019) showed different vibration signal analysis techniques in a turning process. They obtain signal features that allow predicting the roughness

parameter Ra under different cutting conditions obtaining accurate results (correlation coefficient of 0.94 between observed and predicted values) for online prediction through WPT. They also used SSA, Time Direct Analysis (TDA) and Power Spectral Density (PSD) and TDA+PSD obtaining slightly worst results than WPT.

Table 2.6 Summary of indirect roughness monitoring techniques through automatic learning algorithms

Input variables		Process	Algorithm	Training/Testing observations	Result	Ref.
Cutting conditions						
Material hardness						
Dry/Coolant						
Tool diameter						
Tool geometry						
Tool coating						
Vb						
Cutting force						
Spindle power						
Vibrations						
Sound						
Drilling						
Others						
x	x x	x	-ANN	68 28	RMSE=0.0312.	Mia and Dhar (2016)
x	x	x	-ANN	54 8	Error percentage 4.5185%	Venkata Rao et al. (2014)
x	x x	x	-ANN	32 9	RMSE=12.7%	Vrabel et al. (2012)
x	x	x	-ANFIS -ANN -GA-ANFIS	120 36	RMSE=0.0757	Samanta (2009)
x	x	x	-ANN	26 6	RMSE=0.010594 R2=0.999739	Akincioglu et al. (2013)
x	x	x	-Regression	20 -	R2=0.952	Yang et al. (2017)
	x	x	-Regression	360 -	R2=0.94	García Plaza et al. (2019)
	x x	x	-G-SSA	270 90	R2=87.82	García Plaza and Núñez López (2017)
x		x	-Decision trees	225 Cross val.	Accuracy=79.75%	Rodríguez et al. (2016)
x	x x x	x	-ANN	120 30	MAE=1.34% R2=98.76	Deshpande et al. (2019)
x	x	x	-ANN	16 8	MSE=0.023	Zain et al. (2010)
x	x	x	-ANN	55 5	RMSE=0.00069 R2= 0.99985	Nalbant et al. (2009)
x		x	-ANN	243 7	MSE= 1.48%	Erzurumlu and Oktem (2007)

2.3 SUMMARY

The new solutions based on ML techniques published in the last years, despite achieving accurate predictions of the current value of the tool condition, have not yet reached the market. This situation is indicative of the costly work involved in data collection and storage. In laboratory environments, data is limited and accurate approximations to direct measurements are obtained. However, in industrial environments, data acquisition is perhaps more limited because it is time-consuming and costly. Nevertheless, the consideration of failure mechanism and prior knowledge should be utilised and integrated closely to improve diagnostic performance.

The metal cutting process is a complex operation that requires simple solutions as far as possible for process monitoring. In the consulted works, there are successful works as not so successful. The processing and feature extraction methods are highly application-dependent and use sophisticated methods that are difficult to generalise

in a practical and fast way. The most practical methods, however, are believed to be temporal signal analysis and wavelet packet transform. These methods allow a large number of signal features to be obtained directly; however, selecting the most suitable ones for a particular purpose is a difficult task.

The literature review has shown that sensor fusion can be a valuable strategy, achieving higher accuracy in the predictions. If a single sensor malfunctions, it is not known what the response of the system might be. Thus, it involves the maintenance of the measurement systems as a whole. Tool wear monitoring using a dynamometer can be as effective as the more economical accelerometer. The difference in cost between one sensor and the other is significant. In order to achieve cost-effective solutions, the advantages of one sensor over the others must be understood. Thus, the interpretation of the predictive capabilities of each sensor is essential for modern manufacturing. The user must adopt the best flexible data analysis methods to achieve accurate predictions in a range of process input conditions. It seems essential to design and develop hybrid systems, one sensor one ML model and sensor fusion models for industrial applications to benefit from the different characteristics of the different algorithms and signal features. This practice can help reduce false positives caused by both electrical and mechanical noise.

The collection of physical data is limited in terms of machining processes; the measurement of the physical characteristics of both the tool and the machined component is expensive to carry out. The nature of tool wear may allow extrapolation of the measurements made to unlabelled observations. However, the properties of the machined component are more complex due to process uncertainty. In industry, a defined number of components are measured in random order to ensure the quality of a production batch. However, this practice assumes risks in those components that quality is not analysed. To overcome this limitation, it is necessary to deal with unlabelled observations using the data collected throughout the process and the limited measurements to obtain a broader view of the entire production batch.

Significant effort is focused on the use of sensors external to the machine for tool wear monitoring. CNC-controlled machines provide access to internal signals such as spindle motor power and process parameters. The interpretation and relationship of certain features of these signals should be compared with those obtained from external sensors for possible replacement. This would allow process monitoring to be carried out without installing any sensors that could obstruct the process and make prediction models cost-effective.

The selection of the features best suited to the monitoring need is fundamental to achieve an accurate response. The reconfiguration and adaptation of the models to different input parameters (different operations, materials, tool geometries and cutting conditions) to integrate such systems in industrial environments.

Most of the works consulted in the literature as far as component surface quality detection is concerned were based on the use of neural networks for the prediction of the *Ra* parameter, thus supervised learning is needed. Furthermore, most works used

as learning data the cutting conditions used, assuming that the same roughness will always be obtained at specific cutting conditions. These tools can be helpful for the selection of the cutting conditions before starting a cutting process but shall not be used to monitor the characteristics of the machined surface.

The use of signals external (Cutting forces, vibrations or acoustic emissions) or internal (Spindle power, current...) to the machine could deal with the classification of roughness. However, the systematic measurement of a component roughness could be a problem since it is time expensive. Most works are based on changing the cutting conditions, but few repetitions are made with each condition, not achieving a good generalisation. In extended machining time, the probability of an undesirable phenomenon and a resulting defective component is high.

There are still a low number of observations for implementing a simple roughness monitoring system based on machine learning supervised classification algorithms. This low number of observations shows the difficulty in measuring and preparing data for a monitoring system of the roughness in drilling processes. Besides that, the consulted works did not consider different roughness parameters such as Rsk or Rku which explain the non-Gaussian nature of a roughness profile. Roughness characterization based on additional parameters obtained from the roughness profile can give more information, and a model can show a greater generalization of the obtained data.

From another perspective, most of the work observed focuses on supervised learning. This implies the measurement and extraction of the variables to be monitored before the learning phase. On the other hand, clustering is an unsupervised method that allows the understanding of groups and improves the knowledge about the process, dealing with unlabelled data and explaining groups created from this data.

DRILLING PROCESS DATA COLLECTION, PROCESSING AND CLEANING METHODOLOGIES

Monitoring of machining processes is essential for better component quality, higher production and increased automation. Direct measurements of the industrial parameters of interest are dimensional acquisitions of component quality or the cutting tool condition. These methods are expensive and difficult to apply in production environments. Indirect measurement methods are based on measurements of signals related to the cutting process (vibrations, cutting forces, acoustic emissions or spindle power) to correlate them to physical measurements of the industrial parameters (Li and Chen, 2013).

External installed sensors can be intrusive in specific cutting processes. However, they can be installed closer to the area where the material is being cut. CNC-controlled machines provide signals that can be used as a substitute for installed sensors, although these are acquired further away from the cutting area, and do not provide such direct information about the process.

Each sensor measures a physical quantity (mechanical, electrical or thermal energy) and converts it into a signal that acquisition instruments can quantify. Each of these quantities can correlate to a greater or lesser extent to industrial parameters. Therefore, there is a need to assess the suitability of various physical quantities adapted to each monitoring unit.

Set-ups must be designed to be large enough to acquire signals from several information sources (installed sensors and internal machine signals). Besides, the acquisition must be simultaneously and at sampling frequencies adapted to the frequency responses of each of the installed sensors and sufficient to relate the signal features to the industrial parameters to be observed.

Industrial parameters must be measured by direct methods to obtain a target variable that describes the quality of the machined component or the state of the cutting process periodically. It is also essential to trace the physical measurements and the acquisition of the signals to carry out the analyses that make it possible to quantify or relate one to the other. The signals, once acquired, will have parts not related to the cutting process. These segments correspond to machining in an air cutting or transient moments where the tool starts to have or lose contact with the machined material. The processing of the

signal to eliminate the parts irrelevant to the machining and obtain the most related features to the cutting process also requires special attention.

This chapter describes the methodology used for data collection in drilling processes. The data collection was carried out in three test batches. All the tests were carried out on a Lagun B1050 vertical machining centre with Computer Numerical Control (CNC) Fagor 8070. Among the internal signals provided by the CNC, it was unclear which of them would give information about the tool condition or even whether any of them would provide the information necessary to detect defects that may occur during the process. Therefore, other sensors were installed to acquire signals that are not accessible from the CNC.

Both the internal and external variables and the type of sensor used to capture them are shown in Table 3.1. It was decided to install four types of sensors. Among the consulted works are the most used signals for studying industrial parameters of the cutting process.

Among all the signals presented, internal signals are always accessible from the CNC, while the sensors need to be installed. During the execution of the 3 test batches, some sensors were removed or replaced. The following sections will explain which elements have been modified between the different test rounds and the characteristics of each group of tests performed.

Among internal signals, the power produced by the machine to cut the material (TV50, TV51, TV2 and TV3), the position of tool tip and successive derivatives in the three axes (POS, V, ACCEL and JERK) and cutting conditions (SREAL and FREAL) has been obtained.

A Kistler 9123 4-component rotational dynamometer, a PCB piezoelectric accelerometer J356A45, a Brüel & Kjaer 4321 charge output accelerometer, a Kistler 8152C acoustic emission sensor and a G.R.A.S. 40AE microphone were used among all three batches of experiments.

As part of the industrial parameters, the tool condition was measured periodically by a LeicaDMS1000 microscope. No standard has been found to measure tool wear in drilling processes, so the measurements have been based on ISO 8688 : 1989 (tool-life testing in milling) and ISO 3685 : 1993 (tool-life testing with single-point turning tools) standards. The roughness of certain holes drilled and material damage caused by machining was also measured.

The sections in this chapter present the methodology used throughout the thesis to acquire signals related to the drilling process. It also explains the combination of input parameters of the cutting processes, the methods followed for cleaning and obtaining the signal features and the methodologies carried out to measure the industrial parameters related to the cutting process.

Table 3.1 Acquired signals, sampling frequency and sensor details

Source	Signal ID	Description	Units	Range	Sensitivity	Fs (Hz)
Internal	TV50	Spindle motor power feedback	W	± 2147483647	-	250
	TV51	Active power supplied by the drive	W	± 100000 W	-	250
	TV2	Z-axis motor torque	N	± 1000 % of the stall torque of the motor	-	250
	TV3	Power percentage used with respect to the maximum power available in the servo system		0..3276.3%	-	250
	POS_(X-Y-Z)	Tool tip position	mm	-	-	250
	V_(X-Y-Z)	Tool tip speed	$\text{mm} \cdot \text{s}^{-1}$	-	-	250
	ACCEL_(X-Y-Z)	Tool tip acceleration	$\text{mm} \cdot \text{s}^{-2}$	-	-	250
	JERK_(X-Y-Z)	Tool tip jerk	$\text{mm} \cdot \text{s}^{-3}$	-	-	250
	SREAL	Spindle speed	rpm	-	-	250
	FREAL	Feed rate	$\text{mm} \cdot \text{min}^{-1}$	-	-	250
Kistler 9123	F(X-Y-Z)	Cutting force in three axes	N	$\pm 20e3$ N	0.5 mV/lbf	10e3
	Mz	Torque	N · m	± 200 N · m	0.5 mV/N cm	10e3
PCB J356A45	ACC_Z	Vibration in Z axis	$\text{m} \cdot \text{s}^{-2}$	± 50 g pk	100 mV/g	25.6e3
Kistler 8152C	AE	Acoustic emissions	v	10 dB	48 dBref 1Vs/m	1e6
Brüel & Kjaer 4321	ACC_(X-Y-Z)	Vibration in three axis	$\text{m} \cdot \text{s}^{-2}$	± 500 g pk	1pC/ms ⁻²	50e3
G.R.A.S 40AE	SP	Sound pressure	Pascal	15dB(A)to148dB	50mV/Pa	50e3

3.1 PRELIMINARY TESTS ON BLS 35CRMO4 LOW S STEEL WITH PREVIOUSLY INDUCED WEAR

The signals shown in section 2.2.2.1 have been acquired in addition to the internal signals to find correlations between the signals themselves and tool wear. The set-up used in the preliminary tests can be seen in Figure 3.1.

In this set-up, no signal synchronisation architecture was used, and the simultaneous acquisitions are limited to the sampling frequency. The thrust force (F_z) and torque (M_z) (Kistler 9123) ① were acquired through the analogue inputs available on the CNC, so their sampling frequency was equal to that of the internal signals, and thus, they were acquired simultaneously. Vibrations (Brüel & Kjaer 4321) ② and sound pressure (G.R.A.S. 40AE) ③ were acquired at 50kHz, while acoustic emissions (Kistler 8152C) ④ were acquired at 1MHz. NI 9234 and NI USB 6361 were used respectively for the acquisitions. The internal signals ⑤ were acquired at a sampling frequency of 250Hz.

It is worth mentioning that although the accelerometer installed is of the triaxial type. Only the Z-axis signal was acquired due to wiring problems.

The material used for these tests was a steel of composition BLS35CrMo4 (Table 3.2). Two types of drills were used, Kendu R204.6D curved edge drill with a helix angle of 30°, and BH04.5D straight edge drill with a helix angle of 15°, both of $\varnothing 8$ mm diameter. The tests were carried out dry and a jaw was used to clamp the workpiece. The cutting conditions were $V_c = 100$ m/min and $f = 0.15$ mm/rev for tool R204.6D and 3 levels of tool condition were considered, $V_b = 0$ mm, $V_b = 0.1$ mm and $V_b = 0.2$ mm. For tool BH04.5D the cutting conditions were $V_c = 40$ m/min and $f = 0.07$ mm/rev and

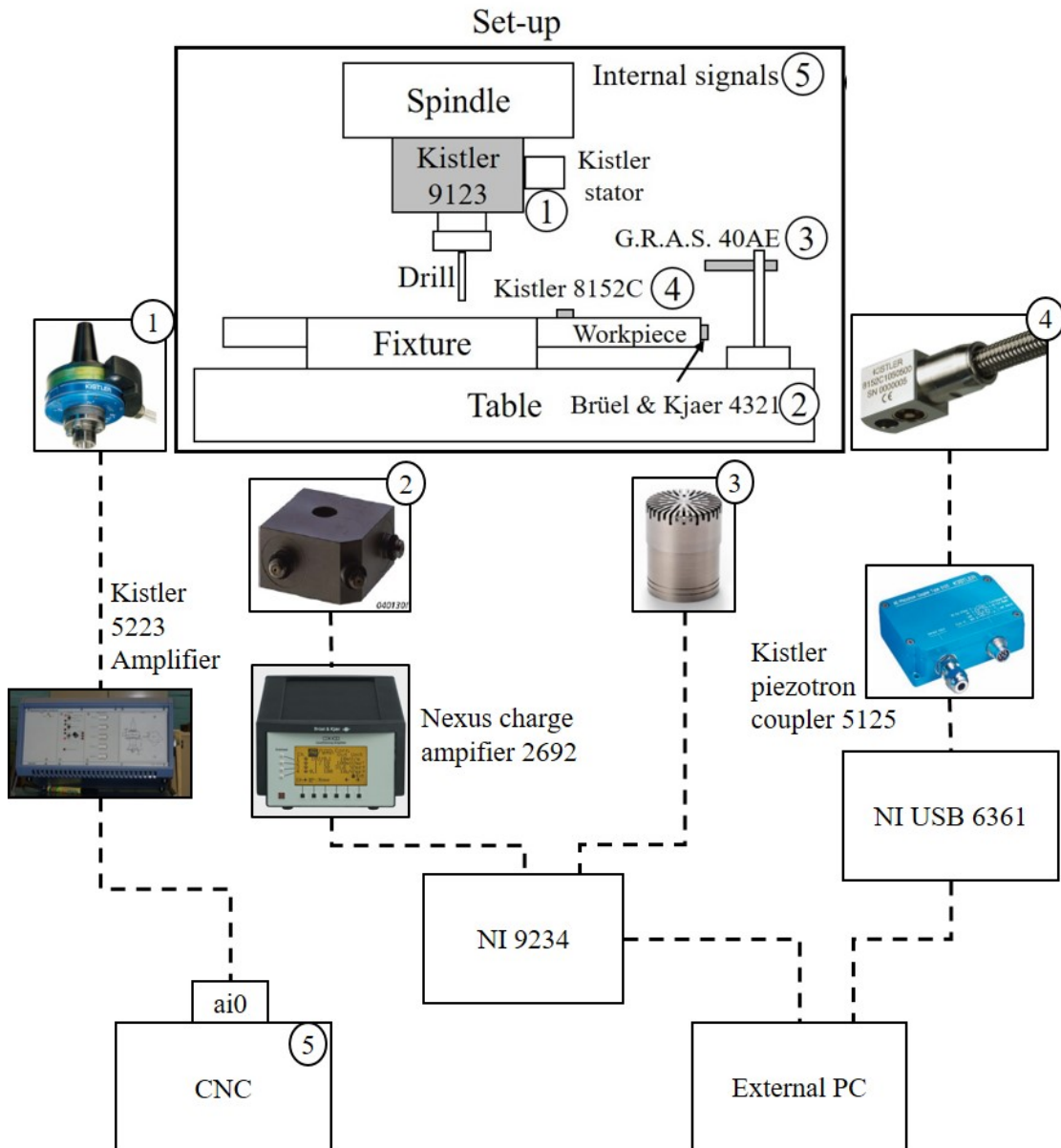


Figure 3.1 Employed set-up configuration, sensor positions and signal acquisition system

4 levels of tool wear were considered, $V_b = 0\text{mm}$, $V_b = 0.1\text{mm}$, $V_b = 0.2\text{mm}$ and $V_b = 0.3\text{mm}$.

Table 3.2 Chemical composition of the workpiece material (BLS 35CrMo4 Low S)

Material	C	Mn	Si	P	S	Cr	Ni	Mo	V	Cu	Al	Sn	Ti
Weight %	0.32	0.79	0.33	0.03	0.003	1.07	0.11	0.21	0.004	0.17	0.007	0.011	0.003

The industrial output parameter measured directly was the tool condition before and after the tests, using a LeicaDMS1000 macroscope and Alicona IFG4 3D profilometer. Fig. 3.2 shows the proposed set-up conceptually.

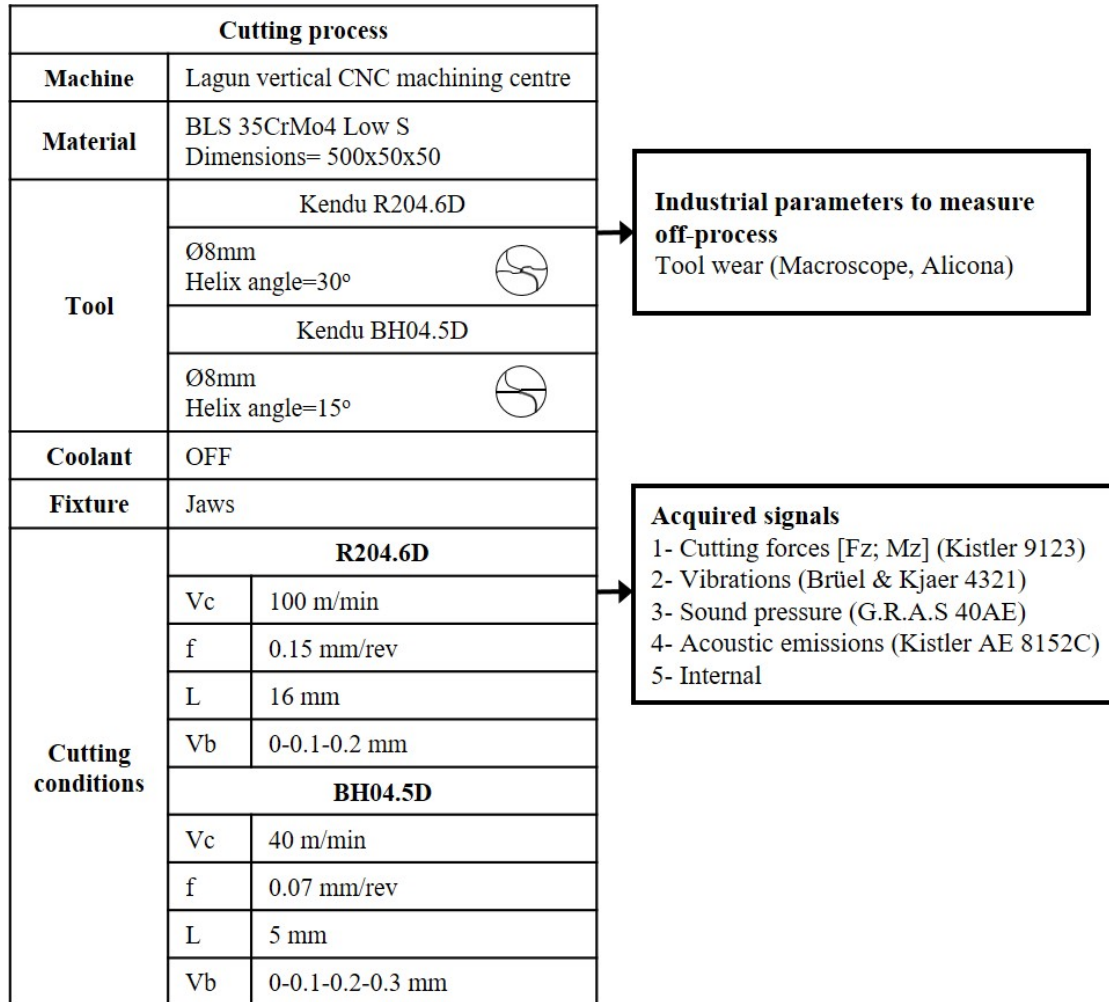


Figure 3.2 Input/Outputs of the proposed experimental set-up on preliminary tests

All the tools were measured before and after performing the trials. These measurements were made in terms of cutting edge geometry. Thus, the flank wear was measured in a Leica DMS1000 macroscope and the cutting-edge radius, and the cutting-edge angle was measured in an Alicona IFG4 3D profilometer. The measurements were taken at the periphery of the cutting edge, where the cutting speed reaches its maximum value, as shown in Figure 3.3 (a-e). In the same Figure 3.3 (b-c-d-f-g-h) can be seen the different levels of wear considered in this work with their cutting edge profile. While in R204.6D the tool flank wear of 0.1mm and 0.2mm was generated, making preliminary tests aside of the experimental test, in BH04.5D tool flank wear was generated by sharpening.

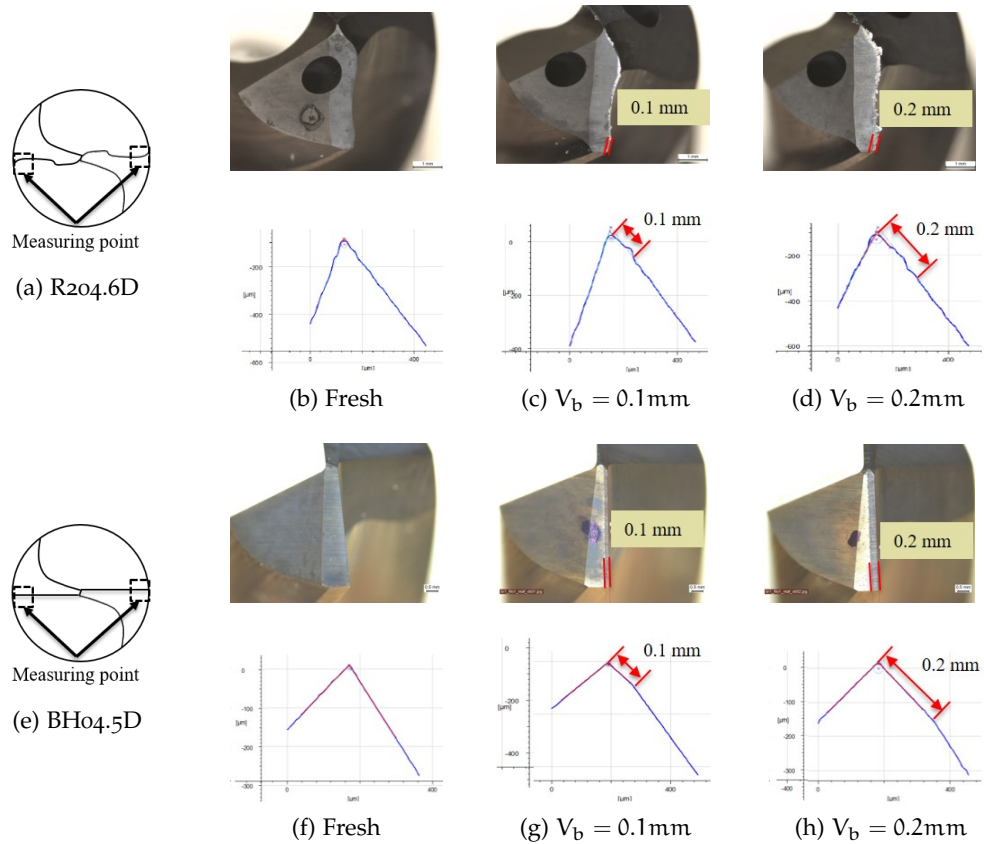


Figure 3.3 Drill bit geometries a-e) General geometry b-c-d-f-g-h) Considered tool wears: fresh, $V_b=0.1$ and $V_b=0.2$ with their cutting edge profile at measuring point

Table 3.3 shows the cutting conditions, tool geometry and tool identification. The main modified parameter was the flank wear, which is considered an input parameter to the cutting operation. Due to the lack of precision in preparing the tools, a unique value was assigned to represent the tool wear. Each of the tools was assigned an approximation of the wear value closest to those considered in this work (0, 0.1, 0.2 mm). The cutting speed, feed rate and hole depth were the same for each type of drill bit. A total of 90 holes were made.

3.2 TESTS ON BLS 35CRMO4 LOW S

In this set-up, some changes were made regarding the external signals. In this case, a Kistler 9123 ① 4-component rotational dynamometer, a PCB J356A45 ② triaxial accelerometer and a Kistler 8152C ③ acoustic emission sensor were installed for signal acquisition. The sound pressure sensor was removed from the set-up because of the inaccurate measurements due to external noise. The accelerometer position is transferred from the workpiece to the spindle, ensuring that there is always the same

Table 3.3 Cutting conditions, cutting edge geometry and number of holes related to drill number

Drill identification		Cutting edge geometry						Cutting conditions				
Drill n°	Drill ID	V_b (mm)		β (°)		r (μ m)		V_c (m · min ⁻¹)	f_n (mm · rev ⁻¹)	L (mm)	\varnothing (mm)	N° of holes
		\bar{V}_b	$\sigma^2 \cdot 10^{-4}$	$\bar{\beta}$	σ^2	\bar{r}	σ^2					
1	R204.6D_1_0	0	0	54.9	0.24	15	2	100	0.15	16	8	5
2	R204.6D_2_0	0	0	53.3	0.6	15	2	100	0.15	16	8	10
3	R204.6D_1_01	0.08	2.2	66.7	12.5	5.5	0.5	100	0.15	16	8	5
4	R204.6D_2_01	0.08	3.1	61.1	2.6	4	0	100	0.15	16	8	5
5	R204.6D_1_02	0.15	5.8	63.8	0.72	3.5	0.5	100	0.15	16	8	5
6	R204.6D_2_02	0.17	26.1	62.7	11.5	11	0	100	0.15	16	8	5
7	BH04.5D_1_0	0	0	79.6	0.32	6	2	40	0.07	5	8	5
8	BH04.5D_2_0	0	0	79.6	0.12	7.5	0.5	40	0.07	5	8	10
9	BH04.5D_1_01	0.14	0.5	91.5	0	7.5	4.5	40	0.07	5	8	5
10	BH04.5D_2_01	0.1	0	92.1	0.02	10.5	4.5	40	0.07	5	8	5
11	BH04.5D_3_01	0.12	2	91.5	0.08	9	2	40	0.07	5	8	5
12	BH04.5D_4_01	0.12	0	90.6	0.08	11	0	40	0.07	5	8	5
13	BH04.5D_1_02	0.28	0	90.2	0.02	11	18	40	0.07	5	8	5
14	BH04.5D_2_02	0.24	0.5	90.2	0.125	11.5	4.5	40	0.07	5	8	5
15	BH04.5D_3_02	0.2	0	90.5	0.125	8	0	40	0.07	5	8	5
16	BH04.5D_4_02	0.28	0.5	89.7	0.4	10.5	0.5	40	0.07	5	8	5
Total												90 holes

distance from the cutting process to the sensor and avoiding collisions between the tool and the sensor. The acoustic emission sensor was placed on the workpiece material. All the internal signals (4) were acquired as in the preliminary tests (i.e. those shown in Table 3.1). Figure 3.4 shows the configuration of the employed set-up.

For the simultaneous acquisition of the signals, the threshold (PFI0) was configured in the acquisition cards (NI cDAQ 9178 and NI USB 6361). When the internal acquisition starts, the external signals will start to be collected simultaneously. An analogue output (ao0 of the CNC) of the machine tool was used to obtain a threshold at the acquisition time. This allows obtaining both internal and external signals simultaneously. The workpiece surface is $Z = 0$ mm, when the position of the tool tip is $Z = 1$ mm, the command is given to start the simultaneous acquisition on the NI USB 6361 and NI cDAQ 9178 acquisition cards. The internal signals of the machine were acquired at the CNC hard disc, while the external signals were acquired in an external PC. Given the deployed simultaneous acquisition system, the dynamometer signals, instead of being acquired together with the internal signals, have been obtained at a higher sampling frequency (10kHz). In this case, in addition to the thrust force and torque signals, the force in the X direction and the Y direction were also acquired. The sampling frequency of the accelerometer signal was also reduced to 25.6kHz.

In this case the set-up configuration did not change much except for the signal acquisition methodology used. The same machine and material BLS35CrMo4 were used. The same tool geometries were used as in the tests described in the previous section (section 3.1) (R204.6D and BH04.5D) and a total of 600 holes were produced with each tool. The cutting conditions have been kept the same for the tool R204.6D ($V_c = 100$ m/min and $f = 0.15$ mm/rev), while for tool BH04.5D have been changed to

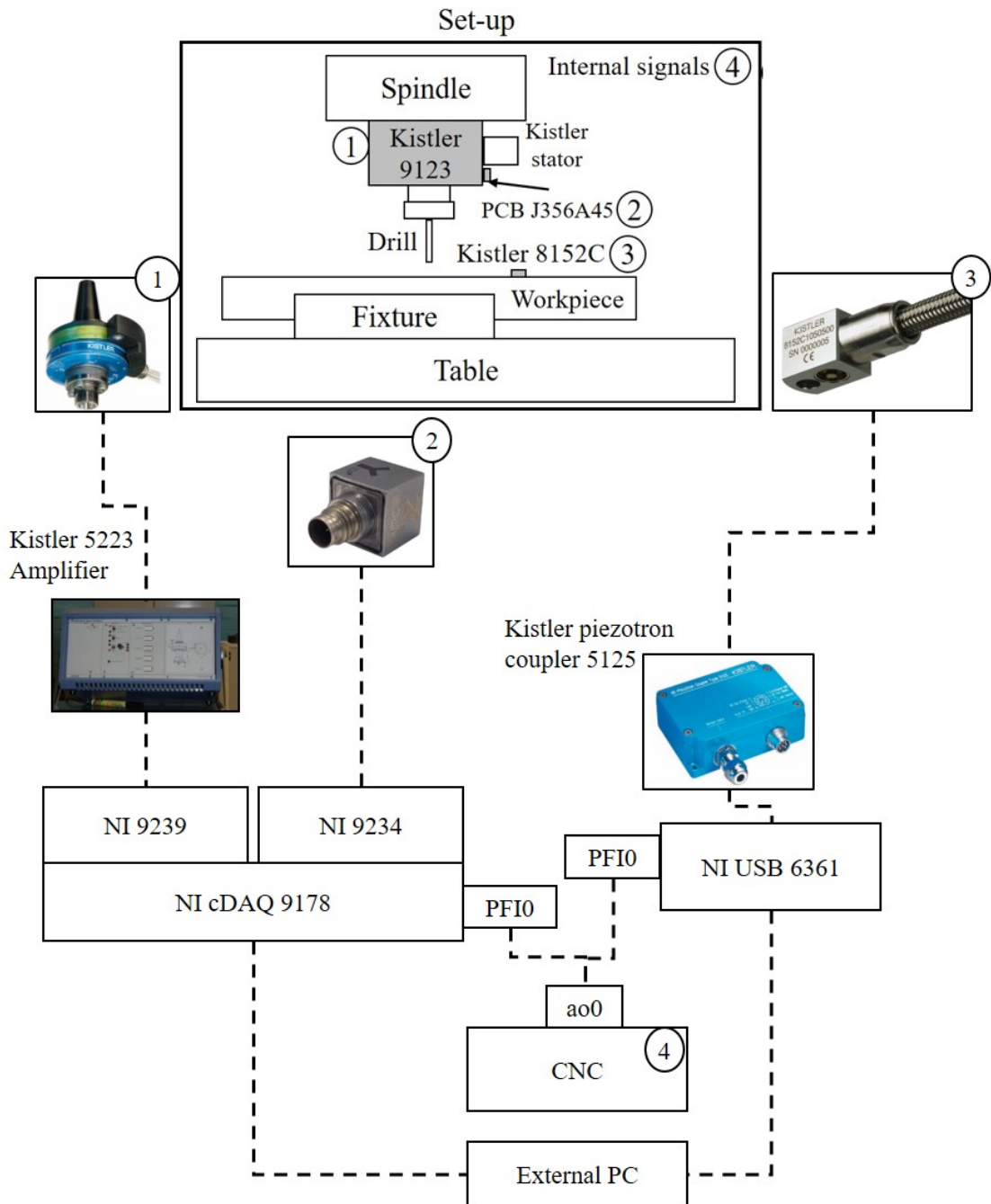


Figure 3.4 Employed set-up configuration and sensor positions and simultaneous acquisition of internal and external signals

$V_c = 70\text{m/min}$ and $f = 0.15\text{mm/rev}$. All the holes were throughout holes with a length of $L = 5\text{mm}$. The conceptual set-up is shown in Figure 3.5.

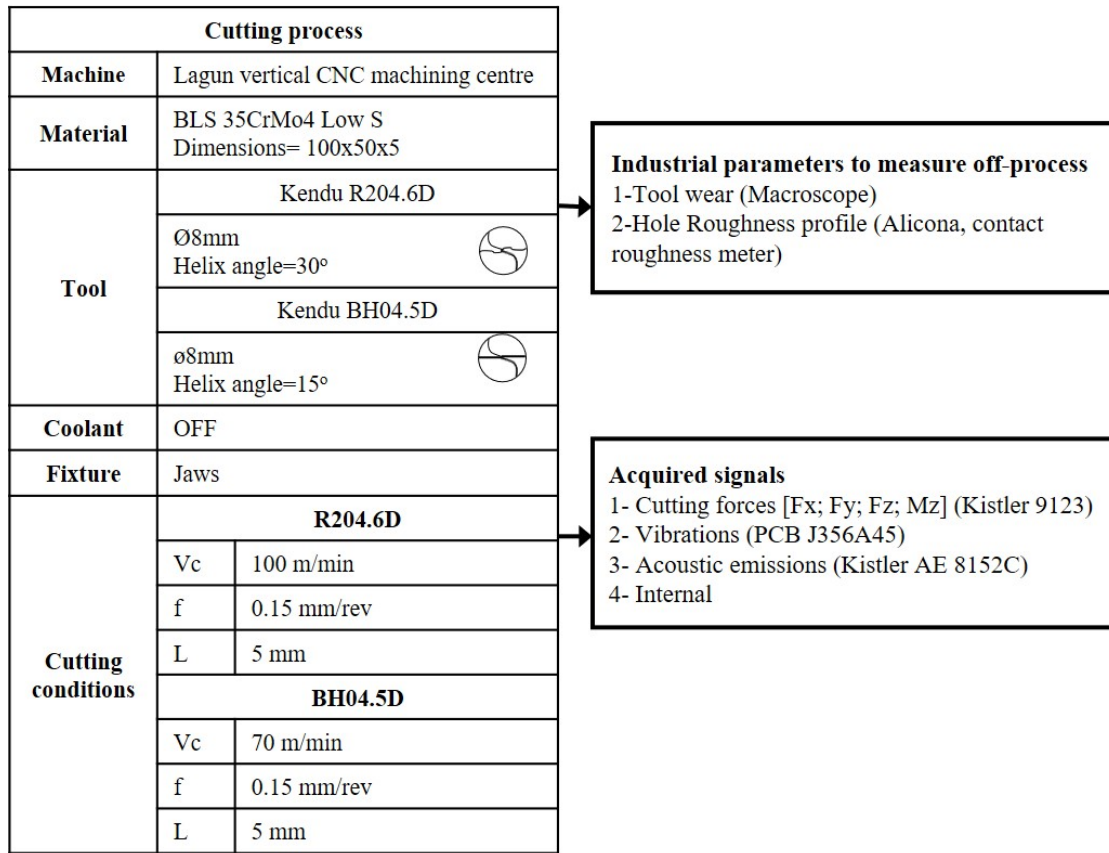


Figure 3.5 Input/Outputs of the proposed experimental set-up on BLS 35CrMo4 Low S steel tests

During tests, the tool was inspected on the lip and outer corner of the point at a periodicity of 20 holes in a Leica DMS1000 macroscope with no evidence of tool wear as shown in Figure 3.6. The workpiece material was a BLS 35CrMo4 Low S steel. This was not expected as the intention was to carry out end-of-life tests. On the other hand, sensor data was obtained from the different data sources over a long time.

3.3 TESTS ON INCONEL 718

In the third batch of tests, the position of sensors was the same as in the previous set-up (section 3.2), and the same system was used to acquire sensor data and internal signals simultaneously.

The tests were performed in the same machine (Lagun vertical machining centre), 3 different tool geometries were used, and 3 repetitions were made with each tool geometry. A total of 9 tools were used. Two of the geometries were used in the two

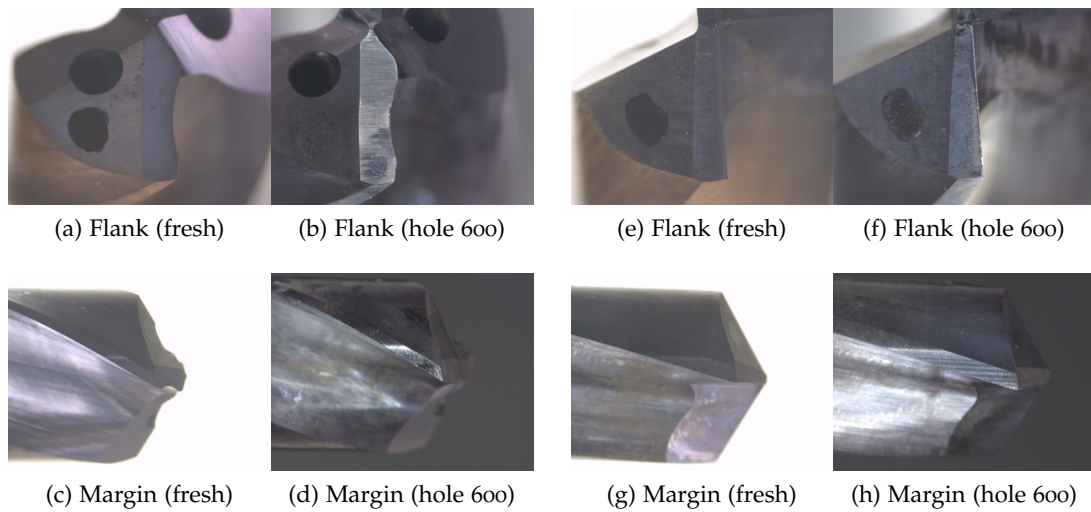





Figure 3.6 Tool condition before and after tests for each tool geometry a-b-c-d) R204.6D tool geometry, e-f-g-h) BH04.5D tool geometry

previous test batches (R204.6D and BH04.5D), the third geometry corresponds to a SUMITOMO solid TiAlN coated carbide tool (MDS080SK) with a helix angle of 30° as shown in Figure 3.7.

Cutting process		
Machine	Lagun vertical CNC machining centre	
Material	Inconel 718	
Tool	3x Kendu R204.6D Ø8mm Helix angle= 30° 	
	3x Kendu BH04.5D Ø8mm Helix angle= 15° 	
	3x Sumitomo MDS080SK Ø8mm Helix angle= 30° 	
	Coolant	ON
	Fixture	Jaws
	Cutting conditions	R204.6D BH04.5D MDS080SK
Vc		15 m/min
f		0.1 mm/rev
L		6.5 mm

Industrial parameters to measure off-process

- 1-Tool wear (Macroscope)
- 2-Hole Roughness profile (Alicona, contact roughness meter)
- 3- Material damage

Acquired signals

- 1- Cutting forces [Fx; Fy; Fz; Mz] (Kistler 9123)
- 2- Vibrations (PCB J356A45)
- 3- Acoustic emissions (Kistler AE 8152C)
- 4- Internal

Figure 3.7 Input/Outputs of the proposed experimental set-up on Inconel 718

The workpiece material was Inconel 718, the chemical composition of this material can be seen in Table 3.4, the following cutting conditions were used for all the repetitions; $V_c = 15\text{m/min}$, $f = 0.1\text{mm/rev}$, $\varnothing 8\text{mm}$ diameter and 6.5mm depth throughout holes for all the repetitions. In contrast to previous tests, these were carried out with coolant.

Table 3.4 Chemical composition of the workpiece material (Inconel 718)

Material	Cr	Fe	Nb	Mo	Ti	Al	Co	Si	Cu	C	Ta	S	Ni
Weight %	18.63	17.66	4.94	2.89	0.92	0.59	0.24	0.13	0.12	0.03	0.01	0.0002	Balance

The tools were periodically measured for every 10 holes. The criteria for the end of the tests was the breakage of the periphery of the tool or flank wear of 0.3mm . The single cutting tool wear measurement was taken as the average between the two cutting edges and estimated as a polynomial of degree 3. R204.6D tool suffered from the beginning, and it was broken in every single repetition during the drilling of the first 10 holes. Therefore, the data concerning this tool was discarded for further analysis. The tool geometries can be seen in Figure 3.8.

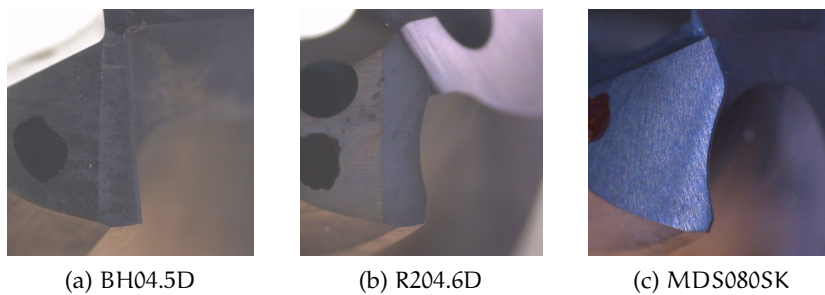


Figure 3.8 Tool geometries used in end-of-life tests on Inconel 718

3.4 SIGNAL CLEANING AND FEATURE EXTRACTION

The data cleaning process was made according to Signal Stable Length Window (SSLW). Figure 3.9 shows the extracted segment. This segment is established from when the tool tip has completely penetrated the workpiece material until it emerges from the bottom. Thus, $\text{SSLW} = \text{HD} - 2\text{TH}$, where HD is the hole depth and TH the tool tip height.

The extraction of information can be done both in the time domain and in the acquired signal frequency domain. In the time domain, the parameters of interest are those statistical features capable of explaining or providing information about the acquired signal. The frequency domain is characterised by representing the frequency components that vary according to the phenomenon to be controlled.

One of the biggest challenges results in the extraction of the features that best represent the analysed process. The features of the acquired signals are statistical indicators that preserve and explain the essential signal elements. On SSLW segment,

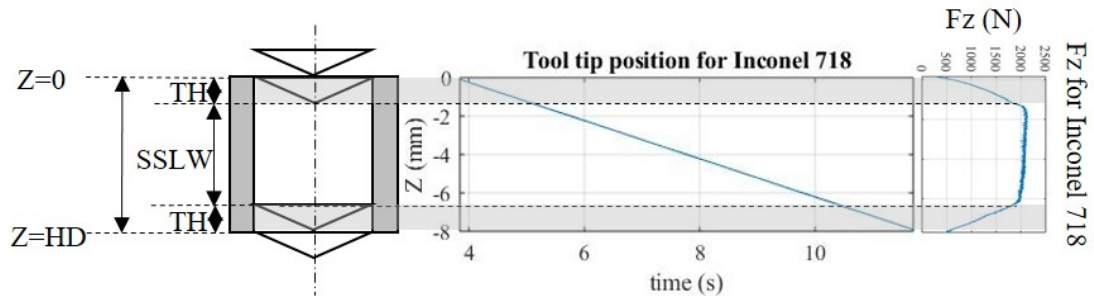


Figure 3.9 Signal segmentation strategy; HD: Hole depth, TH: Tool tip height, SSLW: Signal stable length window. Example for Inconel 718 tests

different statistical features were extracted: mean, RMS, standard deviation, maximum, minimum, kurtosis, skewness and signal amplitude. Additionally, a third level WPT was applied to the external signals, and the same statistical features were extracted from the wavelet packets, Figure 3.10 shows an example for the vibration signal in the Z-axis at Inconel 718.

This part can be seen in Figure 3.12 represented as SSLW. This task was carried out using the tool tip position (POS_Z). Knowing where the tool tip is, and performing a simultaneous acquisition of all the signals, it is possible to obtain the segment belonging to the stable machining zone that runs through the whole hole.

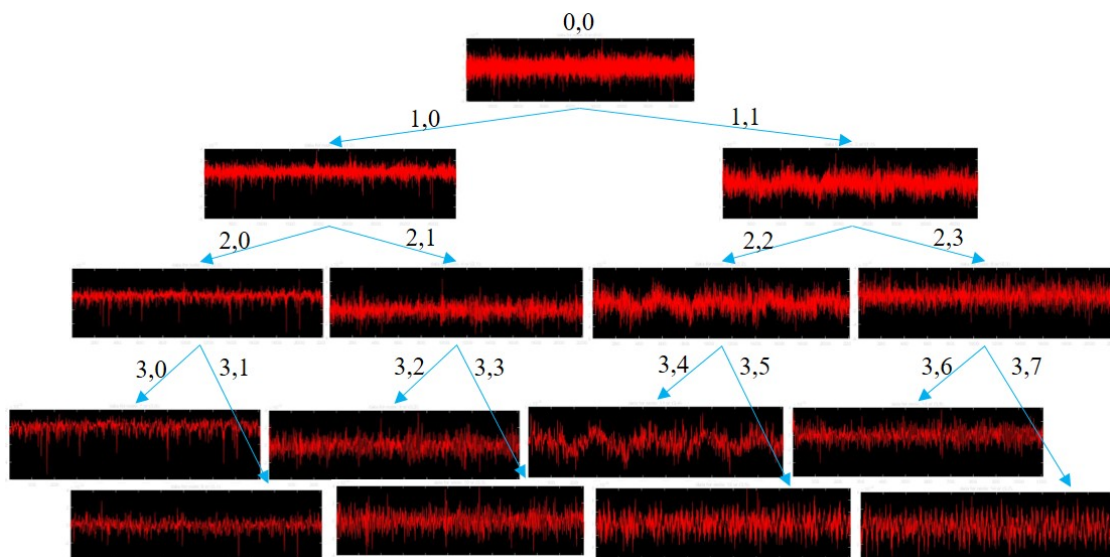


Figure 3.10 Example of Wavelet packet transform obtained from vibrations in Z axis for Inconel 718

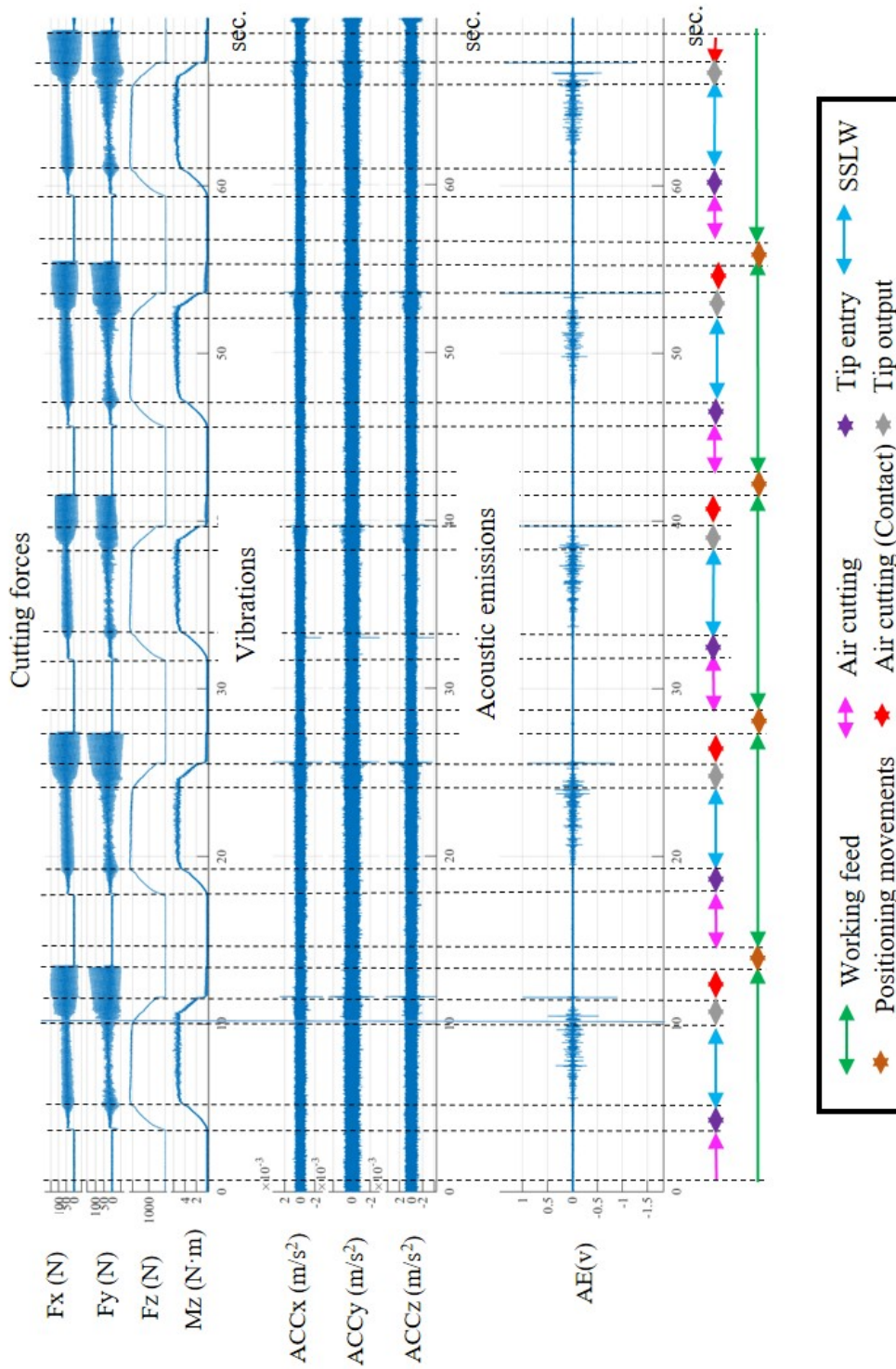


Figure 3.11 Signals acquired by sensors and corresponding drilling states

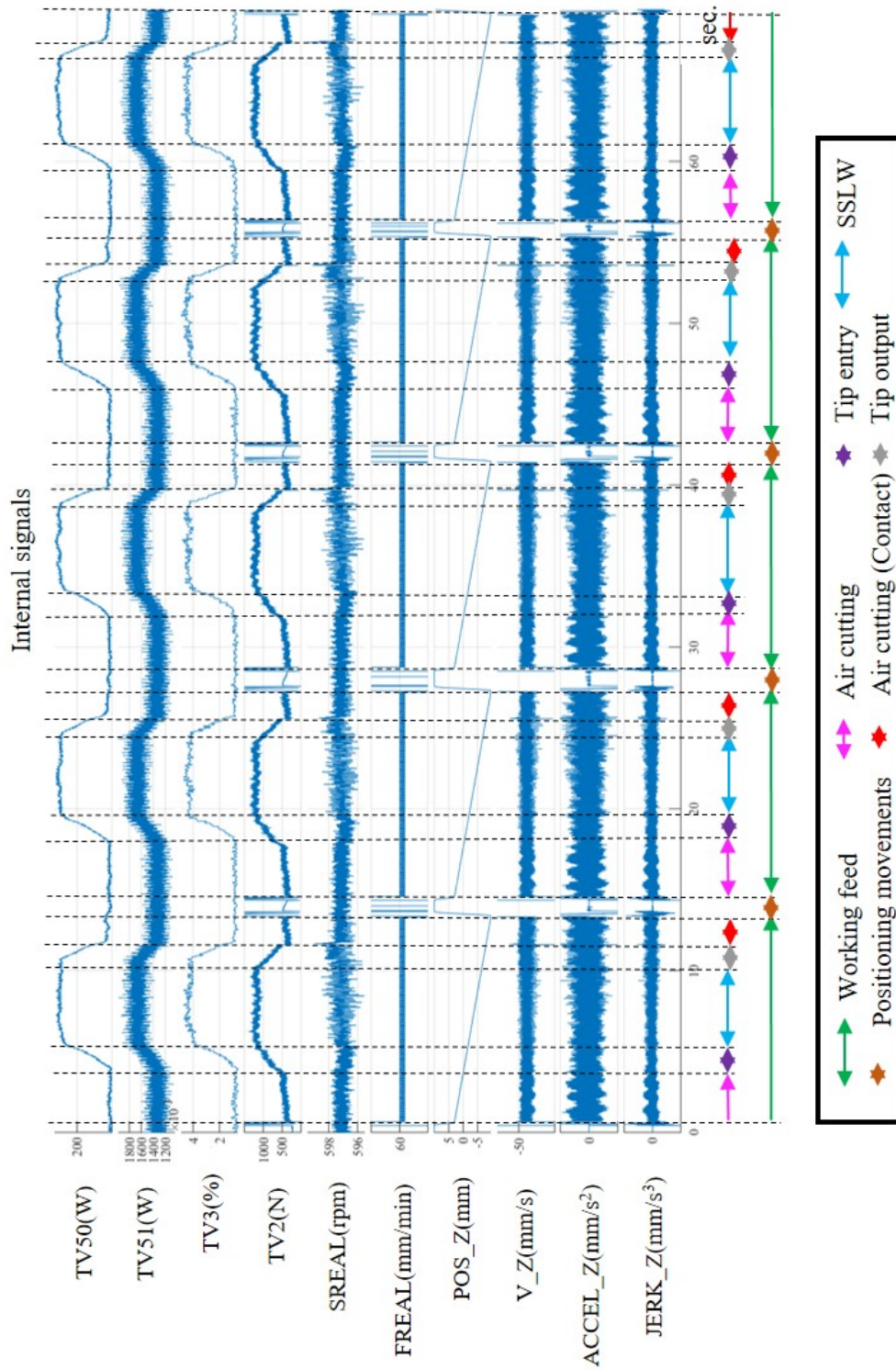


Figure 3.12 Machine internal signals and corresponding drilling states

3.5 SURFACE INTEGRITY DATA COLLECTION

One of the variables to be taken into account is the roughness of the machined surface. These measurements were carried out with the help of a roughness meter and Alicona IFG4 profilometer. The contact roughness meter was used to reference and adapt the Alicona profilometer parameters to the expected roughness ranges. The advantage of Alicona is that it allows obtaining a surface visual profile of the machined material, being able to extract different profiles of a single measurement or to make superficial analysis in 3D. It also makes possible the visual identification of superficial errors that may have occurred during machining.

In addition, the microstructural damage of the material was measured by metallographic analysis for the inspection of the occurrence of White Layer (WL), Heavily Distorted Layer (HDL) or Strain Hardening (SH).

The steps that were followed to analyse the surface integrity are shown in the Figure 3.13. First, the hole was removed by EDM cutting. Then, the hole was cut with a precision cutter to measure the surface generated on opposite sides of the hole in each part cross-section. The parameters used for the roughness measurements were based on ISO 4287 – 1997. A x20 objective, a cut-off wavelength of $\lambda_c = 0.8\text{mm}$ and a measuring width of $r_{tip} = 2\mu\text{m}$. Each of the measurements is 7.16° of the hole perimeter.

One of the two parts was cut out again to obtain two longitudinal sections. Finally, the obtained parts (longitudinal and cross-sections) were crimped together, and thus the material damage caused by the machining process was measured in a cross section $Z = L/2$ and $Z = L$.

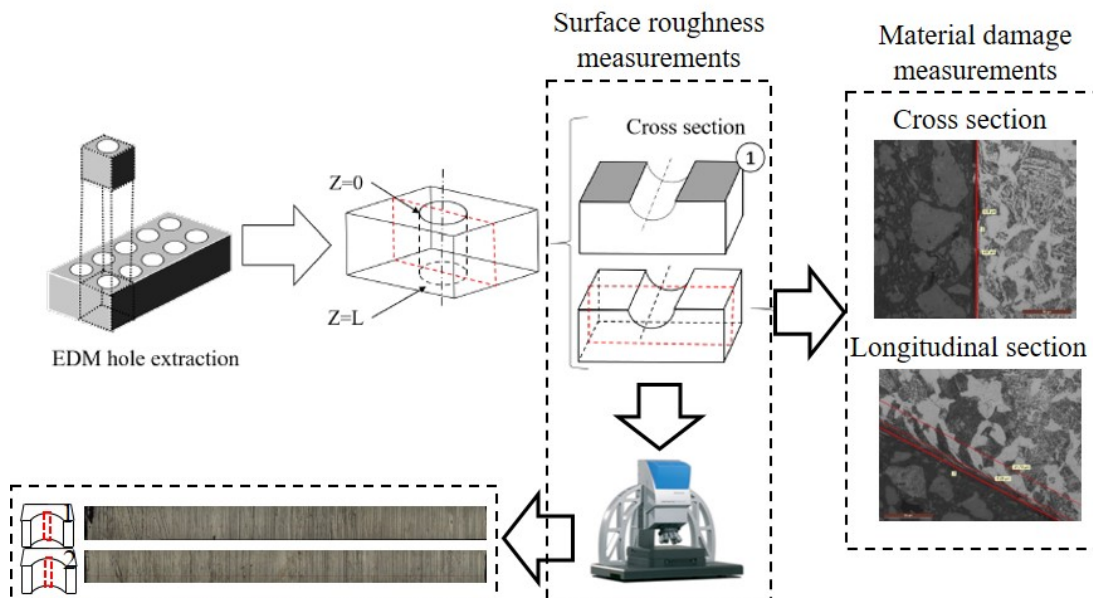


Figure 3.13 Cutting procedure for micro-structural and roughness measurements in EDM and precision cutting machine

TOOL CONDITION CLASSIFICATION THROUGH SIGNAL PERFORMANCE EVALUATION IN BLS 35CRMO4 LOW S STEEL MATERIAL WITH PREVIOUSLY WEAR-INDUCED TOOLS

It is estimated that the non-service time of a machine tool is 20% due to the malfunctioning of the cutting tool (Liang et al., 2004), the incorrect selection of cutting tool geometry and working conditions. This problem can produce a quicker tool wear than expected and thus, can cause components not reaching the expected quality and increased manufacturing costs. Therefore, continuous inspection of the cutting tool condition is essential to reduce machine downtime, reduce the number of components scrapped due to poor cutting tool performance and increase the service life of the tools for more sustainable machining.

Tool wear leads to changes in the micro-geometry of the tool and consequently in the machining performance. The different wear mechanisms observed in cutting (abrasive, diffusion, adhesive, oxidation or fatigue) do not follow a linear wear rate over time. Therefore, the use of suitable sensors for indirect measurement of tool wear is essential to achieve acceptable quality in manufacturing processes.

Tool condition monitoring may be a costly task, and not all sensors can reproduce measured physical phenomena of cutting processes with the same accuracy. Increasing the number of sensors for tool wear prediction allows more data to be obtained. However, this can lead to confusion due to the complexity of the data. During the literature review, it has been observed that works using both individual and fused sensors have obtained successful and not so successful results. However, there is no comprehensive view on which sensors are the most suitable for tool condition monitoring in the different machining operations.

Tool wear is usually measured in the cutting edge formed by the major and minor cutting edge. The most common type of cutting tools wear is flank wear (V_b). The value defining the maximum tool life would be 0.3mm, and this can be reached in drilling after 5 – 20 minutes of machining time.

The main objective in this chapter is to understand the relationship between external and internal sensor measurements and check their capability to detect tool wear under the set-up and experimental plan explained in section 3.1 (Preliminary tests). The replacement of the external signals by the internal signals for tool wear detection

will allow the development of a non-intrusive tool condition detection system. Two drills (R204.6D and BH04.5D) previously ground with flank wear of new tools, 0.1 and 0.2mm in the major cutting edge will be employed to analyse.

The first objective of this chapter is to identify the most sensitive signals to predict tool wear. For this purpose, a statistical comparison of the most widely used signals for tool wear detection was made from the point of view of machine learning. The methodology used identifies the most sensitive signals for both drill bit configurations using the recorded raw data. The second objective is to predict the tool wear of one tool geometry using the model created from the data from another tool geometry. Once the most sensitive signal and the most accurate algorithm were identified, the data acquired using one of the drill bits were used to predict the tool wear of the other drill bit configuration. In this study, only the temporal features of the acquired signals are considered.

4.1 METHODOLOGY

The data used in this chapter corresponds to the setup presented in section 3.1. Therefore, this section explains the data analysis methodology used to compare the different signals acquired during the drilling process to predict the previously induced wear.

4.1.1 Sensitivity analysis through machine learning algorithms

The predictive capacity of the statistical features extracted from the signals was carried out using machine learning algorithms. To that end, the following statistical features were calculated for each signal in the time domain: mean, RMS, standard deviation, maximum, minimum, kurtosis, skewness, variance and coefficient of variation. These statistical features explain the distribution of the signal, so automatic learning is applied to them.

First of all, the data which constituted the dataset was selected. The rows of the dataset are called instances, while the columns are attributes. Table 4.1 shows a generalized dataset of any of the acquired signals. In addition to the calculated statistical features, some process parameters were added to the datasets: cutting speed (V_c), feed per revolution (f_n), drilled depth (L), the cutting-edge angle (β) and the cutting edge radius (r). All these attributes were used to predict the class, which is the tool wear (V_b) measured before the experiments. V_c and f_n variables were obtained acquiring FREAL and SREAL signals, which are penetration rate and spindle speed, respectively acquired from the drilling process.

Overall, eleven datasets were created for each type of drill, one for each of the acquired signals. Among them, the ones with the name TV50, TV51, TV2, Mz, Fz, SP and V_Z were created with 14 attributes and the target or class. In contrast, V(X-Y-Z), ACCEL(X-Y-Z) and JERK(X-Y-Z) were built with 32 attributes and the class. This is

Table 4.1 Generalized example of a signal dataset. Constituted by statistical features extracted from the signal, process input parameters, and the class

Statistical features									Process parameters					C
mean	rms	std. desv.	max.	min.	kurt	skew	var	coef. var	V_c	f_n	L	β	r	V_b
Hole1: 1st instance														
Hole2: 2nd instance														
...														
HoleN: Nth instance														

because signals composed of more than one component were set together in a dataset. The R204.6D drill type datasets had 35 instances, while the BH04.5D type drill datasets had 55, having a total of 90 instances, one for each of the holes made.

Machine learning algorithms were used within a 10 folds cross-validation process. Due to their differences in approximation at the time of generating the models, J48 (Krishnakumar et al., 2015; Ferreiro et al., 2011) (Decision tree), LMT (Logistic Model tree) (Kilundu et al., 2011) (Decision tree with logistic regressions on the leaves), IBk (Krishnakumar et al., 2015; Ferreiro et al., 2011) (Instance-based learning) and NaiveBayes (Probability-based algorithm) available in the Weka platform were tested, each of the strategies followed are briefly explained in the literature review (section 2.2.2.4). 10 folds cross-validation process consists of performing 10 iterations, where in each iteration the data is partitioned in 10 subsets. The analysis (also called training) is performed in 9 of these subsets, while the validation or testing uses the remaining subset. It is repeated 10 times, rotating the validation subset until every instance has been validated once. The same validation process was applied to all datasets.

Further statistical significance of the differences in these algorithm accuracies was also carried out at three different levels of difficulty. From the simplest classification to the more complex one, the three difficulty levels are listed below:

- V1:** In the first version, only the holes made with new drill bits ($V_b = 0\text{mm}$) and those with the maximum flank wear ($V_b = 0.2\text{mm}$) were considered. But, still the classification was in binary mode (false if the hole was made with a new drill bit, true if the hole was made with a worn drill bit)
- V2:** Apart from holes made with new drill bits ($V_b = 0\text{mm}$) and those with the maximum flank wear ($V_b = 0.2\text{mm}$), instances corresponding to holes made with $V_b = 0.1\text{mm}$ drill bit were added. In this case, the classification was also carried out in binary mode (false if the hole was made with a new drill bit, true if the hole was made with a worn drill bit).
- V3:** All flank wear levels were considered, $V_b = 0\text{mm}$, $V_b = 0.1\text{mm}$ and $V_b = 0.2\text{mm}$ in a multi-class classification process.

After the cross-validation process had been applied, a T-test was performed. The sensitivity analysis was performed using the WEKA software experimenter. For the paired T-test, the first signal is the dominant signal, while all other signals are compared against the dominant signal. Therefore, the most accurate signal was chosen as the dominant one. This test aims to obtain the statistical significance of the signals analysed in this work concerning the most accurate signal to predict tool wear. The results of this methodology can be found in section 4.2.

4.1.2 Testing with different drill bits

To test the ability of one model created from one drill geometry to predict the tool wear of the other drill geometry, the models created with the most sensitive signals in drill R204.6D were used to test the wear on instances of both drills.

Figure 4.1 shows a picture explaining the general process. Firstly, statistical features of selected signals and process parameters (V_c , f_n , L , β) along with V_b for R204.6D were used to train ①, and then, the model was tested to predict V_b for both ②.

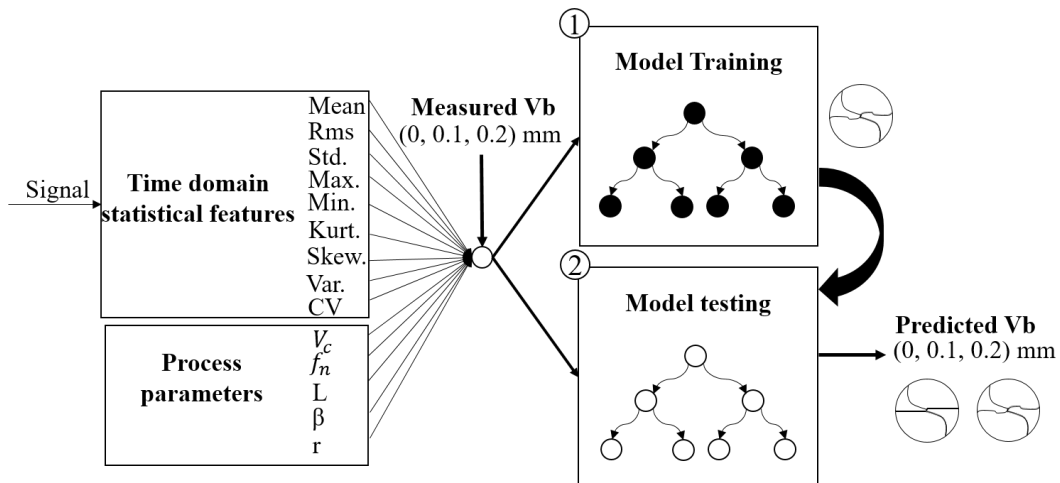


Figure 4.1 Model training and testing using different geometries of drill bits

Further feature extraction processes made us distinguish between three different strategies explained below:

- S1:** Calculates the statistical features of the entire signal for each hole. The signal has been considered from the beginning of the hole to the end of the hole, omitting any part that does not belong to the drilling process.
- S2:** Calculates the statistical features for each millimetre depth of cut, segmenting the signal for one hole in as many segments as mm it has. As both tools are the same diameter, statistical features correspond to the same volume of material removed using this approach. For different cutting conditions, the 1mm window

was calculated using equation 4.1. As a consequence, the number of instances available for the same hole could increase.

$$W_{1\text{mm}} = \frac{f_s \cdot 60}{a_v} \quad (4.1)$$

Where $W_{1\text{mm}}$ is the 1mm window length (Samples \cdot mm⁻¹), a_v is the feed rate (mm \cdot min⁻¹) and f_s is the sampling frequency (Samples \cdot seg⁻¹).

S3: The predictions were made using the predictions made for each segment of the hole in a voting scheme. If the majority of the segments predicted one specific value for V_b , this would be the final decision for the predicted wear in this hole.

4.2 SENSITIVITY OF THE SIGNALS TO TOOL WEAR

As already mentioned, the sensitivity analysis was carried out based on a two-tailed paired T-test using 10-fold-cross-validation 10 times. In the 3 versions proposed (V_1 , V_2 , V_3) and for both types of tools used.

Table 4.2 shows each signal accuracy concerning the algorithm used for the type BH04.5D drill bit. TV2 signal was chosen as the most accurate signal to predict tool wear. Therefore, T paired test is applied against the TV2 signal. In the first version (V_1), only new tools and tools with flank wear were classified. In all signals, at least one or more algorithms fulfil the null hypothesis. In the second version (V_2), although the classification is done in binary form, the degree of difficulty is increased, so the number of signals that fulfil the null hypothesis is considerably reduced. In the last version (V_3), the only signal which fulfils the null hypothesis concerning TV2 that the difference of the means for the accuracy of the paired data is 0, is F_z . About the other signals, none of them is statistically relevant. Therefore, they are not considered as signals with statistical features capable of predicting tool wear in the time domain better than TV2 or F_z do.

Regarding the prediction of the wear for the R204.6D type drill bit, Table 4.3 shows the corresponding results. The signal chosen as most accurate was F_z and the paired-T test was applied against it. As in the previous case, the highest number of signals that accept the null hypothesis is found in the first version (V_1) proposed. However, the same number of successes are not achieved as in the previous case. This may be due to differences in tool geometry. In the second version (V_2), as expected, the number of successes is significantly reduced. In the last one (V_3), results indicate that the TV2 signal is the one that makes most of the algorithms accept the null hypothesis.

The results match both tool geometries. Given the two tool configurations, it can be seen from the results that the straight-edged tool (BH04.5D) has better results for some of the signals. This may be due to geometrical differences between the two tools or the

Table 4.2 Statistical significance of signals in a two tailed paired T-test for accuracy in predicting BH04.5D tool flank wear for three proposed versions for S₁. In white, the signals with the same mean in accuracy as TV2. In grey, the signals with different mean in accuracy

		Internal						External				
		TV2	TV50	TV51	V	ACCEL	JERK	Fz	Mz	AE	Sound	Vib
V ₁	J48	97	97	96	85	88	91	97	90	86	96	86
	LMT	99	91	91	84	84	87	100	96	82	96	84
	IBK	100	94	91	85	86	85	100	99	89	97	89
	NB	100	94	93	91	84	94	100	95	89	95	82
V ₂	J48	98	77	66	81	82	95	97	89	86	98	89
	LMT	98	69	72	85	80	89	100	87	82	95	86
	IBK	100	71	70	84	80	86	100	96	90	90	88
	NB	100	82	75	77	81	90	100	81	83	96	87
V ₃	J48	94	68	55	67	61	78	91	77	70	66	72
	LMT	94	64	69	75	72	80	94	80	73	70	57
	IBK	96	59	63	72	74	72	98	86	78	63	68
	NB	94	77	63	79	72	81	98	75	63	69	53

preparation before testing. The BH04.5D tools were sharpened by the tool manufacturer, leaving more uniform wear along the flank of the tool. As expected, the results showed that the F_z and TV2 signals were the most sensitive when predicting the tool wear.

The location of the hole changes constantly, changing the source of the signal to be measured, so measurements are likely to vary as the hole changes location. In this case, the acoustic emission sensor, the vibration sensor and the sound pressure sensor are affected by this phenomenon.

4.3 MODEL TESTING FOR DIFFERENT TOOL GEOMETRIES

To check the impact of the tool geometry in the models used for tool wear detection, an algorithm was trained using R204.6D drill bits and then tested with R204.6D and BH04.5D tool signals, using for that TV2 and F_z, the most sensitive signals for tool wear detection.

Figure 4.2 shows the proportion of correct and incorrect predictions made for each proposed strategy and considered algorithms. The TV2 signal shows a good performance in terms of the first strategy (S₁). However, despite the percentage of correct results obtained, other classification strategies have been carried out to improve the results. The second strategy (S₂) involves the segmentation of signals and therefore contains a more significant number of instances for both the training and testing phases. The IBk algorithm has optimal performance when training with a more significant number of instances. In the last strategy (S₃), a voting system was added to the previous classification strategy. Comparing S₃ strategy with S₁, it can be seen how it significantly

Table 4.3 Statistical significance of signals in a two tailed paired T-test for accuracy in predicting R204.6D tool flank wear for three proposed versions for S₁. In white, the signals with the same mean in accuracy as Fz. In gray, the signals with different mean in accuracy

		Internal						External				
		TV2	TV50	TV51	V	ACCEL	JERK	Fz	Mz	AE	Sound	Vib
V ₁	J48	96	79	91	60	65	74	99	83	71	54	69
	LMT	99	94	91	64	70	72	100	89	72	72	64
	IBK	96	88	84	73	65	70	100	85	49	73	61
	NB	96	91	91	69	61	57	96	86	66	65	65
V ₂	J48	93	72	73	68	71	71	100	70	58	52	75
	LMT	88	95	87	69	69	73	100	83	53	63	66
	IBK	79	78	76	75	70	71	100	73	58	53	69
	NB	75	77	77	70	69	71	97	72	53	54	68
V ₃	J48	85	56	63	55	59	59	91	63	54	46	65
	LMT	84	90	83	65	60	58	92	74	63	48	67
	IBK	74	69	59	73	56	55	95	63	57	52	67
	NB	87	75	72	74	63	55	91	70	66	38	69

improves all the algorithm behaviour. Thus, the segmentation of signals and the voting system presents better behaviour than the complete signal.

Observing Figure 4.2, the Fz signal shows a worse behaviour regarding the first strategy (S₁) than TV2 signal. As for the second strategy (S₂), the Fz signal appears to have a favourable effect on the number of correctly classified instances. The segmentation of the signal into independent instances seems to affect the precision of the algorithms positively. It does not seem to have the same effect on the TV2 signal with which in this case, the proportion of correctly classified decreases for the first strategy (S₁). As in the first strategy (S₁), in the last strategy (S₃), predictions are made in terms of a hole made. For both signals, the amount of correctly classified increases yields considerable improvement in all the algorithms.

A confusion matrix shows the performance of a classification model, columns represent current values of a target (Measured Vb) and, in rows, the values predicted (Predicted Vb) by a model. the values in the cells represent the number of instances for which the Measured Vb has a certain Predicted Vb. Any value out of the confusion matrix diagonal corresponds to the number of wrongly classified instances. Precision is the fraction of all relevant instances divided among the obtained instances. The recall is the fraction of relevant instances obtained over the total number of relevant instances. The column on the far right of the plot shows the recall for each predicted class, while the row at the bottom of the plot shows the precision for each true class. The cell in the bottom right of the plot shows the overall accuracy.

In S₂, for both signals, an optimal result is achieved using the IBk algorithm. Therefore, this algorithm benefits from the number of instances available for the training

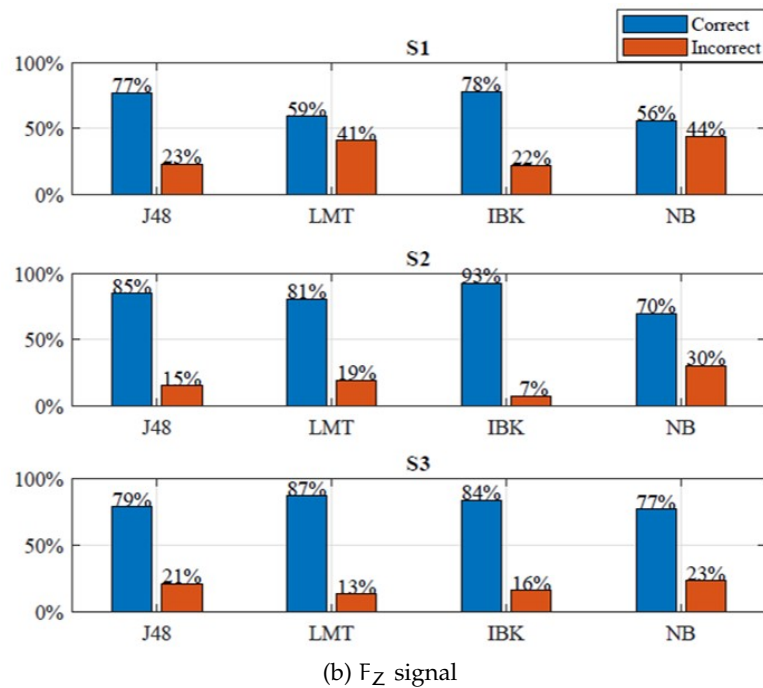
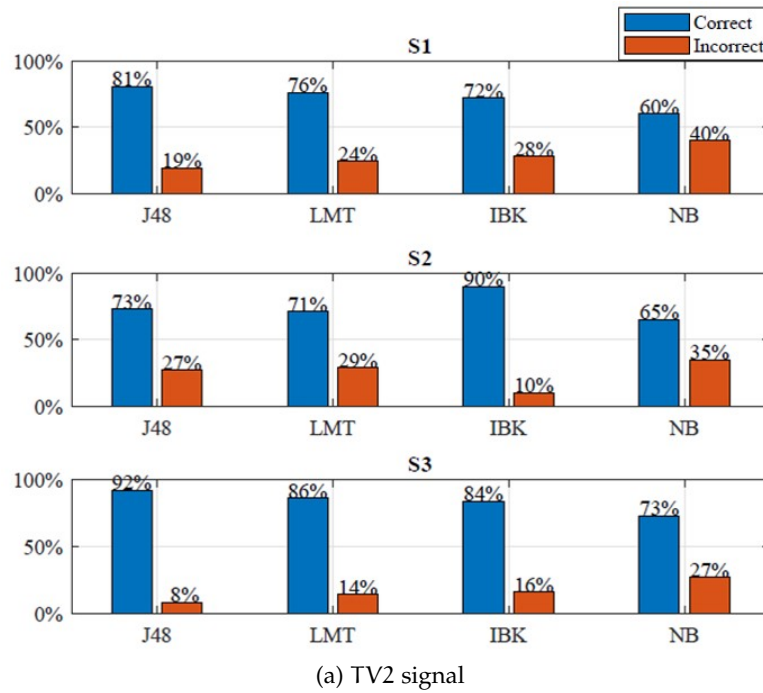


Figure 4.2 Performance of all the strategies and algorithms tested for the third version of dataset (V3)

phase. Figure 4.3 shows the confusion matrices for the predictions made using the IBk algorithm for the S2 and S3 strategies with the TV2 and Fz signals. Using S2 (Figure 4.3 a, c), a good percentage of correctly classified instances is obtained, 90.4% for TV2 and 92.7% for Fz. For both signals in S2, the worst instances at the time of being classified are the worn tools to $V_b = 0.1\text{mm}$. This is because there are overlaps between the proposed labels for wear classification between the different statistical features extracted from the signals. This supposes a challenge when assigning the labels based on the Leica DMS1000 microscope measurements and Alicona profilometer.

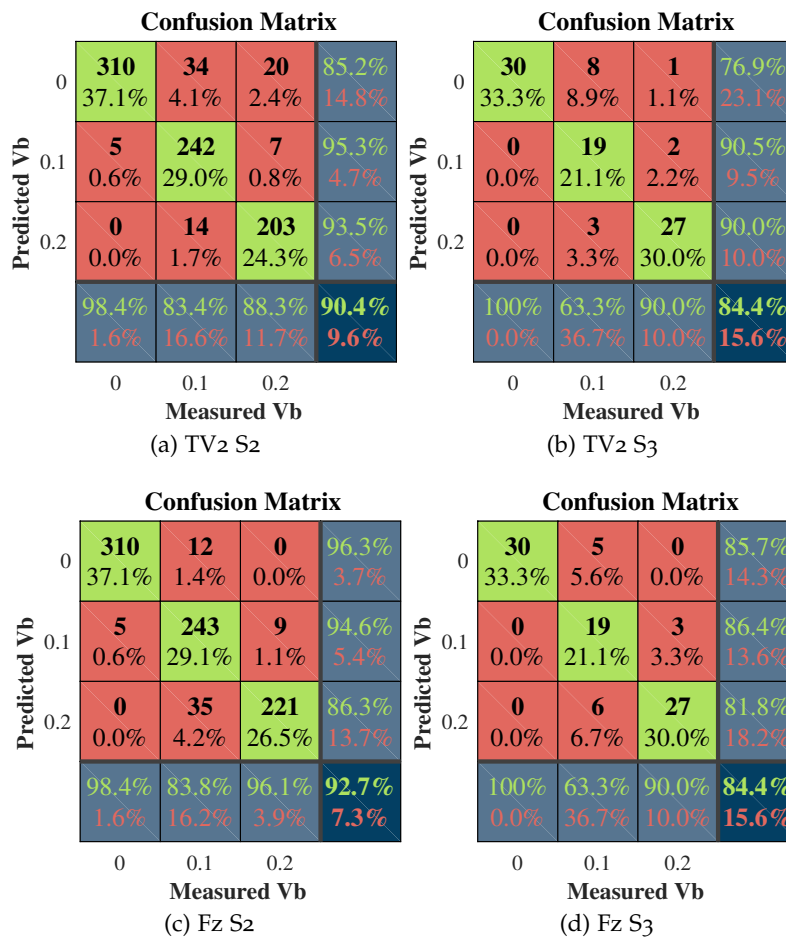


Figure 4.3 Confusion matrices applying strategies 2 and 3 for the IBk algorithm and the TV2 and Fz signals

Figure 4.4 compares the performance of the J48 algorithm using the TV2 for strategies 1 and 3. The improvement is remarkable. The final classification is the same in both strategies. On the one hand, the complete signal (S1) statistical features are taken into account. On the other hand, the classification is made based on the segments obtained (S3). So the difference is in the use that is made of the data obtained from the process. The five holes made with 0.1mm wear tools classified as new tools in S3 belong to a single tool, the tool labelled with ID: BH04.5D_2_01. It is the tool with the lowest

wear measured directly, making it difficult to distinguish them from the new ones. In general, it can be observed that precision and recall increase from S1 to S3. The number of false positives is reduced, observing a considerable improvement when performing a classification based on signal segments. This way of handling the data allows increasing the probability of success of a certain model since, in addition to the current output, it takes into account previous system outputs.

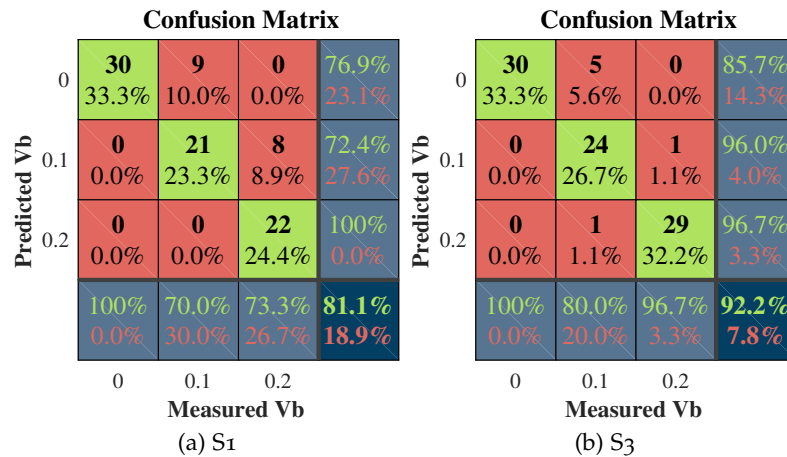


Figure 4.4 Confusion matrix: J48 algorithm for TV2 signal

4.4 CONCLUSIONS

In this chapter, a comparative study of the sensibility of the most commonly used signals for tool wear detection in drilling processes has been carried out. Tests were performed with two different types of drill bits under a complete setup in which multiple signals were acquired to evaluate their sensitivity to tool wear in drilling processes. The methodology used has made it possible to identify the most sensitive signals in the time domain, with the TV2 (Z-axis motor torque) and Fz (thrust force) being the most sensitive to tool wear. Besides, based on the algorithms training phase with the TV2 signal of R204.6D type drill bits, tool wear of BH04.5D type drills has been predicted.

- The methodology used has made it possible to identify the variables of interest for this study. This methodology has helped identify the extent to which the different signals collected can detect tool wear.
- Once the sensitivity analysis has been carried out, it has been possible to see that the most affected signals by tool wear are the Fz and the TV2. With the above mentioned signals, quite precise results have been achieved by predicting tool wear with both types of drill bits.

- The model created with the TV2 signal from R204.6D drill bits shows great accuracy in predicting tool wear for BH04.5D drill bits. The F_z signal does not perform as well as TV2 in this respect.
- The strategy of segmenting the signals with a 1mm hole depth window means an increase in the number of instances available for the algorithm training phase. In both cases (TV2 and F_z) a better result is achieved with the added voting system than in the first pursued strategy.
- The signals have been analysed in the time domain. They need to be analysed further to obtain accurate indicators of tool wear. It is necessary to apply different treatments to the signals to obtain better indicators for detecting tool wear.
- With this work, it has been possible to identify the TV2 signal as the most predictive internal signal for a combination of a given material, two different tool geometry types, and two different cutting conditions for tool wear level prediction.

TOOL FLANK WEAR CURVE RECONSTRUCTION IN END-OF-LIFE TESTS AND SUBSEQUENT PREDICTION OF TOOL BREAKAGE IN INCONEL 718

According to Dudzinski et al. (2004), broaching, turning and drilling are the main operations in the manufacture of discs for gas turbine engines for the aerospace industry. These parts are produced from Nickel-based superalloys due to their resistance to high temperatures and corrosion. Chen and Liao (2003) reported that during the machining of Nickel-based alloys, the tool wear is accelerated, being the abrasion wear the mechanism that predominates in the initial stages. Changes in tool microgeometry due to wear, cause increased friction on the machined material and may cause alterations to the surface integrity. Thus, accurate indirect measurement of tool condition is of great importance on Nickel-based superalloys.

Among the several strategies for detecting tool wear, given the continuous nature and continuous data acquisition from the cutting process, it makes more sense to perform it as a continuous value prediction. The most common algorithm for this purpose is linear regression. However, its insufficient capacity and primitiveness are often not appropriate to real-life data. Therefore, algorithms that attempt to model the non-linear wear of cutting tools must be used.

Sudden changes in the tool, such as the loss of part of the cutting edge, can lead to inadequate cutting and thus produce poor quality surfaces. It is essential to assess the risk of irreversible damage to the tool for premature tool change to prevent machining errors while monitoring the progression of wear. Each sensor or acquired signal can give a different response, so it is essential to evaluate the predictive capability of the acquired signals for a given target before selecting the sensors that can best meet the monitoring requirements of the cutting process.

In the previous chapter, the capacity of each collected signal for the classification of previously induced tool wear levels has been shown. The thrust force (F_z) and the Z-axis motor torque (TV2) signal were the most accurate signals when classifying different tool wear levels. However, the use of dynamometer signals practicability is debatable. O'Donnell et al. (2001) showed that cutting torque is the most informative signal regarding tool wear in the drilling process. Its use in industrial environments is not practical due to a lack of adaptability and geometrical limitations, both measured

by a three-dimensional dynamometer or rotational dynamometer. Thus, the TV2 signal, which corresponds to the Z-axis motor torque of the machine, shows more practical behaviour.

In this chapter, the main objective is to evaluate each sensor signal to reconstruct the wear curve in end-of-life tests and the capacity to detect tool periphery breakage on Inconel 718. The data from the set-up explained in section 3.3 (Tests on Inconel 718) is used. Besides, the effect of wear on surface roughness and material damage has also been analysed. The results indicate that reconstruction of the wear curve is possible using both the internal machine signals and the sensors used. With the exception of the acoustic emissions, which in the analysis carried out and among the features of the extracted signals do not show sufficient capacity to reconstruct the wear curve. The signals acquired with the rotational dynamometer and the internal signals show a greater ability than the signals acquired with the accelerometer to detect tool breakage. Furthermore, roughness and material damage measurements do not show a trend with respect to tool condition.

In the following sections, first, the methodology used is explained, which involves estimation of the class (target) to be predicted. Then, the methodology for feature selection for tool wear prediction, selection of the algorithm that best fits the data for target prediction and modelling based on the selected variables for estimation of the risk that a tool may break are shown. The results obtained for each sensor or sources of information considered in this study are then presented, and finally, the conclusions are outlined.

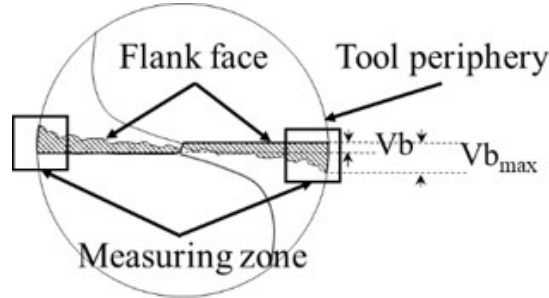
5.1 METHODOLOGY

The presented methodology follows several steps with many interdependences and basically will follow the following steps: a) gather data on different tools and many different sensors and internal signals for the drilling process, adding data relative to the wear, b) extract features and select the best ones using indistinctly data from different tools, c) choose the best algorithm between five of them using indistinctly data from different tools d) use knowledge from steps b and c to predict wear curve on each tool data separately, e) use knowledge from steps b and c to predict wear/breakage on each tool data separately.

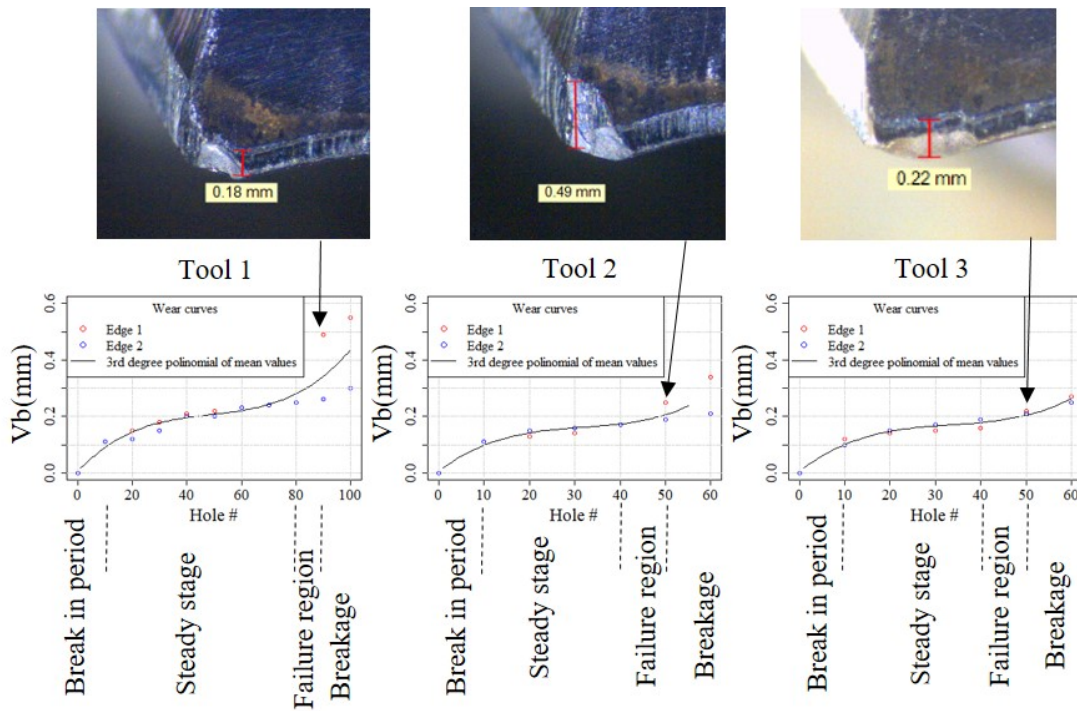
5.1.1 *Wear target estimation*

During the machining process and for the reconstruction of the wear curve, the tool condition at each cutting edge was measured with a periodicity of 10 holes at the periphery of the major cutting edge. (Figure 5.1 a)), calculating then an average of the wear on the two cutting edges. Once the process was finished, using those estimated wear values, a curve was adjusted through a 3rd degree polynomial fitting shown in

Figure 5.1 b). The first hole in which a sign of breakage was observed on the periphery of the tool (intersection point between the minor and major cutting edges) was also identified and labelled. The criteria to finish the test was to achieve a wear value of $V_b = 0.3\text{mm}$ or 10 holes after the first breakage point was identified.



(a) Measuring area



(b) Wear target estimations

Figure 5.1 Tool wear measurements, third-degree polynomial curve and tool breakage measured hole for each repetition

The third-degree polynomial curves estimated from the tests measurements are used as the target for ML algorithms. During the evolution of the wear curve, four phases have been identified. (i) **Break-in period**, is the phase where the tool wears out quickly. At the beginning of the process, for every tool, a $V_b = 0.1\text{mm}$ is reached after the first ten holes (ii) **Steady stage**, the tool wear curve is smoothed and continues growing

progressively. (iii) **Failure region**, where the tool suffers some breakage in the cutting edge (iv) **Breakage period**, one or both cutting edges have suffered irreversible damage.

During the tests, it has been observed in tool 1 that the first occurrence of a breakage appears in between holes 80-90, while in tools 2 and 3, the breakage was observed between holes 40-50, in the Figure 5.1 shown as failure region. Even though the holes were drilled under the same cutting conditions, the breakage on the periphery of the tool has been observed at different periods in the tool life.

Once the polynomial adjustment has been made, the datasets created with internal and external feature values and the estimated wear curve are joined as shown in Figure 5.2 (Complete feature spaces) for each information source, including data for every tool.

5.1.2 Feature selection

The non-relevant or redundant features must be removed from each data-set corresponding to one unique sensor for predicting the wear curve. The final decision regarding feature selection has been carried out through a voting scheme between different methods; a) two embedded methods, b) a wrapper method and c) a filter was used. The methods selected for this step have been Elastic Net (EN), Sequential Backward Search (SBS), Random Forest (RF) and Information Gain (IG).

In this work every decision on selecting (1) or not (0) of a feature by an algorithm is added. In this way, each feature can obtain a maximum score of 4 (all the algorithms considered this specific feature as a candidate for tool wear curve prediction) and a minimum of 0. The selected features for each one of the sensors have been those that would have only features that obtain a score greater or equal to 3. Ensuring that different criteria have been involved in the selection of these features (At least 3 of the algorithms consider the selected features as relevant). The feature selection process is represented in Figure 5.2 and was carried out per each sensor separately.

Specific names are used for the rest of this work to specify these reduced feature spaces. Dynamometer Reduced Feature Space (FC_RFS), Accelerometer Reduced Feature Space (ACC_RFS) and INT_RFS were obtained. In the case of acoustic emissions no relevant features have been found using these algorithms.

5.1.3 Algorithm selection and flank wear curve prediction

The performance of algorithms predicting tool wear curve values was validated before and after the previous variable selection process using 10 fold 10 times cross-validation. This way, the behaviour of the selected algorithms for the prediction of the wear curve is evaluated under different input feature space.

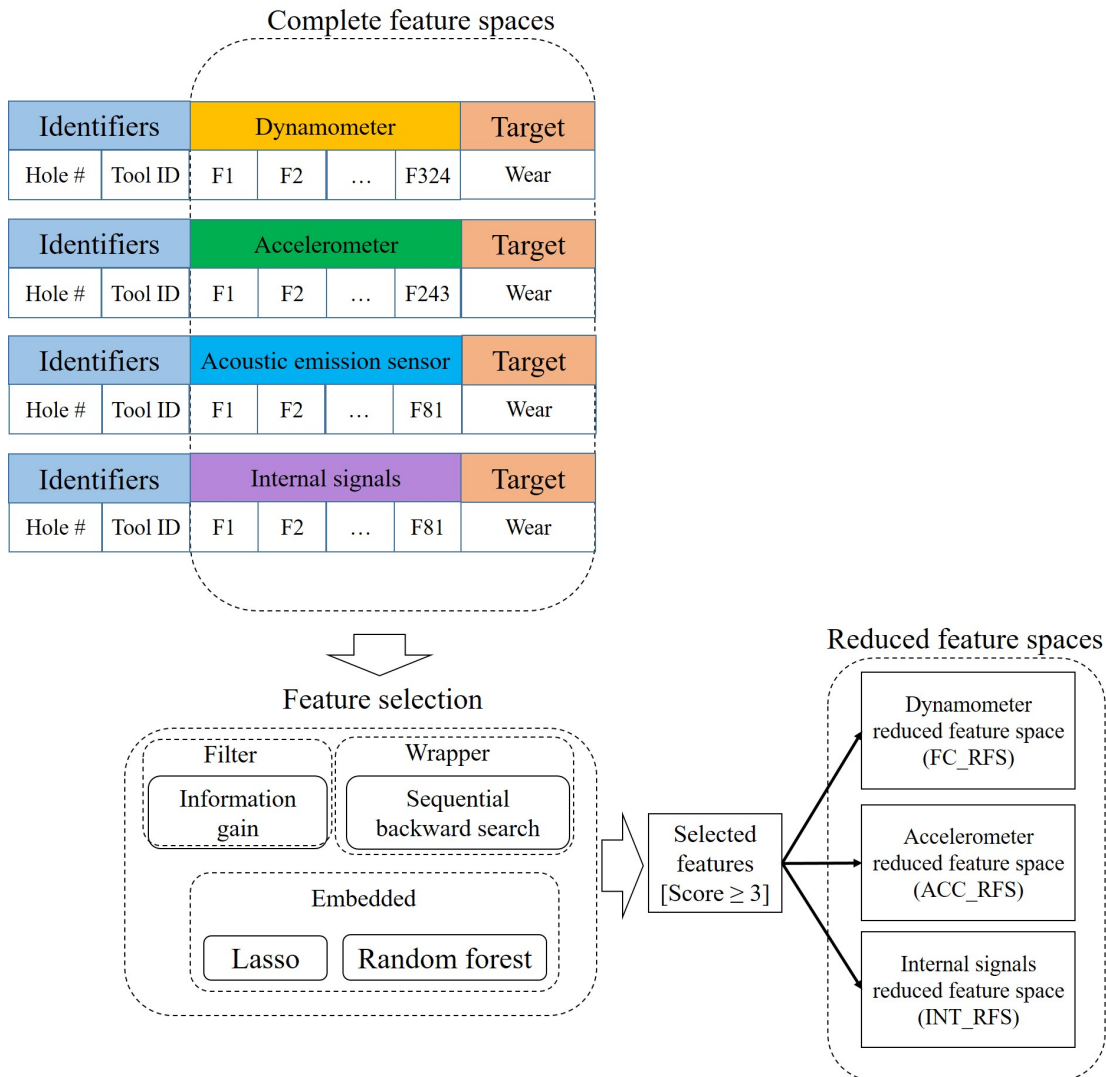


Figure 5.2 Complete feature space, feature selection process and reduced feature spaces for each sensor

The algorithms tested for the prediction of the wear curve were: (i) neural network (NNET) (Artificial neural network), (ii) generalized linear model (GLM) (a generalization of linear regression), (iii) K nearest neighbour (KNN) (Instance-based learning), (iv) M5 model rules (M5) (Decision tree) and (v) Linear SVM for regression (Support vector machine).

To evaluate the capacity to reconstruct the wear curve in another tool, the bootstrap sampling method was used. This method consists of selecting a part of the training data (training samples) and another part for testing (out-of-bag samples) (Kuhn, Johnson, et al., 2013). The training samples belong to two of the three tools used, and the out-of-bag samples belong to the remaining tool. After three iterations, the prediction of the wear curve for the three tools used in this work are obtained.

To measure the behaviour of the model fitting against the measured tool wear curve, Mean Absolute Error (MAE), Root Mean Square Error (RMSE) and R square (R^2) metrics were used, the mathematical notations of these metrics can be found in Table 5.1.

The results obtained from the comparison of the different algorithms in the whole feature space and in the reduced feature space for each sensor can be consulted in section 5.2 as well as results from bootstrapping process.

Table 5.1 Model evaluation metrics used for regression

Model evaluation metrics
$MAE = \frac{1}{n} \sum_{j=1}^n y_j - \hat{y}_j $
$RMSE = \sqrt{\frac{1}{n} \sum_{j=1}^n (y_j - \hat{y}_j)^2}$
$R^2 = 1 - \frac{\sum (y_j - \hat{y}_j)^2}{\sum (y_j - \bar{y}_j)^2}$

5.1.4 Tool breakage prediction

In this section, the selected features during the feature selection process have been used to detect tool periphery breakage according to the levels established in section 5.1.1. The algorithm used to create the models for detecting the tool periphery breakage was the Logistic Model Tree (LMT) because of its simplicity of interpreting the obtained model and identifying the features that evaluate the probability of risk to suffer a tool periphery breakage. LMT combines logistic regression models with tree induction. A logistic model tree is a standard decision tree structure with logistic regression functions in the leaves (Landwehr et al., 2005). Unlike conventional decision trees, the leaves have an associated logistic regression function instead of a class label. At the leaves of the LMT, the functions $F(x)$ and $-F(x)$ determine the class membership probabilities by equations 5.1 and 5.2.

$$\Pr(\text{without failure}) = \frac{e^{F(x)}}{e^{F(x)} + e^{-F(x)}} \quad (5.1)$$

$$\Pr(\text{tool break}) = \frac{e^{-F(x)}}{e^{F(x)} + e^{-F(x)}} \quad (5.2)$$

Where $F(x)$ is a linear model for the leave with the next form,

$$F(x) = a_0^j + \sum_{k=1}^m a_{v_k}^j v_k \quad (5.3)$$

Where a_0^j is the intersection and $a_{v_k}^j$ is the coefficient of the corresponding v_k feature.

Figure 5.3 shows the logistic regression curve of probabilities for each case. $-F(x)$ determines the probability of a tool failure (label=1), while $F(x)$ determines the probability of a tool without failure (label=0).

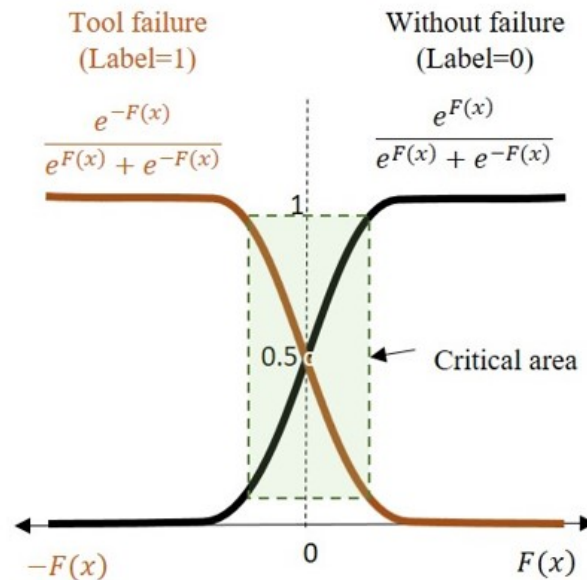


Figure 5.3 Model interpretation through logistic model trees

When $F(x)$ has a high value, the probability of belonging to class 0 "without failure" is higher. When $F(x)$ is closer to 0, the probability of belonging to one class or another is more doubtful, so this is the critical area or failure region, where a tool can go from a "without failure" (label:0) to a "tool failure" (label:1) state.

Before the final model is created that will predict the presence of breakage, several previous stages are used to impute values on unknown data that gradually control the uncertainty. A description of these stages can be seen in Figure 5.4. The results obtained from this methodology can be consulted in section 5.3.

- S1** The first stage only considers those instances correctly labelled for each separate tool, without considering the failure region data where the tool is known to have suffered substantial and irreversible damage. This allows us to observe that the created model effectively differentiates a bad state from a good state of the tool.
- S2** The second stage uses instances of every tool together without considering the failure region, as in the first stage.
- S3** The third stage trains the models with the well-labelled instances of a single tool and tests them using instances on the failure region. In this way, the labels obtained in this stage are used for value imputation for instances in the failure region.

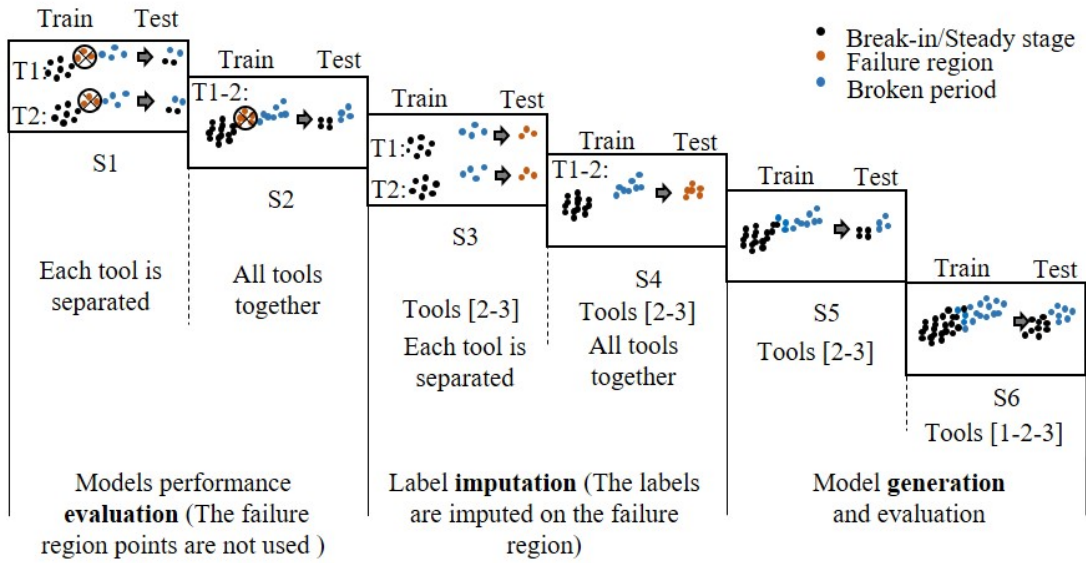


Figure 5.4 Followed methodology for tool breakage detection

- S4** The fourth stage follows the same steps that stage S3 but considering all the instances of all the tools together. This will also help in imputing the appropriate labels to the instances on the failure region.
- S5** With all the instances labelled, in stage S4, training in 70% of the data and testing in the remaining 30% on tools 2 and 3. To ensure the early detection of tool breakage the first instances of this period have been introduced in the test partition.
- S6** The last stage follows the same steps that in S5 but with data of all tools 1,2,3 together.

There are more holes not presenting a breakage in the periphery of the tool than those that are performed with tool breakage, resulting in an imbalanced data problem. Having a few instances that belong to the tool failure class makes it more difficult for the algorithm to learn what the decision boundary is. The training data has been balanced using the Synthetic Minority Oversampling Technique (SMOTE) algorithm to avoid this problem. It chooses two neighbouring minority instances and creates a new minority instance based on selected ones (Chawla et al., 2002). This allows the models to better generalize in terms of the minority class; in this case, the class that indicates tool failure. According to Luque et al. (2019) for this type of imbalanced classification, the best evaluation metric results in the use of Matthews Correlation Coefficient (MCC) since it takes into account the equilibrium ratios of the four categories in the confusion matrix (TP: true positives, TN: true negatives, FP: false positives, FN: false negatives) as seen in equation 5.4. The value of this metric is distributed from -1 to 1 , being -1 the total disagreement between the predicted and the real value, 0 means random predictions and 1 the total agreement between the predicted and the real value.

$$MCC = \frac{TP \cdot TN - FP \cdot FN}{\sqrt{(TP + FP) \cdot (TP + FN) \cdot (TN + FP) \cdot (TN + FN)}} \quad (5.4)$$

5.2 TOOL FLANK WEAR CURVE MODELLING THROUGH MACHINE LEARNING ALGORITHMS

The reconstruction of the wear curve has been carried out with the features of each of the sensors separately. The results obtained with the acoustic emission signal have not been presented since they do not show any predictive capacity concerning the tool wear curve.

Different algorithms have been compared for each of the sensors used in this study. The models obtained were compared using the entire feature space and the reduced feature space for each sensor. In the case of the accelerometer, the reduced feature space is ACC_RFS. These features are those obtaining a score greater or equal to 3 during the feature selection process.

ACC_RFS = [WP5_ACCx_rms, WP5_ACCx_max, WP7_ACCx_rms, WP8_ACCx_rms, WP2_ACCy_rms, WP4_ACCy_kurt, WP3_ACCz_rms, ACCx_max, ACCx_skew, WP2_ACCx_rms, WP2_ACCx_max, WP2_ACCx_peak, WP4_ACCx_rms, WP6_ACCy_rms, WP7_ACCy_mean, WP3_ACCz_max, WP7_ACCz_kurt, WP8_ACCz_max, WP8_ACCz_peak]

The complete feature space obtained from the accelerometer was of 243 features, once the process of feature selection was applied, this number was reduced to 19 features. Figure 5.5 shows the results obtained by cross-validation with the features obtained from the accelerometer sensor. On the one hand, the entire feature space results are shown (243 features). On the other hand, the results obtained after applying the feature selection process (ACC_RFS).

All the algorithms create a model with better behaviour in terms of the accelerometer with the reduced feature space. Considering the complete feature space, the KNN algorithm obtains the best result. Besides, all the other algorithms obtain a p – value < 0.05 concerning KNN, which indicates a statistically significant worse behaviour than KNN. Once the feature space is reduced, the best result is obtained with the NNET algorithm. KNN and M5 obtain the same mean in model performance with a p – value > 0.05 , indicating that there is not a statistically significant difference between the results obtained by each of these algorithms.

In the features obtained from the dynamometer, the feature space was reduced from 324 to 10 features (FC_RFS). Thus, having a considerable feature reduction.

FC_RFS= [WP2_Fy_rms, Fx_mean, Fx_kurt, Mz_mean, WP2_Fy_min, WP2_Fy_skew, WP2_Fy_peak, WP2_Mz_rms, WP2_Mz_kurt, WP2_Mz_skew]

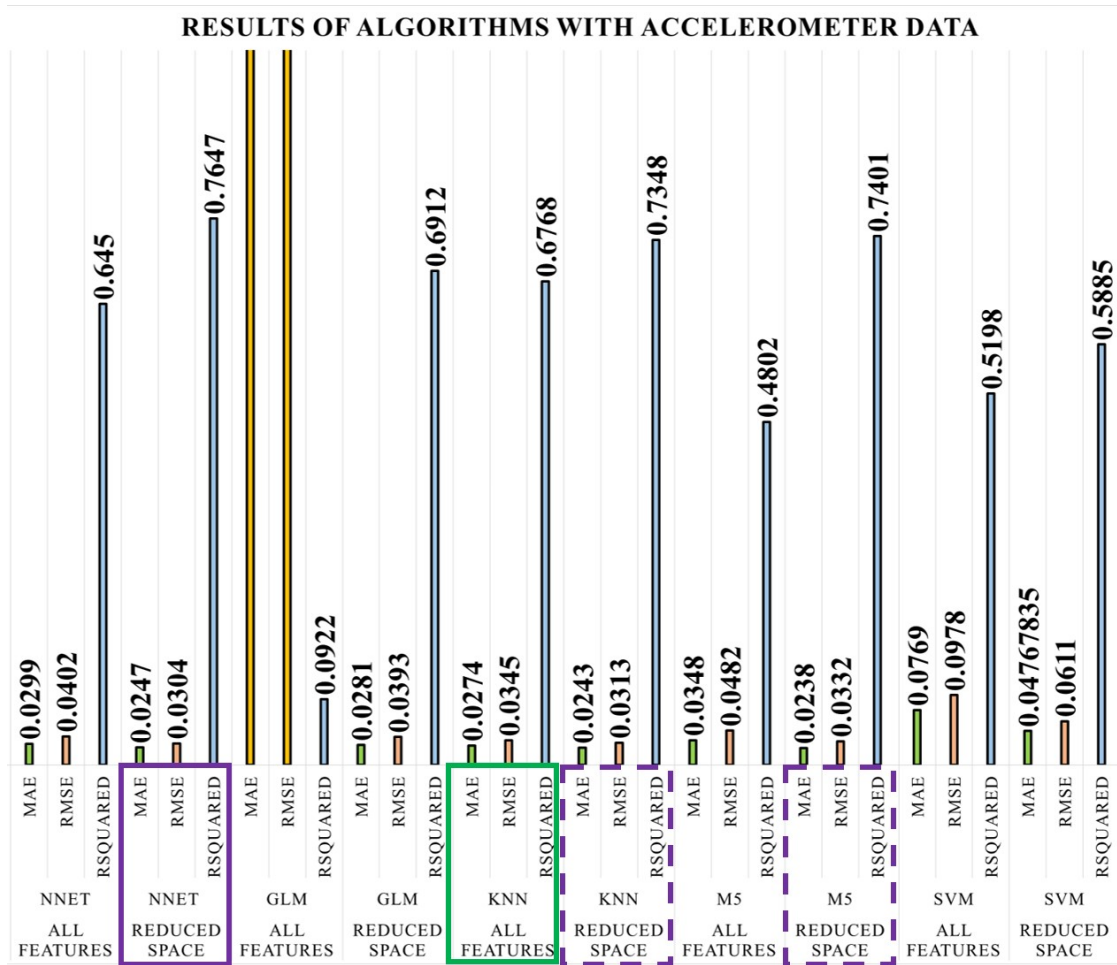


Figure 5.5 Results of algorithms using the accelerometer signals applying 10 folds 10 times cross-validation in all feature space and reduced feature space for each algorithm. The green square indicates the best result achieved with all feature space. The purple square indicates the best result achieved with the reduced feature space and the dashed line purple square indicates those algorithms with the same mean in results to the NNET algorithm ($p - \text{value} > 0.05$)

The results obtained with the signals acquired with the dynamometer can be seen in Figure 5.6. In this case, the same procedure as with the accelerometer has been followed. In the figure below, the metrics of all the algorithms used can be seen for the cross-validation process for both complete feature space and reduced feature space.

Similarly, as with accelerometer signals, better results were obtained in the reduced space using the FC_RFS features. The most remarkable improvement is obtained in the GLM algorithm using the reduced space of the features obtained from the signals of the dynamometer. The best result is obtained with the reduced space of features using the NNET algorithm, KNN and M5 algorithms show similar behaviour, as they do not show a statistically significant difference.

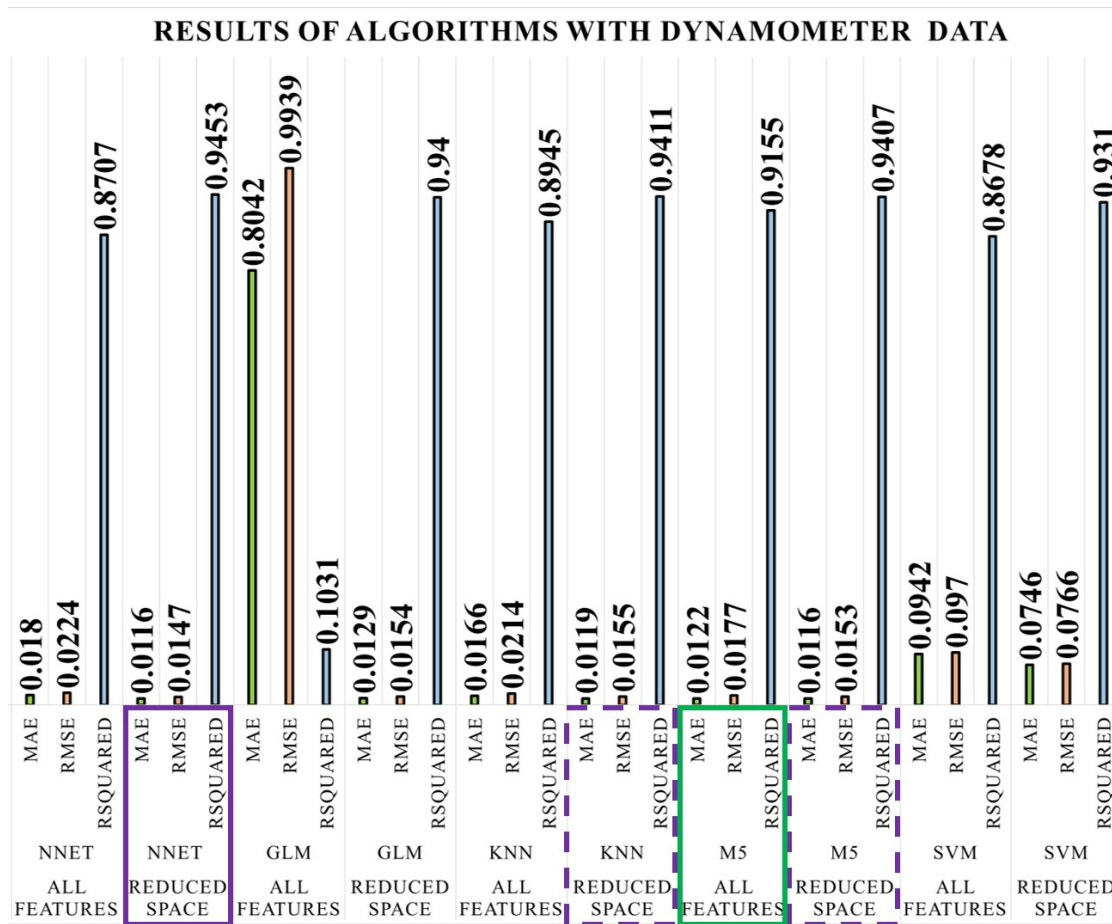


Figure 5.6 Results of algorithms using the dynamometer signals applying 10 folds 10 times cross-validation in all feature space and reduced feature space for each algorithm. The green square indicates the best result achieved with all feature space. The purple square indicates the best result achieved with the reduced feature space and the dashed line purple square indicates those algorithms with the same mean in results to the NNET algorithm (p – value > 0.05)

Regarding CNC internal signals from 81 feature space, it was reduced to 16 as seen in INT_RFS feature vector.

INT_RFS= [TV50_mean, TV50_max, TV50F_std, TV51_max, TV2_mean, TV2_min, Vz_std, Vz_skew, TV50F_max, TV2_max, Vz_rms, Vz_max, JERKx_kurt, TV3_max, TV3_min, CV3_min]

Figure 5.7 shows the results obtained from the cross-validation process of all feature space obtained from the CNC provided signals. It should be noted that obtaining these signals does not require installing any sensor and is, therefore, the most practical option for creating tool condition monitoring systems.

In the case of internal signals, the KNN algorithm is the one that obtains the best results for the reconstruction of the wear curve in the reduced feature space INT_RFS.

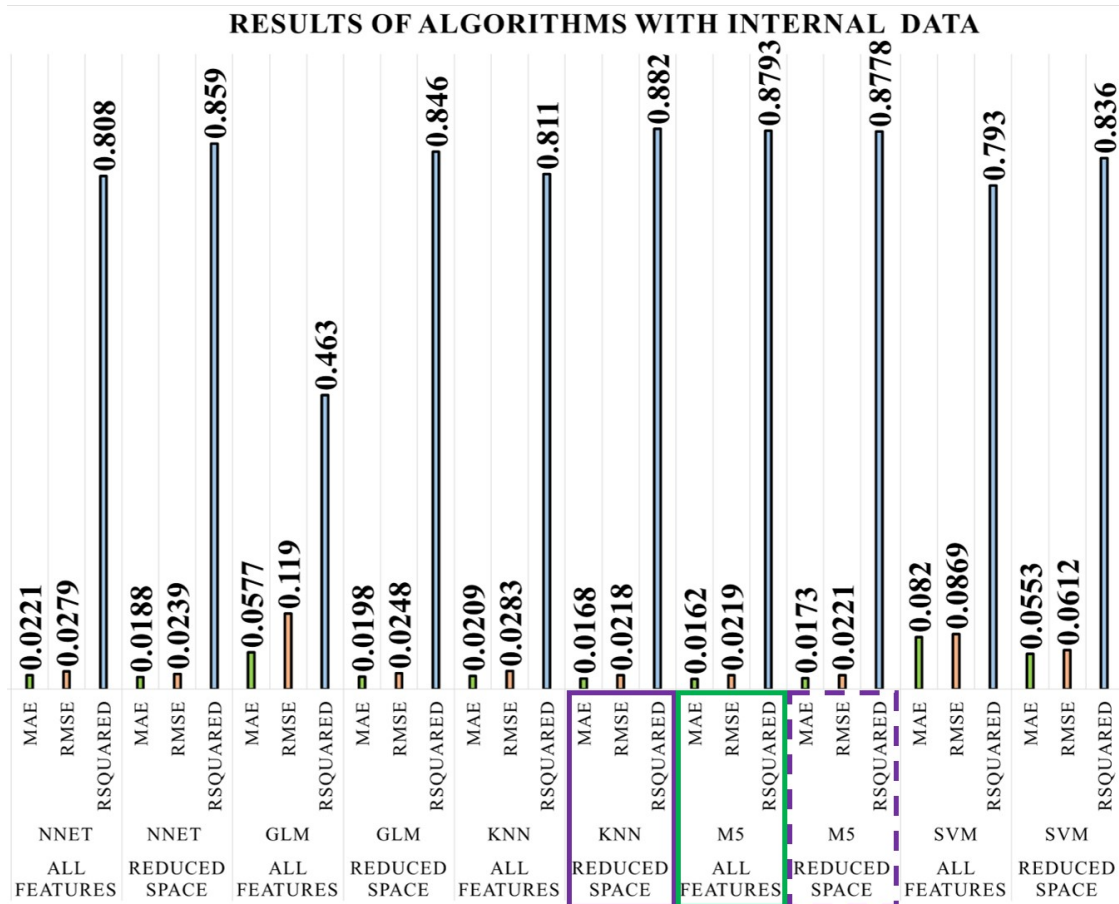
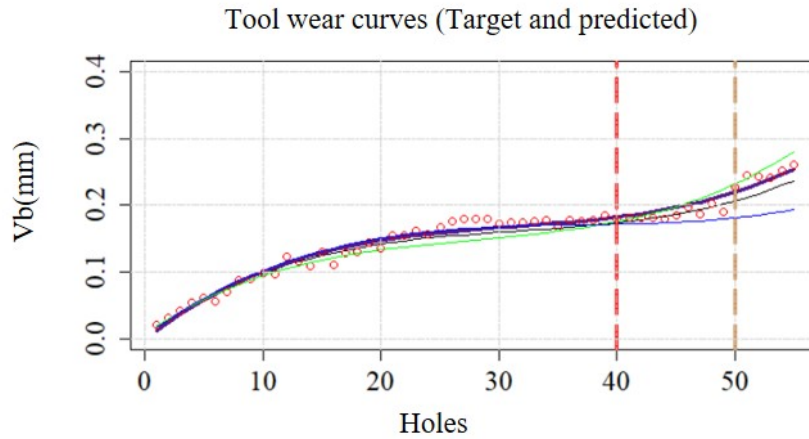


Figure 5.7 Results of algorithms using the internal signals applying 10 folds 10 times cross-validation in all feature space and reduced feature space for each algorithm. The green square indicates the best result achieved with all feature space. The purple square indicates the best result achieved with the reduced feature space and the dashed line purple square indicates those algorithms with the same mean in results with respect to NNET algorithm ($p - \text{value} > 0.05$)

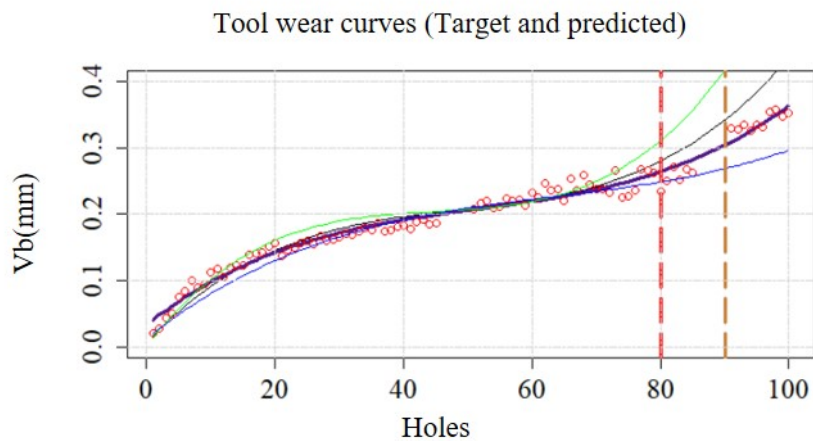
It is possible to reconstruct the wear curve both by using external signals of vibrations and cutting forces and the machine internal signals. Slightly worse results are obtained with the accelerometer, although acceptable for environments that do not have the possibility of collecting internal signals or installing a dynamometer. Although several works show the ability of acoustic emissions to monitor tool wear, in this work, no trend has been observed that would allow good results to be obtained with this sensor.

Once the comparison of the different algorithms has been made, it has been decided to use the NNET algorithm to reconstruct the wear curve. The process has been carried out by training with two of the tools and testing on the remaining tool. Table 5.2 shows the results obtained for each of the repetitions carried out. The best and worst tool wear reconstruction performances with each sensor reduced feature space can be consulted in Figure 5.8, Figure 5.9 and Figure 5.10. The tool in repetition number 1 shows tool breakage later than the other 2 repetitions performed, but even so, the

algorithm generalises well by keeping the predictions within the wear ranges of both cutting edges using the data on each of the sensors analysed.



(a) MAE= 0.009; RMSE= 0.012; R2= 0.985



(b) MAE= 0.017; RMSE= 0.023; R2= 0.982

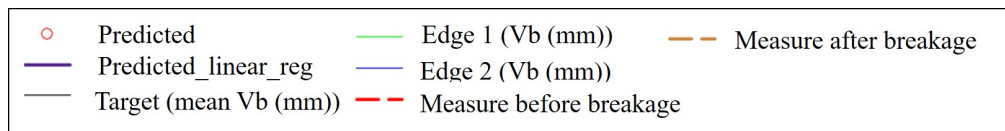
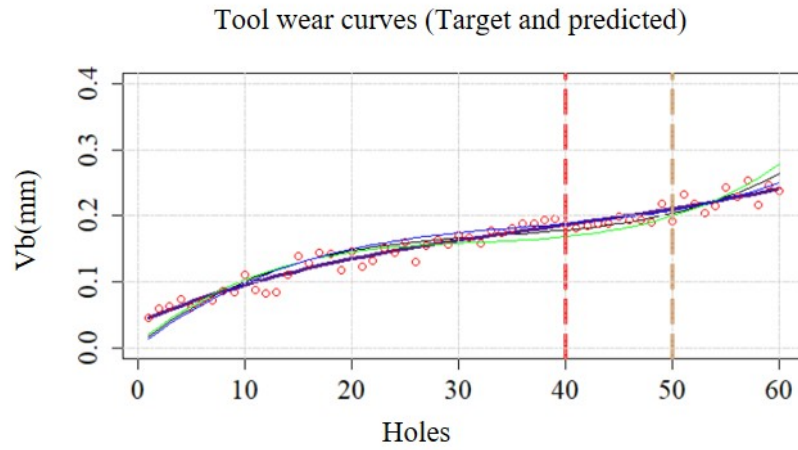
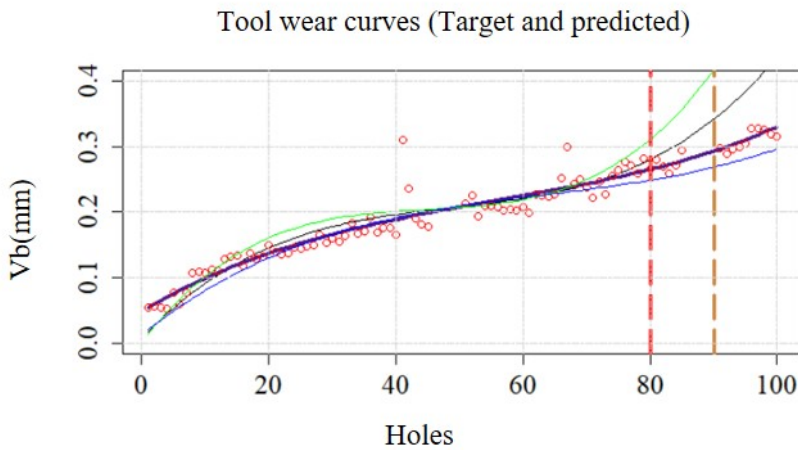


Figure 5.8 Best and worst tool wear prediction performances for each sensor reduced feature space from bootstrapping process on geometry MDS080SK for FC_RFS a) training samples: tools 1 and 3, test on tool 2, b) training samples: tools 2 and 3, test on tool 1

The internal signals obtain the best result since the lowest average error is obtained among the three tools. The cutting force signals tend to obtain a similar result with slightly higher errors. The accelerometer is, in this case, the one that obtains the worst



(a) MAE= 0.012; RMSE= 0.015; R2= 0.960



(b) MAE= 0.023; RMSE= 0.034; R2= 0.944

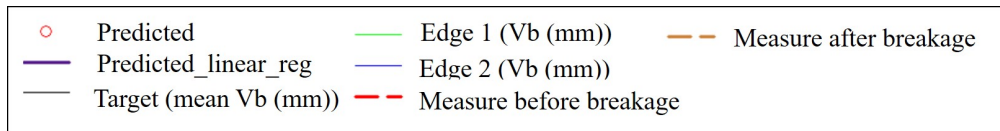
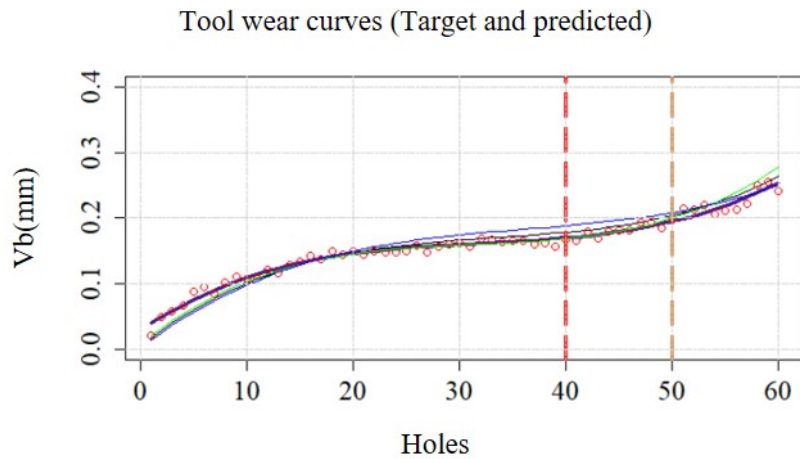
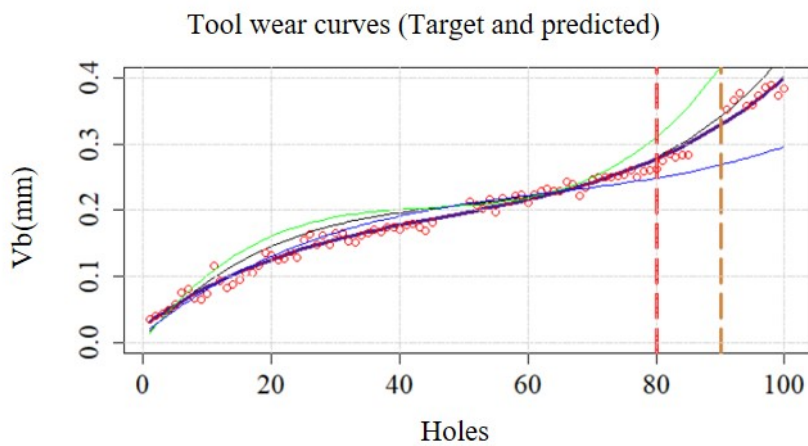


Figure 5.9 Best and worst tool wear prediction performances for each sensor reduced feature space from bootstrapping process on geometry MDS080SK for ACC_RFS a) training samples: tools 1 and 2, test on tool 3, b) training samples: 2 and 3, test on tool 1



(a) MAE= 0.009; RMSE= 0.011; R2= 0.986



(b) MAE= 0.015; RMSE= 0.018; R2= 0.987

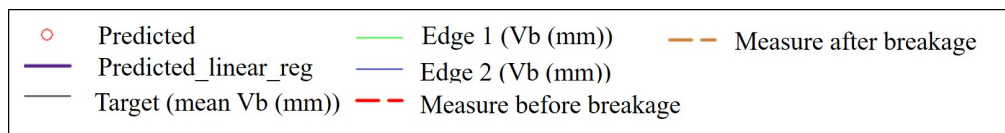


Figure 5.10 Best and worst tool wear prediction performances for each sensor reduced feature space from bootstrapping process on geometry MDS080SK for INT_RFS a) training samples: tools 1 and 2, test on tool 3 b) training samples: tools 2 and 3, test on tool 1

Table 5.2 Model performance from bootstrapping process for each tool and the mean value of considered metrics for each sensor reduced feature space

	FC_RFS			ACC_RFS			INT_RFS		
	MAE	RMSE	R ₂	MAE	RMSE	R ₂	MAE	RMSE	R ₂
Tool 1	0.017	0.023	0.982	0.023	0.034	0.944	0.015	0.018	0.987
Tool 2	0.009	0.012	0.985	0.014	0.016	0.951	0.012	0.014	0.966
Tool 3	0.013	0.018	0.955	0.012	0.015	0.960	0.009	0.011	0.986
Mean	0.013	0.017	0.974	0.016	0.021	0.951	0.012	0.014	0.979

result with the highest error. However, in general terms, good results are obtained in all cases, and all options are valid for a tool wear curve reconstruction.

5.2.1 Model performance in BH04.5D tool geometry

Once the behaviour of the model on the same tool geometry has been observed, the model created with one tool geometry has been tested for the reconstruction of the wear curve on another tool geometry. Specifically, it has been trained with all the data of the MDS080SK geometry and tested on the 3 repetitions made on BH04.5D.

In the first repetition carried out with the BH04.5D tool geometry, there were some errors during signal acquisition, so that the data relevant to the first 15 holes made in the first repetition are not available. Therefore, it has been decided to use the data of BH04.5D as test data for a model created from the MDS080SK geometry. Table 5.3 shows the results obtained from the model created for each of the subsets selected in the variable selection stage. Each of the metrics was obtained with respect to the average between the wear of the two cutting edges.

Table 5.3 Model performance on BH04.5D tool geometry after training on MDS080SK in each sensor selected feature space

	FC_RFS			ACC_RFS			INT_RFS		
	MAE	RMSE	R ₂	MAE	RMSE	R ₂	MAE	RMSE	R ₂
Tool 1	0.054	0.070	0.653	0.019	0.024	0.837	0.061	0.066	0.89
Tool 2	0.026	0.031	0.968	0.065	0.072	0.916	0.054	0.064	0.954
Tool 3	0.046	0.072	0.838	0.042	0.058	0.913	0.097	0.110	0.855
Mean	0.042	0.057	0.819	0.042	0.051	0.888	0.070	0.080	0.89

It should be mentioned that no data from BH04.5D tool geometry was used for the training of the model, but still acceptable results are obtained for the external signals

(ACC_RFS and FC_RFS). A general decreasing trend in performance can be observed for all sensors when predicting the tool wear of BH04.5D tool geometry. The most stable subset appears to be ACC_RFS with a more remarkable ability to adapt the predictions made to other tool geometry. In general, in most cases, the non-linearity is well modelled with correlation coefficients around 0.9; on the other hand, the mean absolute errors are high, indicating that there may be a small offset with respect to measured tool wear value. The standardization is done based on the MDS080SK tool data. The data from tool BH04.5D are subtracted from the mean of the data from tool MDS080SK and divided by the standard deviation. The internal signals show more difficulty in fitting the tool wear prediction in the BH04.5D tool. In the best case, the non-linearity of the curve is well modelled with an $R^2 = 0.95$. However, it shows a high mean absolute error.

5.3 TOOL BREAKAGE PREDICTION THROUGH LOGISTIC REGRESSION

Once the wear curve has been reconstructed, the tool breakage must also be detected not to damage or damage the minimum number of components possible. Rather than detecting the sudden change of a tool breaking, the risk of a tool breakage must be established in order to take appropriate action.

During the first and second stage (S1 and S2), it was not difficult to predict the state of the tool. In all cases, it has been successfully tested that the models created from the features of any of the sensors successfully differentiate between good and bad tool condition. So the results have been satisfactory in 100% of the cases.

In the transition phase, where it is unknown at what point the tool has suffered irreversible damage, it is unknown in which of the holes it has broken. So the breakage or non-breakage label must be attributed based on the pre-breakage and post-breakage labels. The S3 and S4 (3rd and 4th strategies) aim to assign labels to the transition area instances. Table 5.4 shows the label imputations made with each of the sensors. There can be seen the labels obtained with S3 and S4, the third stage consists on training an algorithm with the features of each of the tools separately, and the imputation was made based on each of the tools. The 4th stage involves training the algorithm with both tools and using the holes from the transition area as testing.

Table 5.4 Label imputation for transition phase during tool breakage a) 3rd stage (S3) b) 4th stage (S4). H2 correspond to the labels imputed to the transition phase of the 2nd tool while H3 corresponds to the 3rd tool

a) S3	H2	H3
FC_RFS	0000000001	0001110111
ACC_RFS	0000000000	0001111111
INT_RFS	0000000000	0111111111
[FC_RFS, ACC_RFS, INT_RFS]	0000000000	0111111111
b) S4	H2	H3
FC_RFS	0000000101	0101111101
ACC_RFS	0000000000	1001000000
INT_RFS	0000000001	0111111111
[FC_RFS, ACC_RFS, INT_RFS]	0000000001	0111101111
Imputation	0000000001	0111111111

The labels were imputed through an agreement between the different results. Thus, the final results labels are those from the imputation row.

After allocating the labels corresponding to each of the tools, models were created using all the labels corresponding to tool 2 and tool 3 (those with a comparable tool life). 70% of the data was used to train the models and 30% to test them. The confusion matrices are shown in Figure 5.11.

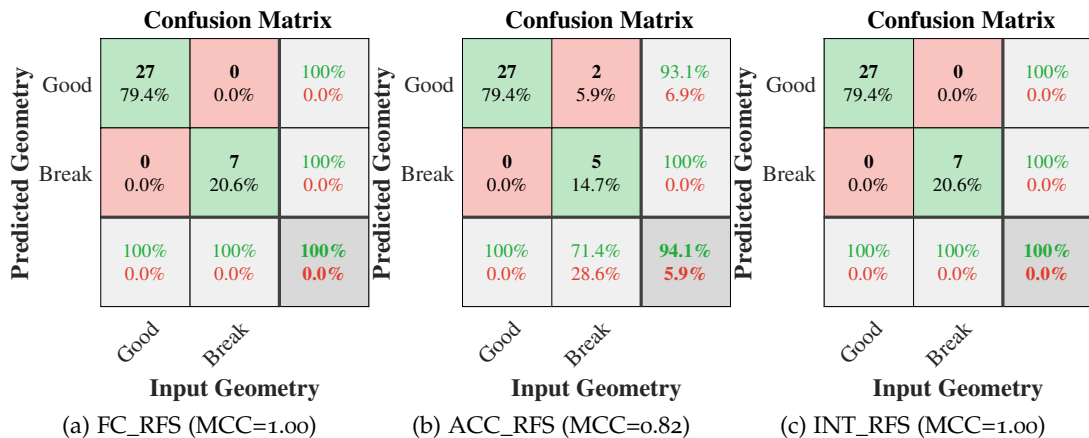


Figure 5.11 Confusion matrices for each sensor reduced feature space for S5 (stage 5)

Only taking into account tools 2 and 3, which have a comparable tool life and are broken in the same failure region, 100% accuracy is achieved with dynamometer and internal signals. The accelerometer sensor has the greatest difficulty for tool breakage detection.

Up to now, only the second and third tools have been tested for tool periphery breakage automatic detection. To see how the behaviour of the created models is altered, the instances of tool 1 have been introduced in S6. Given the limited data available, training with two of the tools and testing with the remaining one is not possible as not all the variability of the data was collected. Given this situation, 70% of the data has been separated to train and create the model and 30% of the data to test it.

The results obtained with all sensors can be seen in Figure 5.12. It shows the confusion matrix and the wear curves indicating the correctly and incorrectly classified instances for each of the classes. False positives are those instances in the "without failure" zone that are classified as "tool failure", while false negative are those instances in the "tool failure" zone classified as "without failure".

Finally, the results obtained by each of the sensors have been statistically compared against INT_RFS obtained results. A sampling (70%-30%) was done 30 times, and a t-test was applied between the results obtained with each of the sensors. Table 5.5 shows the mean values of MCC of the models and the p values.

Table 5.5 Mean in MCC for each of the sensors and p values of t-test results

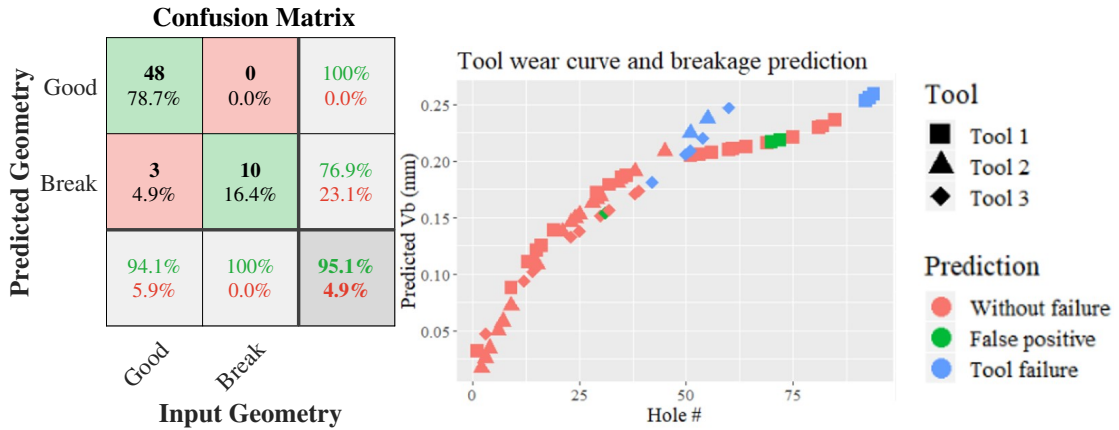
	MCC	INT_RFS	FC_RFS
INT_RFS	0.9807		
FC_RFS	0.8818	7.796e-08	
ACC_RFS	0.3899	2.2e-16	2.2e-16

The results show that the internal signals can detect tool breakage with the best mean in MCC. Both the dynamometer and the accelerometer have significantly different averages with a p – value < 0.05.

Below is an example of the model achieved with the S6 for internal signals. Specifically, it is obtained the probability that the tool is not broken in holes 49 and 50 made with tool 2. It is in these holes where the tool has passed from "without failure" to "tool failure" state.

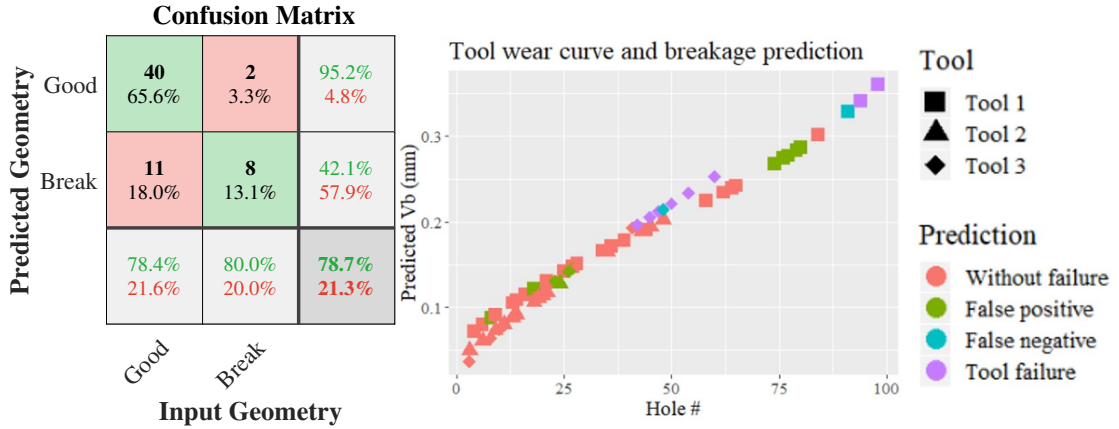
The model for internal signals in S6 shown in section 5.3.1 on Table 5.16 is given by the following equation.

$$F(x) = 10.59 + TV50_{mean} \cdot (-14) + TV51_{max} \cdot 0.61 + TV2_{mean} \cdot (-18.88) + Vz_{std} \cdot 1.42 + Vz_{skew} \cdot 2.41 + TV50_{max} \cdot (-5.78) + TV3_{max} \cdot (-1.82)$$



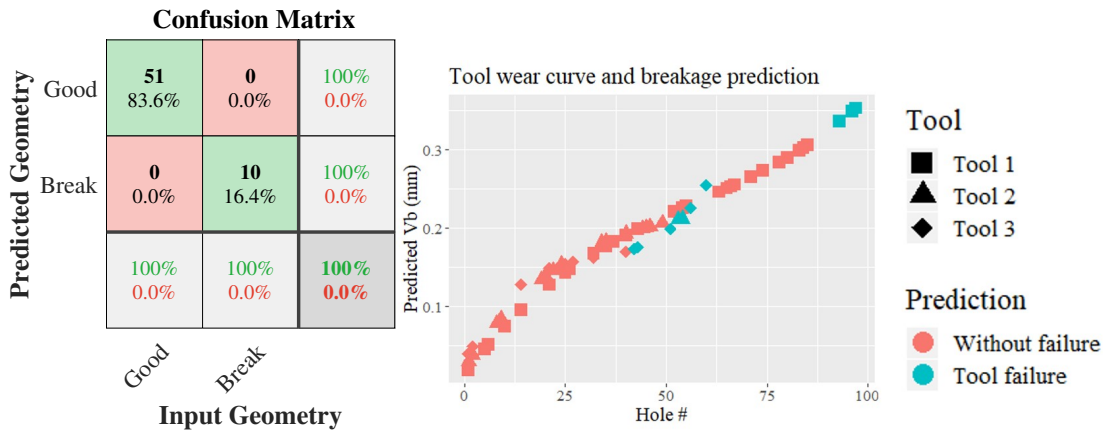
(a) Confusion matrix with FC_RFS (MCC=0.85)

(b) Wear curve/breakage prediction with FC_RFS



(c) Confusion matrix with ACC_RFS (MCC=0.47)

(d) Wear curve/breakage prediction with ACC_RFS



(e) Confusion matrix with INT_RFS (MCC=1.00)

(f) Wear curve/breakage prediction with INT_RFS

Figure 5.12 Results obtained in S6 (stage 6) for each of the sensors in testing subset. a-c-d) Confusion matrices for each sensor reduced feature space on test set. b-d-f) Wear curve prediction and breakage detection for each sensor reduced feature space on test set

Substituting the values of the features by the normalized values ($\mu = 0, \sigma = 1$) of hole 49 the expression is as follows,

$$F_{\text{hole49}} = 10.59 + 0.13 \cdot (-14) + (-0.28) \cdot 0.61 + 0.4 \cdot (-18.88) + 0.39 \cdot 1.42 + 0.07 \cdot 2.41 + 0.10 \cdot (-5.78) + (-0.40) \cdot (-1.82) = 1.4$$

And the probability that in hole 49 the tool has not suffered a breakage is,

$$\Pr(\text{withoutbreakage})_{\text{hole49}} = \frac{e^{1.4}}{e^{1.4} + e^{-1.4}} = 0.94$$

In hole 50, in the same way, making the substitution of the values the expression is,

$$F_{\text{hole50}} = 10.59 + 0.758 \cdot (-14) + 0.097 \cdot 0.61 + 1.194 \cdot (-18.88) + (-0.561) \cdot 1.42 + (-1.431) \cdot 2.41 + 0.654 \cdot (-5.78) + 0.317 \cdot (-1.82) = -31.13$$

And the probability that in hole 50 the tool has not suffered a breakage is,

$$\Pr(\text{withoutbreakage})_{\text{hole50}} = \frac{e^{-31.13}}{e^{-31.13} + e^{31.13}} = 9.137e - 28$$

When $F(x)$ starts to get close to 0, the process should be stopped for premature tool change before the tool breaks.

The following sections show the models obtained for the detection of tool breakage.

5.3.1 Logistic model trees for each sensor for tool breakage detection

The logistic regressions shown in this section belong to class 0 ("without failure") ($F(x)$). The logistic regressions for class 1 ("tool failure") are therefore the opposite of those shown ($-F(x)$). It can be seen that with the dynamometer and the internal signals, simpler and more interpretable expressions were obtained. The coefficients represent the effect of the variable per one unit of change in the predictor feature.

Cutting forces

Model obtained with dynamometer signal reduced feature space (FC_RFS) on stage 5.

Table 5.6 Logistic model for stage 5 using FC_RFS

Inter.	Fx_mean	Mz_mean	WP2_Fy_peak
13.11	3.22	-15.75	0.9

Model obtained with dynamometer signal reduced feature space (FC_RFS) on stage 6.

Table 5.7 Logistic model for stage 6 using FC_RFS

Inter.	WP2_Fy_rms	Fx_mean	Mz_mean	WP2_Fy_min	WP2_Fy_peak
5.42	3.58	1.1	-17.53	-0.23	0.56
WP2_Mz_rms	WP2_Mz_skew				
1	-1.77				

In both strategies a single logistic model is obtained. The complexity added in stage 6 can be clearly seen as there are more features that are part of the decision. However, both models have only one leave. The most relevant feature for tool breakage detection is Mz_mean since it has the highest coefficient on both strategies.

Accelerometer

Model obtained with accelerometer signal reduced feature space (ACC_RFS) on stage 5.

$WP2_ACCx_rms \leq -0.337507 : LM_1$

$WP2_ACCx_rms > -0.337507$

$WP4_ACCx_rms \leq -0.677682 : LM_2$

$WP4_ACCx_rms > -0.677682 : LM_3$

Number of Leaves : 3

LM_1:

Table 5.8 Logistic model 1st leave for stage 5 using ACC_RFS

Inter	WP3_ACCz_max
1.24	-0.19

LM_2:

Table 5.9 Logistic model 2nd leave for stage 5 using ACC_RFS

Inter.	WP2_ACCy_rms	WP4_ACCx_rms	WP3_ACCz_max
-0.55	-1.43	0.47	-0.3

LM_3:

Table 5.10 Logistic model 3rd leave for stage 5 using ACC_RFS

Inter.	ACCx_max	WP4_ACCx_rms	WP3_ACCz_max
0.71	-0.45	0.47	-0.3

Model obtained with accelerometer signal reduced feature space (ACC_RFS) on stage 6.

WP2_ACCy_rms <= 0.719511

WP2_ACCy_rms <= -0.814449 : **LM_1**

WP2_ACCy_rms > -0.814449

WP4_ACCx_rms <= -0.68583 : **LM_2**

WP4_ACCx_rms > -0.68583 : **LM_3** WP2_ACCy_rms > 0.719511 : **LM_4**

Number of Leaves : 4

LM_1:

Table 5.11 Logistic model 1st leave for stage 6 using ACC_RFS

Inter.	WP7_ACCx_rms	WP8_ACCx_rms	WP2_ACCy_rms	WP4_ACCy_kurt	WP3_ACCz_rms
24.96	-0.33	-0.54	-0.55	-1.02	7.56
ACCx_max	ACCx_skew	WP2_ACCx_rms	WP2_ACCx_max	WP2_ACCx_peak	WP4_ACCx_rms
0.16	-262.45	-2.4	0.27	-6.32	0.84
WP6_ACCy_rms	WP7_ACCy_mean	WP3_ACCz_max	WP7_ACCz_kurt	WP8_ACCz_max	
-0.39	1.54	-1.08	-57.62	1.87	

LM_2:**Table 5.12** Logistic model 2nd leave for stage 6 using ACC_RFS

Inter	WP5_ACCx_rms	WP5_ACCx_max	WP7_ACCx_rms	WP8_ACCx_rms	WP2_ACCy_rms
-5.18	0.57	-2.68	-0.33	-1.26	0.3
WP4_ACCy_kurt	WP3_ACCz_rms	ACCx_max	ACCx_skew	WP2_ACCx_rms	WP2_ACCx_max
-1.2	1.78	0.16	-101.13	-0.35	15.74
WP2_ACCx_peak	WP4_ACCx_rms	WP6_ACCy_rms	WP7_ACCy_mean	WP3_ACCz_max	WP7_ACCz_kurt
-0.03	0.95	-0.45	-0.19	-1.17	33.87
WP8_ACCz_max	WP8_ACCz_peak				
-0.2	0.13				

LM_3:**Table 5.13** Logistic model 3rd leave for stage 6 using ACC_RFS

Inter.	WP5_ACCx_rms	WP5_ACCx_max	WP7_ACCx_rms	WP8_ACCx_rms	WP2_ACCy_rms
12.04	0.57	-3.12	-0.33	-1.26	1
WP4_ACCy_kurt	WP3_ACCz_rms	ACCx_max	ACCx_skew	WP2_ACCx_rms	WP2_ACCx_max
-2.9	2.58	0.16	-160.26	-0.64	0.12
WP2_ACCx_peak	WP4_ACCx_rms	WP6_ACCy_rms	WP7_ACCy_mean	WP3_ACCz_max	WP7_ACCz_kurt
-0.75	1.89	-0.97	-0.48	-1.17	3.33
WP8_ACCz_max	WP8_ACCz_peak				
-0.2	0.13				

LM_4:**Table 5.14** Logistic model 4th leave for stage 6 using ACC_RFS

Inter.	WP7_ACCx_rms	WP2_ACCy_rms	WP3_ACCz_rms	ACCx_max	ACCx_skew
21.16	-0.47	0.34	1.1	-0.1	-30.22
WP7_ACCy_mean	WP2_ACCx_rms	WP2_ACCx_max	WP2_ACCx_peak	WP4_ACCx_rms	WP6_ACCy_rms
-0.08	-0.38	0.27	0.1	0.43	-0.39
WP3_ACCz_max	WP7_ACCz_kurt	WP8_ACCz_max	WP8_ACCz_peak		
-0.61	1.53	-0.2	0.01		

In the accelerometer signals, more complex models are obtained; in stage 5, 3 logistic models are obtained while in stage 6, 4 are obtained. To give rise to each of these models, the rules created in the tree must be fulfilled, and therefore the detection of tool periphery breakage is more complex, manifesting itself in the accelerometer signals

in different ways. In stage 6 it is possible to identify the variables $WP7_ACCz_kurt$ and $ACCx_skew$ as the variables on which tool breakage can have the most significant impact.

Internal signals

Model obtained with internal signal reduced feature space (INT_RFS) on stage 5.

Table 5.15 Logistic model for stage 5 using INT_RFS

Inter	TV2_mean
0.56	-0.72

Model obtained with internal signal reduced feature space (INT_RFS) on stage 6.

Table 5.16 Logistic model for stage 6 using INT_RFS

Inter.	TV50_mean	TV51_max	TV2_mean	Vz_std	Vz_skew	TV50F_max	TV3_max
10.59	-14	0.61	-18.88	1.42	2.41	-5.78	-1.82

Regarding the internal signals, the signal with the greatest weight and that can best interpret the breakage of the tool periphery is the TV2_mean feature which appears as relevant in both strategies. In a more complex scenario, the TV50_mean feature is also considered relevant.

It can be seen that by introducing a slightly different tool (with different life expectancy), more complicated models are obtained in which a greater number of features are involved. In the case of the dynamometer, the signal with the highest weight coefficient is Mz_mean for both strategies (S5 and S6). It can also be seen that in both models, the same features are present. However, in S6 a greater number of features are involved. In the accelerometer case, the models obtained are not comparable. Although the variables of stage 5 appear in the stage 6 the obtained models are of great complexity. Thus, it has little ability to generalize the employed data. In the case of internal signals, they present the best results. The variable with the highest weight in the model in both cases is TV2_mean, and it is remarkable that in the S6 only 7 features participate, obtaining a good generalization to testing data.

Figure 5.13 shows the function $F(x)$ obtained based on INT_RFS as a function of the holes drilled, the plot on the right margin shows the density plot of $F(x)$ for each tool. The minimum value among the maximum of $F(x)$ between the 3 tools before the breakage is -17 (the most conservative value), while the maximum value is -13. As can be seen, tools 2 and 3 have a similar tool life, while tool 1 has allowed a greater

number of holes to be drilled. This is because the inherent variability of the process, material properties, variability in tool manufacture or the degree of effectiveness of the coolant in reaching the cutting zone can cause these variabilities. The figure also shows the polynomial fit of each of the curves. In the equations obtained, it can be seen that as the first coefficient increases, the tool has a shorter life. Under the same conditions, there may be situations where the tool is prematurely changed in the hole 40 when double the number of holes could have been made. Therefore, the use of techniques to assess the condition of the tool based on the signals collected during the process is essential to avoid these situations.

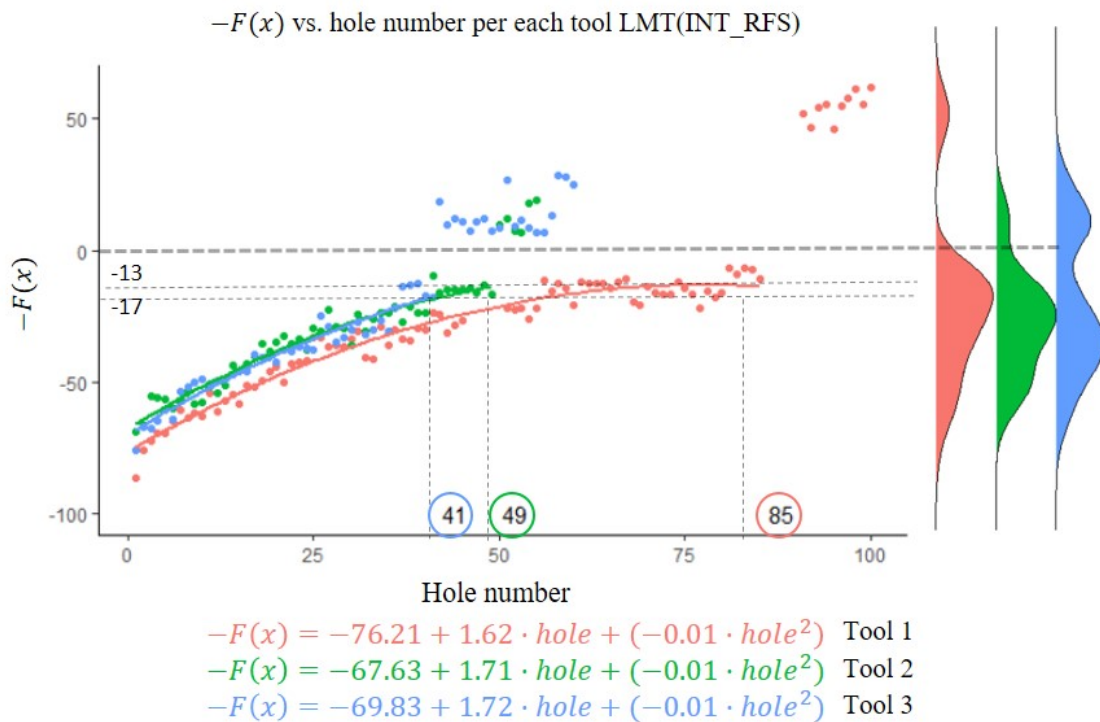


Figure 5.13 Logistic model function based on INT_RFS. On the horizontal axis are marked the holes where tool breakage has been observed for each tool. On the vertical axis are marked the $F(x)$ values at which tool breakage has been observed

5.4 SURFACE INTEGRITY ANALYSIS

Three holes were selected from among the holes made from two of the repetitions made with the BH04.5D tool and two repetitions of the MDS080SK tool. A total of 12 holes have been analysed to see if there is a relationship with tool wear in the end-of-life tests. In each of the repetitions, holes corresponding to different tool conditions were selected. Figure 5.14 shows the test points for each of the repetitions carried out. The figure shows the moment of completion of the tests ($V_b = 0.3\text{mm}$), but some additional holes

were drilled to observe the damage caused to the material when the tool is practically unusable. The moment at which the periphery of the tool breaks has also been marked.

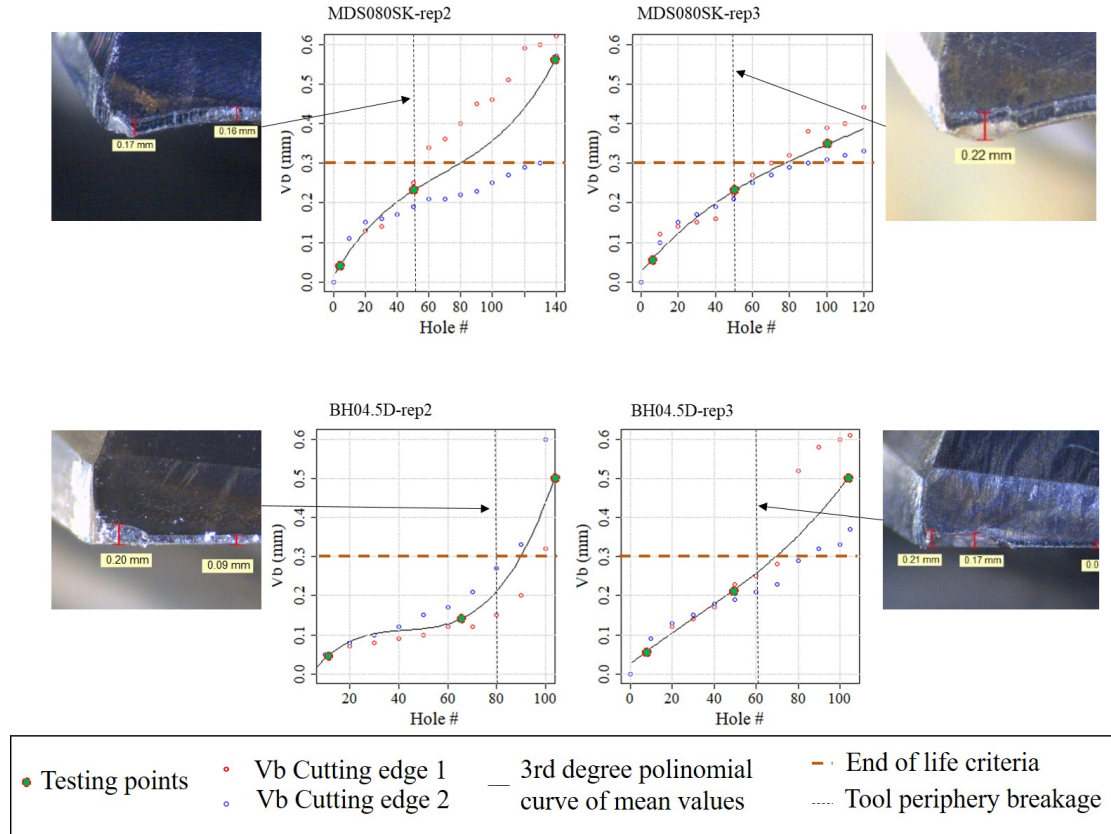


Figure 5.14 Surface integrity testing points for 2 different tool geometries on different tool conditions

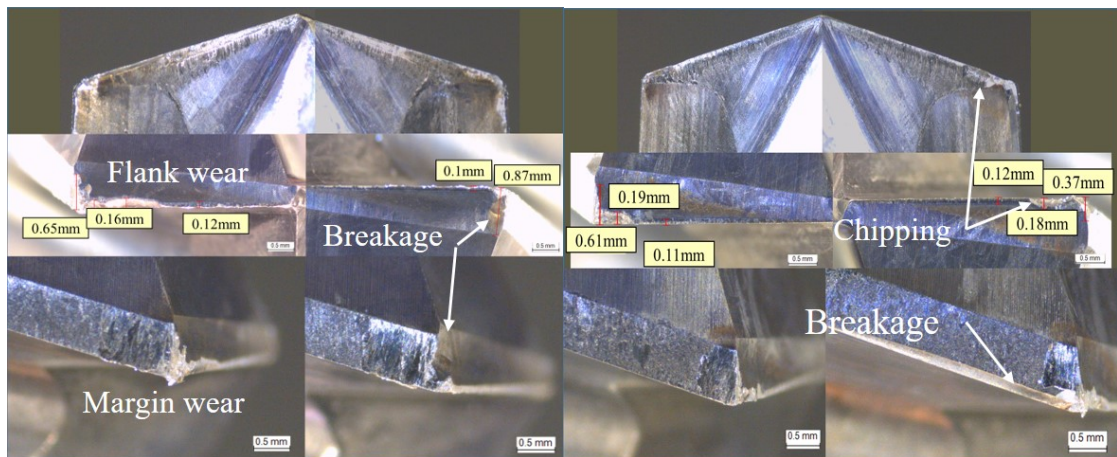
Figure 5.15 shows the condition of the tool for each of the repetitions in the last test point. On tools of type MDS080SK the first breakage was observed earlier than on BH04.5D tools. However, when the tool breaks at the periphery, it becomes unstable and wear is rapidly accelerated.

5.4.1 Roughness

The distribution of each of the holes measured at different tool wears can be seen in Figure 5.16. The kernel density estimation of the two measured roughness profiles on each hole and their corresponding mean are shown, besides their confidence intervals are also pointed. This way of visualising the roughness profile gives an insight into the stability of a roughness profile, i.e. how much deviation the roughness profile data suffers. The kernel density estimation is non-parametric method that shows the probability of a randomly distributed variable. So applying on roughness profile, the frequency distribution of each value in the surface of the component can be seen.

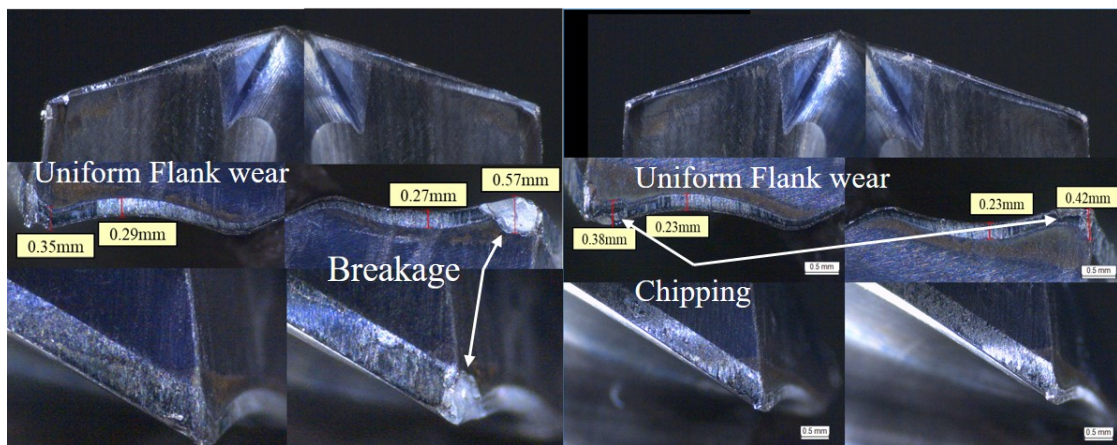
Edge 1	Edge 2
Rake face 1	Rake face 2
Flank face (Major cutting edge) 1	Flank face (Major cutting edge) 2
Margin (minor cutting edge) 1	Margin (minor cutting edge) 2

(a) Schematic view of tool photographs



(b) BH04.5D – rep2

(c) BH04.5D – rep3



(d) MDS080SK – rep2

(e) MDS080SK – rep3

Figure 5.15 Tool condition in the last testing point for each tool in both cutting edges (rake face, flank face and margin)

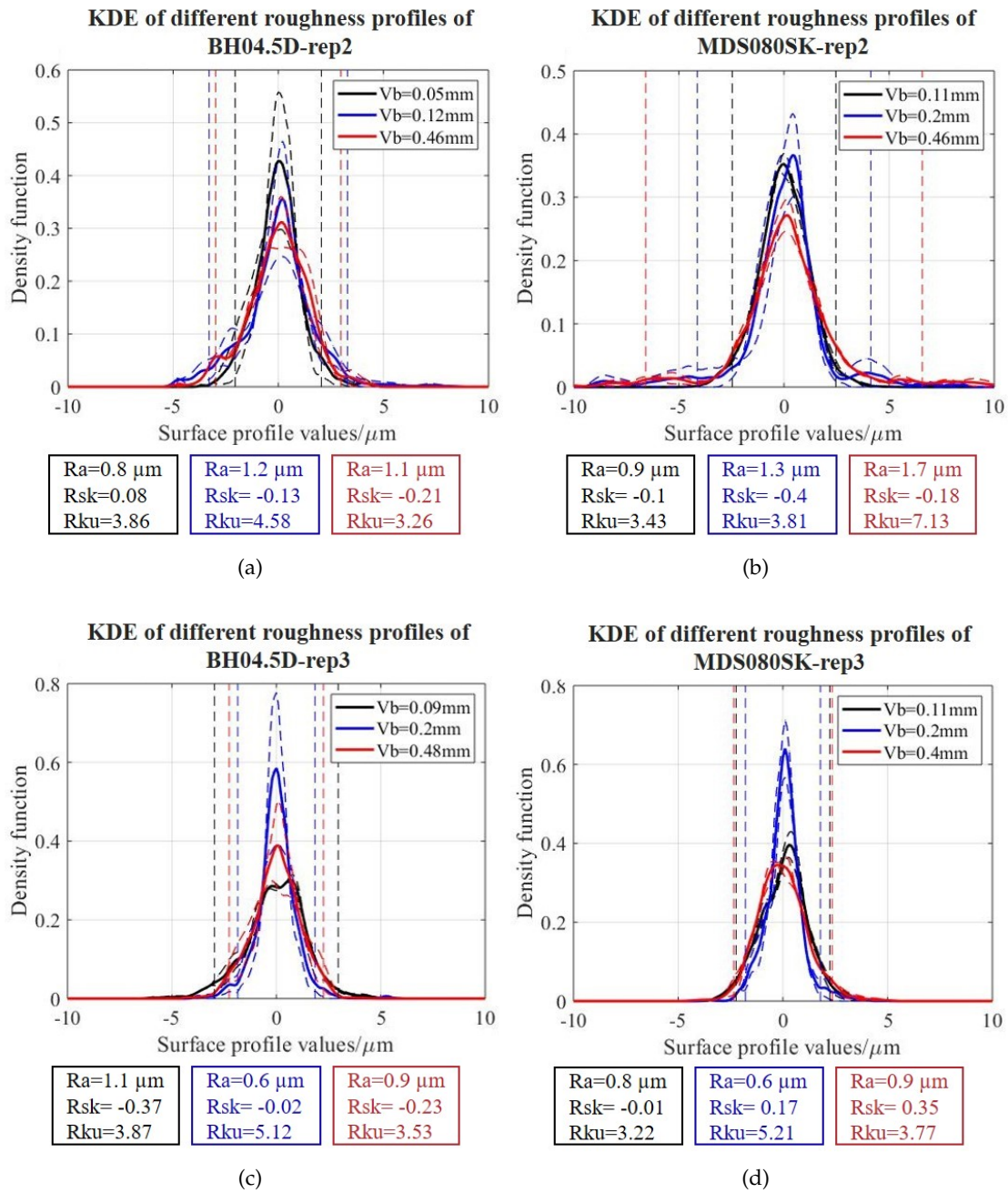


Figure 5.16 Kernel Density estimations of roughness profiles on different tool wear levels and their corresponding confidence interval levels. The dashed lines represent each of the measurement distributions, while the continuous line represents the mean between the two measurements made for each of the holes. The vertical dashed lines correspond to the confidence intervals of each of the means obtained for each tool condition

The 95% confidence interval maintains a proportional relationship to the Ra parameter of the roughness profile in all cases.

In geometry BH04.5D, in the repetition 2, the probability that the central values of the roughness profile remain in the centre decreases with increasing tool wear. The confidence interval is similar on $V_b = 0.46\text{mm}$ and $V_b = 0.12\text{mm}$. The Rsk value decreases with increasing tool wear, indicating a higher probability that more values are in the negative tail of the distribution. So there is an increased risk of fatigue crack initiation on the component.

In repetition 3 of the same tool geometry, the confidence interval is the widest when the tool is worn to a $V_b = 0.09\text{mm}$. When the tool is more worn ($V_b = 0.2\text{mm}$) the confidence interval decreases to the minimum, indicating an improvement of the Ra parameter of the roughness profile, and then worsens when the tool is worn ($V_b = 0.48\text{mm}$). Although in all cases the Rsk value remains below 0, at $V_b = 0.2\text{mm}$ is the instant when it is closest to 0, the Rku value is above 3, indicating a leptokurtic distribution, in which the values are more centred. Regarding the surface generated during the drilling process, this is the distribution in which the probability of crack initiation is reduced, and the best contact properties are obtained.

Concerning repetition 2 of geometry MDS080SK, it can be seen that the confidence intervals are wide, indicating that the values are more dispersed, resulting in rougher surfaces.

With repetition 3, similar values to tool repetition 3 of geometry BH04.5D are obtained, having the most centred distribution with wear $V_b = 0.2\text{mm}$. However, in this case, the Rsk values are positive, indicating a greater probability that the profile values are in the distributions positive tail. This means a higher resistance to cracks but a disadvantage in terms of assembly.

It can be seen that the only cases where more than 50% of the roughness values remain more centred are at $V_b = 0.2\text{mm}$ in repetition 3 of both tool geometries.

In any case, no clear trend is observed for tool wear and roughness obtained. In Figure 5.17 3 roughness profiles are observed of tool geometry MDS080SK on repetition 3 for different tool conditions.

5.4.2 Material damage

Among the repetitions performed on Inconel 718, the material damage was measured in 2 repetitions performed with the BH04.5D tool and 2 repetitions performed with the MDS080SK tool at 3 levels of wear. However, no relationship with tool wear or between the two geometries has been found. Figure 5.18 shows the measured length of the damaged layer in terms of both White/HDL and SH for each of the repetitions.

The only case that maintains a relationship with tool wear is in BH04.5D – rep2, in which an upward trend is observed with tool wear both at the hole entrance and the

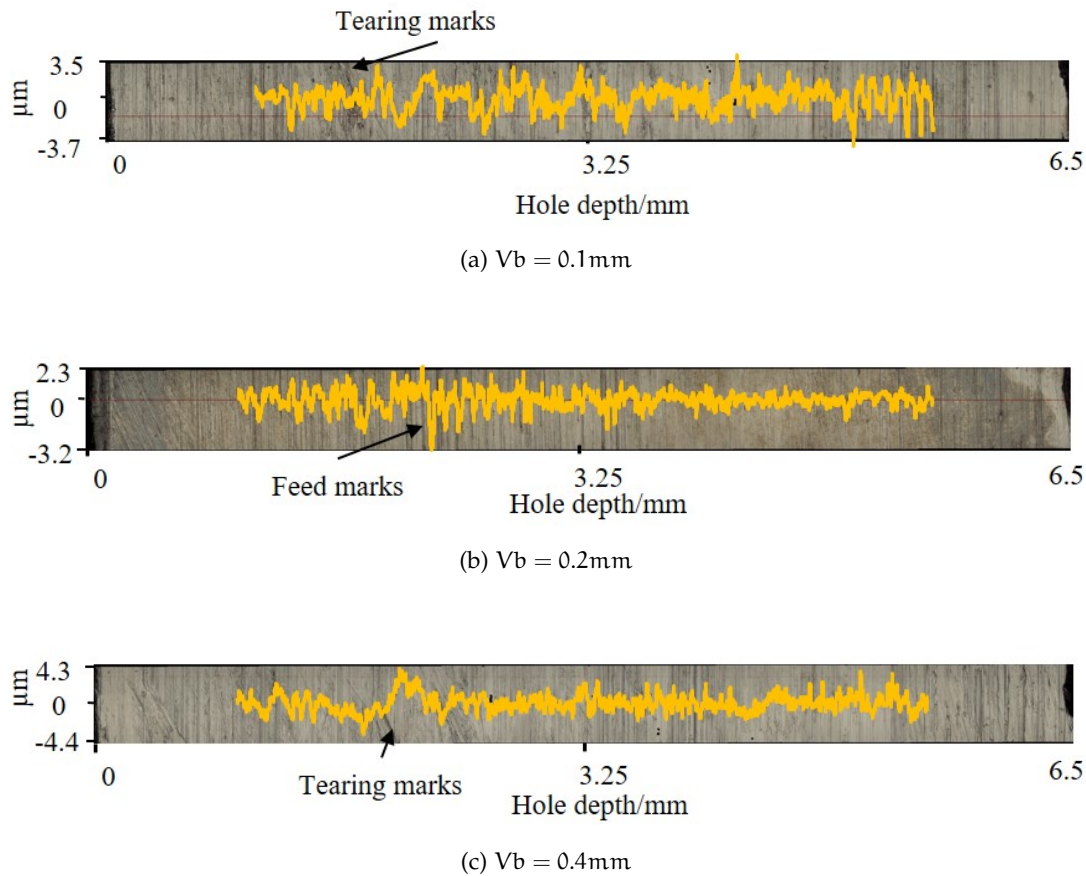
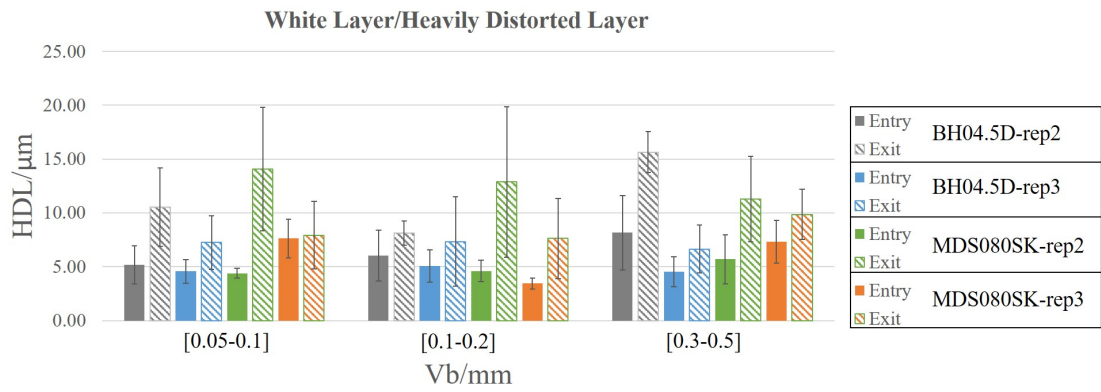


Figure 5.17 Surface roughness profiles on each tool condition for tool geometry MDS080SK on repetition 3

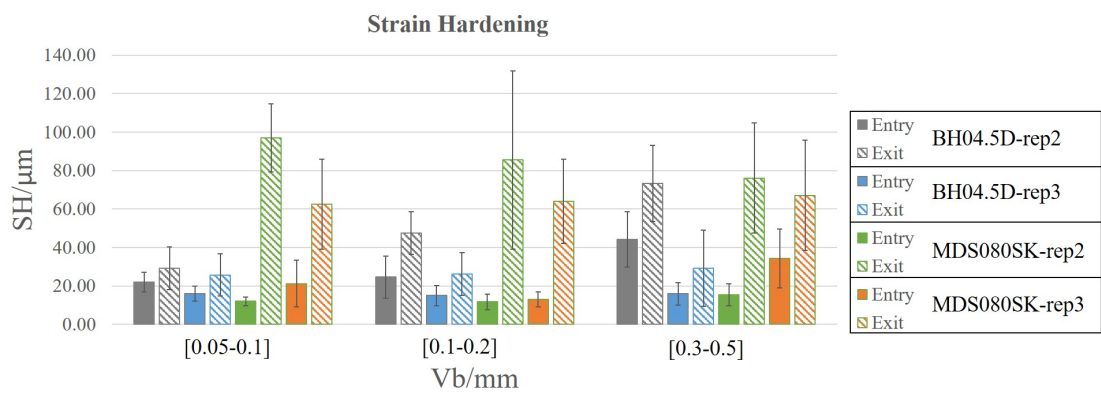
exit concerning both HDL and SH. On the other hand, there is more damage at the hole exit than at the entrance in all cases.

These results were not as expected, as it was thought that a more evident trend in material damage would be observed in relation to tool condition. However, according to Sharman et al. (2008), in drilling, the greatest cutting action occurs on the chisel and major cutting edges, but the surface area is generated at the periphery of the tool due to the minor cutting edge. Even though the periphery of the tool may be broken, the minor cutting edge will remove some of the damaged material. In drilling, the cut is produced by two or more cutting edges. Even if one of the cutting edges shows more damage, the other cutting edge will cut the part of the material that the damaged cutting edge has not cut.

Figure 5.19 shows the material damage caused by MDS080SK tool geometry on repetition 3 in different the last testing point. In the hole exit for a $V_b = 0.4\text{mm}$, more surface drag can be observed in the direction of the cutting speed. However, there is no clear trend on the layer of damaged material concerning tool wear.

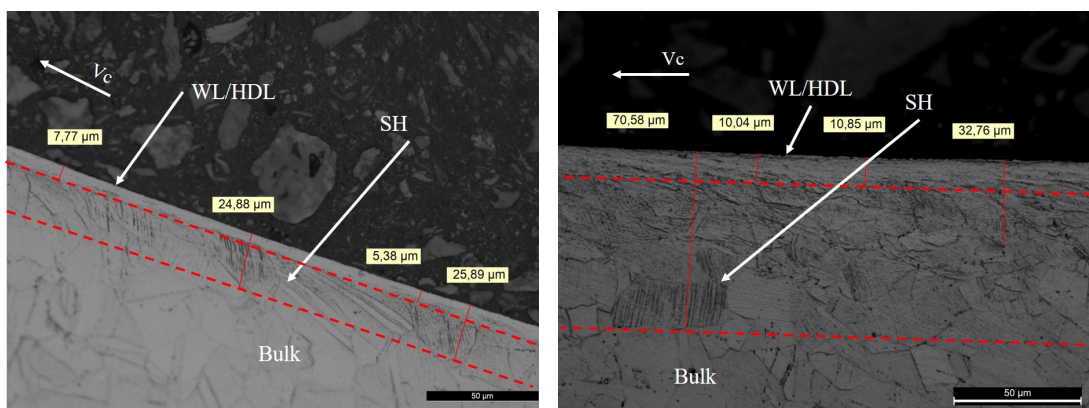


(a) White Layer/Heavily Distorted Layer



(b) Strain Hardening

Figure 5.18 Material damage on holes performed with MDS080SK and BH04.5D tool geometries in different tool conditions



(a) Hole entry ($V_b = 0.4\text{mm}$)

(b) Hole exit ($V_b = 0.4\text{mm}$)

Figure 5.19 Material damage generated on the last testing point for tool geometry MDS080SK on repetition 3 at hole entry and hole exit

For tool BH04.5D in the 2 repeat, an increase in roughness can be seen as tool wear increases. This trend is also seen in the material damage for the same tool. However, it is the only tool that shows a trend of worsening surface integrity in all the repeats analysed. The rest of the measurements show a constant trend both at the entrance and exit of the hole.

5.5 CONCLUSIONS

The deployed set-up results in the use of different sensors to monitor tool wear and detect peripheral tool breakage. A methodology based on ML techniques is used to select the most suitable sensor for tool wear monitoring. On the one hand, the reconstruction of the wear curve is addressed using features obtained from each of the sensors separately and comparing different algorithm performances. Besides, the ANN model created for wear curve reconstruction is tested on a different tool geometry. On the other hand, tool breakage is detected automatically using a methodology for the imputation of labels that are not known which class they belong to. Surface integrity has also been analysed in terms of roughness and material damage caused by the drilling process under different tool conditions.

- In all cases, better results are obtained once the feature selection process has been applied, so applying feature selection can improve the behaviour of the used algorithms. In this way, irrelevant and redundant features that can penalise the result obtained are removed.
- The feasibility of each of the sensors lies in (i) the implementation of the sensor in the machine environment, (ii) the amount of data generated by each of the sensors, (iii) the cost of installing the sensor in the work environment and (iv) the prediction capacity provided. In our experience, the most practical signals for monitoring the tool condition are those provided by the machine itself (Internal signals). No sensor installation is required, the highest sampling frequency is 250Hz, so it does not generate a large amount of data and provides good predictive capabilities in terms of tool wear, both for the reconstruction of the wear curve and the detection of tool breakage. In cases where it is not possible to collect this type of signal, the most practical option is the accelerometer, as it results in a cheaper sensor than a dynamometer and less invasive although it generates a more significant amount of data than internal signals. Nevertheless, the accelerometer does not give the capacity to detect tool breakage, or at least in the feature space analysed in this work.
- During the model testing for the reconstruction of the wear curve on another tool geometry, it has been observed that the internal signals are the most affected in terms of performance. However, with another tool geometry (BH04.5D) and having standardised the data based on the MDS080SK geometry, fairly good results have been obtained, and the non-linearity of the wear curve has been

modelled quite well. The search for mechanisms to compensate the offset of the predictions is of great interest given the results presented in this chapter.

- The simplest models are those that best generalise to the test data. Stage 6 (S6) involves 7 features in the models created with the dynamometer and the internal signals, having interpretable models.
- The most relevant features with the highest coefficients for tool periphery breakage detection were Mz_mean , $WP7_ACCz_kurt$ and $ACCx_skew$ and $TV50_mean$ and $TV2_mean$ for the reduced spaces of the FC_RFS , ACC_RFS and INT_RFS respectively. Using FC_RFS , 95% accuracy has been obtained with misclassification occurring late in the process, having few false positives. With ACC_RFS , 75% accuracy has been obtained and the time point at which false positives occur is early in the process. However, even more serious are the cases in which false negatives are detected, determining that a bad tool is still in good condition. The best result in these experiments was obtained with INT_RFS with 100% accuracy for the three tools used.
- It has been observed that the same tool geometry under the same cutting conditions in the same material can vary in terms of tool life. Tool 1 has a life of 70 holes during the steady stage phase, while tools 2 and 3 have a life of 30 holes in the same phase. Creating hybrid models to simultaneously predict two phenomena at the same time is a strategy that not only provides information about where the wear curve is at any given moment, one of the two models can warn that the process is not in the ideal conditions to continue gaining in robustness in terms of monitoring tool condition.
- As far as surface integrity is concerned, the expected results were not observed. However, the main wear measured was flank wear. The interaction between the margin and the surface can cause the results seen. The first hole measured was hole number 6, in which the wear progression is in the break-in period. Measuring hole number 1 would be interesting, as the tool is completely new and differences could be observed with respect to the holes measured in this work. In the absence of differences, surface integrity in drilling processes on Inconel 718 may be affected by other factors.

SURFACE ANOMALY DETECTION IN BLS 35CRMO₄ LOW S STEEL ON A LONG MACHINED TIME

The roughness of the machined part is an essential industrial parameter concerning the durability property of the component. The monitoring of the surface condition is not widespread because of the low number of observations for machine learning models creation and the challenge of getting reliable predictions. At present, most of the works on the prediction and analysis of errors that may appear on the machined surface focuses on the analysis of the *Ra* parameter, which is the average roughness of the profile. The works consulted in section 2.2.2.6 test the models on a small number of measurements, which suppose a challenge in obtaining reliable model performance metrics. There are many parameters of the roughness profiles that retain the information of the generated surface distribution. These are described in Table 2.1 in the literature review. These parameters characterise the surface and inform about the contact properties of a component. With the increasing demand for more precise requirements, it is necessary to analyse the obtained surface profile distributions based on more parameters than the mere use of the *Ra* parameter.

In drilling processes, the chip required for a better finish is in the fan-shaped form, as this is evacuated more efficiently, thus preventing the chip from rubbing against the machined surface and chip clogging. Currently, in industrial environments the method used for the evaluation of the generated surface is randomly chosen test points. This is a dangerous practice as it could risk the non-detection of errors that could lead to future problems in the operational life of the components. Although most research is focused on developing tool condition monitoring systems that can extend tool life and anticipate possible tool breakage, the development of new methodologies that allow detecting surface or subsurface machining errors is still in its infancy. This is a fundamental branch of research into the monitoring of cutting processes to achieve better-finished components and reduce the probabilities of component malfunctions. In the given input conditions, one of the biggest challenges is to replicate the surface finish on all parts machined under these conditions. However, given the dynamics of the machine, this is still hardly achievable.

Clustering algorithms can help to measure the degree of replicability of surface roughness of a particular process under established cutting conditions. The major challenge is to select those features of the signals that maintain a relationship with

the measured roughness parameters that allow to evaluate the differences between the distributions of the roughness profiles.

Mingoti and Lima (2006) compared different partitioning and hierarchical clustering algorithms, SOM (Self Organizing Map) networks, Fuzzy *c*-mean, K-means and hierarchical agglomerative clustering on simulated overlapped data. In the study, they showed that Fuzzy *c*-means behaves well concerning the other partitioning algorithms. Regarding the hierarchical agglomerative algorithm, among the various measures used of inter-group proximity, they showed that the Ward linkage method is the one that obtains the most stable behaviour. Diaz-Rozo et al. (2017) used both hierarchical and partitioning clustering algorithms to diagnose the state of a spindle. Xiaoli and Zhejun (1998) used fuzzy partitioning algorithms to classify different tool wear levels in boring operations. Partitional Around Medoids (PAM) algorithm was used by Li et al. (2017) for tool condition clustering in milling operations showing its superiority over *k* means, and fuzzy *c* means algorithms based on cutting force signal. Zhou et al. (2017) used vibration signal time-frequency features, and fuzzy *c* means algorithm to classify 3 roughness *Ra* ranges in the drilling operation. They assumed the Gaussian nature of the surface roughness, and they classified a high and low *Ra* value categories by relating each hit of acoustic emission with each tool pass. Kubišová et al. (2019) used hierarchical clustering to compare original surface roughness with replicated surface roughness based on Euclidean distances of various roughness parameters showing that it can be a good tool for replicability measurements of obtained surface profiles.

Based on the work done by Kubišová et al. (2019), where supported by different roughness parameters, compare an original surface with a replicated surface employing a hierarchical clustering. In this chapter, the same idea is followed, but the proposal is to perform it with the signals acquired during the drilling process instead of using roughness parameters. A mapping between signal features and roughness parameters is performed. In this way, a set of signal features that allow to create the same similarity groups created based only on the roughness parameters is obtained. Consequently, based on a limited number of roughness measurements, a series of signal features are selected to create clusters for a larger population of holes. Once the clusters were obtained, a series of additional measurements were carried out for validation purposes.

6.1 METHODOLOGY FOR SURFACE ANOMALY DETECTION

The data obtained from the setup presented in the section 3.2 (Tests on BLS 35CrMo4 Low S) is used. Several potential statistical features are evaluated using agglomerative hierarchical clustering to create the same groups obtained from roughness parameters of a limited number of holes measured in the Alicona profilometer.

6.1.1 Acquired signal segmentation and feature extraction

As seen in chapter 3, the signals have been filtered to obtain the stable part or zone of the machining. In Figure 6.1 the signals of each of the tool geometries used for this analysis can be seen.

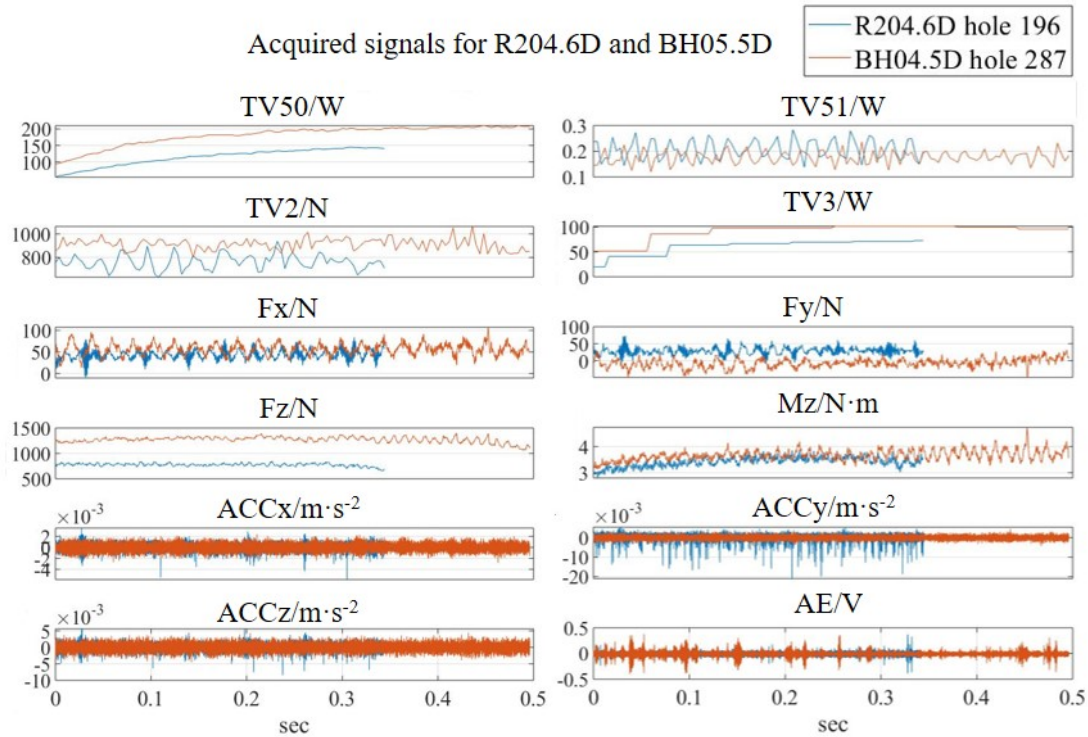


Figure 6.1 External and Internal signal acquired for each tool geometry on hole 196 for R204.6D tool geometry and hole 287 for BH04.5D tool geometry

As part of the first stage, pre-processing task, to eliminate some noise introduced by the machine in the vibration signals, these have been filtered with a low pass Butterworth filter of order 10 with cut-off frequency $F_c = 3600\text{Hz}$ and a bandpass filter with $F_{c1} = 4000\text{Hz}$ and $F_{c2} = 6000\text{Hz}$. On the one hand, we have the vibrations that happen below 3600Hz (named $\text{ACC}(x - y - z)_1$) and in the other hand, vibrations in the sub-band $4000 - 6000\text{Hz}$ (named $\text{ACC}(x - y - z)_2$). Six vibration signals overall, two for each signal acquired on each of the three axes.

15 signals are available for the clustering of the holes roughness. After extracting eight statistical features for each one, mean, rms, standard deviation, maximum, minimum, kurtosis, skewness and variance, 120 statistical features are available.

Hole roughness measurements (post-process measurements) and sensor signals (in-process measurements) obtained in the drilling process were obtained and related to each other. These main analysis steps can be seen schematically represented in Figure 6.2.

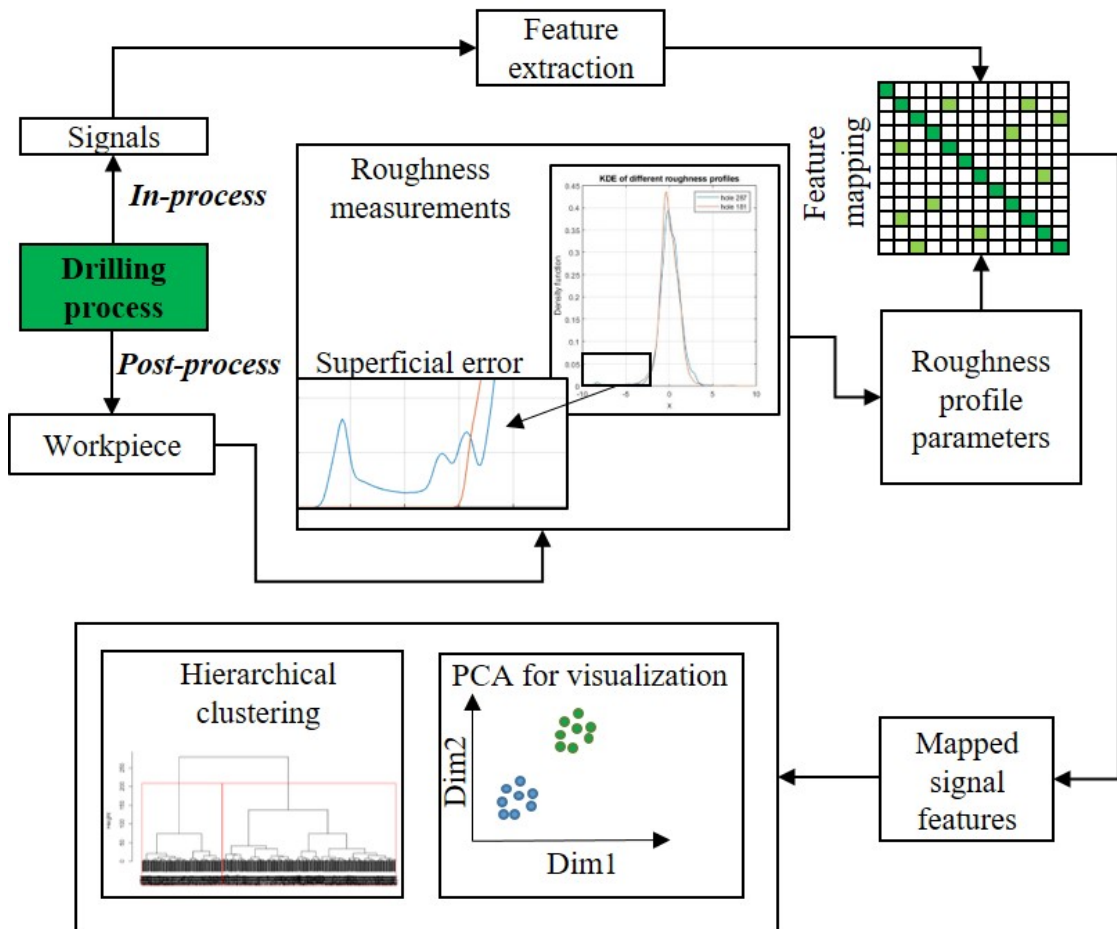


Figure 6.2 External and Internal signal statistical feature selection for hole surface anomaly detection

After obtaining the signal statistical features and the roughness parameters, redundant roughness parameters are removed (those having a coefficient above 99%), and a clustering performed with the filtered parameters to see hole surface differences shown in section 6.1.2. The roughness parameters obtained in this filter are used to observe linear relationships with the acquired signal features that have a correlation coefficient above 90%.

To evaluate the suitability of the selected signal features, hierarchical clustering is carried out only considering the features that belong to the measured holes. These results can be seen in section 6.1.3.

For the creation of the bottom-up dendrograms in hierarchical clustering, the Euclidean distance was used. For linkage purposes, Ward's minimum variance method, in which the fusion of two clusters is based on the size of an error sum-of-squares criterion (this is the criterion for joining two subgroups that are at a minimum distance to create the dendrogram). The objective at each stage is to minimize the increase in the

total within-cluster error sum of squares. Finally, the rest of the holes are projected on these clusters to see if they are representative of the extended population of holes.

6.1.2 Roughness parameter selection for clustering

Hierarchical clustering was used to classify the deviation on the machined surface roughness profiles, using initially 6 measured holes for each tool. The clusters were created from the roughness parameter data obtained from the Alicona system measurements after the tests. As many of these parameters were highly related, those highly correlated variables were removed to avoid redundancies. Then, parameters have been normalized to have an average equal to 0 and a standard deviation of 1 ($\mu = 0, \sigma = 1$).

From the 13 initial variables, $Ra, Rp, Rv, Rsm, Rsk, Rku, Rdq, Rq, Rt, Rz, Rmax, Rc, Rt/Rz$, 7 were not highly correlated ($R^2 < 0.99$). Figure 6.3 shows the parameters selected and their respective dendrograms for each of the measured holes corresponding to each tool.

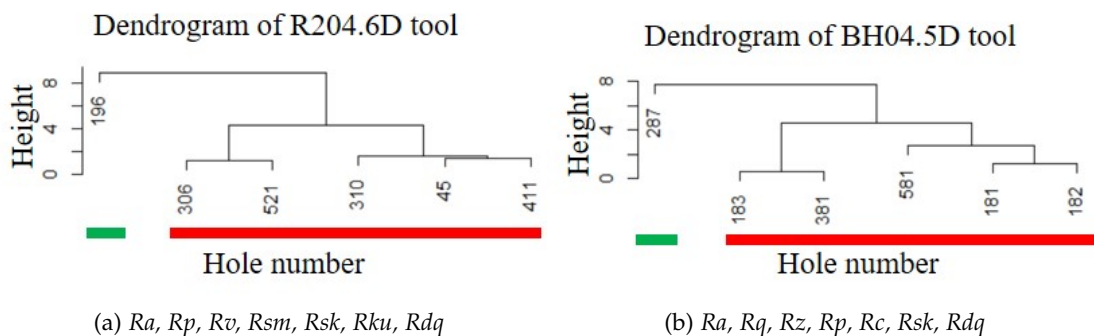


Figure 6.3 Uncorrelated ($R^2 < 0.99$) surface parameters and their respective dendrograms for the different tools, a) R204.6D tool with uncorrelated parameters $Ra, Rp, Rv, Rsm, Rsk, Rku, Rdq$, b) BH04.5D tool with uncorrelated parameters $Ra, Rq, Rz, Rp, Rc, Rsk, Rdq$

The y-axis shows how similar the observations or groups of observations are. Each connection of two groups is represented in the graph by dividing a vertical line into two vertical lines. The vertical position of the division, shown by the horizontal bar, gives the distance (dissimilarity) between two groups. As shown in Figure 6.3, holes 196 and 287 are remarkably different from the rest of the observations for tools R204.6D and BH04.5D, respectively.

Specifically, for the holes made with tool R204.6D, the parameters $Rq, Rt, Rz, Rmax, Rc, Rt/Rz$ have been neglected and not taken into account in the analysis. For the holes made with the BH04.5D tool, $Rt, Rmax, Rp, Rv, Rku, Rt/Rz$ are the parameters that were neglected. Using two clusters, holes 196 and 287 were identified as different from the rest of the holes for tools R204.6D and BH04.5D respectively.

The observation of the differences of hole roughness parameters through clustering results was the next step. Figure 6.4 shows Ra , Rsk and Rku parameters obtained by each of the tools where the different groups obtained during the clustering of the holes can be seen represented in colours. Each point represents the average of the two measurements made on each of the holes and is labelled with the number of the hole made with each tool and coloured with results of clustering groups shown in Figure 6.3.

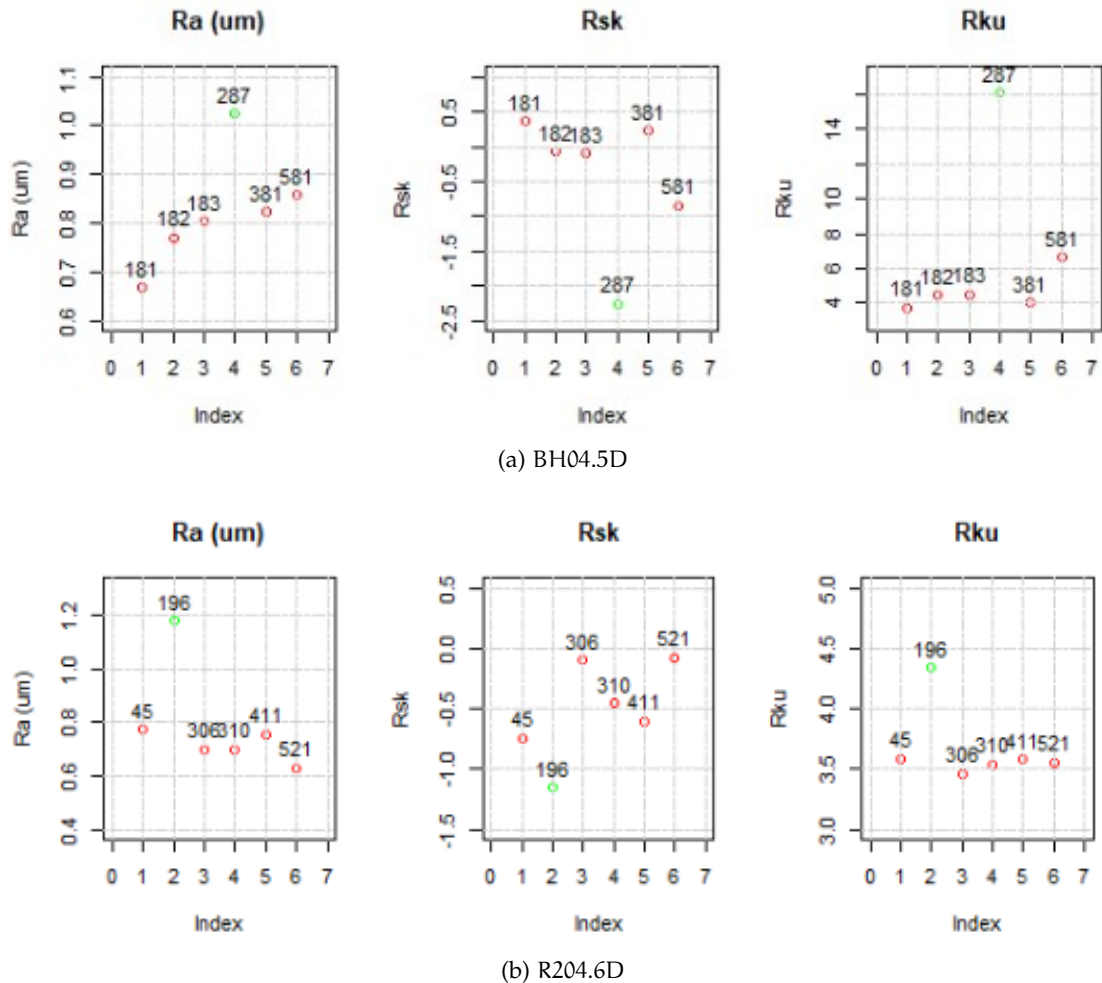


Figure 6.4 Individual roughness parameters (Ra , Rku , Rsk) coloured based on clustering results a) BH04.5D b) R204.6D. The index is the number of measurement (6 holes per each tool geometry)

For every hole made with each of the tools, two types of surface profiles have been observed. On the one hand, in the hole 287, made with tool BH04.5D, there were marks that did not correspond to the tool feed rate (surface tearing), and holes with no visible damage have been observed. In hole 196, made with the tool R204.6D, deep feed marks were seen compared to the rest of the holes. These observed phenomena caused the roughness to be affected at certain points of the process.

Discarding the damaged surface values (hole 196 for R204.6D and hole 287 for BH04.5D of which the measured profiles can be seen in the Figure 6.5) the average Ra values are $0.71\mu\text{m}$ and $0.78\mu\text{m}$ for R204.6D and BH04.5D tools respectively.

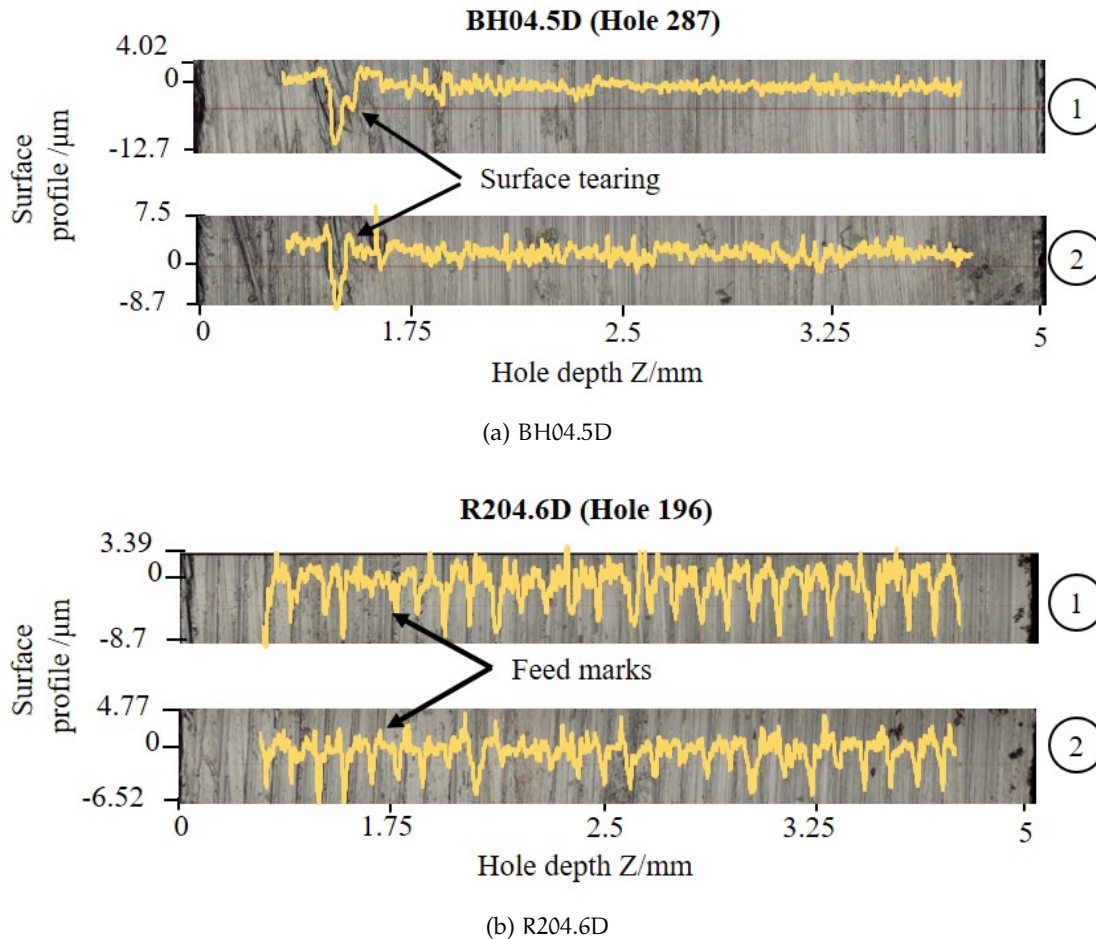


Figure 6.5 Example of Alicona measurements for hole 196 of R204.6D tool and hole 287 of BH04.5D tool a) 1st and 2nd measurement of hole number 196 made with BH04.5D tool b) 1st and 2nd measurement of hole number 287 made with R204.6D tool

The holes shown in the previous figure have a very similar Ra value (in the range of $(1 - 1.2\mu\text{m})$), however, the profile distribution is very different. Figure 6.6 shows the difference assuming that the distribution is normal and a kernel density estimation for two holes made with R204.6D and two holes made with BH04.5D. It can be seen that assuming the distribution is normal, there are no large differences between distributions with a similar Ra value. Instead, the kernel density estimation gives an insight into the differences between the holes. The 306 hole made with the R204.5D tool and the 181 hole made with the BH04.5D tool have a lower Ra and show a similar distribution, whereas the 196 holes from the R204.6D tool and the 287 hole from the BH04.5D tool

have a higher Ra and show differences in the roughness profile distributions due to surface errors occurred during machining.

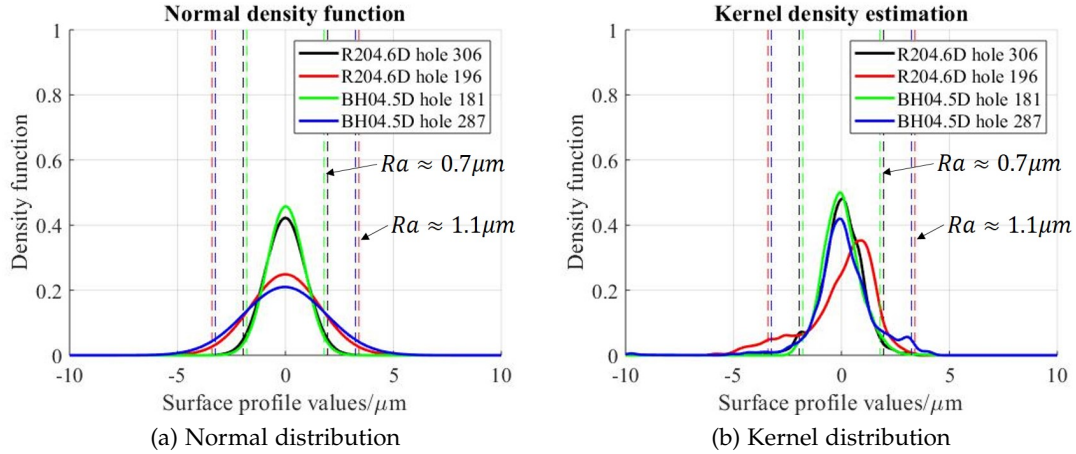


Figure 6.6 Comparison of different distribution function assumption for roughness profiles a) Normal distribution b) Kernel density estimation

6.1.3 Surface roughness clustering based on signal features

For selecting the most representative signals regarding roughness, correlation analysis has been carried out concerning the filtered roughness parameters among all the statistical features obtained from the signals. Statistical features with correlations to roughness measures above 90% were selected and neglected below 90% independently of whether the correlation coefficient is positive or negative. Table 6.1 shows features with a high correlation coefficient with one or more roughness parameters.

Table 6.1 Correlations higher than 90% between acquired signal statistical features and roughness measured parameters and a) R204.6D tool measured holes b) BH04.5D tool measured holes

a) R204.6D	Ra	Rp	Rv	Rsm	Rsk	Rku	Rdq	b) BH04.5D	Ra	Rq	Rz	Rp	Rc	Rsk	Rdq
Fy_skew	0.81	0.45	0.84	0.91	-0.89	0.82	0.21	Mz_mean	0.03	-0.11	0.14	0.20	-0.01	0.33	0.91
ACCx1_min	-0.89	-0.75	-0.86	-0.81	0.78	-0.92	-0.56	ACCy_max	0.06	-0.04	0.24	0.32	0.08	0.26	0.97
ACCx1_kurt	0.94	0.76	0.91	0.79	-0.78	0.96	0.68	ACCx2_mean	-0.76	-0.76	-0.82	-0.93	-0.81	-0.62	-0.55
ACCy2_skew	0.93	0.68	0.92	0.79	-0.77	0.97	0.7	ACCx2_rms	-0.82	-0.86	-0.81	-0.94	-0.87	0.75	-0.33
AE_kurt	0.93	0.67	0.91	0.81	-0.77	0.88	0.61	ACCz2_rms	-0.84	-0.93	-0.81	-0.81	-0.9	0.96	0.08
TV2_max	0.63	0.96	0.48	0.40	-0.24	0.67	0.81	ACCz2_min	0.75	0.84	0.71	0.62	0.81	-0.93	-0.26
TV3_min	0.82	0.31	0.89	0.96	-0.98	0.71	0.04	TV50_mean	0.23	0.11	0.34	0.43	0.21	0.12	0.96
								TV50_max	0.21	0.09	0.32	0.43	0.19	0.13	0.95

Both the roughness parameters and the acquired signal features have been filtered differently for each tool, as the phenomena observed in the roughness profiles are also different. In the holes made with the R204.6D tool, in the worst-case scenario, more visible feed marks are seen (Figure 6.5), which causes the roughness to increase,

having a negative impact in the profile skewness value. In the worst-case scenario measured with the BH04.5D tool (hole 287), the surface tearing can be seen, which highly increases the Ra value.

In a next step, the statistical features of the signals shown in Table 6.1 were the inputs for another hierarchical clustering to compare the similarities shown by these statistical features and those obtained from the roughness parameters in Figure 6.3. Figure 6.7 shows the dendrograms obtained as a result of this process. At low levels of similarity, differences can be seen between the groups created with respect to the dendrograms in Figure 6.3, however the differences observed at high levels of similarity are identical.

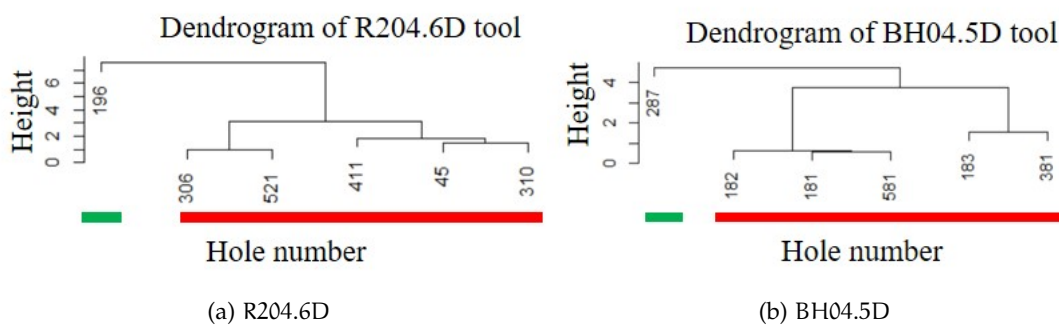


Figure 6.7 Clustering of measured holes using the signal statistical features of signals shown in Table 6.1

Following with the proposed methodology, hierarchical clustering has been applied to the entire set of observations made for each of the tools using the signal features during the selection of variables to see how accurately the selected signals can predict the differences between the profile distributions. Figure 6.8 shows the dendrograms obtained for the holes made with each of the tools, in the dendrograms, two groups can be seen clearly.

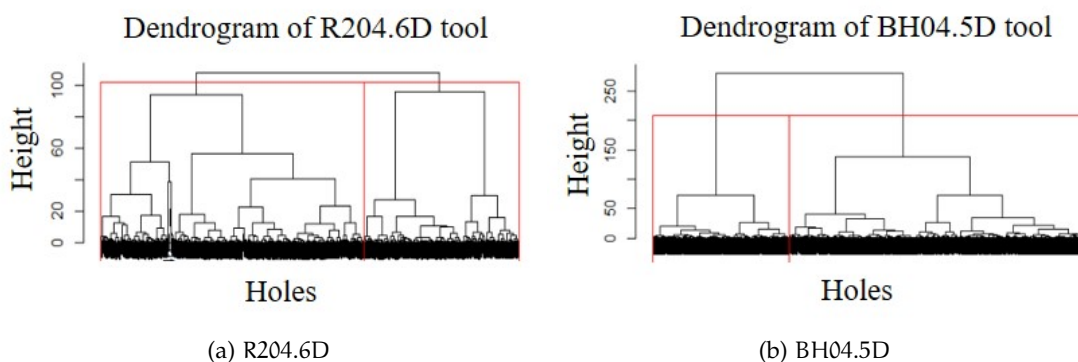


Figure 6.8 Dendrograms using the statistical features of all the holes for each of the cutting tools used

During the assignment of the clusters, the S_i (silhouette coefficient) of each one of the observations has been evaluated. The silhouette coefficient (S_i) measures how similar an object i is to the other objects in its cluster compared to those in the neighbouring cluster. Those observations with a silhouette coefficient below 0 have been taken to the nearest neighbour; this operation is carried out recursively until all the observations assigned to a given cluster have a S_i higher than 0.

6.2 VISUALIZATION OF OBTAINED CLUSTERS AND ANALYSIS OF THE PRINCIPAL COMPONENTS

For the display of the clusters, the principal component analysis was used. Figure 6.9 shows the two principal components for the holes made with each of the tools. The colours show each of the clusters. The length of the original variables represents the weight of each variable on each principal component.

For tool R204.6D, holes 45, 196, 411 belongs to cluster 2 while holes 306, 310, and 521 belongs to cluster 1. Holes 45 and 411 that was supposed to be in cluster 1 falls in cluster 2. The holes are in the boundary of the two clusters, so they are more confusing. Regarding tool BH04.5D hole 287 belong to group 2 (green), the rest of the measured holes belongs to group 1 (red).

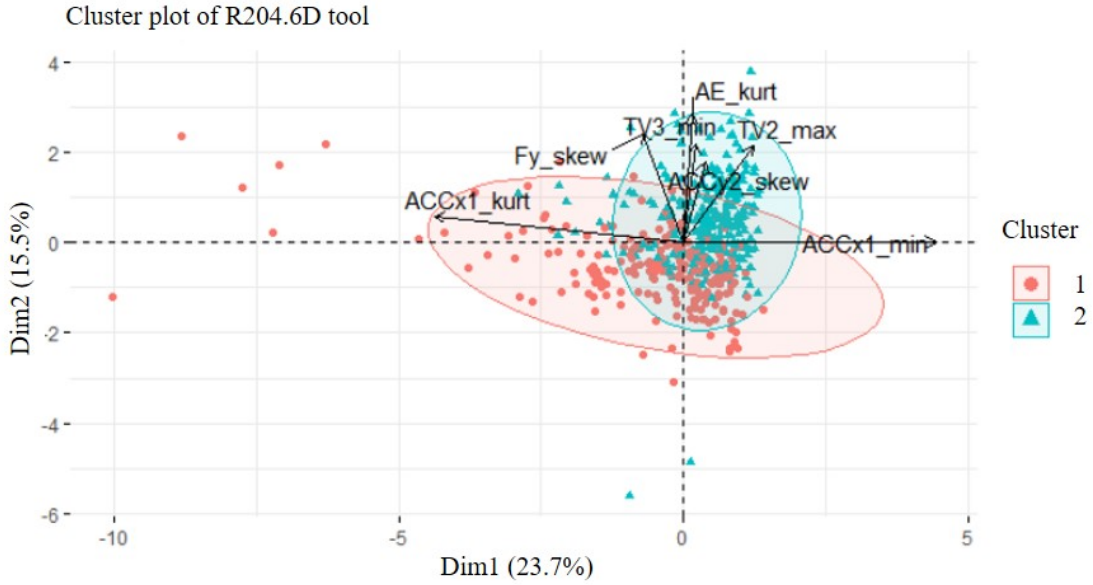
The percentage of the variance of each dimension obtained in the principal component analysis and the contribution of each of the features in the two principal components have been obtained, to find out which variables have the greatest variability in each of the dimensions. This can be seen in Figure 6.10.

In the holes made with the R204.6D tool, in the first dimension, the kurtosis value of the vibrations in the X-axis at low frequencies (ACC_{x1_kurt}) and the minimum of the same signal (ACC_{x1_min}) are the ones that have the most significant contribution. In the second dimension TV_{2_max} , TV_{3_min} , AE_kurt and Fy_skew are the ones that have the most significant contribution.

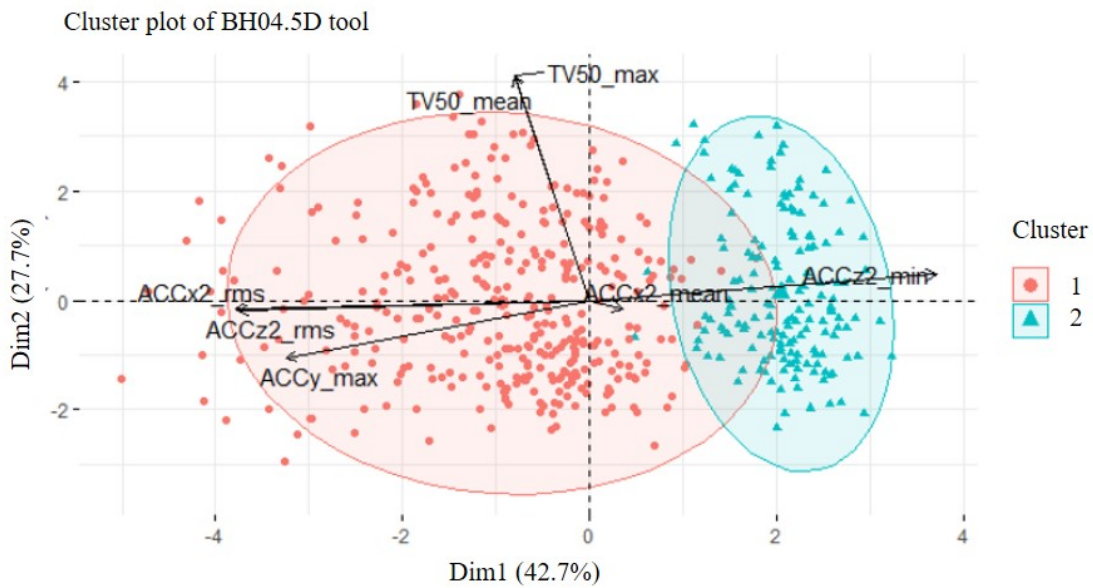
The holes made with the BH04.5D tool, the statistical features ACC_{x2_rms} , ACC_{z2_rms} , ACC_{z2_min} and ACC_{y_max} are the ones that contribute most to the first dimension. In this tool, the vibration signals are more affected by what happens on the working material surface. In the second dimension, TV_{51_max} and TV_{51_mean} have an equal contribution. The ACC_{x2_mean} feature has a null contribution; this was expected since the centre of the vibration signal is around 0, so this feature could be removed to reduce the feature space.

In Table 6.2 the centroids of each of the clusters can be seen for R204.6D tool. The centroids are the mean value of each variable for each cluster and explain how the roughness has suffered on that particular variable. The contributions of each variable to dimensions 1 and 2 of the principal component analysis can also be seen in the table.

The same procedure can be seen in table 6.3 for tool BH04.5D.



(a) R204.6D



(b) BH04.5D

Figure 6.9 Visualization of two principal components for obtained clusters a) R204.6D tool b) BH04.5D tool

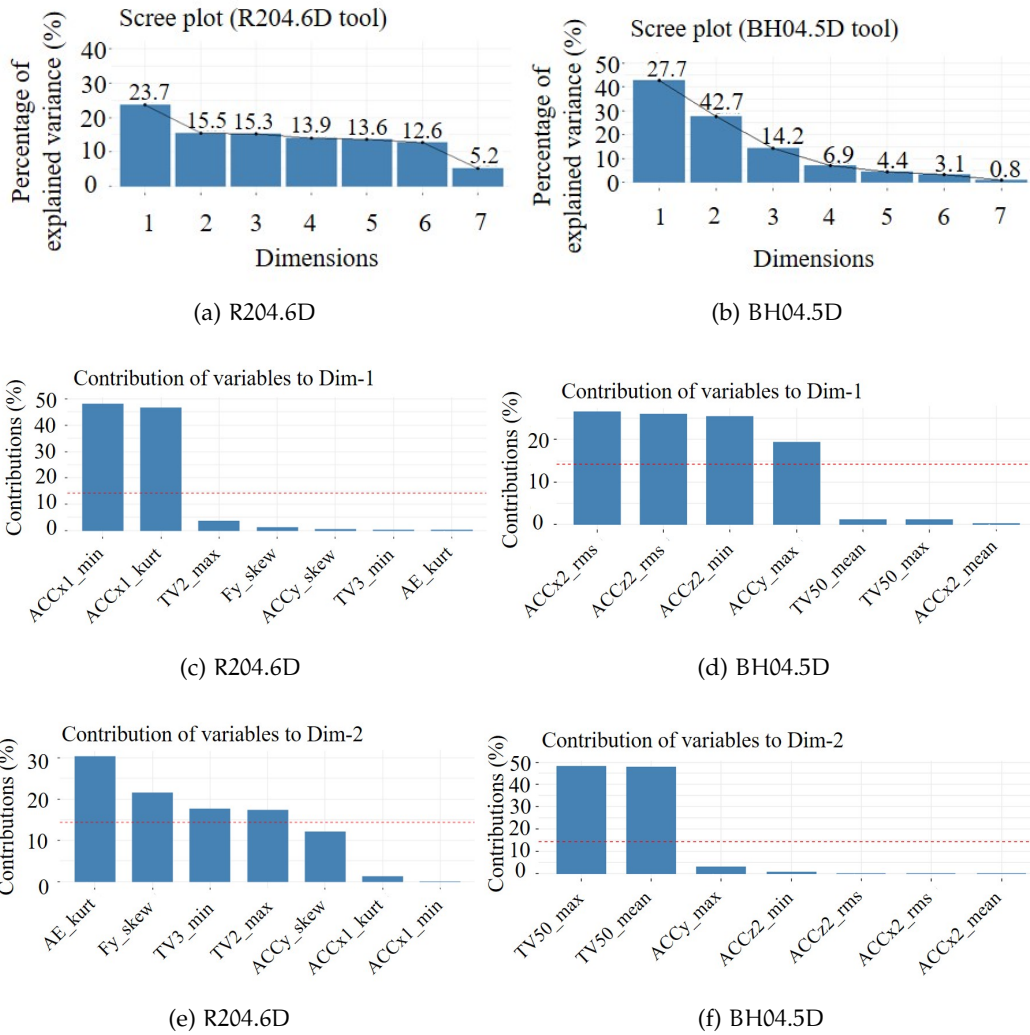


Figure 6.10 Principal component analysis a) Percentage of explained variance for R204.6D tool c) Contribution of each statistical feature to Dim1 of R204.6D tool e) Contribution of each statistical feature to Dim2 of R204.6D tool b)Percentage of explained variance for BH04.5D tool d) Contribution of each statistical feature to Dim1 of BH04.5D tool f) Contribution of each statistical feature to Dim2 of BH04.5D tool

Table 6.2 Cluster centroids for R204.6D tool drilled holes and feature contribution to each dimension

Cluster	Holes	Dim2	Dim1	Dim1		Dim2	Dim2	Dim2
		Fy_skew	ACCx1_min	ACCx1_kurt	ACCy2_skew	AE_kurt	TV2_max	TV3_min
		(15%)	(49%)	(49%)	(-)	(21%)	(34%)	(24%)
1	45,196,411	-0.1582	-0.1722	0.1694	-0.0304	-0.2964	-0.1994	-0.4003
2	306,310,521	0.2697	0.2935	-0.2887	0.0518	0.5053	0.3398	0.6822

Table 6.3 Cluster centroids for BH04.5D tool drilled holes and feature contribution to each dimension

Cluster	Holes	Dim1		Dim1		Dim1		Dim2	
		ACCy_max	ACCx2_mean	ACCx2_rms	ACCz2_rms	ACCz2_min	TV50_mean	TV50_max	
		(19%)	(-)	(37%)	(36%)	(35%)	(49%)	(49%)	
1	183,381,181,182,581	0.3765	-0.0276	0.5508	0.5099	-0.4339	0.0517	0.0650	
2	287	-0.8189	0.06	-1.1980	-1.1090	0.9438	-0.1124	-0.1414	

To analyse the compactness of each of the clusters, the intra-cluster distance has been measured, which indicates how compact a cluster is. For this purpose, the mean of the distances from the observations to the centroid of their cluster is calculated. Besides, the distances of the holes considered for measurement to the centre of the clusters have been included. This information can be seen in Tables 6.4 and 6.5. The numbers in bold are the distances to the clusters to which each hole belongs.

Table 6.4 Intra cluster distance and distance between measured holes and cluster centroids R204.6D tool

Cluster	Intra cluster distance	Distance between measured holes and cluster centroids					
		Hole 45	Hole 196	Hole 306	Hole 310	Hole 411	Hole 521
1	2.14	2.069	3.426	1.576	1.448	1.844	1.157
2	2.57	1.588	2.533	1.773	1.871	1.345	1.713

In the case of tool R204.6D, holes 45 and 411 belong to cluster 2, and are located at the boundary of the clusters, as shown in Figure 6.13 a). These were expected to be in cluster 1, and as they are located in a boundary region between two clusters, the correct assignment is more complicated.

Table 6.5 Intra cluster distance and distance between measured holes and cluster centroids BH04.5D tool

Cluster	Intra cluster distance	Distance between measured holes and cluster centroids					
		Hole 181	Hole 182	Hole 183	Hole 287	Hole 381	Hole 581
1	2.252	2.268	2.224	1.206	3.226	2.221	2.417
2	3.499	3.355	2.982	3.360	1.430	4.109	3.067

Concerning the BH04.5D tool, cluster 1 is the most compact, and cluster 2 show an increase in the mean values of their corresponding observation distances. The randomly selected holes for this tool are more central to their cluster centroids.

6.3 VALIDATION OF OBTAINED CLUSTERS

A new branch of holes has been selected again to validate the obtained clusters.

The clusters obtained for the BH04.5D tool are shown in Figure 6.11. In this case, all the holes measured for the validation correspond to their respective clusters. Figure 6.11 a) shows the clusters in the first two principal components of the signal features considered for creating the clusters. Figure 6.11 b) shows the dendrogram of the roughness parameters obtained from the profiles measured in Alicona. The mapping made between the signal statistical features and the measured holes matches 100% of the total measured holes.

Expressions 6.1 and 6.2 show the linear combinations of the two principal components used to display the obtained clusters in Figure 6.11 a).

$$\text{Dim1} = -0.51 \cdot \text{ACCx2}_{\text{rms}} - 0.51 \cdot \text{ACCz2}_{\text{rms}} + 0.5 \cdot \text{ACCz2}_{\text{min}} - 0.44 \cdot \text{ACCy}_{\text{max}} \quad (6.1)$$

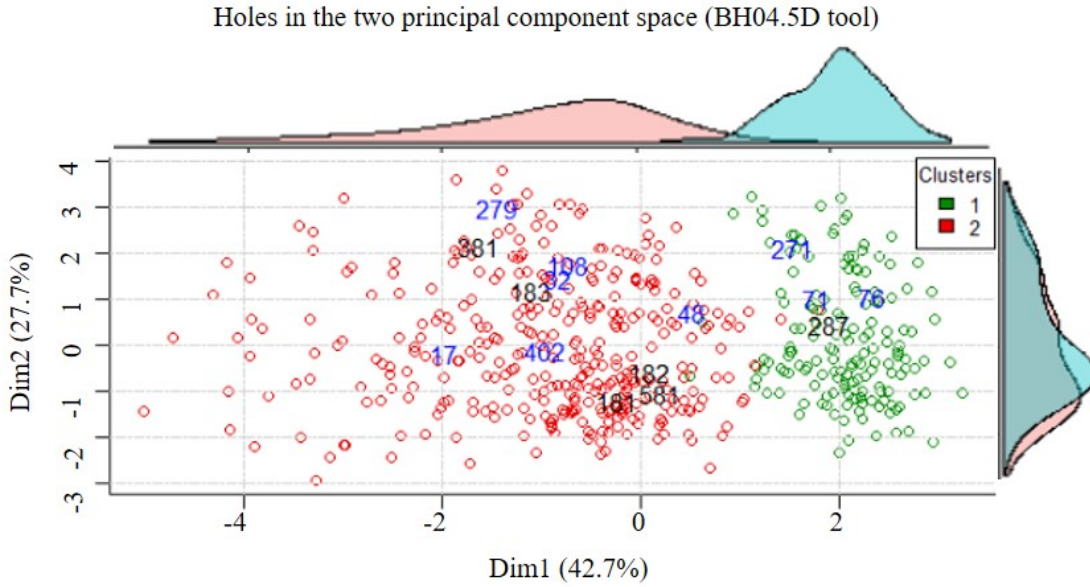
$$\text{Dim2} = 0.69 \cdot \text{TV50}_{\text{max}} + 0.69 \cdot \text{TV50}_{\text{mean}} \quad (6.2)$$

To establish the space covered by the selection of the statistical features, the corresponding area to the two principal components $A = 55.45$ and the area corresponding to the holes measured for the creation of the clusters $A(181, 182, 183, 287, 381, 581) = 11.82$ has been calculated. Overall, 21% of the area has been covered and the distance between two clusters, that is, the inter-cluster distance, is 3.014. Figure 6.12 shows the measured surfaces and their corresponding roughness profiles. Figure 6.12 a) shows the surfaces where some error has been observed, in this case, surface tearing. Figure 6.12 b) shows those surfaces that are free of visible defects.

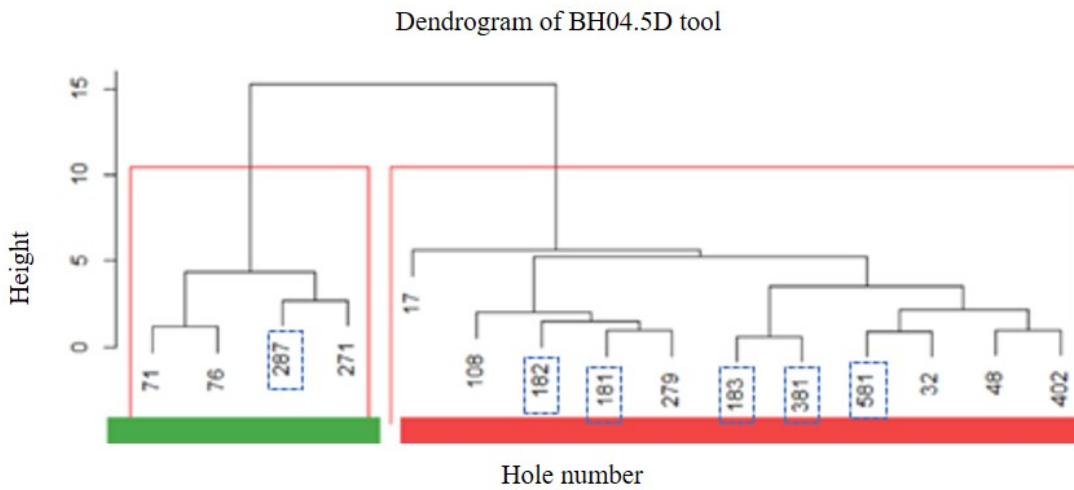
Concerning tool R204.6D, Figure 6.13 a) shows the clusters from the features of the acquired signals and the boundary between the two clusters. Figure 6.13 b) shows the dendrogram made with the roughness parameters obtained from the profiles.

The dendrogram shows that holes 45, 411 and 376 (marked in green) belong to cluster 2 although they were expected to be in cluster 1. The same happens with holes 27 and 173, which should belong to cluster 2 and are classified in cluster 1. In the zoom made in Figure 6.13 a), it can be observed that these holes belong to the cluster boundary. Holes that are not in the boundary and are observed further away are correctly classified.

Expressions 6.3 and 6.4 show the linear combinations of the two principal components used to display the obtained clusters in Figure 6.13 a).

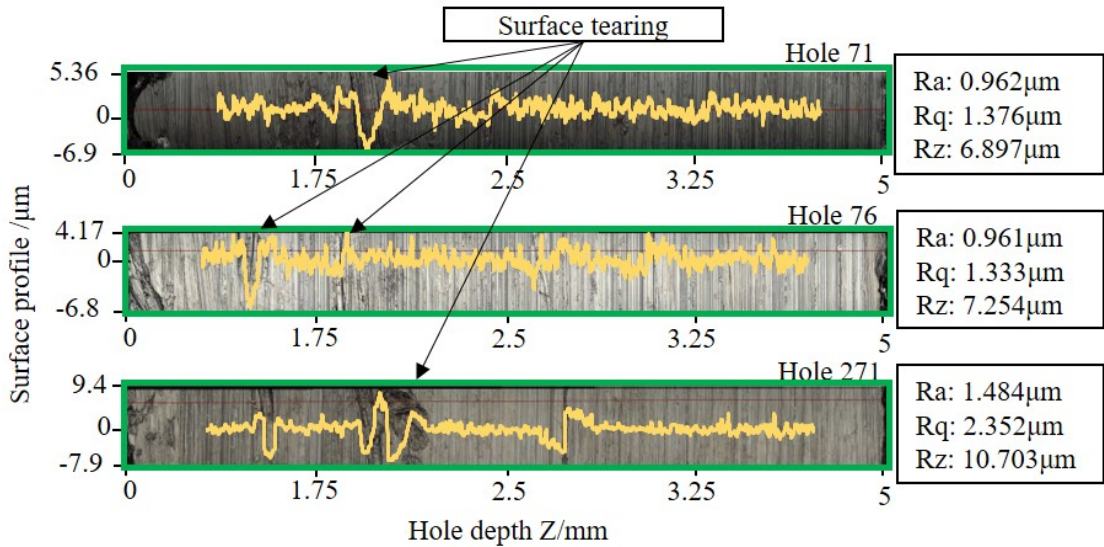


(a) 2 Principal components of features and density plots

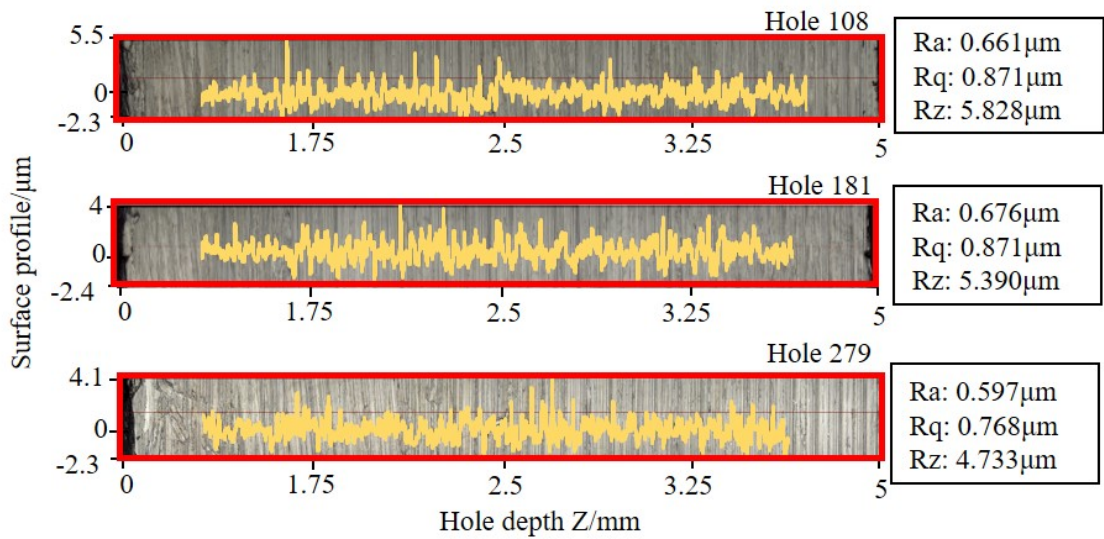


(b) Roughness parameters dendrogram (R_a , R_q , R_z , R_p , R_c , R_{sk} , R_{dq})

Figure 6.11 Validation data for BH04.5D (straight edge) tool, a) Obtained clusters from sensor data in two principal component space of the selected features, labels in black are the holes used for the cluster creation, labels in blue are the holes measured after the clusters where created b) Obtained clusters from surface measurement data (green and red colours express the clusters of the figure a)

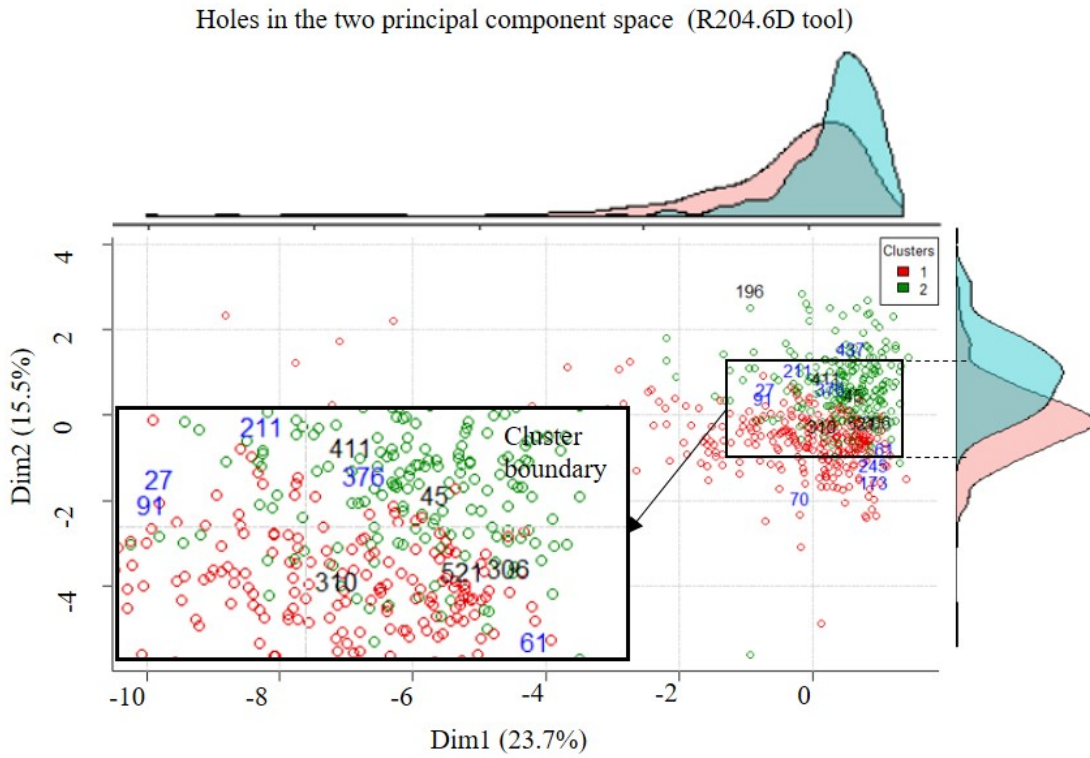


(a) Surface tearing observed profiles

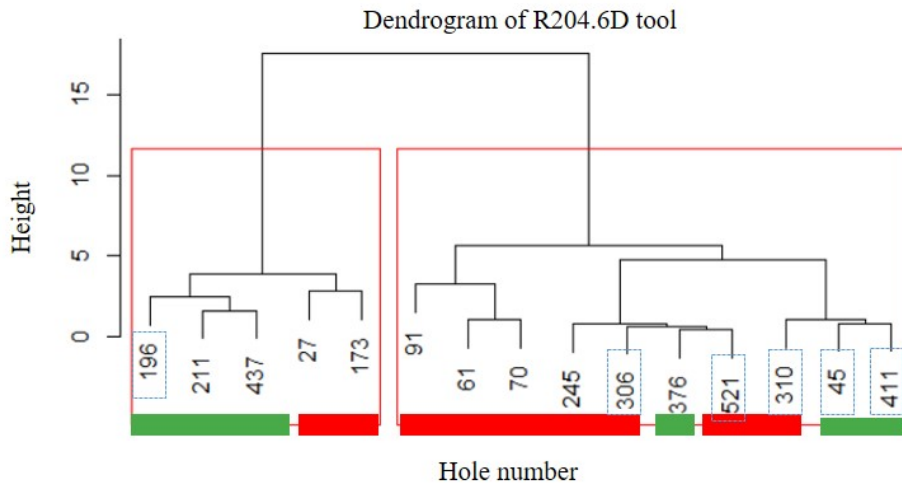


(b) Damage free surfaces

Figure 6.12 Hole surfaces and surface profiles obtained with BH04.5D tool a) Observed surface tearing b) Free damage surfaces



(a) 2 Principal components of features and density plots



(b) Roughness parameters dendrogram (R_a , R_p , R_v , R_{sm} , R_{sk} , R_{ku} , R_{dq})

Figure 6.13 Validation data for R204.6D (curved edge) tool, a) Obtained clusters from sensor data in two principal component space of the selected features and holes in clusters boundary b) Obtained clusters from surface measurement data. Red colour corresponds to cluster 1 and green color to cluster 2 of Figure a)

$$\text{Dim1} = 0.69 \cdot \text{ACCx1}_{\min} - 0.68 \cdot \text{ACCx1}_{\text{kurt}} \quad (6.3)$$

$$\text{Dim2} = 0.55 \cdot \text{AE}_{\text{kurt}} + 0.46 \cdot \text{Fy}_{\text{skew}} + 0.41 \cdot \text{TV3}_{\min} + 0.41 \cdot \text{TV2}_{\max} + 0.34 \cdot \text{ACCy2}_{\text{skew}} \quad (6.4)$$

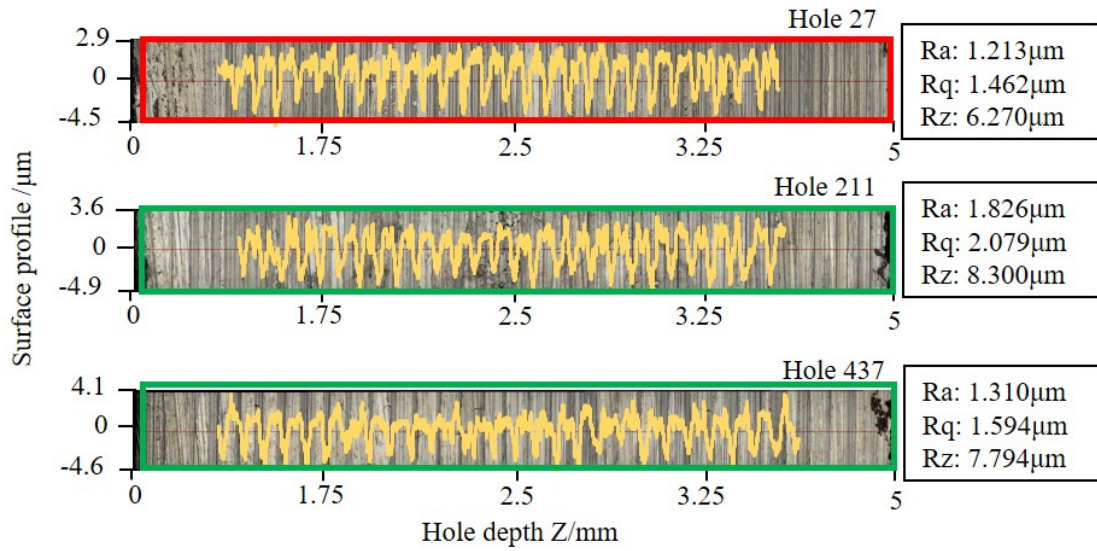
The area corresponding to the two principal components is $A = 107.45$ and the area corresponding to the holes measured for the creation of the clusters is $A(45, 196, 306, 310, 411, 521) = 6.02$. Therefore, 5.6% of the area has been covered. The inter-cluster distance is 1.65. Figure 6.14 shows the measured surfaces and their corresponding roughness profiles. Figure 6.14 a) more visible feed marks can be seen, whereas in Figure 6.14 b) holes with a lower surface roughness are seen with no visible feed marks. These feed marks do not show a trend in terms of the time series in which the holes have been made and could be due to other factors such as a built-up edge on the periphery of the tool.

In the BH04.5D tool, the area covered by the measured holes is more extensive than in the R204.6D tool, and better results are obtained, achieving a better separation between the clusters.

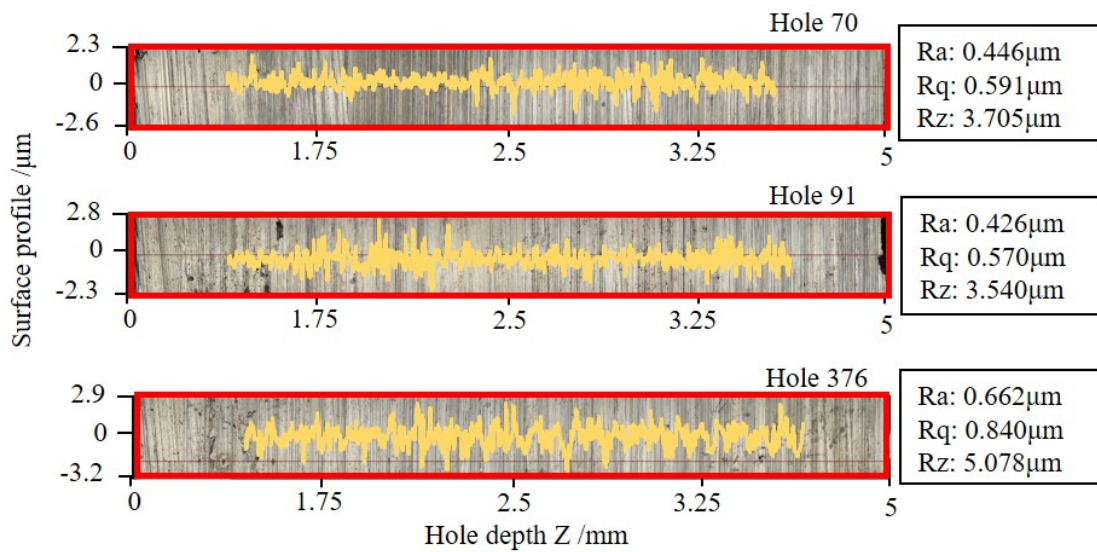
The creation of a supervised learning system requires the measurement of a large number of observations. The feasibility of this depends on the resources and time available. Obtaining classification models of roughness, in case of not having internal or external signals or only having process parameters is a complex task. Several parameters influence the roughness of a component and influence the features of the signals that can be collected during an operation. In this work, we show a methodology that can create descriptors of the roughness obtained by measuring a small sample of the set of observations to be evaluated. Although it is not an exact value of roughness, the descriptors are based on different parameters of the measured profile to create a model capable of classifying each of the holes made without the need for physical measurement. As in work done by Kubišová et al. (2019) the use of hierarchical clustering is highly valued to obtain information about the replicability of surfaces under specific cutting conditions.

The area covered by the holes measured on the map of the principal components plays an essential role in the methodology developed. It was found that with the R204.6D tool some of the holes were in the cluster boundary, while with the BH04.5D tool all the holes measured, both prior and for the validation, were identified in 100% of the measured cases on each respective clusters.

There is no direct effect on the features of a given signal directly related to the roughness profile of a component as can be the case with tool wear, which has been shown that the increase in thrust force in drilling processes is very closely related to



(a) Feed marks observed profiles



(b) Damage free surfaces

Figure 6.14 Hole surfaces and surface profiles obtained with R204.6D tool a) Observed feed marks b) Free of feed marks

the tool wear curve Lin and Ting (1995). Although many works show an increase in roughness values and tool wear, some temporal event in the middle of the process may cause the surface of the component to be damaged or the roughness value to increase for some reason with the same tool condition. This study shows that with two different cutting tools blocking the cutting conditions, surface roughness variations can be seen without tool wear.

The works consulted to date only contemplate the parameter Ra for monitoring the roughness of a given component (Deshpande et al., 2019; Mia and Dhar, 2016), as seen in Djebala et al. (2015) other roughness parameters can describe the fatigue or assembly properties. The Rsk value of a roughness profile can be of great importance; thus, an excessively negative skewness could lead to early fracture occurrence. However, it can be beneficial for assembly. Conversely, a positive skewness can lead to assembly problems and be beneficial for components where long useful life is expected. Therefore, the system proposed in this work has the benefit of using several roughness profile parameters. This leads to a better interpretation of the surface property characteristics of a component depending on the sector for which it is being manufactured.

The chip is fan-shaped on the R204.6D tool, which occurs when the chip is broken before a complete revolution; this is the ideal chip in drilling processes and the one that is best evacuated (Batzer et al., 1998). On the BH04.5D tool, the chip is somewhat longer and is a mixture of fan-shaped and conical, presenting a higher difficulty in the evacuation, and therefore could lead to surface tearing on the machined surface.

The surface tearing observed in the holes made with tool BH04.5D (straight edge) could be due to chip clogging. The phenomenon has been observed in the first half of the hole, in all cases ($Z < 2.5\text{mm}$), which suggests that it is the part of the surface that experiences the most damage during drilling.

Concerning the descriptors (categories) created, it is possible that for each of the tools used in other cutting conditions, there are other possible phenomena not visualised in the measurements made under the cutting conditions used. Tool wear, which is not analysed in this study, could also lead to the appearance of other types of defects that cause the machined surface to be negatively affected. So it is of interest to analyse the phenomena that may appear to decrease the limitations of this system. The statistical features related to the roughness profiles shown could change. Thus, a study of different cutting conditions and different tool conditions that increase the space of variables used and, consequently, creating a greater number of clusters is of interest.

6.4 CONCLUSIONS

Hierarchical clustering of holes is made with different tool geometries to describe the surface roughness obtained. For the characterization of the roughness of the machined components, several surface profile parameters measured in the Alicona profilometer were used. Once the statistical features of collected signals during drilling have been

identified, clustering is carried out for 600 holes made with each of the tools. The major contribution of this work results in the development of a new methodology capable of giving a descriptor of the quality of the surface generated in drilling processes based on the least number of measurements possible through the use of hierarchical clustering and internal and external signals to the cutting process. The result is a virtual metrology system for a more extensive set of holes than those physically measured. The following are the main conclusions:

- As contact properties of machined surfaces depend on the parameters of the roughness profile distribution, more than one parameter extracted from the profile must be taken into account for predictive modelling.
- It should be noted, in any case, that the measurement of roughness is a costly task but affordable in case of parts belonging to critical sectors.
- There was no tool wear identified during the tests. However, there was a variation in roughness. Events that occur at specific points in the cutting process cause the surface profile of the machined component to be affected.
- The events or phenomena observed on the machined surface that appear using two tool geometries are different. Consequently, the signals used to characterise the roughness result to be different, avoiding the use of the same variables to characterise the surface generated in the drilling processes.
- Clustering algorithms used with signals can approximate the roughness obtained and perform a classification of the holes without the need to measure a large number of them. In this way, a roughness estimation can be obtained by measuring just a few holes and projecting them in the signal space.
- The area covered with the measurements on the data observation space is of great relevance for a good mapping of the roughness parameters using the data gathered during the process. As can be seen with the R204.6D tool, not all the erroneous holes have been identified in their respective clusters, while with the BH04.5D tool, 100% have been identified.

INFLUENCE OF TOOL GEOMETRY, MATERIAL AND CUTTING CONDITIONS IN SENSOR SIGNALS: DIMENSIONALITY REDUCTION AND DATA ANALYSIS

Sensor measurements are affected by the input parameters of the cutting process (workpiece material, cutting conditions, tool geometry, tool material or coolant). This represents a challenge in terms of monitoring the cutting process. The measurement accuracy of the sensors must be interpreted using statistical tools. In such a way that it helps to reflect the detection sensitivity to a series of phenomena that are desired to predict. Using algorithms that allow classification through probability theory and the clustering of similar data groups, it is possible to identify data patterns related to the cutting process.

In general, the learning algorithms have as input variables, all the input conditions set for a cutting process for generalization purpose. The cost of developing a model that adapts to different machining conditions is high. An interpreter that identifies sensor data changes to adapt wear curves based on the set input conditions could abstract the design of predictive models to a wider process window. A single value (feature) from the set of sensor features can automatically recognise the change in input conditions of the machining process. If an equivalent set of features could be identified for different cutting processes (turning, milling, drilling), the trained algorithm would even be equivalent to the same in all cases. This can be done by transforming the feature set into two dimensions that can rearrange the data points to be easily identifiable.

The main idea of this chapter is that from the feature spaces of the sensors, it is possible to visualise the input parameters in two dimensions by analysing dimensionality reduction techniques. A comparison of PCA and tSNE is made to classify the input parameters used during the tests. This analysis allows the creation of data maps capable of identifying and visualising the differences between input parameters in two dimensions through sensor signals.

7.1 METHODOLOGY

The data used in this chapter correspond to the tests described in sections 3.2 and 3.3. Figure 7.1 represents input parameters variation concerning the acquired signals. In

steel BLS 35CrMo4, one feed rate, two cutting speeds and two different tool geometries were used, while in Inconel 718, one feed rate, one cutting speed and three different tool geometries were used. The main idea is the automatic identification of each of the set of input parameters used.

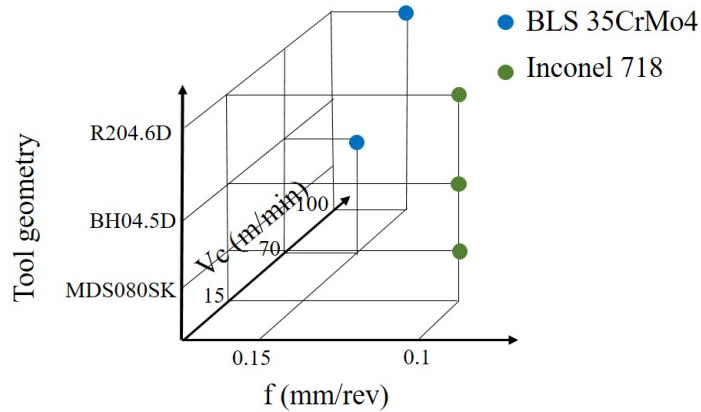


Figure 7.1 Different input parameters to the drilling process considered in this chapter

The comparison of the two strategies was made taking into account the schemes shown in Figure 7.2. The difference lies in the fact that applying PCA a direct transformation is learned to apply in new data. While tSNE can produce different visualization maps in each execution, a neural network is trained to predict the dimensions created by the tSNE algorithm.

Figure 7.2 a) shows the methodology involved in the use of PCA. In the training phase, principal component analysis is applied to obtain the projection of the statistical features in two-dimensions on the 70% of all available observations. The kNN algorithm is applied to the transformed new features to identify the different input parameters. In the testing phase, the PCA transform and the created model are applied to 30% of the remaining data to obtain the metrics that allow us to evaluate the pursued strategy. On the other hand, in Figure 7.2 b) the strategy followed with the tSNE algorithm is observed. As the model cannot be reproduced on new data, a neural network is trained to transform new data to the new projection of the components obtained by this method.

A backpropagation neural network was developed in R using keras for tSNE dimension multi-output predictions. The neural network has the following architecture [$n : n : 32 : 2$], where n is the number of input features of each of the sensor feature space. The loss function used was MAE and two regularization methods were used for training purpose and to get a better generalization. On the one hand, a dropout layer was used between the two hidden layers with a 0.2 rate, and on the other hand, an early stopping callback to get the best weights with a patience of 5, this means that the training will stop 5 epoch later if a better performance is not achieved. This configuration was used

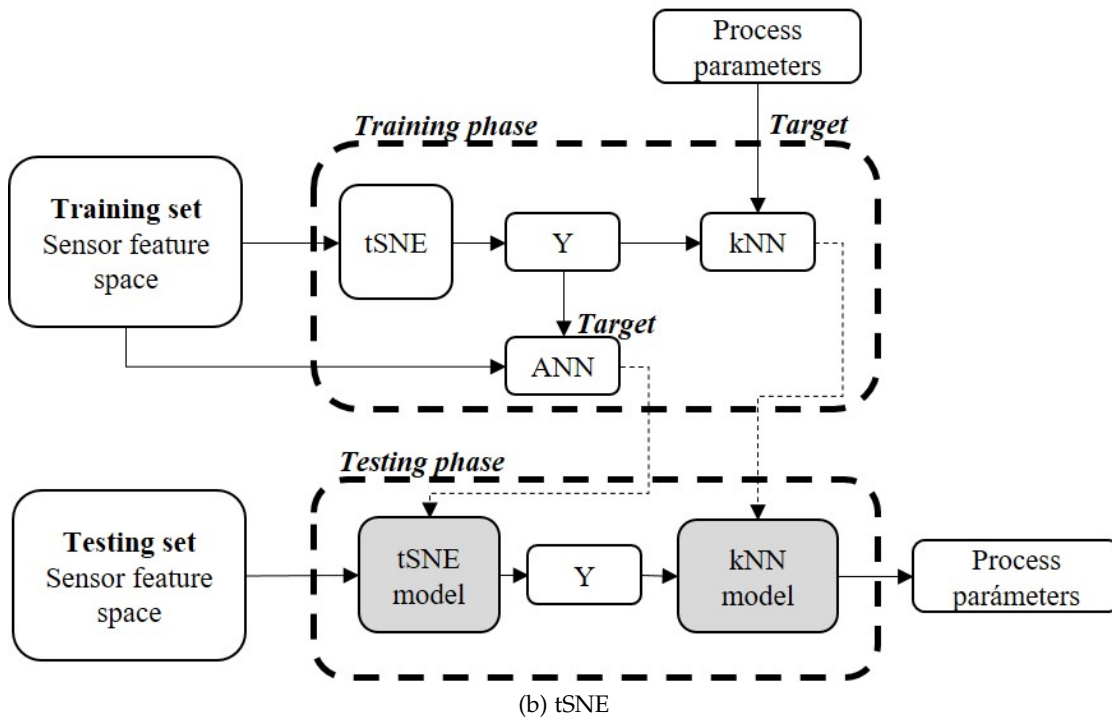
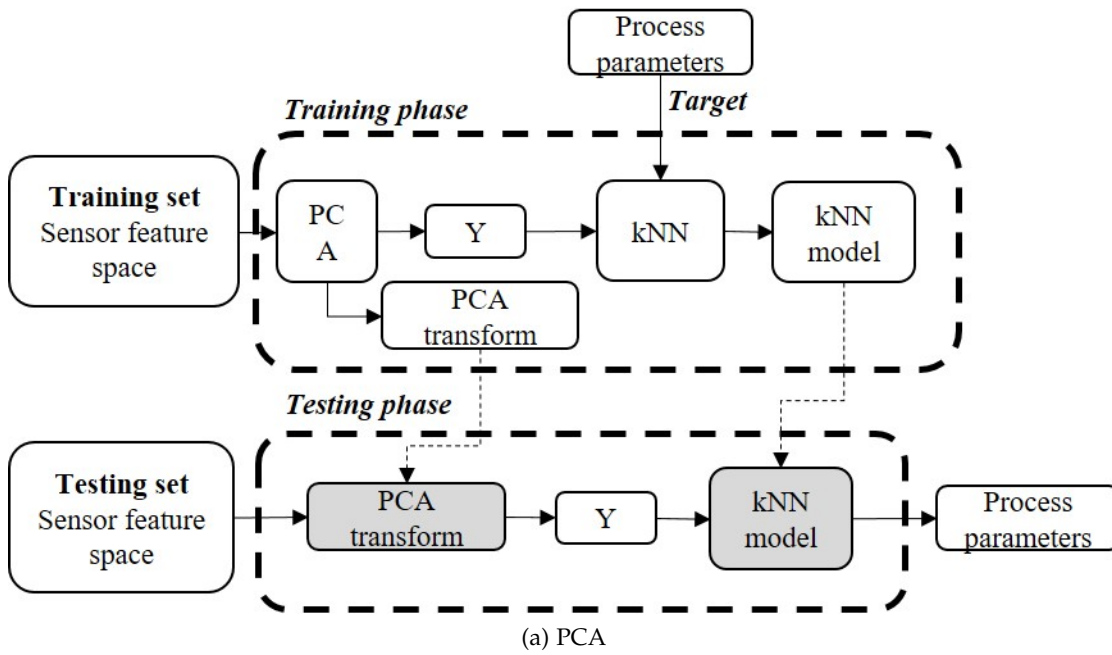


Figure 7.2 Compared two scenarios for the same objective a) PCA based model b) tSNE based model)

for each feature space used in this work. One epoch is when an entire dataset is passed forward and backward through the neural network only once.

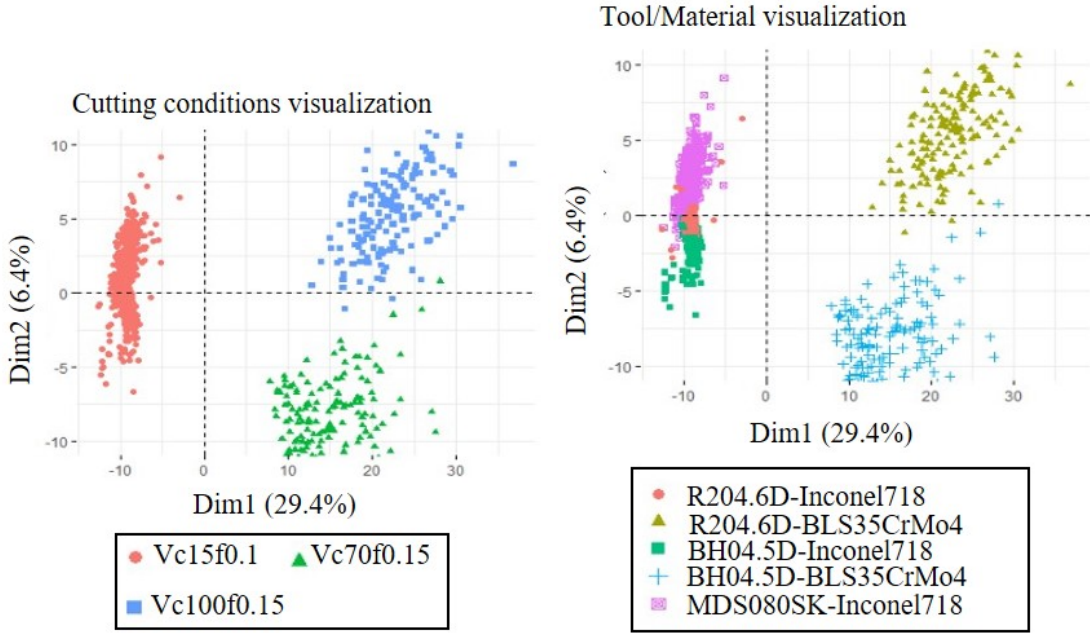
To compare the same algorithm performance with both methods a kNN algorithm was selected as it is based on the k neighbours between data points. And, as the idea is to group the similar data points and kNN classifier is generally used in this type of paradigms we chose this algorithm. The training dataset used does not have so much data points (750) and the reduced feature space is of 2 dimensions. (i) The algorithm first compute the distances of the new point to the rest of data points in the training dataset. (ii) Then, it selects the k nearest neighbours, that is, the ones with the lower distances. (iii) Finally, a voting is made between the classes of these k nearest neighbours. The class that predominates in the voting is assigned to the new point.

7.2 VISUALIZATION AND CLASSIFICATION OF DIFFERENT INPUT PARAMETERS USING PCA AND TSNE ON DIFFERENT SENSORS

Visualisations and classifications of the different input parameters have been made using each installed sensor and sensor fusion. Only the results obtained in the case of sensor fusion are shown in Figures 7.3 and 7.4 as there would be too many graphs, however the results achieved with each of the sensors are commented and discussed. The data have been coloured based on the interaction of cutting conditions (Vc-f) and tool geometry and material interaction. The summary of the results achieved using both the PCA and tSNE method for each sensor can be seen in Table 7.1.

Using the features of all the signals in the strategy pursued with PCA, visually, 3 large clusters can be observed in the case of the cutting conditions (Figure 7.3 a)). However, in Figure 7.3 b), although the groups created with the 3 geometries in Inconel 718 are very close together, they are easily identifiable. The classification results indicate that the material and cutting conditions are identified with 100% and 98.4% accuracy respectively. However, this classification is reduced to 90% when it comes to classifying tool geometry. The worst case is obtained by predicting the R204.6D used in Inconel 718 with only 55.6% success rate. The behaviour of this tool geometry on Inconel 718 was weak as it broke in the first few holes drilled.

Using tSNE with all the available signal features, the visualisation of the data is similar to that obtained with PCA. However, in this case, more compact and more separated clusters can be seen in Figure 7.4. The tests performed in the same material are closer to each other; on the right, the data for steel and the left, the data for Inconel 718 can be seen. The differences between the two groups on steel are due to the cutting conditions and tool geometry. Observing the distances of the groups in the same cutting conditions and different tool geometries in Inconel 718, the separation of the groups in steel is more pronounced by cutting condition differences. In Inconel 718, the data are more similar; the only parameter varied between them is the tool geometry, keeping all other parameters fixed. However, in this visualization, more significant differences can be observed than those obtained in PCA. Both material and cutting conditions are



(a) Cutting conditions

(b) Geometry/Material interaction

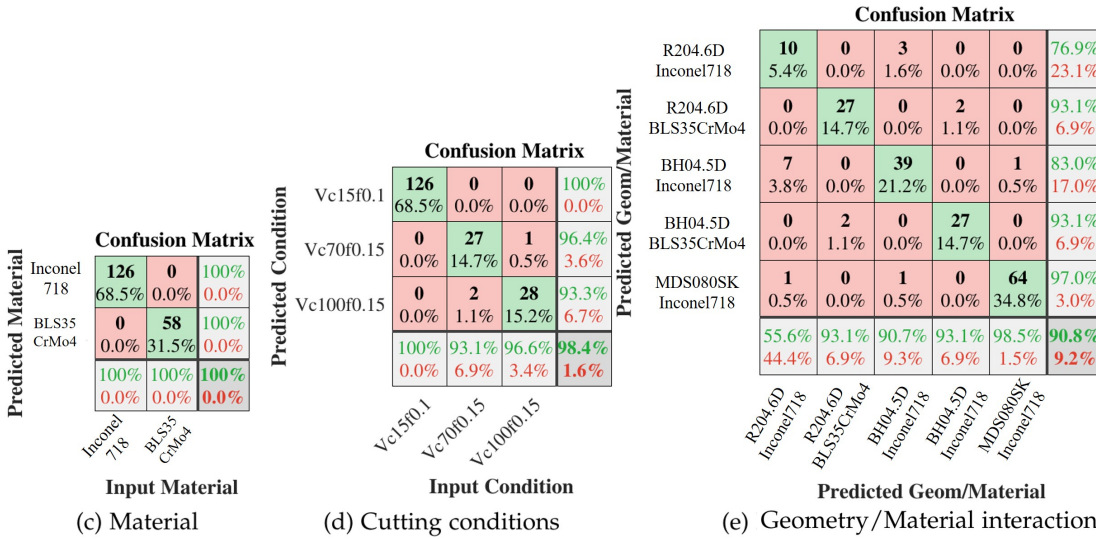


Figure 7.3 PCA based on sensor fusion a) Visualization based on cutting conditions b) Visualization based on Geometry/Material interaction c) Classification of material d) Classification of cutting conditions e) Classification of Geometry/Material interaction

predicted with a 100% success rate, tool geometry is predicted with a 98% success rate with only 4 misclassified holes being made on Inconel 718 with R204.6D and BH04.5D tool geometries.

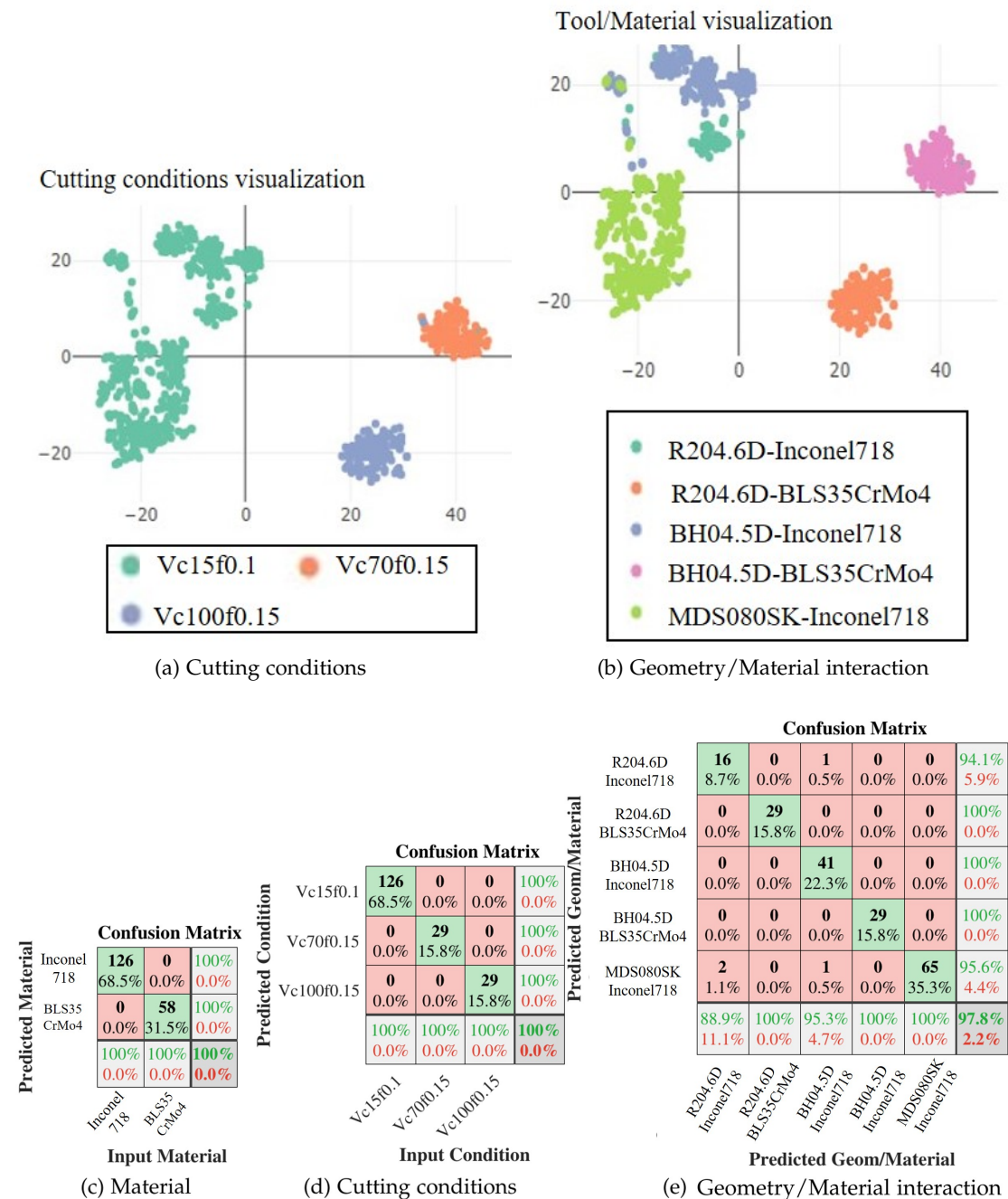


Figure 7.4 t-SNE based on Sensor fusion a) Visualization based on cutting conditions b) Visualization based on Geometry/Material interaction c) Classification of material e) Classification of cutting conditions f) Classification of Geometry/Material interaction

The same analysis has been carried out for each of the sensors separately. Table 7.1 shows the summary and comparison of each of the sensors for each of the methods used. Internal signals are those that can be acquired from the CNC, the sensor fusion are the features of [ACC, FC, AE, Internal] together.

Table 7.1 Comparison of the success rate between PCA and tSNE for identifying process input parameters

Method	Sensor	Material	Conditions	Geom/Mat
PCA	ACC	100	94.6	83.7
	FC	100	97.8	70.1
	AE	95.1	90.2	75.5
	Internal	100	100	88.6
	Sensor fusion	100	100	90.8
tSNE	ACC	100	98.4	84.2
	FC	100	98.9	91.3
	AE	98.4	92.9	77.7
	Internal	100	100	91.3
	Sensor fusion	100	100	97.8

Using both PCA and tSNE, the material and cutting conditions give good results. In terms of the material used, the worst result is obtained using acoustic emissions and PCA with a 95% success rate, and this percentage is improved by using tSNE with a 98% success rate. All other sensors can determine the material (Inconel 718 or BLS35CrMo4 steel) with a 100% accuracy. The cutting conditions are more misclassified, and slightly worse results are obtained. The worst result is again obtained using the acoustic emissions with 90% correct, with the accelerometer and cutting forces 94% and 97% of the cases are correctly classified respectively, all of them using PCA. In the tSNE scenario, all these results are improved, indicating that tSNE can better join the most similar data and separate the different ones. Finally, the geometry of the tool is the most difficult to classify. The best case using PCA is obtained with sensor fusion (shown in Figure 7.3), the worst case is obtained using cutting forces with a 70% success rate. The tSNE obtains better results, and the most noticeable improvement is obtained by using cutting forces, increasing the success rate to 91%.

One of the advantages of PCA is that it is possible to analyse those characteristics that contribute most to each of the principal components obtained. However, the t-SNE can facilitate the separation of the groups with greater precision.

The cutting conditions and the material used are easily identifiable using both PCA and t-SNE, although better results are obtained using t-SNE as it allows the separation of the groups according to the parameters in a more noticeable way.

Tool geometry is the most challenging input parameter to identify using the signals acquired during the drilling process. This indicates a lower variability of the acquired signals concerning this input; by merging the sensors used, the separation of the groups for the identification of the used geometry results in an increased probability of identifying this condition.

Similarly, the same occurs with the cutting conditions used except for the accelerometer and the PCA strategy, which places the cutting conditions used in BLS 35CrMo4 as if they were both carried out at $V_c = 100\text{m/min}$ and $f = 0.15\text{mm/rev}$. This is not the case for the t-SNE based strategy as it allows to increase the classification accuracy to 100% of the cases with the accelerometer signal.

The achieved two dimensional visualisation of the input parameters of the drilling process based on the acquired signals is interesting. Reducing the dimensions of the features of the individual sensors allows the construction of visualisation maps in which both similarities and differences that these parameters produce on the acquired signals can be identified. In flexible machining processes, where there are changes in input parameters, this form of visualisation can help develop the intelligence of the sensors. It can identify the changes and adapt the predictions to the specific combination of input parameters of the cutting process since the sensor data will be in other range of measurement. It is a form of visualisation which allows the identification of errors in the cutting conditions used at any given stage.

An illustration of the predictions made in the section 5.2.1 where the model was trained with the tool MDS080SK and predictions were made about the tool BH04.5D to predict the tool flank wear (V_b) on Inconel 718 can be seen on Figure 7.5. The lack of predictive ability shown by the model was because of geometry modification on the combination of input parameters. These visualisation maps inform that a model was trained to predict data for a specific input parameter combination and that the predictions intended to be made do not belong to the same process window as the data used to train the model. Consequently, the predictions may not be accurate, or at least were not validated at the time of model training.

7.3 CONCLUSIONS

In this chapter the dimensionality reduction of the features obtained from the sensors installed during the drilling process have been visualised and the accuracy of the kNN algorithm for the identification of the groups created from the reduced dimensionality has been evaluated.

- In general, the machined material properties have a significant effect on all the signals analysed. The cutting conditions used, or at least the cutting speed, which is the only one that has been modified on the steel material, also have an important effect. The tool geometry is the one that presents the most problems when it comes to being identified with either of the 2 methods used.

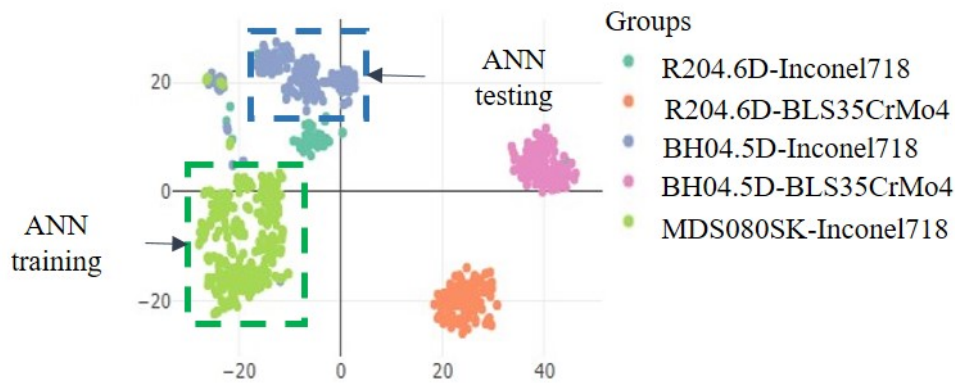


Figure 7.5 Input parameter combination changes used on section 5.2.1 to predict tool flank wear

- The tSNE method allows to separate the different groups with a more significant effect by joining those holes that have more similarities in the group of features analysed, and distancing those with differences.
- Instead of analysing each of the features separately, dimension reduction can provide a broader view of the effect on sensor signals when modifying one of the input parameters.
- PCA allows for the analysis of linear combinations of signal features that preserve the highest variance and at the same time do not present a redundancy. The tSNE allows for better visualisations but does not preserve the original structure of the data. This means that it does not allow the direct transformation of the new data to the dimensions created, requiring a neural network trained to obtain the new data in the transformed dimensions. The other way to transform the new data is to apply the whole process from the beginning, including the old and the new data.
- Sensor data can identify changes in the combination of input parameters to create data-driven models. In many cases, changes made to some parameter of the input conditions may not generate the expected sensor acquisition (measurement range for accurate prediction) for data-driven prediction, so identifying the combination of input parameters just based on the acquired sensor data can help to create more reliable models.

CONCLUSIONS AND FUTURE LINES

The drilling operation involves several industrial outputs that must be controlled for the proper operation of the machined component. Uncertain and random instabilities can cause errors in the component, leading to premature failure. The general framework of this research project was to create data-driven predictive models for the prediction of laboratory-measured errors. To this end, external (sensors) and internal (machine) signals were collected from the drilling process, and statistical analysis was applied to determine the signal features best suited to specific process monitoring (tool wear evolution, tool breakage or surface integrity condition). Modern manufacturing requires strategies to identify the type of error that may have occurred during machining and enable automatic detection of incorrect machining process behaviour. However, there are a wide variety of cutting process parameters that require monitoring. This makes it difficult to identify the sensors that better adapt or relate to the cutting process-specific parameters.

In this research project, a setup complete enough to acquire different drilling operation signals simultaneously was developed. Tests were carried out with different tool geometries on BLS 35CrMo4 Low S steel and Inconel 718 in three batches. The errors analysed and measured in detail in the laboratory were tool wear and hole surface roughness. Material damage was also measured, to evaluate the relationship between tool wear, surface roughness and material damage under specific cutting conditions.

The results show the high capability of specific signal features for detecting tool condition or determining a tool breakage risk. The analysis carried out has made it possible to assess the capacity of each of the signals acquired for the identification or reconstruction of the tool condition.

However, the installation of several sensors is an impractical solution that can challenge the indirect measurement of the tool condition, and each signal can achieve different robustness. Thus, the requirements for monitoring the cutting process must be determined to select the sensors best suited to the specific monitoring needs.

Identifying signal features related to errors that compromise the machined surface integrity is a difficult task. Depending on the type of error that may occur during machining, the signals can show greater or lesser sensitivity to process instabilities. The roughness profile parameters can help to identify the signal features that are best suited

to surface errors. However, the results show that changes in the input parameters cause different surface errors. Therefore, the features selected to determine the type of error that may have occurred can change, or might not be effective in all cases.

8.1 TOOL CONDITION MONITORING

Chapters 4 and 5 are mainly focused on the evaluation of information sources (sensors and internal machine signals) for the prediction of the cutting tool condition. This evaluation was carried out, considering that not all information sources have the same capacity to predict the tool condition. The signals acquired during the cutting process were compared following two strategies for predicting tool wear.

On the one hand, the analysis of each of the signals was carried out separately to classify different wear levels on previously worn tools on steel BLS 35CrMo4 employing two different tool geometries (Kendu BH04.5D and R204.6D). On the other hand, a reconstruction of the tool condition with three different tool geometries (Kendu BH04.5D and R204.6D and SUMITOMO MDS080SK) on Inconel 718, was performed in three repetitions with each of the tool geometries. The tool R204.6D broke prematurely at the beginning of the drilling process, and was excluded from further analysis.

The results of these analyses indicate that both internal and external signals can perform the task adequately. Hence, it is possible to exchange some of the acquired external signals for some of the acquired internal signals, without compromising robustness for tool wear prediction.

In the process conditions established in this study, the best external sensor was found to be the dynamometer for both classification and regression. However, given their predictive capability for tool wear, the internal signals were identified as candidates for replacing the dynamometer since they indirectly monitor cutting force signals. The cost of acquiring internal signals is less expensive, and there is no need to install sensors on the machine.

From the signal features extracted, acoustic emissions were not able to predict the wear curve. It may be however, that another sensor location or another pre-processing would allow the reconstruction of the said curve. The accelerometer is a sufficiently robust candidate for the reconstruction of the wear curve. However, after the variable selection process, the sensor has the highest number of features shown to be needed.

Using the data of a specific tool geometry as training, the prediction of another tool geometry is possible up to a point. Chapter 4 focuses on a classification strategy, in which the models can identify the class membership of second tool geometry with a high degree of accuracy using the internal signal of the Z-axis torque TV2. The reconstruction is more complicated however, when the strategy employed is to reconstruct the wear curve, as seen in chapter 5. The signal that presented the most notable adaptation was the accelerometer. Although the accelerometer was able to model the non-linearity of the wear curve, it was more difficult to compensate the offset

of the predictions and achieve accurate results. This indicates that these systems are case sensitive and need calibration with data from different input conditions to the cutting process for fine tuning (tool geometries, cutting conditions or materials).

The risk of tool periphery breakage was predicted using logistic model trees. This algorithm is particularly valuable in determining the probability breakage at the tool periphery. In this case, the signals identified as the most capable of performing the task were the internal signals and cutting forces, since they produced more simple and interpretable models.

The amount of data generated by each sensor and the capacity of the monitoring unit to process and store it should also be considered when selecting features. In controlled laboratory environments, as in this study, the volume of data generated is limited. However, in industrial environments, data volume can grow considerably and limit the available resources, causing system degradation.

8.2 SURFACE CONDITION MONITORING

Although monitoring the Ra parameter is a widespread practice, direct measurement to create supervised learning models is costly. Furthermore, the same Ra level on two "identically" machined components does not necessarily mean the same contact properties. Thus, the surface condition was evaluated by performing unsupervised learning on several roughness profile parameters to compare the repeatability of the drilling process and acquire the desired surface contact properties. The applied methodology is the closest to the methods used in production environments. By measuring a sub-population of holes randomly selected from the total number of holes drilled and applying hierarchical clustering, the similarity between the measured holes is established. The developed unsupervised learning methodology can respond to a more significant unknown than merely evaluating a single roughness profile parameter. When the surface errors that can appear on a given component with a given tool geometry and cutting conditions are characterised, it is possible to create clusters from the signals that distinguish those damaged surfaces with different contact properties.

The findings show that vibration signals are the most likely to be related to the generated surface. However, other signals such as cutting torque, spindle power, Y-axis cutting force, acoustic emissions, or Z-axis motor torque or current could also be present.

In the tool BH04.5D, dimension 1 of the principal components in which the features $ACCx2_rms$, $ACCz2_rms$, $ACCz2_min$ and $ACCy_max$ have the greatest contribution, is where a greater separation of the obtained groups (clusters) is observed. Therefore it can be concluded that the features obtained from the accelerometer contribute to the identification of the holes that present a surface error. In the case of this tool, surface tearing.

In the case of tool R204.6D no specific sensor contribution is observed. In dimension 1, ACCx1_min and ACCx1_kurt contribute, while in dimension 2 a larger number of features (AE_kurt, Fy_skew, TV3_min, TV2_max, ACCy_skew) contribute. Cluster separation and visualisation based on PCA show that the cluster boundary separates the clusters in dimension 2. Although most of the measured holes belong to their cluster there are a number of holes that are misclassified.

No direct relationship was found between roughness and tool wear. This is thought to be because minor cutting edges generate the final surface of the hole.

8.3 INPUT PARAMETER RECOGNITION THROUGH SENSORS

A broader analysis of the signals acquired was conducted by reducing the feature set dimensionality and visualising these new dimensions according to the cutting process input parameters. The results showed that PCA and tSNE are capable of representing input parameters based on sensor data. This can help process monitoring systems reconfigure and adapt to various metals, tool geometries and cutting conditions, and even different processes.

tSNE and PCA methods effectively identified the change of workpiece material and cutting conditions. Tool geometry changes however, proved more challenging to identify. In this case, tSNE identified the tool geometry with better results than that achieved with PCA using any of the employed sensors. The best result was obtained by sensor fusion in both PCA and tSNE however, this identification must be based on the sensor or sensors used to monitor the cutting process.

8.4 FUTURE DEVELOPMENT

Future monitoring systems must obtain as many signal features as possible, differentiate those that are unrelated to the monitoring unit, eliminate redundancy that may introduce undesirable features into the prediction models, and make robust predictions for accurate and automatic decision making. The quality of model predictions must also be monitored to ensure adequate feedback. This indicates that the deployment and implementation of predictive models in production environments are not static. Continuous feedback has to be received to guarantee prediction accuracy. Active learning also plays a key role in model deployment. As new data is produced, this should be validated to update predictive capacity.

In the context of the set of input parameters used in this work, the signals have performed quite accurately. However, their use may be limited to specific cutting parameters. The definition of the process window (tool diameter, cutting conditions or different materials) in which each signal can operate for wear monitoring is critical. For this purpose, tests need to be carried out on different materials and under different input conditions to establish the capability limits of each specific sensor.

In processes such as drilling, there is no direct relationship between tool wear and the level of roughness. The measurement of the similarity of two machined surfaces under established cutting conditions is thus of considerable interest. Methodologies that assess whether two components manufactured under the same conditions meet the specified requirements can increase productivity and speed up decision-making without expensive direct inspections.

The results show that material damage does not depend only on tool wear or tool geometry. The parameters that can affect material damage in drilling processes should be investigated in more detail to identify the signal features that can maintain a relationship with these parameter.

In this research work, only tool condition and surface integrity were analysed. However, as reported in the literature, more parameters influence the lifetime of the machined component, such as dimensional tolerances, residual stresses or burr formation. These industrial parameters should also be related to the acquired signals, so as to increase machining accuracy by adapting input parameters to the machined component.

CONTRIBUTIONS

ARTICLES IN PEER-REVIEWED JOURNALS

- Aitor Duo, Rosa Basagoiti, Pedro J. Arrazola, Javier Aperribay, and Mikel Cuesta. 2019. "The Capacity of Statistical Features Extracted from Multiple Signals to Predict Tool Wear in the Drilling Process." *International Journal of Advanced Manufacturing Technology*, 5-8. <https://doi.org/10.1007/s00170-019-03300-5>.
- Aitor Duo, Erika Domínguez, Larraitz Azpitarte, Javier Aperribay, Mikel Cuesta, Ainhara Garay, Rosa Basagoiti, and Pedro J. Arrazola. 2020. "Qualitative estimation of roughness using automatic learning algorithms in a drilling operation." *DYNA*, 1-9. <https://doi.org/https://doi.org/10.6036/9388>.
- Aitor Duo, Rosa Basagoiti, Pedro J. Arrazola, Mikel Cuesta and Miren Illarramendi. 2021. "Surface roughness assessment on hole drilled through the identification and clustering of relevant external and internal signal statistical features " *CIRP Journal of Manufacturing Science and Technology*, Under review.
- Aitor Duo, Rosa Basagoiti, Pedro J. Arrazola and Mikel Cuesta. 2021. "Sensor signal selection for tool wear curve estimation and subsequent tool breakage prediction in a drilling operation" *International Journal of Computer Integrated Manufacturing*, Under review.

INTERNATIONAL CONFERENCES

- Aitor Duo, Rosa Basagoiti, Pedro J. Arrazola, Javier Aperribay,. 2018. "A Comparative Study between Internal and External Signals for Tool Wear Detection in Drilling Processes." 14th *International Conference on High Speed Machining*, Donostia-San Sebastian. Apr. 17, 2018-Apr. 18, 2018 (presenting author).
- Aitor Duo, Tiziana Segreto, Alessandra Caggiano, Rosa Basagoiti, Roberto Teti, and Pedro J Arrazola. 2020. "Drilling Process Monitoring: A Framework for Data Gathering and Feature Extraction Techniques." 14th *CIRP Conference on Intelligent*

Computation in Manufacturing Engineering, Gulf of Naples, Italy. Jul 15, 2020 - Jul 18, 2020. <https://doi.org/10.1016/j.procir.2021.03.123> (presenting author).

NATIONAL CONFERENCES

- Aitor Duo, Erika Domínguez, Larraitz Azpitarte, Javier Aperribay, Mikel Cuesta, Ainhara Garay, Rosa Basagoiti and Pedro J Arrazola. 2019. "Estimación cualitativa de la rugosidad mediante algoritmos de aprendizaje automático en una operación de taladrado." 22 *Congreso de máquina herramienta*, Donostia-San Sebastian. Oct. 23, 2019-Oct. 25, 2019 (presenting author).

OPEN-ACCESS DATASETS

- Aitor Duo, Rosa Basagoiti, Pedro J. Arrazola, Javier Aperribay, and Mikel Cuesta. Drilling test data from new and worn bits [Dataset]. 2019. <http://hdl.handle.net/20.500.11984/1477>

BIBLIOGRAPHY

- Abdelhafeez, A. M. et al. (2015). "Burr formation and hole quality when drilling titanium and aluminium alloys." In: *Procedia CIRP*. Vol. 37, pp. 230–235. ISBN: 9781510815216. DOI: 10.1016/j.procir.2015.08.019.
- Abu-Mahfouz, Issam (2003). "Drilling wear detection and classification using vibration signals and artificial neural network." In: *International Journal of Machine Tools and Manufacture* 43:7, pp. 707–720. ISSN: 08906955. DOI: 10.1016/S0890-6955(03)00023-3.
- Abubakr, Mohamed et al. (2021). "Sensors selection for tool failure detection during machining processes: A simple accurate classification model." In: *CIRP Journal of Manufacturing Science and Technology* 32, pp. 108–119. ISSN: 17555817. DOI: 10.1016/j.cirpj.2020.12.002.
- Akincioğlu, Sitki et al. (2013). "ANN-based prediction of surface and hole quality in drilling of AISI D2 cold work tool steel." In: *International Journal of Advanced Manufacturing Technology* 68.1-4, pp. 197–207. ISSN: 02683768. DOI: 10.1007/s00170-012-4719-6.
- Amor, Meriem Bel Hadj et al. (2015). "Effect of skewness and roughness level on the mechanical behavior of a rough contact." In: *Lecture Notes in Mechanical Engineering* 789, pp. 377–386. ISSN: 21954364. DOI: 10.1007/978-3-319-17527-0_38.
- Ao, Yinhui and George Qiao (2010). "Prognostics for drilling process with wavelet packet decomposition." In: *International Journal of Advanced Manufacturing Technology* 50.1-4, pp. 47–52. ISSN: 02683768. DOI: 10.1007/s00170-009-2509-6.
- Arrazola, P J. et al. (2014). "Correlation between tool flank wear, force signals and surface integrity when turning bars of Inconel 718 in finishing conditions." In: *International Journal of Machining and Machinability of Materials* 15.1/2, p. 84. ISSN: 1748-5711. DOI: 10.1504/IJMMM.2014.059193.
- ARTIS (n.d.). *Machine condition monitoring brochure*. Tech. rep. URL: <https://www.marposs.com/spa/product/tool-and-process-monitoring-system>.
- Astakhov, Viktor P (2010). *Geometry of single-point Turning Tools and Drill: Fundamental and Practical Applications*, p. 562. DOI: 10.1007/978-1-84996-053-3.
- Babatunde, O P et al. (2017). "Acoustic Emission in Stainless Steel End Milling with Carbide Tools." In: *International Symposium on Advanced Material Research* 753 KEM, pp. 206–210. DOI: 10.4028/www.scientific.net/KEM.753.206.
- Balazinski, Marek et al. (2002). "Tool condition monitoring using artificial intelligence methods." In: *Engineering Applications of Artificial Intelligence* 15.1, pp. 73–80. ISSN: 0952-1976. DOI: [https://doi.org/10.1016/S0952-1976\(02\)00004-0](https://doi.org/10.1016/S0952-1976(02)00004-0).
- Balsamo, Vittorio et al. (2016). "Multi Sensor Signal Processing for Catastrophic Tool Failure Detection in Turning." In: *Procedia CIRP* 41, pp. 939–944. ISSN: 22128271. DOI: 10.1016/j.procir.2016.01.010.

- Batzer, S. A. et al. (1998). "Chip morphology and hole surface texture in the drilling of cast Aluminum alloys." In: *Journal of Materials Processing Technology* 79.1-3, pp. 72–78. ISSN: 09240136. DOI: 10.1016/S0924-0136(97)00324-5.
- Benardos, P. G. and G. C. Vosniakos (2003). "Predicting surface roughness in machining: A review." In: *International Journal of Machine Tools and Manufacture* 43.8, pp. 833–844. DOI: 10.1016/S0890-6955(03)00059-2.
- Bhuiyan, M. S H et al. (2016). "Application of acoustic emission sensor to investigate the frequency of tool wear and plastic deformation in tool condition monitoring." In: *Measurement: Journal of the International Measurement Confederation* 92, pp. 208–217. ISSN: 02632241. DOI: 10.1016/j.measurement.2016.06.006.
- Bhuiyan, M. S.H. and I. A. Choudhury (2014). *Review of Sensor Applications in Tool Condition Monitoring in Machining*. Vol. 13. Elsevier, pp. 539–569. ISBN: 9780080965338. DOI: 10.1016/B978-0-08-096532-1.01330-3. arXiv: arXiv:0901.0931.
- Bhushan, Bharat (2000). "Surface Roughness Analysis and Measurement Techniques." In: *Revista clínica española* 5, pp. 49–119. DOI: 10.1201/9780849377877.
- Brinksmeier, E. (1990). "Prediction of Tool Fracture in Drilling." In: *CIRP Annals* 39.1, pp. 97–100. ISSN: 0007-8506. DOI: [https://doi.org/10.1016/S0007-8506\(07\)61011-7](https://doi.org/10.1016/S0007-8506(07)61011-7).
- Caggiano, Alessandra (2018). "Tool wear prediction in Ti-6Al-4V machining through multiple sensor monitoring and PCA features pattern recognition." In: *Sensors (Switzerland)* 18.3. ISSN: 14248220. DOI: 10.3390/s18030823.
- Caggiano, Alessandra et al. (2017). "Dry Turning of Ti6Al4V: Tool Wear Curve Reconstruction Based on Cognitive Sensor Monitoring." In: *Procedia CIRP* 62, pp. 209–214. ISSN: 22128271. DOI: 10.1016/j.procir.2017.03.046.
- Caggiano, Alessandra et al. (2018a). "Dimensionality Reduction of Sensorial Features by Principal Component Analysis for ANN Machine Learning in Tool Condition Monitoring of CFRP Drilling." In: *Procedia CIRP* 78, pp. 307–312. ISSN: 22128271. DOI: 10.1016/j.procir.2018.09.072.
- Caggiano, Alessandra et al. (2018b). "Multiple Sensor Monitoring for Tool Wear Forecast in Drilling of CFRP/CFRP Stacks with Traditional and Innovative Drill Bits." In: *Procedia CIRP* 67, pp. 404–409. ISSN: 22128271. DOI: 10.1016/j.procir.2017.12.233.
- Cai, Jie et al. (2018). "Feature selection in machine learning: A new perspective." In: *Neurocomputing* 300, pp. 70–79. ISSN: 18728286. DOI: 10.1016/j.neucom.2017.11.077.
- Caron (n.d.). *TOOL MONITORING ADAPTIVE CONTROL*. URL: <https://www.caroneng.com/products/tmac-tool-monitoring-adaptive-control>.
- Chawla, Nitesh V. et al. (2002). "SMOTE: Synthetic minority over-sampling technique." In: *Journal of Artificial Intelligence Research* 16.Sept. 28, pp. 321–357. ISSN: 10769757. DOI: 10.1613/jair.953. arXiv: 1106.1813.
- Chen, Y. C. and Y. S. Liao (2003). "Study on wear mechanisms in drilling of Inconel 718 superalloy." In: *Journal of Materials Processing Technology* 140.1-3 SPEC. Pp. 269–273. ISSN: 09240136. DOI: 10.1016/S0924-0136(03)00792-1.
- Childs, Thomas et al. (2000). "Chip formation fundamentals." In: *Metal Machining* 1878, pp. 35–80. DOI: 10.1016/B978-0-08-052402-3.50005-8.

- Corne, Raphael et al. (2017). "Study of spindle power data with neural network for predicting real-time tool wear/breakage during inconel drilling." In: *Journal of Manufacturing Systems* 43, pp. 287–295. ISSN: 02786125. DOI: 10.1016/j.jmsy.2017.01.004.
- Dechow, Henning (1998). "Influence of tool geometry on hole quality when drilling Ti-6Al-4V." In: *Lma*, p. 43.
- Deshpande, Yogesh V. et al. (2019). "Application of ANN to estimate surface roughness using cutting parameters, force, sound and vibration in turning of Inconel 718." In: *SN Applied Sciences* 1.1. ISSN: 2523-3963. DOI: 10.1007/s42452-018-0098-4.
- Dheeraj Simon, Galipothu and R. Deivanathan (2019). "Early detection of drilling tool wear by vibration data acquisition and classification." In: *Manufacturing Letters* 21, pp. 60–65. ISSN: 22138463. DOI: 10.1016/j.mfglet.2019.08.006.
- Diaz-Rozo, Javier et al. (2017). "Machine Learning-based CPS for Clustering High throughput Machining Cycle Conditions." In: *Procedia Manufacturing* 10, pp. 997–1008. ISSN: 23519789. DOI: 10.1016/j.promfg.2017.07.091.
- Dimla, D.E and P.M Lister (2000). "On-line metal cutting tool condition monitoring." In: *International Journal of Machine Tools and Manufacture* 40.5, pp. 769–781. ISSN: 08906955. DOI: 10.1016/S0890-6955(99)00085-1.
- Dimla Snr., Dimla E. (2000). "Sensor signals for tool-wear monitoring in metal cutting operations - a review of methods." In: *International Journal of Machine Tools and Manufacture* 40.8, pp. 1073–1098. ISSN: 08906955. DOI: 10.1016/S0890-6955(99)00122-4.
- Djebala, Abderrazek et al. (2015). *Design and Modeling of Mechanical Systems - II*. Vol. 789, pp. 169–178. ISBN: 978-3-319-17526-3. DOI: 10.1007/978-3-319-17527-0.
- Drouillet, Cyril et al. (2016). "Tool life predictions in milling using spindle power with the neural network technique." In: *Journal of Manufacturing Processes* 22. DOI: 10.1016/j.jmapro.2016.03.010.
- Dudzinski, D. et al. (2004). "A review of developments towards dry and high speed machining of Inconel 718 alloy." In: *International Journal of Machine Tools and Manufacture* 44.4, pp. 439–456. ISSN: 08906955. DOI: 10.1016/S0890-6955(03)00159-7.
- Duo, Aitor et al. (2019). "The capacity of statistical features extracted from multiple signals to predict tool wear in the drilling process." In: *International Journal of Advanced Manufacturing Technology*, pp. 5–8. ISSN: 14333015. DOI: 10.1007/s00170-019-03300-5.
- Eckstein, Martin et al. (2016). "Tool Wear and Surface Roughness Evolution in Hole Making Process of Inconel 718." In: *Materials Science Forum* 862, pp. 11–17. ISSN: 1662-9752. DOI: 10.4028/www.scientific.net/MSF.862.11.
- Ehmann, K. F. et al. (1997). "Machining process modeling: A review." In: *Journal of Manufacturing Science and Engineering, Transactions of the ASME* 119.4B, pp. 655–663. ISSN: 15288935. DOI: 10.1115/1.2836805.
- El-Hofy, Hassan (2019). *Fundamental of Machining Processes*. Third edit. CRC press, p. 6. ISBN: 9781138334908.
- El-Wardany, T.I. et al. (1996). "Tool condition monitoring in drilling using vibration signature analysis." In: *International Journal of Machine Tools and Manufacture* 36.6,

- pp. 687–711. ISSN: 0890-6955. DOI: [https://doi.org/10.1016/0890-6955\(95\)00058-5](https://doi.org/10.1016/0890-6955(95)00058-5).
- Elangovan, M. et al. (2011). "Evaluation of expert system for condition monitoring of a single point cutting tool using principle component analysis and decision tree algorithm." In: *Expert Systems with Applications* 38.4, pp. 4450–4459. ISSN: 09574174. DOI: 10.1016/j.eswa.2010.09.116.
- Equeter, Lucas et al. (2020). "Cutting Tools Replacement: Toward a Holistic Framework." In: *IFAC-PapersOnLine* 53.3, pp. 227–232. ISSN: 24058963. DOI: 10.1016/j.ifacol.2020.11.037.
- Erzurumlu, Tuncay and Hasan Oktem (2007). "Comparison of response surface model with neural network in determining the surface quality of moulded parts." In: *Materials and Design* 28.2, pp. 459–465. ISSN: 18734197. DOI: 10.1016/j.matdes.2005.09.004.
- Everitt, Brian S. et al. (2011). *Cluster analysis: Fifth edition*, pp. 1–330. ISBN: 9780470977811. DOI: 10.1002/9780470977811.
- Ferreiro, Susana et al. (2011). "Data mining for quality control: Burr detection in the drilling process." In: *Computers and Industrial Engineering* 60.4, pp. 801–810. ISSN: 03608352. DOI: 10.1016/j.cie.2011.01.018.
- Franco-Gasca, Luis Alfonso et al. (2006). "Sensorless tool failure monitoring system for drilling machines." In: *International Journal of Machine Tools and Manufacture* 46.3-4, pp. 381–386. ISSN: 08906955. DOI: 10.1016/j.ijmachtools.2005.05.012.
- Gadelmawla, E. S. et al. (2002). "Roughness parameters." In: *Journal of Materials Processing Technology* 123.1, pp. 133–145. DOI: 10.1016/S0924-0136(02)00060-2.
- Gao, R. et al. (2015). "Cloud-enabled prognosis for manufacturing." In: *CIRP Annals - Manufacturing Technology* 64.2, pp. 749–772. DOI: 10.1016/j.cirp.2015.05.011.
- García Plaza, E. and P. J. Núñez López (2017). *Surface roughness monitoring by singular spectrum analysis of vibration signals*. DOI: 10.1016/j.ymsp.2016.06.039.
- García Plaza, E. et al. (2019). "Efficiency of vibration signal feature extraction for surface finish monitoring in CNC machining." In: *Journal of Manufacturing Processes* 44.March, pp. 145–157. ISSN: 15266125. DOI: 10.1016/j.jmapro.2019.05.046.
- Garg, Saurabh et al. (2010). "Engineering Applications of Artificial Intelligence Genetically evolved radial basis function network based prediction of drill flank wear." In: *Engineering Applications of Artificial Intelligence* 23.7, pp. 1112–1120. ISSN: 0952-1976. DOI: 10.1016/j.engappai.2010.02.012.
- Gómez, Martín P. et al. (2010). "Tool wear evaluation in drilling by acoustic emission." In: *Physics Procedia* 3.1, pp. 819–825. ISSN: 18753892. DOI: 10.1016/j.phpro.2010.01.105.
- Gouarir, A et al. (2018). "In-process Tool Wear Prediction System Based on Machine Learning Techniques and Force Analysis." In: *Procedia CIRP* 77.Hpc, pp. 501–504. ISSN: 2212-8271. DOI: <https://doi.org/10.1016/j.procir.2018.08.253>.
- Grosse, Christian U and Lindsay M Linzer (2008). "Signal-Based AE Analysis." In: *Acoustic Emission Testing: Basics for Research - Applications in Civil Engineering*. Ed. by Christian Grosse and Masayasu Ohtsu. Berlin, Heidelberg: Springer Berlin

- Heidelberg, pp. 53–99. ISBN: 978-3-540-69972-9. DOI: 10.1007/978-3-540-69972-9_5.
- Han, Jiawei et al. (2012). *Data Mining: Concepts and Techniques*, p. 745. DOI: 10.1016/B978-0-12-381479-1.00001-0.
- Harun, M. H.S. et al. (2017). "Analysis of tri-axial force and vibration sensors for detection of failure criterion in deep twist drilling process." In: *International Journal of Advanced Manufacturing Technology* 89.9-12, pp. 3535–3545. ISSN: 14333015. DOI: 10.1007/s00170-016-9344-3.
- Herbert, C. R.J. et al. (2012). "An evaluation of the evolution of workpiece surface integrity in hole making operations for a nickel-based superalloy." In: *Journal of Materials Processing Technology* 212.8, pp. 1723–1730. ISSN: 09240136. DOI: 10.1016/j.jmatprotec.2012.03.014.
- Heyns, P. Stephan (2007). "Tool condition monitoring using vibration measurements - A review." In: *Insight: Non-Destructive Testing and Condition Monitoring* 49.8, pp. 447–450. ISSN: 13542575. DOI: 10.1784/insi.2007.49.8.447.
- Huo, Pengcheng et al. (2014). "On-Line Tool Condition Detection Based on Acoustic Signal." In: *International Journal of Applied science technology* 4.4, pp. 202–207.
- ISO 4287-1997 (1998). "Surface Texture Parameters." In: *ASTM International*, pp. 1–65. ISSN: 4288-1996.
- Jaini, Siti Nurfadilah Binti et al. (2020). "Indirect tool monitoring in drilling based on gap sensor signal and multilayer perceptron feed forward neural network." In: *Journal of Intelligent Manufacturing* 0123456789. ISSN: 15728145. DOI: 10.1007/s10845-020-01635-5.
- Jawahir, I. S. and X. Wang (2007). "Development of hybrid predictive models and optimization techniques for machining operations." In: *Journal of Materials Processing Technology* 185.1-3, pp. 46–59. ISSN: 09240136. DOI: 10.1016/j.jmatprotec.2006.03.133.
- Jemielniak, K. (1999). "Commercial tool condition monitoring systems." In: *International Journal of Advanced Manufacturing Technology* 15.10, pp. 711–721. ISSN: 02683768. DOI: 10.1007/s001700050123.
- Jemielniak, K. and J. Kossakowska (2010). "Tool wear monitoring based on wavelet transform of raw acoustic emission signal." In: *Tool wear monitoring based on wavelet transform of raw acoustic emission signal* 34.March, pp. 5–17. ISSN: 0137-4478.
- Jemielniak, K. et al. (2011). "Application of wavelet transform of acoustic emission and cutting force signals for tool condition monitoring in rough turning of Inconel 625." In: *Proceedings of the Institution of Mechanical Engineers, Part B: Journal of Engineering Manufacture* 225.1, pp. 123–129. ISSN: 09544054. DOI: 10.1243/09544054JEM2057.
- Jemielniak, Krzysztof (2019). "Contemporary challenges in tool condition monitoring." In: *Journal of Machine Engineering* 19.1, pp. 48–61. ISSN: 23918071. DOI: 10.5604/01.3001.0013.0448.
- Jindal, Anil (2012). "Analysis of Tool Wear Rate in Drilling Operation Using Scanning Electron Microscope (SEM)." In: *Journal of Minerals and Materials Characterization and Engineering* 11.01, p. 43.

- Kandilli, Ismet et al. (2007). "Online monitoring of tool wear in drilling and milling by multi-sensor neural network fusion." In: *Proceedings of the 2007 IEEE International Conference on Mechatronics and Automation, ICMA 2007*, pp. 1388–1394. DOI: 10.1109/ICMA.2007.4303752.
- Karagiannopoulos, M et al. (2007). "Feature Selection for Regression Problems." In: *The 8th Hellenic European Research on Computer Mathematics & its Applications, HERCMA 2007 i*, pp. 20–22. DOI: 10.1109/ICDM.2014.63.
- Karnik, S. R. and V. N. Gaitonde (2008). "Development of artificial neural network models to study the effect of process parameters on burr size in drilling." In: *The International Journal of Advanced Manufacturing Technology* 39.5-6, pp. 439–453. ISSN: 0268-3768. DOI: 10.1007/s00170-007-1231-5.
- Karpuschewski, Bernhard (2001). *Sensoren zur Prozessüberwachung beim Spanen*. VDI-Verlag, p. 243.
- Khleif, Ali Abbar and Mostafa Adel Abdullah (2017). "Effect of Cutting Parameters on Wear and Surface Roughness of Stainless Steel (316L) Using Milling Process." In: *Al-Nahrain Journal for Engineering Sciences* 19.2, pp. 286–292.
- Kilicaslan, Cenk (2009). "Modelling and Simulation of Metal Cutting By Finite Element Method." PhD thesis, p. 86.
- Kilundu, Bovic et al. (2011). "Tool wear monitoring by machine learning techniques and singular spectrum analysis." In: *Mechanical Systems and Signal Processing* 25.1, pp. 400–415. ISSN: 08883270. DOI: 10.1016/j.ymssp.2010.07.014.
- König, W. et al. (1993). "Turning versus Grinding - A Comparison of Surface Integrity Aspects and Attainable Accuracies." In: *CIRP Annals - Manufacturing Technology* 42.1, pp. 39–43. DOI: 10.1016/S0007-8506(07)62387-7.
- Kothuru, Achyuth et al. (2017). "Application of audible sound signals for tool wear monitoring using machine learning techniques in end milling." In: *The International Journal of Advanced Manufacturing Technology*, pp. 1–12. ISSN: 0268-3768. DOI: 10.1007/s00170-017-1460-1.
- Krishnakumar, P. et al. (2015). "Tool wear condition prediction using vibration signals in high speed machining (HSM) of Titanium (Ti-6Al-4V) alloy." In: *Procedia Computer Science* 50, pp. 270–275. ISSN: 18770509. DOI: 10.1016/j.procs.2015.04.049.
- Kubišová, Milena et al. (2019). *Statistical Comparison of Original and Replicated Surfaces*. Vol. 88. 872, pp. 1–10. ISBN: 9783030186814. DOI: 10.1007/978-3-030-18682-1_1.
- Kudryavtsev, YuriF. (2008). "Residual Stress." In: *Springer Handbook of Experimental Solid Mechanics SE - 15*, pp. 371–388. DOI: 10.1007/978-0-387-30877-7_15.
- Kuhn, Max, Kjell Johnson, et al. (2013). *Applied predictive modeling*. Vol. 26. Springer.
- Kumar, Adarsh et al. (2015). "Detection and classification for faults in drilling process using vibration analysis." In: *2014 International Conference on Prognostics and Health Management, PHM 2014*, pp. 3–8. DOI: 10.1109/ICPHM.2014.7036393.
- Kwong, J et al. (2009a). "Minor cutting edge-workpiece interactions in drilling of an advanced nickel-based superalloy." In: *International Journal of Machine Tools and Manufacture* 49.7-8, pp. 645–658. DOI: 10.1016/j.ijmachtools.2009.01.012.

- Kwong, J et al. (2009b). "The sensitivity of Ni-based superalloy to hole making operations: Influence of process parameters on subsurface damage and residual stress." In: *Journal of materials processing technology* 209.8, pp. 3968–3977.
- Landwehr, Niels et al. (2005). "Logistic model trees." In: *Machine Learning* 59.1-2, pp. 161–205. ISSN: 08856125. DOI: 10.1007/s10994-005-0466-3.
- Lee, Kiha and David A. Dornfeld (2005). "Micro-burr formation and minimization through process control." In: *Precision Engineering* 29.2, pp. 246–252. ISSN: 01416359. DOI: 10.1016/j.precisioneng.2004.09.002.
- Li, Huaizhong and Yun Chen (2013). *Handbook of Manufacturing Engineering and Technology*, pp. 1–33. ISBN: 9781447149767. DOI: 10.1007/978-1-4471-4976-7.
- Li, Zhimeng et al. (2017). "Milling tool wear state recognition based on partitioning around medoids (PAM) clustering." In: *International Journal of Advanced Manufacturing Technology* 88.5-8, pp. 1203–1213. ISSN: 14333015. DOI: 10.1007/s00170-016-8848-1.
- Liang, Steven Y. et al. (2004). "Machining process monitoring and control: The state-of-the-art." In: *Journal of Manufacturing Science and Engineering, Transactions of the ASME* 126.2, pp. 297–310. ISSN: 10871357. DOI: 10.1115/1.1707035.
- Lin, S. C. and C. J. Ting (1995). "Tool wear monitoring in drilling using force signals." In: *Wear* 180.1-2, pp. 53–60. ISSN: 00431648. DOI: 10.1016/0043-1648(94)06539-X.
- Liu, Huan and Hiroshi Motoda (1998). "Feature Selection for Knowledge Discovery and Data Mining." In: *Feature Selection for Knowledge Discovery and Data Mining*, p. 368. DOI: 10.1007/978-1-4615-5689-3.
- Liu, T. I. and K. S. Anantharaman (1994). "Intelligent Classification and Measurement of Drill Wear." In: *JOURNAL OF ENGINEERING FOR INDUSTRY* August 1994, pp. 1–3. ISSN: 00220817. DOI: 10.1115/1.2901957.
- Lu, J. (2002). "Prestress Engineering of Structural Material: A Global Design Approach to the Residual Stress Problem." In: *Handbook of residual stress and deformation of steel*. Chap. 2, pp. 11–26.
- Luque, Amalia et al. (2019). "The impact of class imbalance in classification performance metrics based on the binary confusion matrix." In: *Pattern Recognition* 91, pp. 216–231. ISSN: 00313203. DOI: 10.1016/j.patcog.2019.02.023.
- Maaten, Laurens Van Der and Geoffrey Hinton (2008). "Visualizing Data using t-SNE." In: *Journal of Machine Learning Research* 9, pp. 2579–2605.
- Maia, Luis Henrique Andrade et al. (2015). "A new approach for detection of wear mechanisms and determination of tool life in turning using acoustic emission." In: *Tribology International* 92, pp. 519–532. ISSN: 0301679X. DOI: 10.1016/j.triboint.2015.07.024.
- Maimon, Oded and Lior Rokach (2011). *Data mining and knowledge discovery handbook*. Vol. 48. 10, pp. 48–5729–48–5729. ISBN: 9780387244358. DOI: 10.5860/choice.48-5729.
- Markopoulos, Angelos P (2013). *Finite Element Method in Machining Processes [electronic resource]*, p. 96. ISBN: 9781447143307.

- Mehmood, Tahir et al. (2012). "Review of Input Variable Selection Methods for Artificial Neural Networks." In: *Chemometrics and Intelligent Laboratory Systems* 118, pp. 62–69. ISSN: 01697439. DOI: 10.1016/j.chemolab.2012.07.010.
- Mia, Mozammel and Nikhil Ranjan Dhar (2016). "Prediction of surface roughness in hard turning under high pressure coolant using Artificial Neural Network." In: *Measurement: Journal of the International Measurement Confederation* 92, pp. 464–474. ISSN: 02632241. DOI: 10.1016/j.measurement.2016.06.048.
- Min, Sangkee et al. (2001). "Development of a drilling burr control chart for low alloy steel, AISI 4118." In: *Journal of Materials Processing Technology* 113.1-3, pp. 4–9. ISSN: 09240136. DOI: 10.1016/S0924-0136(01)00589-1.
- Mingoti, Sueli A. and Joab O. Lima (2006). "Comparing SOM neural network with Fuzzy c-means, K-means and traditional hierarchical clustering algorithms." In: *European Journal of Operational Research* 174.3, pp. 1742–1759. ISSN: 03772217. DOI: 10.1016/j.ejor.2005.03.039.
- Mohsen, Marani et al. (2020). "Prediction of cutting tool wear during a turning process using artificial intelligence techniques." In: *The International Journal of Advanced Manufacturing Technology* 32.2, pp. 174–182. ISSN: 13623052. DOI: 10.1080/0951192X.2018.1550681.
- Montronix (n.d.). *Operating manual spectra brochure*. Tech. rep. o. URL: <https://www.montronix.com/en/>.
- Moussaoui, Kamel et al. (2013). "Influence of milling on surface integrity of Ti6Al4V-study of the metallurgical characteristics: Microstructure and microhardness." In: *International Journal of Advanced Manufacturing Technology* 67.5-8, pp. 1477–1489. ISSN: 02683768. DOI: 10.1007/s00170-012-4582-5.
- Nakandhrakumar, R. S. et al. (2016). "A novel normalisation procedure for the sensor positioning problem in vibration monitoring of drilling using artificial neural networks." In: *Insight: Non-Destructive Testing and Condition Monitoring* 58.10, pp. 556–563. ISSN: 17544904. DOI: 10.1784/insi.2016.58.10.556.
- Nalbant, Muammer et al. (2009). "The experimental investigation of the effects of uncoated, PVD- and CVD-coated cemented carbide inserts and cutting parameters on surface roughness in CNC turning and its prediction using artificial neural networks." In: *Robotics and Computer-Integrated Manufacturing* 25.1, pp. 211–223. ISSN: 07365845. DOI: 10.1016/j.rcim.2007.11.004.
- Nordmann (n.d.). *NORDMANN Tool Monitoring*. URL: <https://www.toolmonitoring.com/>.
- O'Donnell, Garret et al. (2001). "Towards the improvement of tool condition monitoring systems in the manufacturing environment." In: *Journal of Materials Processing Technology* 119.1-3, pp. 133–139. ISSN: 09240136. DOI: 10.1016/S0924-0136(01)00928-1.
- Oliveira, Henrique M et al. (2018). "On the Use of t-Distributed Stochastic Neighbor Embedding for Data Visualization and Classification of Individuals with Parkinson's Disease." In: *Computational and Mathematical Methods in Medicine* 2018. DOI: 10.1155/2018/8019232.

- Panda, S. S. et al. (2006). "Drill wear monitoring using back propagation neural network." In: *Journal of Materials Processing Technology* 172.2, pp. 283–290. ISSN: 09240136. DOI: 10.1016/j.jmatprotec.2005.10.021.
- Patra, Karali (2011). "Acoustic emission based tool condition monitoring system in drilling." In: *Proceedings of the world congress on engineering*. Vol. 3, pp. 6–8.
- Patra, Karali et al. (2006). "Drill wear monitoring through current signature analysis using wavelet packet transform and artificial neural network." In: *Proceedings of the IEEE International Conference on Industrial Technology*, pp. 1344–1348. DOI: 10.1109/ICIT.2006.372577.
- Pearson, Karl (1901). "On lines and planes of closest fit to systems of points in space." In: *The London, Edinburgh, and Dublin Philosophical Magazine and Journal of Science* 5982. DOI: 10.1080/14786440109462720.
- Promicron (n.d.). *Spike*. URL: <https://www.pro-micron.de/spike/?lang=en{\#}drilling>.
- Rafezi, Hamed et al. (2012). "Time Domain and Frequency Spectrum Analysis of Sound Signal for Drill Wear Detection." In: *International Journal of Computer and Electrical Engineering* 4.5, p. 722.
- Rahim, E A and S Sharif (2007). "Tool failure modes and wear mechanism of coated carbide tools when drilling Ti-6Al-4V." In: *Int. J. Precision Technology* Vol. 1 No.1, pp.30–39. ISSN: 1755-2060. DOI: 10.1504/IJPTech.2007.015342.
- Rahim, Erween Abd. and Safian Sharif (2006). "Investigation on Tool Life and Surface Integrity when Drilling Ti-6Al-4V and Ti-5Al-4V-Mo/Fe." In: *JSME International Journal Series C* 49.2, pp. 340–345. ISSN: 1344-7653. DOI: 10.1299/jsmec.49.340.
- Rajeev, D. et al. (2017). "Artificial neural network based tool wear estimation on dry hard turning processes of AISI4140 steel using coated carbide tool." In: *Bulletin of the Polish Academy of Sciences: Technical Sciences* 65.4, pp. 553–559. ISSN: 02397528. DOI: 10.1515/bpasts-2017-0060.
- Ranjan, Jitesh et al. (2020). "Artificial intelligence-based hole quality prediction in micro-drilling using multiple sensors." In: *Sensors (Switzerland)* 20.3, pp. 1–14. ISSN: 14248220. DOI: 10.3390/s20030885.
- Ren, Qun et al. (2010). "TSK fuzzy modeling for tool wear condition in turning processes : An experimental study." In: *Engineering Applications of Artificial Intelligence* 24.2, pp. 260–265. ISSN: 0952-1976. DOI: 10.1016/j.engappai.2010.10.016.
- Rmili, Wafaa et al. (2016). "An automatic system based on vibratory analysis for cutting tool wear monitoring." In: *Measurement: Journal of the International Measurement Confederation* 77, pp. 117–123. DOI: 10.1016/j.measurement.2015.09.010.
- Rodríguez, Juan et al. (2016). "A decision-making tool based on decision trees for roughness prediction in face milling." In: *International Journal of Computer Integrated Manufacturing* 00.00, pp. 1–15. ISSN: 0951-192X. DOI: 10.1080/0951192X.2016.1247991.
- Samanta, B (2009). "Surface roughness prediction in machining using soft computing." In: *International Journal of Computer Integrated Manufacturing* September 2012, pp. 37–41. DOI: 10.1080/09511920802287138.

- Sandvik Coromant (n.d.). "CoroPlus Process Control brochure." In: (). URL: <https://www.sandvik.coromant.com/en-gb/products/coroplus-processcontrol/Pages/default.aspx>.
- Scheffer, C. and P. S. Heyns (2001). "Wear monitoring in turning operations using vibration and strain measurements." In: *Mechanical Systems and Signal Processing* 15.6, pp. 1185–1202. ISSN: 08883270. DOI: 10.1006/mssp.2000.1364.
- Schmitz, Tony L. and Kevin S. Smith (2009). *Machining Dynamics*. Ed. by Kai Cheng. ISBN: 978-1-84628-367-3. DOI: 10.1007/978-1-84628-368-0.
- Seemuang, N. et al. (2016). "Using spindle noise to monitor tool wear in a turning process." In: *International Journal of Advanced Manufacturing Technology* 86.9-12, pp. 2781–2790. DOI: 10.1007/s00170-015-8303-8.
- Shah, Mihir et al. (2010). "Tool control monitoring applied to drilling." In: *Proceedings of the 6th MUGV conference, Cluny, France*, pp. 1–10.
- Shankar, S et al. (2018). "Prediction of cutting tool wear during milling process using artificial intelligence techniques." In: *International Journal of Computer Integrated Manufacturing* 00.00, pp. 1–9. ISSN: 0951-192X. DOI: 10.1080/0951192X.2018.1550681.
- Sharman, A. R C et al. (2008). "Tool life and surface integrity aspects when drilling and hole making in Inconel 718." In: *Journal of Materials Processing Technology* 200.1-3, pp. 424–432. ISSN: 09240136. DOI: 10.1016/j.jmatprotec.2007.08.080.
- Smith, Graham T. (2008). *Cutting Tool Technology*. Vol. 1. 9. Springer-Verlag London, pp. XII, 600. ISBN: 9788578110796. arXiv: arXiv:1011.1669v3.
- Souza, Cláudio Costa et al. (2012). "A contribution to the measurement of circularity and cylindricity deviations." In: *ABCM symposium series in Mechatronics*. Vol. 5, p. 791.
- Stavropoulos, P. et al. (2016). "Tool wear predictability estimation in milling based on multi-sensorial data." In: *International Journal of Advanced Manufacturing Technology* 82.1-4, pp. 509–521. DOI: 10.1007/s00170-015-7317-6.
- Subramanian, K. and N. H. Cook (1977). "Sensing of Drill Wear and Prediction of Drill Life." In: *The ASME International Mechanical Engineering Congress and Exhibition, Orlando* 65.10, p. 854. ISSN: 00099260. DOI: 10.1016/j.crad.2010.04.020.
- Sudev, LJ and HV Ravindra (2008). "Tool wear estimation in drilling using acoustic emission signal by multiple regression and GMDH." In: *ASME International Mechanical Engineering Congress and Exposition*. Vol. 48722, pp. 97–106.
- Sultan, A. Z. et al. (2015). "Effect of Machining Parameters on Tool Wear and Hole Quality of AISI 316L Stainless Steel in Conventional Drilling." In: *Procedia Manufacturing* 2.February, pp. 202–207. ISSN: 23519789. DOI: 10.1016/j.promfg.2015.07.035.
- Sun, Shixu et al. (2020). "Detection of tool breakage during milling process through acoustic emission." In: *International Journal of Advanced Manufacturing Technology* 109.5-6, pp. 1409–1418. ISSN: 14333015. DOI: 10.1007/s00170-020-05751-7.
- Swinburne, Richard (2005). *Metal cutting principles*. 2nd editio. Oxford University Press, Inc. ISBN: 0471359297. DOI: 10.1007/s007690000247.
- Terrazas, German et al. (2018). "Online Tool Wear Classification during Dry Machining Using Real Time Cutting Force Measurements and a CNN Approach." In: *Journal*

- of *Manufacturing and Materials Processing* 2.4, p. 72. ISSN: 2504-4494. DOI: 10.3390/jmmp2040072.
- Teti, R. et al. (2010). "Advanced monitoring of machining operations." In: *CIRP Annals - Manufacturing Technology* 59.2, pp. 717–739. DOI: 10.1016/j.cirp.2010.05.010.
- Thakur, A. and S. Gangopadhyay (2016). "State-of-the-art in surface integrity in machining of nickel-based super alloys." In: *International Journal of Machine Tools and Manufacture* 100, pp. 25–54. ISSN: 08906955. DOI: 10.1016/j.ijmachtools.2015.10.001.
- Trent, Edward Moor and Paul K. Wright (2000). *Metal cutting*. Butterworth-Heinemann.
- Ucun, Ismail and Serdar Kaplan (2017). "Determination of tool wear and chip formation in drilling process of AISI 1045 material using plasma-nitrided high-speed steel drill bits." In: *Proceedings of the Institution of Mechanical Engineers, Part B: Journal of Engineering Manufacture* 231.10, pp. 1725–1734. ISSN: 20412975. DOI: 10.1177/0954405415608105.
- Ulutun, Durul and Tugrul Ozel (2011). "Machining induced surface integrity in titanium and nickel alloys: A review." In: *International Journal of Machine Tools and Manufacture* 51.3, pp. 250–280. ISSN: 08906955. DOI: 10.1016/j.ijmachtools.2010.11.003.
- Umbrello, Domenico et al. (2004). "Hardness-based flow stress and fracture models for numerical simulation of hard machining AISI 52100 bearing steel." In: *Materials Science and Engineering A* 374.1-2, pp. 90–100. ISSN: 09215093. DOI: 10.1016/j.msea.2004.01.012.
- Venkata Rao, K. et al. (2014). "Prediction of cutting tool wear, surface roughness and vibration of work piece in boring of AISI 316 steel with artificial neural network." In: *Measurement: Journal of the International Measurement Confederation* 51.1, pp. 63–70. ISSN: 02632241. DOI: 10.1016/j.measurement.2014.01.024.
- Vrabel, Marek et al. (2012). "Surface roughness prediction using artificial neural networks when drilling UDIMET 720." In: *Procedia Engineering* 48, pp. 693–700. ISSN: 18777058. DOI: 10.1016/j.proeng.2012.09.572.
- Wang, Guofeng et al. (2013). "Tool wear monitoring based on cointegration modelling of multisensory information." In: *International Journal of Computer Integrated Manufacturing* August 2014, pp. 37–41. DOI: 10.1080/0951192X.2013.814162.
- Waqar, Saad et al. (2016). "Effect of Drilling Parameters on Hole Quality of Ti-6Al-4V Titanium Alloy in Dry Drilling." In: *Materials Science Forum* 880, pp. 33–36. ISSN: 1662-9752. DOI: 10.4028/www.scientific.net/MSF.880.33.
- Wattpilote (n.d.). *Tool wear and breakage monitoring system WattPilote brochure*. Tech. rep. URL: <http://www.danffor.com/productos/wattpilote.html>.
- Wei, Yingying et al. (2016). "Effect of drilling parameters and tool geometry on drilling performance in drilling carbon fiber-reinforced plastic/titanium alloy stacks." In: *Advances in Mechanical Engineering* 8.9, pp. 1–16. DOI: 10.1177/1687814016670281.
- Wern, C. W. et al. (1993). "A study of the surface texture of composite drilled holes." In: *Journal of Materials Processing Tech.* 37.1-4, pp. 373–389. ISSN: 09240136. DOI: 10.1016/0924-0136(93)90103-D.
- Wu, Dazhong et al. (2017a). "A Comparative Study on Machine Learning Algorithms for Smart Manufacturing: Tool Wear Prediction Using Random Forests." In: *Journal of*

- Manufacturing Science and Engineering, Transactions of the ASME* 139.7. ISSN: 15288935. DOI: 10.1115/1.4036350.
- Wu, Dazhong et al. (2017b). "Cloud-Based Parallel Machine Learning for Prognostics and Health Management: A Tool Wear Prediction Case Study." In: *Journal of Manufacturing Science and Engineering* c. ISSN: 1087-1357. DOI: 10.1115/1.4038002.
- Xiaoli, Li and Yuan Zhejun (1998). *Tool wear monitoring with wavelet packet transform - fuzzy clustering method*. DOI: [https://doi.org/10.1016/S0043-1648\(98\)00165-3](https://doi.org/10.1016/S0043-1648(98)00165-3).
- Xu, Ke et al. (2020). "Advanced Data Collection and Analysis in Data-Driven Manufacturing Process." In: *Chinese Journal of Mechanical Engineering (English Edition)* 33.1. ISSN: 21928258. DOI: 10.1186/s10033-020-00459-x.
- Yang, Aimin et al. (2017). "Optimum surface roughness prediction for titanium alloy by adopting response surface methodology." In: *Results in Physics*. ISSN: 22113797. DOI: 10.1016/j.rinp.2017.02.027.
- Zain, Azlan Mohd et al. (2010). "Prediction of surface roughness in the end milling machining using Artificial Neural Network." In: *Expert Systems with Applications* 37.2, pp. 1755–1768. ISSN: 09574174. DOI: 10.1016/j.eswa.2009.07.033.
- Zhang, Lin et al. (2014). "Cloud manufacturing: a new manufacturing paradigm." In: *Enterprise Information Systems* 8.2, pp. 167–187. ISSN: 17517575. DOI: 10.1080/17517575.2012.683812.
- Zhao, Qing et al. (2015). "Tool life and hole surface integrity studies for hole-making of Ti6Al4V alloy." In: *International Journal of Advanced Manufacturing Technology* 79.5-8, pp. 1017–1026. ISSN: 14333015. DOI: 10.1007/s00170-015-6890-z.
- Zhou, Youhang et al. (2017). "Consistency evaluation of hole series surface quality using vibration signal." In: *International Journal of Advanced Manufacturing Technology* 92.1-4, pp. 1069–1079. ISSN: 14333015. DOI: 10.1007/s00170-017-0184-6.
- Zou, Hui and Trevor Hastie (2005). "Regularization and variable selection via the elastic net." In: *Journal of the Royal Statistical Society. Series B: Statistical Methodology* 67.2, pp. 301–320. ISSN: 13697412. DOI: 10.1111/j.1467-9868.2005.00503.x.